KU Leuven
Group Biomedical Sciences
Faculty of Pharmaceutical & Pharmacological Sciences
Laboratory for Radiopharmacy

Development of Radiolabeled PET Tracers for *in vivo* Visualization of Phosphodiesterase Type 5 (PDE5)

Rufael CHEKOL

Jury:

Promoter:	Prof. Dr. Guy Bormans
Co-promoters:	Prof. Dr. Alfons Verbruggen
	Prof. Dr. Olivier Gheysens
Chair:	Prof. Dr. Pieter Annaert
Jury members:	Prof. Dr. Erwin Adams
	Dr. Peter Pokreisz
	Prof. Dr. Heinz Coenen
	Prof. Dr. Joel Aerts

Leuven, 2014

Doctoral thesis in Pharmaceutical Sciences

21st of March, 2014, 5 pm

Auditorium BMW3 04.216

Herestraat 49, Campus Gasthuisberg

Leuven, Belgium

Promoter:	Prof. Dr. Guy Bormans
Co-promoters:	Prof. Dr. Alfons Verbruggen
	Prof. Dr. Olivier Gheysens

Laboratory for Radiopharmacy
Faculty of Pharmaceutical &
Pharmacological Sciences
O&N II, Box 821, Herestraat 49
B-3000 Leuven

Dedicated to the City of Leuven, what it entails and the good memories

Acknowledgement

If someone suggested few years ago that I would spend the coming years (more than 16 % of my life so far) out of my home country I would have replied "'No way!". Nonetheless, here I am, short of one day for 6 years and one month in Belgium. I vividly remember how cold it was when I arrived (by the standards of my experience). I also clearly remember the first question from Guy during my first interview, "to explain S_2N reaction". I hope, I can answer that question adequately after 5 years and 5 months in the Laboratory of Radiopharmacy.

The door of radiopharmacy world was opened for me first by Prof. Alfons Verbruggen and then Prof. Guy Bormans. Fons, thank you very much for giving me the opportunity to study under your guidance. You have always been helpful and understanding. After my first spell in radiopharmacy at lower level, the door to the world of radiopharmacy was again opened for me by Prof. Guy Bormans. Thank you Guy zillion times for giving me the opportunity to undertake my doctoral study under your supervision. It has been a great honour to work under your guidance. Your technical, scientific and managerial knowledge/skill have been a great lesson in my life. You have always tirelessly and passionately tried to improve my skill and knowledge in radiopharmacy, I appreciate it. Your enthusiasm, passion, hard work, and determination to make yourself available to your students (however, busy you were) are rare qualities to find in a single person. I hope, you would feel partly compensated for your precious time you spent (including nights and weekends) on the manuscript when you go through the dissertation in its final printed version. It is my wish and hope that you draw satisfaction when you finally witness the launch of one of our compounds (and many other from your research team) in clinical practice.

This research work have been greatly influenced and improved by my co-promoters Prof. Alfons Verbruggen and Prof. Olivier Gheysens. This dissertation would not have its current content, structure and outlook with out your continuous comments and suggestions. Olivier, thank you very much for the discussion on how to improve the research work and the contents of the thesis. I would also like to thank the co-authors of the manuscripts for their contribution.

I wish to express my gratitude to Prof. Pieter Annaert, Prof. Erwin Adams, Dr. Peter Pokreisz, Prof. Joel Aerts, and Prof. Heinz Coenen for spending their precious time reading the manuscript and giving very valuable comments and suggestions.

The research work would not have been possible without the collaboration between different departments: Department of Imaging and Pathology (KU Leuven) and Nuclear Medicine (UZ Leuven) for production of radiolabeled compounds (from radionuclide production to formulation and quality control), Nuclear Medicine and Molecular Imaging (MoSAIC, KU Leuven) for animal experiments, Department of Cardiovascular Sciences (KU Leuven) for providing transgenic mice, pig for PET study, TAC and LAD mice and their expert advice on cardiac hypertrophy, Discovery Sciences (Janssen Pharmaceutica) for determination of *in vitro* phosphodiesterase inhibitory activity of compounds discussed in this dissertation. I have to extend my acknowledgement and appreciation for aforementioned departments and organizations for their contribution to the success of this research work and the resulting manuscript.

We (Nuclear Medicine, UZ Leuven and Radiopharmacy, KU Leuven) are truly two big and happy families. The collaboration is an amazing experience and an example to others. I would like to take this opportunity to express my gratitude to the members of this big family: Prof. Koen Van Laere (Head of Nuclear Medicine, UZ Leuven), Tjibbe De Groot and Marva Bex you were always willing to help me during radioisotope production despite the hectic situation during working hours. Tjibbe you were always forthright spoken and I like that character of yours! Bert Vanbilloen (thanks for the supervision during my first year in post graduate studies), Stef Verschoren (for the nice after-work hours :), Christelle Terwinghe; Nathalie Devolder; Mireille Heroes; Anja Wilberts; Mieke Steukers; Magdalena Sojka; Kim Serdons, Kim Deliege; Katrien Seré and Annemie Morel: thank you all for the help and nice time. Jan Cleynhens, thank you for your great work and help on the organic synthesis of molecules. Your presence in the lab made a big difference both scientifically and socially and you were the spice of the lab! Sofie thank you for valuable and practical input. Ivan, Julie and Jana: thank you for your technical assistance during animal experiments. Maarten, thank you for your help on microPET image processing and also for the great time we had while on lab trip (Parma, Amsterdam...). Ahamed, thank you for your help on organic synthesis and NMR elucidation. I greatly appreciate for forwarding links to job postings and also for little chit-chats we had. Matthias, Kristof, Vamsi, Daisy, Sofie, Dieter, Maarten, Frederick, Lieven, Ivan, Julie Jana, Ahamed and Joan the Catalan: thank you all for the lovely discussions, the chats and the great nights I enjoyed with you. Thanks to An, Chantal, Ann and Jenny for taking away the headache of administrative work. Rita thanks for keeping things in order and the little chats we had.

Ces amigo, thank you for your friendship and making my stay in Belgium a memorable one! Ant, thanks for the brotherly advices and pastime. Zelalem, Sol and Getu thanks for your company and Pangaea nights.

The custom is to reserve the last paragraph for family members though they come first in our lives. Dunge, I greatly appreciate everything you have done, including relieving me of my paternal responsibilities especially during the last hectic months of thesis writing. Thank you for your insistence, encouragement and editing the thesis manuscript. When I started my journey in radiopharmacy I was a man but now I am a father of two energetic boys. Kenusha and Libentje, you are a source of happiness in my life! "I look forward to the day you call me papa" was my wish in my master's thesis. Now, I get papa call every 5 minutes (though most of the time to accuse each other or I resolve a conflict between you to guys!). My wish for you two boys is to grow up and give me many grand children who will call me grandpa :)

Leuven has been kind to me and my family. The boys have been well taken care of starting from Créche (from 3 months old) to preparatory school. My appreciation goes to those who helped raise Kena and Liben particularly Saar Bironț (Kabouterberg) and Tatjana Adriaens (Fabota). I will miss the City of Leuven immensely!

Rufael Chekol

Leuven, 2014

Table of Contents

List of Acronyms and Abbreviations

% ID	Percent Injected Dose
[^{11}C]CH_3OTf	[^{11}C]Methyl trifluoromethanesulfonate
[^{18}F]FEtOTf	2-[^{18}F]FluoroEthyl trifluoromethanesulfonate
AC	Adenylyl Cyclase
sAC	Soluble Adenylyl Cyclase
sGC	Soluble Guanylyl Cyclase
Ala	Alanine
ALT	Alanine Transaminase
AST	Aspartate Transaminase
ATP	Adenosine TriPhosphate
BBB	Blood-Brain Barier
cAMP	cyclic Adenosine MonoPhosphate
cGMP	cyclic Guanosine MonoPhosphate
CPM	Counts Per Minute
cN	cyclic Nucleotide
CNS	Central Nervous System
CT	Computed Tomography
DAG	Diacylglycerol
EDRF	Endothelium-Derived Relaxing Factor
EMA	European Medicines Agency
Epac/EPAC	Exchange Proteins directly Activated by cAMP
ET	EndoThelin
GC	Guanylyl Cyclase
GEF	Guanine nucleotide Exchange Factor
Gly	Glycine
GTP	Guanosine TriPhosphate
Hct	Hematocrit
HPLC	High Pressure Liquid Chromatography
IC_{50}	Inhibitory Concentration of 50 %
ID	Injected Dose
ICH	Internation Conference on Harmonization
IHC	ImmunoHistoChemistry
IP_3	Iinositol 1,4,5-trisphosphate

ISH	In Situ Hybridization
kBq	killo Becquerel (10^3 Bq)
MBq	Mega Becquerel (10^6 Bq)
MC	Metabolic Cage
MCH	Mean Corpuscular Hemoglobin
MCHC	Mean Corpuscular Hemoglobin Concentration
MCV	Mean Corpuscular Volume
Met	Methionine
MPV	Mean Platelets Volume
MRI	Magnetic Resonance Imaging
NADPH	Nicotinamide Adenine Dinucleotide Phosphate
NMRI	North Medical Research Institute
NO	Nitric Oxide
NOS	Nitric Oxide Synthases
eNOS	Endothelial (Type III) Nitric Oxide Synthases
iNOS	Inducible (Type II) Nitric Oxide Synthases
nNOS	Neuronal (Type I) Nitric Oxide Synthases
NP	Natriuretic Peptide
ANP	A-type (Atrial) Natriuretic peptide
BNP	B-type (Brain) Natriuretic Peptide
CNP	C-type Natriuretic Peptide
NSAID	Non Steroidal Anti-Inflammatory Drug
PAH	Pulmonary Arterial Hypertension
PCR	Polymerase Chain Reaction;
PDE5	Phosphodiesterase type 5
PDE5 TG	Phosphodiesterase type 5 TransGenic
PET	Positron Emission Tomography
pi	Post Injection
pGC	Particulate Guanylyl Cyclase
PKA	cAMP dependent Protein kinase
PKG	cGMP dependent protein kinase
Rap1	Ras-related protein 1
Ras	Rat sarcoma
RBC	Red Blood Cell
RCY	RadioChemical Yield

RDW	Red Blood Cell distribution Width
RP-HPLC	Reversed Phase - High Pressure Liquid Chromatography
SGOT	Serum Glutamic Oxaloacetic Transaminase
SGPT	Serum Glutamic-Pyruvic Transaminase
SMC	Smooth Muscle Cell
SPECT	Single Photon Emission Computed Tomography
SUV	Standardized Uptake Value
TAC	Timi-Activity-Curve
tmAC	Transmembrane Adenylyl Cyclase
TNF	Tumor Necrosis Factor
Tyr	Tyrosine
VASP	Vasodilator-Stimulated Phosphoprotein
VIP	Vasoactive Intestinal Peptide
VSMC	Vascular Smooth Muscle Cell

Summary

Phosphodiesterase type 5 (PDE5) is highly expressed in vascular smooth muscle cells, and its inhibition is a primary target for the treatment of erectile dysfunction and pulmonary hypertension. Besides, PDE5 plays a pivotal role in disease progressions such as, cardiac hypertrophy and ventricular remodeling, myocardial ischemia, aortic stenosis, end stage congestive heart failure and atherosclerosis.

Several PDE5 inhibitors are approved for clinical use or have been introduced in preclinical development. Vardenafil, sildenafil, tadalafil, RPP07 (**PF-5**), JC4712, and RBQ05 are among the many to mention few that have been shown to possess avid PDE5 inhibitory activity and are in clinical use and/or at development stage.

Positron emission tomography (PET) is a non-invasive molecular imaging modality that uniquely allows exploration of biochemical processes and can quickly be translated from the laboratory to clinical application. Hence, the use of radiolabeled PDE5 inhibitors with short lived radionuclides such as carbon-11 and fluorine-18 could potentially enable localization and quantification of PDE5 expression *in vivo*. Exploitation of a suitable PDE5 specific PET radioligand(s) would allow quantifying and evaluating changes in PDE5 expression, select patients that would benefit from PDE5 inhibitor treatment early during disease progression and assess PDE5 occupancy and optimize dose regimens in patients treated with PDE5 inhibitors.

In order to realize this goal, PDE5 inhibitors reported in literature to have high *in vitro* PDE5 inhibitory activity and specificity were selected and synthesized, radiolabeled and biologically evaluated for their suitability to non-invasively visualize PDE5 expression. The binding and specificity of radiolabeled radiotracers were evaluated by *in vivo* and *in vitro* studies in mice and rats. Binding of radiolabeled tracers to PDE5 was initially evaluated by comparing the lung retention of the radiotracers in mice and subsequently their specificity for PDE5 was verified with a pre-blocking study by pre-treating mice with a structurally different PDE5 inhibitor. In addition, radiolabeled tracers were evaluated in transgenic mice with cardiomyocyte specific PDE5 over-expression.

In conclusion, four classes of PDE5 inhibitors were radiolabeled and biologically evaluated among which the imidazotriazine family ([^{11}C]NMVardenafil and [^{18}F]Fluorovardenafil) and pyridopyrazinone family ([^{11}C]RPP07B and [^{18}F]FRPP07) showed the highest *in vivo* retention in the lungs of healthy mice where the enzyme is abundantly expressed. Although

the pyrazolopyrimidinone derivative [^{11}C]JC4714 showed favorable properties in initial biological evaluation in healthy mice, further investigation in PDE5 TG mice showed moderate to low *in vivo* binding of the tracer to PDE5. The other investigated compounds [^{11}C]PVardenafil**,** [^{11}C]sildenafil, [^{11}C]RBQ08 and [^{11}C]JC4687 showed low *in vivo* binding and/or specificity for PDE5 rendering them unsuitable for *in vivo* visualization and/or quantification of PDE5. Based on preclinical evaluation of our studies [^{11}C]NMVardenafil has been selected for further clinical investigation in selected patients with end-stage heart failure awaiting cardiac transplantation.

Samenvatting

Het enzym fosfodiesterase type 5 (PDE5) is verantwoordelijk voor de hydrolyse van cyclisch guanosinemonofosfaat (cGMP) naar guanosinemonofosfaat (GMP). PDE5 heeft een hoge expressie in de gladde spiercellen van bloedvaten en verschillende PDE5 inhibitoren (zoals Viagra) werden geregistreerd voor farmacologische behandeling van erectiele dysfunctie en pulmonaire hypertensie. Daarnaast speelt PDE5 ook een belangrijke rol bij aandoeningen zoals myocardiale ischemie en hypertrofie, ventriculaire remodeling, aorta stenose, eindstadium van congestief hartfalen en atherosclerose.

Verschillende structureel uiteenlopende PDE5 inhibitoren (o.a. Vardenafil, Sildenafil, Tadalafil, RPP07 (**PF-5**), JC4712 en RBQ05) werden reeds goedgekeurd voor humaan gebruik of zijn in het stadium van preklinische of klinische ontwikkeling.

Positronemissie tomografie (PET) is een niet-invasieve moleculaire beeldvormingstechniek die gebruik maakt van radioactieve verbindingen en toelaat biochemische processen *in vivo* te visualiseren en te kwantificeren. Daar er slechts een uiterst kleine massahoeveelheid van een radioactieve tracerverbinding voor beeldvorming moet worden toegediend kan een nieuwe PET tracerverbinding relatief snel translationeel toegepast worden bij de mens.

Het gebruik van PDE5 inhibitoren gemerkt met een radionuclide dat met een korte halveringstijd vervalt via positronemissie zoals koolstof-11 of fluor-18 laat mogelijk toe om de PDE5 expressie in vivo in beeld te brengen en te kwantificeren.

De toepassing van een gevalideerde PDE5 specifieke PET radioligand zou dus toelaten patiënten te selecteren met een lokaal pathologisch verhoogde PDE5 expressie (bij voorbeeld na myocardinfarct) die baat kunnen hebben van farmacologische behandeling met een PDE5 inhibitor. Bovendien zou een geschikte PDE5 tracerverbinding ook toelaten de relatie tussen de plasmaconcentratie van een PDE5 inhibitor en de effectieve PDE5 bezetting te kwantificeren zodat aan de hand van deze relatie de dosering met PDE5 inhibitoren kan worden geoptimaliseerd.

Verschillende in de literatuur beschreven PDE5 inhibitoren werden geselecteerd voor merking met koolstof-11 of fluor-18. De benodigde precursoren en referentieverbindingen werden gesynthetiseerd en de radioactief gemerkte verbindingen werden geëvalueerd in proefdieren met betrekking tot hun PDE5 specifieke binding.

Initieel werden de verschillende onderzochte tracerverbindingen vergeleken aan de hand van hun PDE5 specifieke longretentie in muizen daar PDE5 een hoge expressiegraad in dit orgaan heeft. Daarnaast werden de verbindingen ook geëvalueerd in transgene muizen met myocard specifieke PDE5 overexpressie.

Uit de biologische evaluatie van radioliganden uit vier onderzochte structurele klassen van PDE5 inhibitoren bleek dat verbindingen van de imidazotriazine familie ([^{11}C]NMVardenafil en [^{18}F]fluorovardenafil) en de pyridopyrazinon familie ([^{11}C]RPP07B en [^{18}F]FRPP07) de hoogste retentie in longen vertoonden bij muizen.

Op basis van de preklinische evaluatie werd [^{11}C]NMVardenafil geselecteerd voor verdere klinische evaluatie in patiënten met eindstadium hartfalen cardiomyopathie die in aanmerking komen voor harttransplantatie. Een beperkte toxiciteitsstudie volgens de “microdosing” benadering toonde aan dat [^{11}C]NMVardenafil veilig kan gebruikt worden als PET tracerverbinding bij klinische studies.

Different names used to designate the PDE5 inhibitors radiolabeled in the dissertation

Compound	Other names	Other names/radioactive	Class	Chapters discussed
14	Sildenafil	[^{11}C]Sildenafil, [^{11}C]**14**	pyrazolopyrimidine	Chapter 2 and 6
Tadalafil			β-carboline	
Vardenafil			imidazotriazine	
7	NMVardenafil	[^{11}C]NMVardenafil, [^{11}C]-**7**, [^{11}C]RC01	imidazotriazine	Chapter 2, 3 and 6
8	PVardenafil	[^{11}C]PVardenafil, [^{11}C]**8**	imidazotriazine	Chapter 2 and 6
11	Fluorovardenafil	[^{18}F]Fluorovardenafil, [^{11}C]**11**	imidazotriazine	Chapter 2
19	RBQ04		quinoline	Chapter 2 and 6
21	RBQ08	[^{11}C]RBQ08, [^{11}C]**21**	quinoline	Chapter 2 and 6
22	RBQ05		quinoline	Chapter 2 and 6
33	**JC4687**	[^{11}C]JC4687, [^{11}C]**33**	pyrazolopyrimidine	Chapter 2 and 6
35	**JC4712**		pyrazolopyrimidine	Chapter 2 and 6
37	**JC4714**	[^{11}C]JC4714, [^{11}C]**37**	pyrazolopyrimidine	Chapter 2 and 6
10	**RPP011B**		pyridopyrazinone	Chapter 4 and 6
12	**RPP07B**	[^{11}C]RPP07B	pyridopyrazinone	Chapter 4 and 6
14	**RPP07**	**PF-5**	pyridopyrazinone	Chapter 4, and 6
17	**FRPP07**	[^{18}F]FRPP07		Chapter 4, and 6
18	**RPP012**		pyridopyrazinone	Chapter 4, and 6

Chapter I

General Introduction

Phosphodiesterase inhibitors have been used for more than two thousand years since the advent of coffee in East Africa (Ethiopia) but only in the last 60 years their targets have been identified. The active ingredient caffeine inhibits the degradation of cyclic nucleotide second messengers [1].

Second messengers are molecules that relay signals from receptors on the cell surface to target molecules inside the cell, in the cytoplasm or nucleus. They relay the signals of hormones like adrenaline, growth factors, light, natriuretic peptides (NPs), nitric oxide (NO) and others, and cause a change in the activity of the cell. They greatly amplify the strength of the signal and are a component of signal transduction cascades. Some examples of second messengers include cyclic adenosine monophosphate (cAMP), cyclic guanosine monophosphate (cGMP), Ca^{2+}, inositol 1,4,5-trisphosphate (IP_3) and diacylglycerol (DAG) [2, 3].

1. Cyclic nucleotides (cNs)

A cyclic nucleotide (cN) or a cyclic nucleoside monophosphate (cNMP) is a single phosphate nucleotide with a cyclic bond arrangement between the sugar and the phosphate group. Cyclic nucleotides are composed of three functional groups: a sugar, a nitrogenous base, and a single phosphate group (figure 1). cAMP and cGMP are currently the most well documented cyclic nucleotides. They are ubiquitous second messengers responsible for transducing effects of various extracellular mediators including hormones, light and neurotransmitters [2, 3]. cAMP is formed from adenosine triphosphate (ATP) by the catalytic action of adenylyl cyclases (ACs). There are two types of AC: (a) transmembrane AC (tmAC) which is activated/regulated by heterotrimeric G proteins, which transduce extracellular signals via G protein-coupled receptors and can also be activated by forskolin and (b) soluble AC (sAC) which is regulated by the intracellular signaling molecules bicarbonate and calcium. The effector proteins of cAMP include protein kinase A (PKA), exchange proteins activated by cAMP (Epac), cyclic nucleotide gated ion channels and potentially phosphodiesterase type 10 (PDE10). cAMP modulates physiological responses such as learning and memory, cardiac myocyte function, olfaction, sperm activation, pH regulation in epididymis, and tumor necrosis factor (TNF) activation of granulocytes [4].

cGMP is formed from guanosine triphosphate (GTP) by the catalytic action of guanylyl cyclases (GCs). There are two subtypes of guanylyl cyclases: particulate GC (pGC), a

membrane bound protein which is activated by natriuretic peptides and soluble GC (sGC), a cytosolic protein which is activated by nitric oxide (NO) [5].

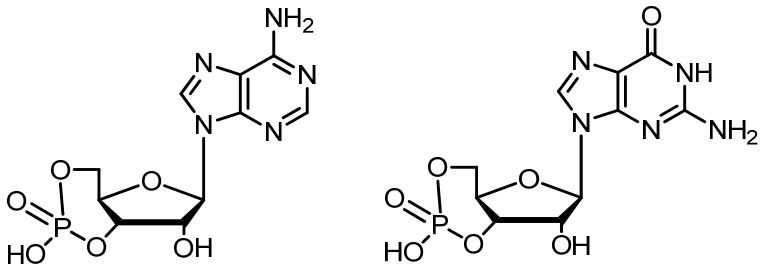

***Figure 1**. Structures of cAMP (left) and cGMP (right).*

1.1. Natriuretic peptide-mediated biosynthesis of cGMP

Natriuretic peptides are a family of three structurally related hormone/paracrine factors. Atrial natriuretic peptide (ANP) and B-type natriuretic peptide (BNP) are secreted from the cardiac atria and ventricles, respectively. ANP signals in an endocrine and paracrine manner to decrease blood pressure and cardiac hypertrophy. BNP acts locally to reduce ventricular fibrosis. C-type natriuretic peptide (CNP, secreted by the vascular endothelium) primarily stimulates long bone growth. ANP and BNP activate the transmembrane guanylyl cyclase, natriuretic peptide receptor-A (NPR-A). CNP activates a related cyclase, natriuretic peptide receptor-B (NPR-B). Both receptors catalyze the synthesis of cGMP, which mediates most known effects of natriuretic peptides. A third natriuretic peptide receptor, natriuretic peptide receptor-C (NPR-C), clears natriuretic peptides from the circulation through receptor-mediated internalization and degradation [6].

1.2. Nitric oxide-mediated biosynthesis of cGMP

Nitric oxide, also known as endothelium-derived relaxing factor (EDRF) and proclaimed "Molecule of the Year" in 1992 (also an area of research for the Nobel prize award in 1998) is a simple but the only known gaseous neuromessenger molecule that readily crosses cell membranes [7]. It is synthesized by the catalytic action of nitric oxide synthases (NOS) from L-arginine, oxygen, and NADPH (figure 2) [8, 9]. There are three isoforms of NOS: neuronal NOS (nNOS or Type I, NOS-I) being the isoform first found in the neuronal tissue; inducible NOS (iNOS, Type II, NOS-II) being the isoform which is inducible in a wide range of cells and tissues; and endothelial NOS (eNOS, Type III, NOS-III) being the isoform first found in vascular endothelial cells. eNOS and nNOS are calcium dependent for their activation whereas iNOS is calcium independent [9]. The NOS isoforms were named by order of their

discovery and initially reported expression pattern. However, all three isoforms have been detected in vascular smooth muscle cells (VSMCs) and vascular endothelial cells [10].

The biosensor of NO is soluble guanylyl cyclase (sGC) which is a heterodimer with an α and β subunit. The amino-terminal of the cyclase contains a heme domain to which nitric oxide binds with distinct specificity [11].

1.3. Physiological role of cAMP and cGMP

The second messengers cAMP and cGMP are important regulators of various physiological processes. The main effectors of cAMP are cAMP dependent protein kinase A (PKA) and cyclic nucleotide-gated ion channels [5]. cAMP and its associated kinases play a role in several biochemical processes, including the regulation of glycogen, sugar and lipid metabolism. Other functions of cAMP and PKA include activation of calcium channels, providing a minor pathway by which growth hormone-releasing hormone causes a release of growth hormone. However, the view that the majority of the effects of cAMP are controlled by PKA is outdated. In 1998 a family of cAMP-sensitive proteins with guanine nucleotide exchange factor (GEF) activity was discovered. These are termed 'exchange proteins directly activated by cAMP (Epac)' and the family comprises Epac1 and Epac2. Upon binding of cAMP, the GEF domain becomes active allowing Epac to activate small Ras-like GTPase proteins, such as Ras-related protein 1(Rap1) [4].

The main effectors of cGMP are cGMP dependent protein kinase G (PKG), cyclic nucleotide-gated ion channels and phosphodiesterases (PDEs, figure 2). Three isotypes of PKGs have been identified, two of which are splice variants of a single gene. PKG type I (PKG-I), which consists of an α and a β isoform (76 kDa), is the prominent isotype in the cardiovascular system. It is expressed at very high levels (> 0.1μM) in vascular smooth muscle cells (both PKG-Iα and PKG-Iβ) and endothelial cells (PKG-Iβ) and at lower levels in cardiac myocytes (PKG-Iα). PKG type II (PKG-II, 86 kDa) is mainly expressed in the kidney, brain, and intestines. Both PKG-I and PKG-II exist as homodimers with identical structures. Each subunit consists of three functional domains, i.e. an N-terminal domain, a regulatory domain, and a kinase domain. The N-terminal domain mediates PKG homodimerization, suppresses kinase domain activity in the absence of cGMP, and interacts with target substrate proteins [10]. Upon cGMP binding to specific sites in the regulatory domain, PKG undergoes a conformational change, resulting in the release of the N-terminus inhibition of the kinase domain. The kinase domain then catalyzes the phosphorylation of a serine/threonine side

chain of the target substrate protein [10]. The other main effector proteins of cGMP are the phosphodiesterases which are a superfamily of intracellular enzymes involved in the degradation of cNs. This will be discussed in the next section.

2. Phosphodiesterases

Early studies by Sutherland and colleagues demonstrated that tissue extracts contained a PDE-activity that could ablate the biological actions of cAMP. This was subsequently identified as PDE catalytic activity, which was increased in the presence of divalent cations and inhibited by methylxanthines such as caffeine and theophylline [12, 13].

Based on differences in primary structure of known PDEs, they have been subdivided into three classes (Class I, II, and III). Class I contains the largest number of PDEs and includes all known mammalian PDEs. Each class I PDE contains a conserved segment of ~250 - 300 amino acids in the C-terminal portion of the proteins (which show high affinity for cAMP and/or cGMP), and this segment has been demonstrated to include the catalytic site of these enzymes. All known class I PDEs are contained within cells and vary in subcellular distribution, with some being primarily associated with the particulate fraction or the cytoplasmic fraction of the cell, others being more evenly distributed in both compartments [13].

Twenty-one classes of genes and diverse spliced transcriptional variants for the PDE class I of humans, rats and mice have been identified. They have been classified into 11 families based on particular subcellular distributions, structural similarities, mechanisms of regulation, amino acid sequences, proteic domains and enzymatic properties among which are specificity for the substrate, kinetic properties, and sensitivity to endogenous regulators and inhibitors [3]. According to the nomenclature used for each PDE isozyme (e.g., HsPDE5A1), the first two letters indicate the animal species (Humans) and the first Arabic number after PDE designates the PDE gene family. This number is followed by a single capital letter indicating a distinct subfamily gene. The last Arabic number indicates a specific splice variant or a specific transcript generated from a unique transcription initiation site [13].

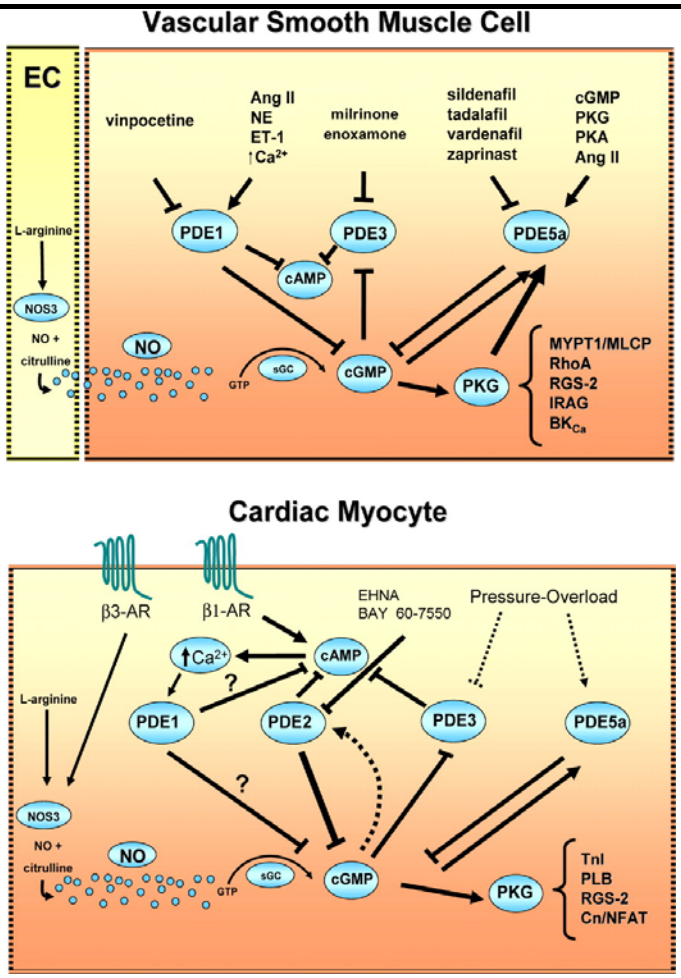

***Figure 2**. Schematics of PDE regulation of NOS–NO generated cGMP in a vascular smooth muscle cell and cardiac myocyte. Small molecule inhibitors and signal-activators for each PDE are shown at the top. **Smooth muscle cell**: NOS3-derived NO diffuses from neighboring endothelial cells (EC) interacting with soluble guanylate cyclase (sGC) to convert GTP to cGMP. cGMP can be hydrolyzed by PDE1 in the presence of Ca^{2+}/calmodulin (Ca/CM) stimulation, and PDE1 may also hydrolyze cAMP. PDE3 hydrolyzes primarily cAMP, but this can be inhibited competitively by cGMP. PDE5 selectively hydrolyzes cGMP, and cGMP and its distal effector kinase-protein kinase G (PKG) also activate the enzyme. Activation of PKG results in phosphorylation of myosin light chain phosphatases (MLCP), RhoA, regulator of g-protein signaling (RGS-2), inositol 1,4,5-trisphosphate receptor-associated PKG substrate; IRAG, and calcium-sensitive potassium channels (BKc_a) that serve to reduce smooth muscle tone. **Cardiac myocyte**: NO possibly derived from several intracellular NOS isoforms (eNOS being coupled to β3 adrenergic receptors) stimulates cGMP synthesis. PDE regulation is similar to that in vascular smooth muscle, with the addition of PDE2, which increases cAMP hydrolysis when stimulated by cGMP, but may also hydrolyze cGMP. Agonists and small molecule inhibitors would be similar for those shown in the upper panel. Chronic stimulation by pressure over-load lowers PDE3 but increases PDE5 activity to alter the balance of cAMP/cGMP regulation. Adapted from reference [11].*

2.1 Structure of phosphodiesterases

All PDEs are chimeric proteins comprising a catalytic domain (C domain) and a regulatory domain (R domain) (figure 3). R domains of mammalian PDEs (PDE 2, 5, 6, 10, and 11) contain either one or two predicted homologous GAF domains (cGMP binding PDEs, *Anabaena adenylyl cyclases*, and *Escherichia coli* (Fh1A) modules) of ~ 120 amino acids (aa) [13, 14]. The PDE superfamily is the only group of mammalian proteins known to have an abundance of GAFs; all isoforms of five PDE families (2, 5, 6, 10, and 11) contain two GAFs (*a* and *b*) arranged in tandem, and in PDEs 2, 5, and 6, at least one GAF forms an allosteric site for cGMP binding (figure 3). The GAF domain thus provides an allosteric binding site for cGMP which results in increased catalytic activity of the enzyme [14, 15].

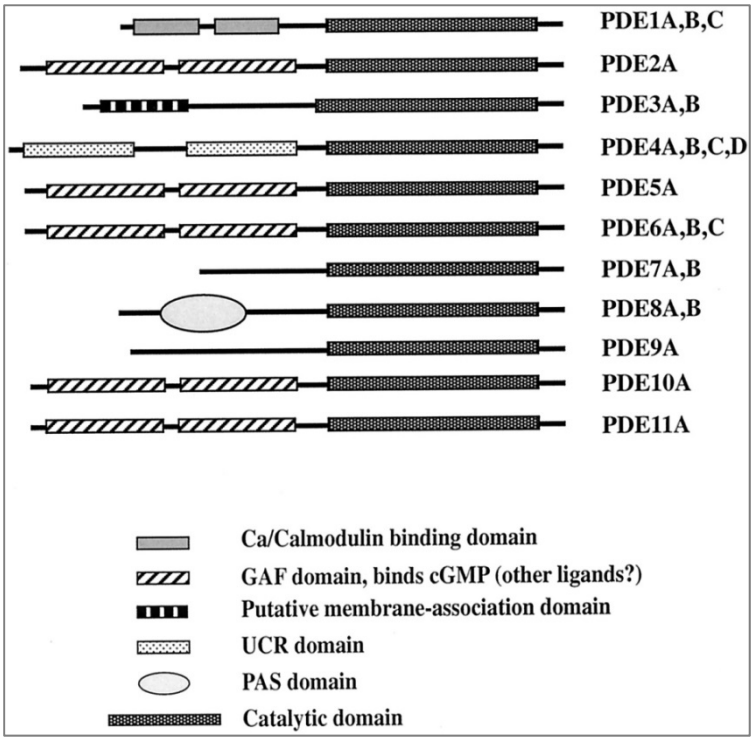

***Figure 3**. Domain organization of 11 PDE gene families. All PDEs share significant homology in their catalytic domain but differ greatly in their N-terminal parts, which contain different types of regulatory domains. UCR domain is an upstream conserved region found only in PDE4. GAF domains were originally defined in PDE2, PDE5, and PDE6 and later shown in PDE10 and PDE11. PAS domain (Per, ARNT, and Sim proteins) was found only in PDE8. Adapted from reference [16].*

Two structural components of cAMP and cGMP, i.e., the cyclic phosphodiester ring and the purine moiety, provide for the specificity with which these compounds interact with PDEs. Some PDEs are highly specific for cAMP (PDE4, PDE7, PDE8), others are highly specific for

cGMP (PDE5, PDE6, PDE9), and some have mixed specificity (PDE1, PDE2, PDE3, PDE10) [3, 13].

PDEs contain three functional domains, including a conserved catalytic core, a regulatory N-terminus and a C-terminus. Regulatory N-terminal domains of these enzymes that vary widely among the PDE classes contain a calmodulin binding domain in PDE1, cyclic GMP binding sites in PDE2, 5, 6, 10 and 11, phosphorylation sites for various protein kinases in PDE1 - 5, and a transducin binding domain in PDE6 [3]. Due to the need to develop selective PDE inhibitors as therapeutic drugs, the structures of the catalytic domains of PDEs, which contain the active pocket that accommodates inhibitors, have been elucidated. The crystal structure of the catalytic domain of PDE5A has shown that catalytic domains of PDEs have three helical subdomains (figure 4, left): an N-terminal cyclin-fold region (which adopts the cyclin-fold topology), a linker region (10 aa residues) and a C-terminal helical bundle. The active site of PDE5 is located at the centre of the C-terminal helical bundle domain. The substrate pocket is approximately 10 Å deep, with a narrow opening and a wide inner space, giving a total volume of about 330 $Å^3$ (figure 4, right). It is composed of four subsites: a metal-binding site (M site), core pocket (Q pocket), hydrophobic pocket (H pocket) and lid region (L region). The M site contains both a zinc ion and a second metal (presumably magnesium) ion which are assumed to play a role in stabilization of the structure and activation of hydroxide to mediate catalysis (figure 4, right) [3, 17].

In the crystal structure of PDE5A in complex with sildenafil (a known PDE5 specific inhibitor), the Q pocket accommodates the pyrazolopyrimidinone group of sildenafil. This Q pocket provides the key hydrogen bonding of the conserved glutamine residue with substrates or inhibitors of PDEs, and the hydrophobic interactions, which come from the residues on both sides of the pyrazolopyrimidinone group, forming a ‘clamp’ like structure. The ethoxyphenyl group of sildenafil fits into the hydrophobic H pocket. The variation of hydrophobic residues in the H pocket among PDEs can give PDE inhibitors the selectivity to corresponding PDEs. The L region of PDE5A, composed of residues Tyr 664, Met 816, Ala 823 and Gly 819, surrounds the methylpiperazine group of sildenafil. The conformational change between closed and open forms of this region seems to be involved in inhibitor binding [3, 17].

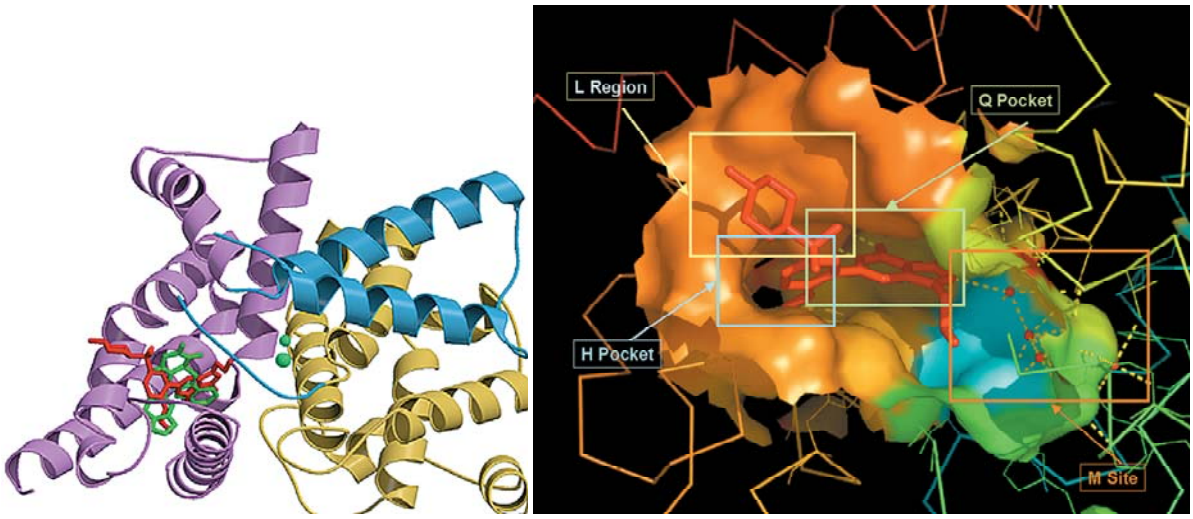

***Figure 4. Left**: Overview of the PDE5 complex structures. Stereo ribbon diagram of the human PDE5 structure. The catalytic domain of the PDE5 molecule can be divided into three subdomains: an N-terminal cyclin-fold domain (residues 537–678, yellow), a linker helical domain (residues 679–725, blue) and a C-terminal helical bundle domain (residues 726–860, violet). The bound sildenafil and tadalafil molecules are overlapped and shown as stick models (red and green, respectively). Two metal ions are represented as green spheres. **Right**: Surface representation of the active site of PDE5A occupied by sildenafil. The active site can be divided into four subsites: a metal-binding site (M site), core pocket (Q pocket), hydrophobic pocket (H pocket) and lid region (L region). Adapted from reference [3].*

2.2. Tissue expression and distribution of PDE5

First purified from rat lung, phosphodiesterase 5 (PDE5) has now been identified in many species and in a wide variety of tissues. So far, three PDE5 isoforms, PDE5A1, PDE5A2 and PDE5A3 have been identified in humans and dogs [18]. While PDE5A1 and PDE5A2 are found in nearly all tissues, with PDE5A2 being more widespread, the distribution of PDE5A3 is limited to smooth muscle (tables 1 and 2). There are no known differences in cGMP catalytic activity among these isoforms [19].

Tissue and cellular expression of PDE5 has been examined by Northern blot analysis, in situ hybridization (ISH), and real time-polymerase chain reaction (RT-PCR) for mRNA expression and by Western blot analysis, immunohistochemistry (IHC), enzymatic assay, and inhibitor binding for protein expression [19-21]. Lakics et al reported that PDE5 mRNA is most abundantly expressed in the lung, bladder, stomach, pancreas and intestine [21]. However, the expression of PDE5 in the lungs was the highest both relative to other PDEs present in the lungs and to PDE5 expression in other tissues.

Table 1. *Distribution of PDE5 in selected tissues. Adapted from references [19, 20].*

	Detection method								
	mRNA			Proteins			PDE5 isoforms		
Tissue	PCR	Northern	ISH	IHC	Western	Activity	A1	A2	A3
Brain	+	+			+		+	+	-
Cerebellum	+	+	+	+	+	+			
Retina	+								
Lung	+	+/-	+		+	+	+	+	-
Heart	+	+/-		+	+/-	+/-	+	+	+
Liver	+	-			-		+	+	-
Stomach	+	+			+	+			
Pancreas	+	+		+					
Spleen	+								
SI	+	+			+	+			
Colon	+	+			+	+			
Kidney	+	+		+			+	+	-
Bladder	+	+			+	+	+	+	+
Prostate	+	+			+		+	+	+
Urethra	+			+	+		+	+	+
Penis	+	+	+	+	+	+	+	+	+
Ovary	+				+				
Uterus	+	+			+		+	+	+
SkM	+	+			-		+	+	-
Platelet					+	+			

+: detected; -: negative; PCR: Polymerase chain reaction; ISH: in situ hybridization; IHC: immunonhistochemistry; Activity: cGMP catalysis; SI: small intestine; SkM: Skeletal muscle immunonhistochemistry; Activity: cGMP catalysis; SI: small intestine; SkM: Skeletal muscle

Most authors agree on the abundant expression of the enzyme in the lungs with two notable exceptions by Loughney et al [22] and by Yanaka et al [23] who reported the absence of lung PDE5 activity. This of course contradicts with the fact that PDE5 was first identified and purified from lung and was first cloned from lung as well [24, 25].

***Table 2**. Cellular distribution of PDE5 isoforms. Adapted from reference [19].*

Cell lines/strains	**PDE5 isoforms**		
	A1	*A2*	*A3*
T47-D (breast cancer)	-	+	-
Ishikawa (uterine cancer)	-	+	-
			-
HT1080 (fibrosarcoma)	-	+	
COS-7 (fibroblasts)	-	+	-
Aorta SM	-	+	+
Bladder SM	-	+	+
Urethra SM	-	+	+
Penis SM	-	+	+
Penis endothelia	-	+	-
Aorta endothelia	-	+	-
CEM (leukemia)	-	+	-
Jurkat (leukemia)	-	+	-
K562 (leukemia)	-	+	-
Molt-4 (leukemia)	-	+	-

SM: smooth muscle

Most authors agree that PDE5 is expressed in vascular smooth muscle cells, platelets, lungs, penis and Purkinje fibers of the cerebellum [19, 21, 25]. However, each of the detection techniques used for identification of PDE5 or its mRNA has its advantages and disadvantages and because certain experimental variables (e.g., animal species, cultured cells *vs* tissues, with or without detergents, etc.) do exist, it is inevitable that disagreements between studies do occur. In particular, since vascular smooth muscle contains an abundance of PDE5, its possible inclusion in tissue preparations should always be considered for having a positive

result that is generated by RT-PCR, Northern blot, or Western blot analyses. On the other hand, while contamination of the tissue of interest by smooth muscles is not an issue with immunohistochemical detection of PDE5, the presence of nonspecific immunological activities in most anti-PDE5 antibodies can be problematic [19, 21]. Selected cellular and tissue distribution of PDE5 with the assay method used for detection is given in tables 1 and 2.

2.3. Physiological role of PDE5

The physiological role of PDE5 ranges from its classic player as a regulator of smooth muscle cells (SMCs) to a new emerging role as a regulator of apoptosis. Much of the information available on the role of cGMP comes from studies on smooth muscle, in which one of the earliest clearly defined effects of cGMP on cell function was described [10, 16, 20]. PDE5 has been shown to participate in many physiological and pathological processes. Particularly, with the convenience of using PDE5-selective inhibitors to discriminate PDE5 from other cGMP-hydrolyzing enzymes, many new possible regulatory roles have been uncovered in recent years. In addition to the classic role of regulation of smooth muscle tone and the emerging role of regulation of apoptosis that will be discussed in more detail below, some of the interesting roles are (1) regulation of neuronal excitability and synaptic plasticity in Purkinje cells [26], (2) activation and inhibition of platelet aggregation [27], (3) regulation of antidepressant-sensitive serotonin transporter [28], (4) control of ion and fluid secretion in intestinal cells [29], (5) regulation of memory formation [30], and (7) handling of sodium secretion in renal cells [31].

The best characterized physiological role of PDE5 is the termination of the cGMP-signaling pathway in smooth muscle, be it vascular, cavernous, or intestinal [10, 16, 20]. The cGMP signaling pathway in corpus cavernous smooth muscle is briefly discussed below (figure 2). Sexual stimulation triggers the release of nitric oxide (NO) from nerve endings. NO diffuses into cavernous smooth muscle cells and activates guanylyl cyclase, which then catalyzes the conversion of GTP to cGMP. Elevated levels of cGMP activate protein kinase G (PKG), which then phosphorylates gap junctions, potassium (K) channels, and calcium (Ca) channels. Phosphorylation of the K and Ca channels leads to increase of potassium efflux and reduction of calcium influx, respectively. When the cytoplasmic calcium concentration falls below a certain level (~500 nM), calcium dissociates from calmodulin, which in turn dissociates from the myosin light-chain kinase, thus inactivating it. With its kinase being inactivated and its

phosphates being removed by phosphatase, the myosin light chain thus becomes dephosphorylated. Dephosphorylated myosin light chain inhibits the binding of the myosin head to actin, resulting in smooth muscle relaxation. Relaxed cavernous smooth muscle allows the entry of blood into the cavernous spaces, thus expanding the penis. To return the penis to the flaccid state, cGMP is principally degraded by PDE5 – despite of the co-presence of several other cGMP-hydrolyzing PDEs [16, 20].

It is currently accepted that cGMP inhibits platelet activation via reduction in intracellular Ca^{2+} [27]. This concept is supported by the finding that pre-incubation of cGMP analogs with platelets inhibits platelet activation. Consistent with this concept, NO donors that inhibit platelet activation enhance intracellular cGMP. However, Li et al [27] showed that the cGMP-stimulated platelet responses are biphasic, consisting of an initial transient stimulatory response that promotes platelet aggregation and a subsequent inhibitory response that limits the size of thrombi. This might be a reason for experimental use of PDE5 inhibitors in stroke rat model as increased cGMP concentrations shorten the time for initiation of the inhibitory phase and consequently resulting in smaller thrombi [33]. Thus, cGMP exerts a time and concentration dependent biphasic effect on platelet activation. Besides, other PDEs (such as PDE2 and PDE3) may come into interplay [27, 33].

PDE5 expression in the brain is limited; however, expression of PDE5 mRNA and protein has been reported for cerebellar Purkinje cells and there is a considerable literature indicating that the cerebellum has a significant role in cognitive processing [30, 34, 35]. In addition, there is a small body of preclinical literature that suggests that PDE5 inhibitors could affect cognitive function [30, 35, 36]. Prickaerts et al [36] reported that several PDE5 inhibitors facilitate memory consolidation in rodent novel object recognition tasks. The mechanism for these precognitive effects remains to be determined. An increase in cGMP concentrations in Purkinje cells, which are the principal output neurons of the cerebellum, could therefore conceivably account for the effects of PDE5 inhibitors in the rodent cognition assays. There are also scattered cells in hippocampus and cortex that express PDE5 mRNA as visualized by in situ hybridization [37]. In humans, a PDE5 inhibitor enhanced auditory evoked potentials during a selective attention and verbal recognition memory task [38]. This could be indicative of the capacity of PDE5 inhibitors to focus attention. Zhu et al in another manuscript reported the role of cGMP-targeted PDE5 in limiting the regulation of antidepressant-sensitive 5-HT transport in RBL-2H3 cells (cell line that supports G-protein coupled receptor stimulation of

the serotonin transporter through a PKG linked pathway) [39]. Therefore, it is probable that the cGMP-PDE5 pathway is involved in early memory consolidation in at least rodents and inhibition of PDE5 improves brain function such as memory consolidation and plasticity [30, 34-37]. Nonetheless, it remains to be determined whether the distribution of PDE5 in human brain is similar to that in rodents.

An emerging and intriguing role for PDE5 is the regulation of apoptosis in both cancer and normal cells. It appears that PDE5 plays both a pro-apoptotic and anti-apoptotic role in different tissues. Fukuo et al reported that NO released from vascular smooth muscle cells (VSMCs) of rats may induce apoptosis in VSMCs themselves. It also induces up-regulation of Fas receptor (apoptosis stimulating factor, an important cell surface receptor protein of the TNF receptor family known also as CD95, that induces apoptosis on binding Fas ligand) via a cGMP-independent mechanism [40]. Hence, in VSMCs PDE5 could play an anti-apoptotic role. Taimor et al also reported that NO induces apoptosis in a cGMP dependent manner in isolated adult cardiomyocytes of rats where PDE5 could play an anti-apoptotic role [41]. However, De Meester et al reported that NO played an anti-apoptotic role in porcine aortic endothelial cells [42].

When breast cancer cells were treated with exisulind (an oxidative metabolite of sulindac that will be discussed under section 3, the PDE5 inhibitors), growth inhibition and apoptotic death were observed [43]. Similar observations have now been made in cancer cells of the prostate [44], bladder [45], colon [46-48], and lung [49]. In colon cancer cells, exisulind induced apoptosis was found to involve the inhibition of PDE2 and PDE5 and activation of PKG [47].

Induction of apoptosis through PDE5 inhibition has also been observed in normal cells, albeit requiring concomitant activation of the cGMP-signaling pathway. First, in human pulmonary artery smooth muscle cells, stimulation of soluble guanylyl cyclase (by BAY41-2272) and inhibition of PDE5 (by sildenafil) not only reduced DNA synthesis and cell proliferation but also increased apoptosis [50]. Second, in pulmonary arterial endothelial cells, stimulation of particulate guanylyl cyclase (by atrial natriuretic peptide, ANP) and inhibition of PDE5 (by zaprinast) also reduced cell growth and induced apoptosis. In pulmonary microvascular endothelial cells, which do not express PDE5, ANP alone was able to induce apoptosis, thus further illustrating the importance of the suppressive role of PDE5 on apoptosis [51].

2.4. Pathophysiological role of PDE5

Phosphodiesterase 5 has been implicated in a number of diseases including pulmonary arterial hypertension, cardiac hypertrophy and ventricular remodeling, myocardial ischemia, atherosclerosis, and others [10, 52]. The main focus of this dissertation is on the pathophysiological role of PDE5 in the pulmonary vasculature and heart. Hence, the role of PDE5 in these organs will be discussed in some detail while its role in other diseases will be mentioned as a passing remark.

The billion dollar income generating drug Viagra® (sildenafil) is used in the treatment of sexual dysfunction where it inhibits PDE5 in corpus cavernosum [19, 34, 53]. To date, we have not come across any publication that claims up-regulation of PDE5 in erectile dysfunction (ED). The use of PDE5 inhibition in ED is to retard enzymatic hydrolysis of cGMP in the corpus cavernosum as the enzyme is relatively abundantly expressed in the penis. To a certain extent the use of PDE5 inhibition to treat pulmonary arterial hypertension is also based on abundant expression of the enzyme in the lungs [25] though a recent publication reported that PDE5 was up-regulated in lambs with pulmonary hypertension, induced by an aortopulmonary vascular graft (shunt) [54]. Pulmonary arterial hypertension (PAH) is a debilitating chronic disease of the small pulmonary arteries characterized by vascular narrowing leading to a progressive increase in pulmonary vascular resistance [55]. The consequence of this increased right ventricle afterload is a failure of the afterload-intolerant right ventricle. Vasoconstriction, remodeling of the pulmonary vessel wall and thrombosis contribute to the increased pulmonary vascular resistance in PAH. There are a number of factors involved at both the molecular and cellular level [56].

At the cellular level, smooth muscle cells, fibroblasts, inflammatory cells and platelets play an important role in disease progression of PAH. Stimuli such as hypoxia, shear stress, inflammation, or response to drugs or toxins may lead to disorganized endothelial cell proliferation which ultimately leads to narrowing of the arteries [57]. On the other hand inflammatory mechanisms appear to play a significant role in some types of pulmonary hypertension including monocrotaline induced PAH in rats and PAH of various origins in humans [57, 58].

At the molecular level, prostacyclin (prostaglandin I2, an important endogenous pulmonary vasodilator), vasoactive intestinal peptide (VIP, a neuropeptide primarily functioning as a neurotransmitter with potent systemic and pulmonary vasodilator effects), endothelin (ET-1, a

potent pulmonary vasoconstrictor) and NO appear to play an important role in PAH. Pulmonary vasoconstriction is believed to be an early component of the pulmonary hypertensive process. Excessive vasoconstriction has been related to abnormal function of endothelial dysfunction. Endothelial dysfunction leads to chronically impaired production of vasodilators such as NO and prostacyclin along with prolonged over-expression of vasoconstrictors such as endothelin (ET-1). Besides, the abundant expression of PDE5 in the pulmonary vasculature further aggravates the vasoconstriction by degrading the already impaired production of cGMP (figure 5) [56].

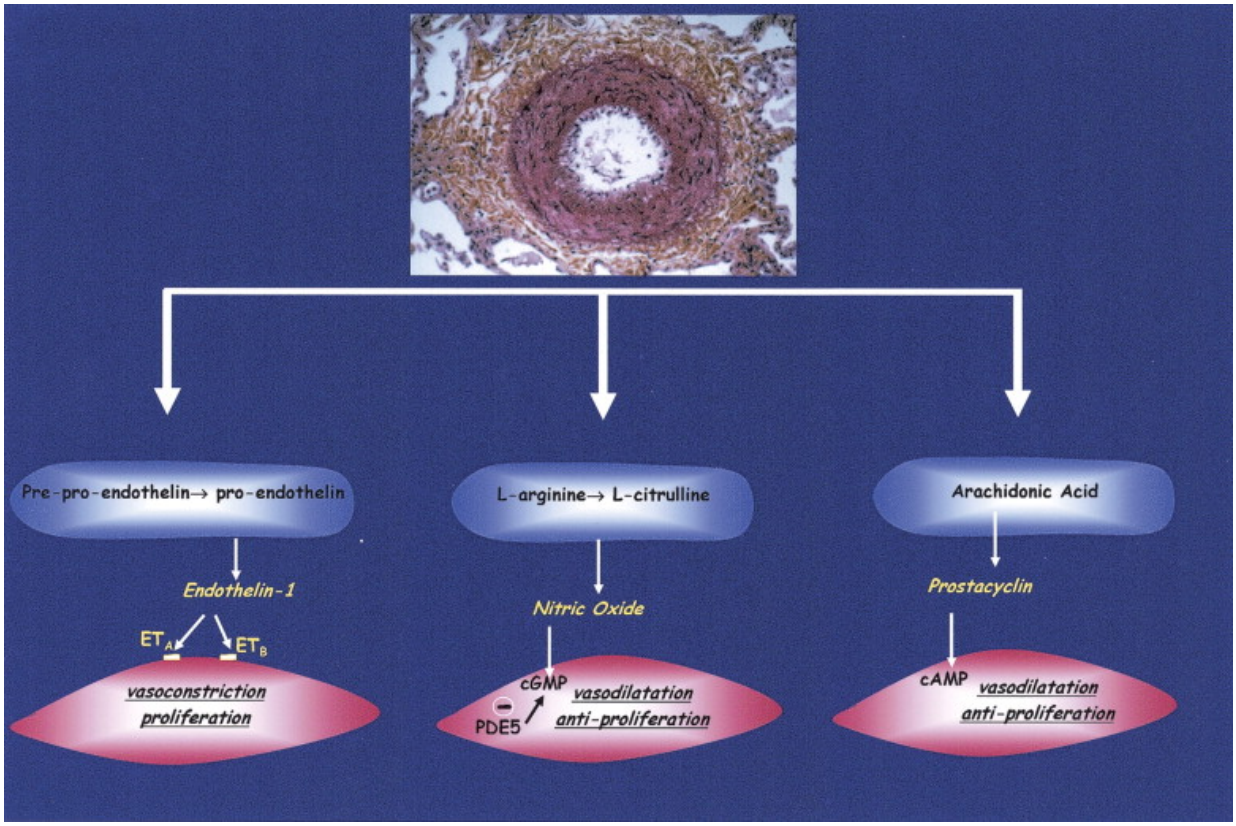

Figure 5. *Consequences of pulmonary artery endothelial cell dysfunction on pulmonary artery smooth muscle cell tone and proliferation. Dysfunctional pulmonary artery endothelial cells* ***(blue)*** *have a decreased production of prostacyclin and nitric oxide, with an increased production of endothelin-1- promoting vasoconstriction and proliferation of pulmonary artery smooth muscle cells* ***(red).*** *ET = endothelin; ET_A = endothelin receptor A; ET_B = endothelin receptor B. (Adapted from reference [56].*

Physiological hypertrophy is a normal part of the growth response of cells, including cardiomyocytes, which are terminally differentiated and cannot undergo hyperplastic growth. This form of hypertrophy is described as both concentric (characterized by addition of sarcomeres in parallel, leading to increased width of the myocyte) and eccentric

(characterized by the addition of sarcomeres in series, leading to increased length). Concentric cardiac hypertrophy can also develop as a response to stressors, in most cases an excess load placed on the heart, for example, with uncorrected hypertension or valvular disease, or post-myocardial infarction (MI) when the remote non-infarcted myocardium hypertrophies. Hypertrophy is initially believed to be adaptive, normalizing systolic wall stress, though this concept has been challenged recently and it is not clear that hypertrophy is really necessary to maintain systolic function in the face of moderately elevated afterloads. Eccentric hypertrophy most often results from volume overloads such as those seen with valvular insufficiency [59, 60]. Though there are a number of factors that cause cardiac hypertrophy, here the discussion is limited to the role of PDE5 in cardiac hypertrophy.

Despite early evidence of myocardial PDE5 gene expression, protein synthesis and enzyme activity in cardiomyocytes are rather low compared with lung tissue, and have been traditionally thought to be physiologically insignificant [52]. The action of NO in the vascular smooth muscle cells is via cGMP mediation which is mainly terminated by PDE5; however, NO regulation of the cardiovascular system involves both cGMP-dependent and independent mechanisms (figure 2). The former directly interacts with the family of catabolic PDEs that control cGMP levels and thus distal effects such as protein kinase G stimulation where the latter involves the cross-talk between cAMP and cGMP downstream. Growing evidence supports an important role of several PDEs, including PDE1, PDE2, PDE3 and PDE5, in the regulation of cGMP in cardiac myocytes (figure 2) [5, 11].

Although the role of PDE5 in the myocardiocytes in healthy condition is considered minimal or negligible, several authors have reported its deleterious effect in different cases of cardiac hypertrophy. Nagendran et al reported a marked up-regulation of PDE5 in hypertrophied right ventricles sampled from nine patients with right ventricle hypertrophy [61]. In addition, Pokreisz et al reported a 5-fold up-regulation of PDE5 in the left ventricles of patients with dilated and ischemic cardiomyopathy [62]. This group also showed that transgenic mice with cardiomyocyte specific PDE5 over-expression (PDE5 TG) responded poorly after myocardial infarction induced by coronary artery ligation. Vandenwijngaert et al from the same laboratory reported up-regulation of PDE5 in patients with severe aortic stenosis and in mice subjected to high pressure overload by transverse aortic constriction (TAC) [63]. The findings of Pokreisz were further strengthened by the report from Shan et al who reported a 4-fold up-regulation of PDE5 in 20 patients with ischemic cardiomyopathy or idiopathic dilated

cardiomyopathy [64]. Lu et al also reported a 4.5-fold increase in expression of PDE5 in patients with end stage congestive heart failure (CHF) [65]. Despite the low expression of PDE5 in the myocardium during healthy condition, many experts in the field showed its important but deleterious effect in cardiac remodelling.

Inconsistent changes in the expression of sGC have been reported in different animal models of hypercholesterolemia and atherosclerosis [66]. However, sGC activity appears dysfunctional as endothelium-dependent and independent vasodilations are markedly inhibited [66]. While PKG expression remains unchanged, its activity as assessed by phosphorylated- Vasodilator-Stimulated Phosphoprotein (VASP) is strongly reduced [67].

3. Phosphodiesterase 5 inhibitors

For many years, nonselective PDE5 inhibitors such as caffeine (1,3,7-trimethylxanthine), theophylline (1,3-dimethylxanthine) and 3-isobutyl-1-methylxanthine (IBMX) have been used to investigate the physiological effects of cyclic nucleotides [1, 34]. But in the early 1990s a drug which was being investigated by Pfizer for its role as an anti-hypertensive and anti-angina medication was serendipitously found to have an erectile side effect in a Phase I angina trial. This compound, sildenafil, was the first PDE5-selective competitive inhibitor approved by FDA for treatment of male erectile dysfunction (MED). Later in 2005, sildenafil was approved for treatment of PAH [34].

Thanks to this discovery, thousands of compounds have been synthesized and screened against PDE5. Due to the wide variety of structures reported for PDE5 inhibitors, rigid classification of the currently available compounds becomes difficult. Here, a limited number of selected PDE5 inhibitors which are deemed to have some relevance with this dissertation are discussed based on a loose classification system.

Currently, there are a number of PDE5 inhibitors that are available on the market for treatment of erectile dysfunction: sildenafil, vardenafil, tadalafil, udenafil, avanafil and mirodenafil. Except for tadalafil and avanafil, all approved PDE5 inhibitors share a similar core structure (figure 6) [68]. Zaprinast was among the earliest reported PDE5 inhibitors that did not make it to the clinic but served as a precursor for many subsequent PDE5 inhibitor discoveries.

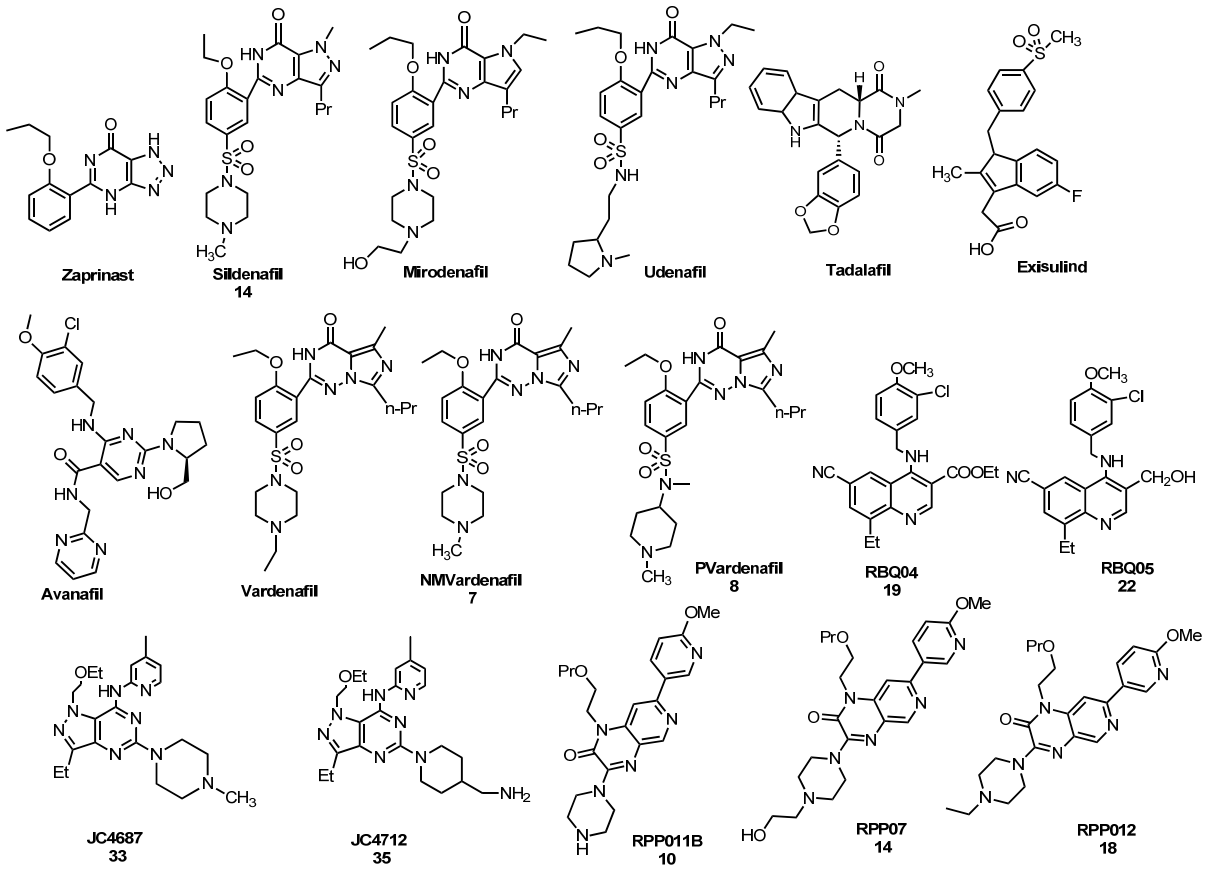

***Figure 6**. Structures of selected PDE5 inhibitors.*

The pyrazolopyrimidinone (**14**, **33**, **35**, udenafil) derivatives were among the first PDE5 specific inhibitors reported and approved. The representative molecule in this group is **14** which was the first approved PDE5 inhibitor for the treatment of MED [34, 53]. **33** and **35** were among the most potent compounds patented by Pfizer/Pharmacia & Upjohn based on IC_{50} values (table 3) [68-70]. Other PDE5 inhibitors patented by the same company belong to the pyridopyrazine derivatives (RPP07, RPP011B and RPP012) [71, 72]. These compounds attract special attention as, unlike other PDE5 inhibitors, they are claimed to readily cross the blood-brain barrier [32, 72, 73]. RPP07 (**PF-5**) was investigated by Mannit et al for its effect on improving functional recovery after stroke in a rat model and it was tested in healthy human volunteers and proved to be well tolerated with a mean apparent elimination half-life of 17 - 25 h after oral dosing [72-74,76]. No further development has been reported, however rat studies indicate significant CNS exposure. Hence RPP07 may have potential as a brain penetrant tool allowing clinical evaluation of the role of PDE5 in the CNS.

The imidazotriazine group, to which vardenafil, **7**, and **8** belong was the second class of PDE5 inhibitors to be approved for the treatment of ED [74-76]. The other group that contains an

approved PDE5 inhibitor is that of the β-carbolines to which tadalafil belongs [77]. The quinoline PDE5 inhibitors (e.g., **19** and **22**) are among a series of potent and selective inhibitors described in a patent filed by Bristol-Myers Squibb in 2001 [78, 79]. The IC_{50} value reported for **19** (50 pM) is among the highest PDE5 inhibitory activity reported so far and also in our in vitro PDE5 inhibitory assay it was found to have the highest inhibitory activity. There has not been any follow up report on this compound from the same group but a recent article reported the potential use of a close derivative of **19** for the treatment of Alzheimer's disease [80].

***Table** 3. In vitro PDE inhibitory activity (IC_{50}) for selected PDE5 inhibitors.*

Compounds	**Class**	**Reported PDE inhibitory activity**			**Ref.**
		PDE5[a]	PDE6-fold[b]	PDE11-fold[c]	
Sildenafil **(14)**	pyrazolopyrimidine	3.6	8	NA	74
Tadalafil	β-carboline	5	1000	NA	77
Vardenafil	imidazotriazine	0.7	11	NA	74
7	imidazotriazine	0.6	NA	NA	74
19	quinoline	0.6	110	NA	79
22	quinoline	0.05	7800	NA	79
33	pyrazolopyrimidine	0.89	91	99	70
35	pyrazolopyrimidine	0.007	170	47	70
10	pyridopyrazine	3.28	51	2460	72
14	pyridopyrazine	0.2	158	2460	72
18	pyridopyrazine	0.22	198	4920	72

[a]PDE5 IC_{50} (nM); [b]PDE6 selectivity defined as (PDE6 IC_{50})/(PDE5 IC_{50}); [c]PDE11 selectivity defined as (PDE11 IC_{50})/(PDE5 IC_{50}); Ref: References; NA: No data available.

Exisulind is a metabolite derived from the irreversible oxidation of the nonsteroidal anti-inflammatory drug (NSAID) sulindac to sulindac sulfone and, unlike its precursor which is an inhibitor of cyclooxygenase, it is able to inhibit the cGMP degrading enzymes PDE2 and PDE5 [43-47, 68, 81]. Exisulind as PDE5 inhibitor is being investigated for its apoptosis-

inducing property in the treatment of colon cancer, non small-cell lung cancer and prostate cancer [43-47, 81].

3.1. Potential application of PDE5 inhibitors

PDE5 inhibitors were originally investigated as drugs for the treatment of cardiovascular diseases, but their success is attributable to their potency in the treatment of erectile dysfunction. Sildenafil (Viagra®) was the first PDE5 inhibitor drug marketed and, at present, all the commercially available PDE5 inhibitors have been registered for erectile dysfunction and some are also approved for the treatment of pulmonary arterial hypertension (sildenafil and tadalafil). In Europe and North-America, sildenafil, vardenafil and tadalafil are approved for marketing whereas udenafil and mirodenafil are approved in South Korea for human use [68]. In the treatment of erectile dysfunction, PDE5 inhibitors work in synergy with endogenous NO and exert their effect by increasing the level of cGMP in corpus cavernosum smooth muscle. Without the concomitant production of NO in the penis PDE5 inhibitors are not effective [82]. cGMP functions and the potential therapeutic use of PDE5 inhibitors are outlined in figure 7.

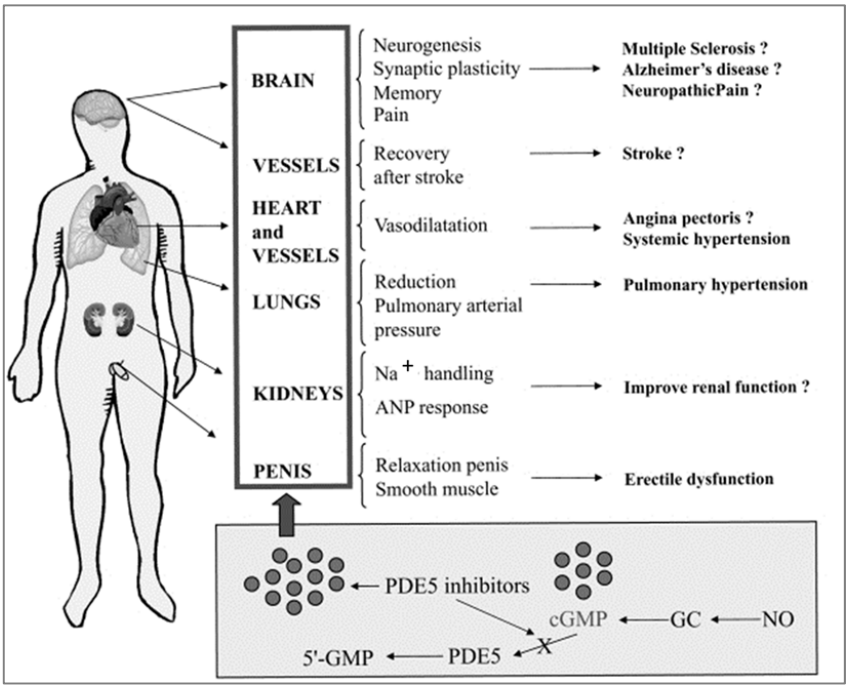

***Figure 7**. cGMP functions and possible therapeutic use of PDE5 inhibitors. PDE5 inhibitors block the degradation of cGMP (bottom panel) leading to an increase of the level of cGMP that can exert its action on several target organs. On the right side, both the approved and possible (question mark) therapeutic applications of PDE5 inhibitors in humans. Adapted from reference [34].*

Sildenafil was approved for the treatment of severe pulmonary hypertension in 2005 and tadalafil is the other PDE5 inhibitor approved for PAH. The principle for the use of PDE5 inhibitors in the treatment of PAH is the same vasodilatory effect in the pulmonary vasculature [83]. More recently, investigations in the paediatric population suggest that PDE5 inhibitors could also be useful for treatment of neonatal pulmonary hypertension [84].

PDE5 inhibitors were shown to be able to prevent the development of cardiac hypertrophy and, more important, they were able to reverse existing cardiac hypertrophy [85]. Sildenafil was reported to suppress myocyte hypertrophy and improve *in vivo* heart function in mice exposed to chronic pressure overload induced by transverse aortic constriction (TAC) [87]. The same study showed that sildenafil reversed pre-established hypertrophy induced by pressure load while restoring chamber function to normal. Another group also showed the effectiveness of sildenafil in decreasing cardiac hypertrophic response to isoproterenol in rats. Vardenafil was also shown to reduce myocardial infarct size following ischemia/reperfusion injury in rabbits [88]. Szabo et al described the protective nature of vardenafil against myocardial and endothelial injuries after cardiopulmonary bypass with hypothermic cardiac arrest [89]. In a 1-year prospective study in heart failure patients, sildenafil was shown to improve left ventricular diastolic function, cardiac geometry, and clinical status [90]. All these findings strongly suggest the potential role of PDE5 inhibitors for treatment of cardiac hypertrophy.

Raynaud's phenomenon is a vasospastic disorder in which there is a constriction of digital arteries and precapillary arterioles, and it can be a primary (where the cause is unknown) or a secondary phenomenon (the cause is secondary to another primary disease, most commonly connective tissue disorders such as systemic lupus erythematosus). Two studies reported the benefit of the use of PDE5 inhibitors in Raynaud's phenomenon [91, 92]. The use of PDE5 inhibitors with secondary Raynaud's phenomenon was associated with an improved microcirculation due to vascular dilation and with a symptomatic improvement; an improved blood flow was observed also in patients with primary Raynaud's phenomenon but few data are available till now [91].

McPherson and co-workers first described in 1999 the potential use of PDE5 inhibitors for treatment of cystic fibrosis, a severe autosomal pathology with dramatic consequences at pulmonary level due to the secretion of abnormally viscous mucus [93]. Preclinical studies

demonstrated that PDE5 inhibitors are able to correct the functional abnormalities resulting from mutation in the cystic fibrosis transmembrane regulator protein [94].

cGMP regulation plays a crucial role in a variety of processes and signal transduction in the CNS and, consequently, PDE5 inhibitors have been investigated for the treatment of central nervous system (CNS) disorders [35, 95]. In different experiments it has been demonstrated that PDE5 inhibitors produce an improvement of memory in different animal models such as object recognition and avoidance learning [30, 36, 96]. Some PDE5 inhibitors were shown to have an effect on functional improvement in rats after stroke [32, 73]. They were also shown as neurorestorative agent for the treatment of stroke, as demonstrated by studies in rat models of stroke by measuring neurogenesis, synaptogenesis and angiogenesis [31, 97].

Many other applications have also been proposed for PDE5 inhibitors such as treatment of idiopathic achalasia, a disease characterized by a reduced ability to move food down the oesophagus [98]; treatment of altitude-induced hypoxaemia [99]; the cure of lower urinary tract symptoms in men with benign prostatic hyperplasia [100]; to enhance the neurohypophysial excitability and the release of oxytocin [101].

Despite the apparent role of phosphodiesterases in a multitude of diseases, there has not been much interest from molecular imaging professionals to develop probes labeled with short lived radionuclides that could be employed in imaging of PDE related pathophysiological processes with positron emission tomography. However, in recent years there has been a revival in interest to develop such probes for *in vivo* imaging of PDEs [102]. In this regard a notable success is the development of a carbon-11 labeled rolipram ([^{11}C]rolipram) used for quantification of PDE4 in brain [103]. Another success was the development of fluorine-18 labeled tracer for *in vivo* visualization of PDE10 in the brain [104]. A potential PET radioligand to visualize PDE1 was reported in a patent application [105]. Despite the commercial availability of several PDE5 inhibitors and the successful application in various diseases, there has been only one report on a PET radioligand for *in vivo* visualization of PDE5 [106]. A compound named [^{11}C]RAL-01 (a close derivative of tadalafil, figure 8) was evaluated in pigs and showed a rapid uptake in liver and extensive elimination in bile. There was also considerable (self)-displaceable binding in the myocardium whereas retention in lungs was relatively low. The absence of retention in lungs was unexpected in view of the high levels of expression of PDE5 in lung tissue, and further it was not unequivocally demonstrated that the displaceable binding was PDE5 specific. The tracer readily entered the

brain and showed a relatively homogeneous distribution; however, its specificity for PDE5 in the brain is questionable as the enzyme is expressed in a restricted manner (the cerebellum).

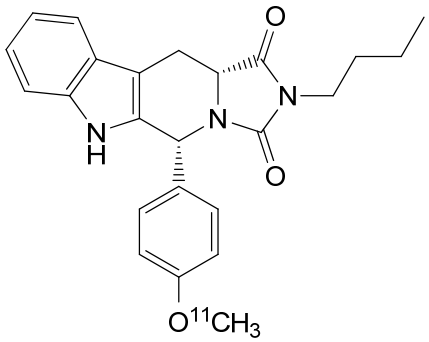

***Figure 8**. Structure of [^{11}C]RAL-01*

4. Molecular imaging

Molecular imaging is a rapidly emerging multidisciplinary field that studies the visual representation, localization and quantification of biological processes at the cellular and subcellular levels within intact living organisms. Imaging of molecular changes enables understanding of fundamental biochemical and physiological processes and, thereby, offers insights for disease characterization and detection. Furthermore, molecular imaging has an important relevance for patient care, as it allows early diagnosis of disease and a personalized approach for treatment follow-up. The field of molecular imaging covers imaging modalities such as positron emission tomography (PET), single photon emission computed tomography (SPECT), magnetic resonance imaging (MRI), computed tomography (CT), optical imaging, ultrasound imaging and photoacoustic tomography [102, 107]. Here, the discussion is limited to PET and PET related radiopharmaceutical because in this dissertation only radionuclides used in PET imaging are evaluated.

PET is an exciting field of molecular imaging that uniquely explores the biochemical process at the cellular (subcellular) level. It is a non-invasive molecular imaging technique used in nuclear medicine. Radioactive molecules that decay by positron emission are used as PET is based on the detection of two coincident gamma rays emitted during annihilation of positroniums, formed by collision of positrons with electrons. Nevertheless, the development of PET-radiopharmaceuticals requires a multidisciplinary approach including organic synthesis of the standard non-radioactive reference compound and precursors, effective incorporation of radionuclides into the precursor (radiochemistry), isolation of the desired radiolabeled molecule (purification), radiochemical and chemical purity determination (quality control), confirmation of radiolabeled molecule identity, and formulation of the

radiolabeled molecule in such a way that it is appropriate for administration to experimental animals or humans (sterile, pyrogen free, pH value, osmolarity, toxicity and physical state of the sample). The basics from production of radionuclides to radiopharmaceutical formulation will be discussed in brief in the subsequent paragraphs.

4.1. PET Radiopharmaceutical: development and requirements [108-113]

The initial step towards developing radiolabeled molecules begins with organic synthesis of precursors suitable for incorporating radionuclides. Radionuclides (radioactive nuclides or radioisotopes are unstable atoms due to the unsuitable composition of neutrons and protons, or excess energy, and therefore decay by emission of radiations such as α particles, β^- particles, β^+ particles, electron capture, and isomeric transition. The stability of a nuclide is governed by the structural arrangement and binding energy of the nucleons in the nucleus. One criterion of stability is the neutron-to-proton ratio (N/Z) of the stable nuclides; the radionuclides decay to achieve the N/Z of the nearest possible stable nuclide. Radioactive decay by particle emission or electron capture changes the atomic number of the radionuclide, whereas decay by g-ray emission does not.

α decay occurs in heavy nuclei such as ^{235}U, ^{239}Pu, etc. In the decay process two protons and two neutrons, i.e. nucleus of helium molecule are emitted. α particles are emitted with discrete energy and have a very short range in matter, e.g., about 0.03 mm in human tissues.

β decay occurs in radionuclides that are neutron rich. In the decay process, a neutron in the nucleus is converted to a proton along with the emission of a β^- particle and an anti-neutrino ($\overline{\nu}$). β^- decay is usually represented as $n \rightarrow p + \beta^- + \overline{\nu}$. Examples are ^{131}I and ^{90}Y.

Positron decay: β^+ occurs when a radionuclide is proton rich; it decays by the emission of a positron β^+ along with a neutrino ν. In essence, a proton in the nucleus is converted to a neutron in the process. β^+ decay is usually represented as ($p \rightarrow n + \beta^+ + \nu$) and some examples of positron-emitting nuclides are: ^{11}C, ^{13}N, ^{15}O, ^{19}F, ^{66}Ga, ^{68}Ga, ^{82}Rb and ^{124}I. Since a neutron is one electron mass heavier than a proton, the right hand side of decay representation is two electron mass more than the left-hand side, i.e., 2 X 0.511 MeV = 1.022 MeV more on the right side. For conservation of energy, therefore, the radionuclide must have transition energy of at least 1.022 MeV to decay by β^+ emission. The energy beyond 1.022 MeV is shared as kinetic energy by the β^+ particle and the neutrino. PET is based on the principle of coincidence

detection of the two 511 keV photons arising from positron emitters, which will be discussed in certain detail later.

Electron capture (EC) occurs when a radionuclide is proton rich, but has energy less than 1.022 MeV, then it decays by electron capture. In the process, an electron from the nearest shell, i.e., *K*-shell, is captured by a proton in the nucleus to produce a neutron. EC decay is usually represented as ($p + e^- \rightarrow n + \nu$) and some examples radionuclides that decay by EC are: ^{11}C (1.9 %), ^{19}F (3 %), ^{68}Ga (11 %), and ^{124}I (23 %).

Isomeric transition: when a nucleus has excess energy above the ground state, it can exist in excited (energy) states, which are called the isomeric states. The lifetimes of these states normally are very short (10^{-15} to 10^{-12} s); however, in some cases, the lifetime can be longer in minutes to years. When an isomeric state has a longer lifetime, it is called a metastable state and is represented by "m" as superscript after the mass number (e.g. ^{99m}Tc). In isomeric decay, γ-ray is emitted as radionuclides decay to ground state. Having an energy state of 140 keV above ^{99}Tc and decaying with a half-life of 6 h, ^{99m}Tc is an isomer of ^{99}Tc. Isomeric transition for ^{99m}Tc is represented as (^{99m}Tc → ^{99}Tc +γ).

Internal conversion is a radioactive decay process where an excited nucleus interacts electromagnetically with an electron in one of the lower atomic orbitals, causing the electron to be emitted (ejected) from the atom. Thus, in an internal conversion process, a high-energy electron is emitted from the radioactive atom, but not from a nucleon in the nucleus. The electron emitted is called an Auger electron.

The most commonly used PET radionuclides including ^{11}C and ^{18}F with a half life of 20.4 min and 109.7 min, respectively are cyclotron produced (table 5). This necessitates the presence of on-site cyclotron for production of radionuclides because the desired short-lived radionuclides need to be incorporated into the desired molecule, purified, formulated for administration and analyzed for (radio)chemical purity and identity within a brief time frame (< three half-lives) to ensure there is enough tracer left to administer to the subject undergoing the PET-scan.

In a cyclotron, charged particles such as hydride ion (H^-), deuterons, α particle from the ion source (S) are accelerated in circular paths in dees under vacuum by means of an electromagnetic field (figure 9). The charged particles move along the circular paths under a magnetic field with gradually increasing energy, the larger the radius of the particle trajectory,

the higher the energy of the particle. The negative charge in hydride ion is stripped of its electron by a carbon foil (D) placed perpendicular along its path and directed via the window (W) to the target where it interacts with the molecules which then can cause nuclear reactions in nuclei.

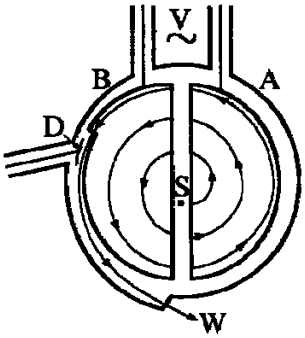

***Figure 9**. A schematic illustration of a cross-section of a cyclotron: V, alternating voltage; S, ion source; A and B, dees under vacuum; D, carbon foil stripper; W, window.*

The type of radionuclide produced during the nuclear reaction depends on the molecules kept in the target. Here, the production of fluorine-18 and carbon-11 is discussed.

Fluorine-18 ($t_{1/2}$ = 110 minutes) is commonly produced by the $^{18}O(p,n)^{18}F$ reaction on water target enriched with oxygen-18 ($H_2{}^{18}O$) using 11 to 18MeV protons in medical cyclotrons. This produces nucleophilic fluorine-18 ($[^{18}F]F^-$). For F-18 production, an enrichment of > 95 % is used, because ^{16}O can also undergo a nuclear reaction ($^{16}O(p,\alpha)^{13}N$) in the cyclotron. The $^{18}F^-$ is present as $[^{18}F]HF$ in the target water, and can easily be extracted from it by ion exchange cartridges. $[^{18}F]F^-$ is passed through a carbonated anion exchange cartridge to get rid of the bulk of the $H_2{}^{18}O$. The $[^{18}F]F^-$ can be eluted from the cartridge by carbonate/cryptand mixture (usually K_2CO_3/4,7,13,16,21,24-Hexaoxa-1,10-diazabicyclo[8.8.8]-hexacosane). However, any remaining water should be removed as solvated fluoride is a poor nucleophile (this can be achieved by azeotropic distillation with acetonitrile). $[^{18}F]F^-$ can be converted to different synthons (such as 1-bromo-2-$[^{18}F]$fluoroethane by reaction with 2-bromoethyl trifluoromethane-sulfonate at 120 ^oC which can be further converted to the more reactive 2-$[^{18}F]$fluoroethyl trifluoromethane-sulfonate by passing through a silver triflate column at 225 ^oC). Other methods to produce radioactive fluorine are given in table 4.

Table 4. *Nuclear reactions for ^{18}F-production.*

$^{20}Ne(d,\alpha)^{18}F$
$^{20}Ne(p,2pn)^{18}F$
$^{16}O(^{3}He,p)^{18}F$
$^{16}O(\alpha ,pn)^{18}F$
$^{18}O(p ,n)^{18}F$
$^{20}Ne(^{3}He,\alpha n)^{18}Ne$, ^{8}Ne ($t_{1/2}$ 1.67 s) decays to ^{18}F
$^{6}Li(n , \alpha)^{3}H$, the ^{3}H reacts in a following nuclear reaction $^{16}O(^{3}H ,n)^{18}F$

The most convenient method for producing carbon-11 in a cyclotron is by the $^{14}N(p,\alpha)^{11}C$ nuclear reaction. With O_2 (0.1-0.5 %) present, $[^{11}C]CO$ or $[^{11}C]CO_2$ is produced in-target from the nuclear reaction of protons from the accelerator with $^{14}N_2$, while by adding H_2 (5-10 %) to the target gas $[^{11}C]CH_4$ is produced. $[^{11}C]CO_2$ or $[^{11}C]CH_4$ is recovered by initially trapping in a column trap inserted into liquid nitrogen filled cup (Deware) and later removing it by flushing with helium or heating the trap. Several reactive molecules have been prepared by simple on-line or one-pot procedures from $[^{11}C]CO_2$ or $[^{11}C]CH_4$. Some of the most important of those secondary precursors are shown in figure 10. The most common production method for other commonly used PET tracers are given in table 5.

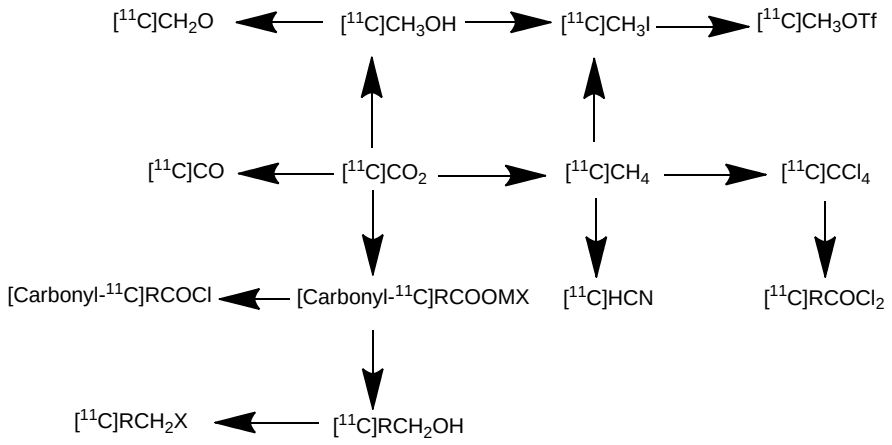

Figure 10*. The most important ^{11}C precursors used in the synthesis of ^{11}C-labeled compounds produced from either $[^{11}C]CO_2$ or $[^{11}C]CH_4$.*

Table 5. *Frequently used PET-radionuclides, their nuclear reactions for production, decay nuclides and some physical characteristics. Adapted from van Veghel [108].*

Radionuclide	Reaction	$t_{1/2}$	Daughter	E_{max} (keV)	R_{max}
^{11}C	$^{14}N(p,\alpha)^{11}C$	20.4 min	^{11}B	961	3.9
^{18}F	$^{18}O(p,n)^{18}F$	109.8 min	^{18}O	634	2.3
^{13}N	$^{16}O(p,\alpha)^{13}N$	9.97 min	^{13}C	1198	5.1
^{15}O	$^{15}N(d,n)^{15}O$	2.04 min	^{15}N	1732	8.0
^{124}I	$^{124}Te(p,n)^{124}I$	4.17 d	^{124}Te	2138	10.2
^{68}Ga	^{68}Ge generator	67.6 min	^{68}Zn	1899	8.9
^{64}Cu	$^{64}Ni(p,n)^{64}Cu$	12.7 h	^{61}Ni	653	2.4
^{89}Zr	$^{89}Y(p,n)^{89}Zr$	78.4 h	^{89}Y	897	3.6

p: proton; n: neutron; d:deuteron; α: helium nucleus (2p+2n); Reaction: nuclear reaction for production of radioisotopes;$t_{1/2}$: physical half-life; Daughter: daughter product/nuclide of the decay; Emax: maximum energy of the β; R_{max}: maximum range of β^+ in H_2O (mm)

Once, a radioisotope is produced in the target and transferred to a reactive synthon the next step is radiolabeling where priority is given for effective incorporation of the positron emitting radionuclide in the desired precursor molecule. Due to the high energies of the gamma rays emitted upon decay of the radioisotopes, traditional bench-top chemistry is not an option and radiolabeling reactions are performed in synthesis modules housed in lead shielded "hot cells" (figure 11) to avoid high radiation doses.

The most commonly used methods employed in the preparation of labeled compounds for clinical use are: *Isotope exchange reactions.*In isotope exchange reactions, one or more atoms in a molecule are replaced by isotopes of the same element having different mass numbers. Examples are ^{125}I-triiodothyronine (T3) and ^{125}I-thyroxine (T4).

Introduction of a foreign label: in this type of labeling, a radionuclide is incorporated into a molecule that has a known biological role, primarily by the formation of covalent or coordinate covalent bonds. The tagging radionuclide is foreign to the molecule and does not

label it by the exchange of one of its isotopes. Examples are ^{18}F-fluorodeoxyglucose ([^{18}F]FDG) ^{99m}Tc-labeled albumin, ^{51}Cr-labeled red blood cells, and many iodinated proteins and enzymes.

Labeling with bifunctional chelating agents: in this approach, a bifunctional chelating agent is conjugated to a macromolecule (e.g., protein, antibody) on one side and to a metal ion (e.g. Tc) by chelation on the other side. An example is ^{68}Ga-octreotide (^{68}Ga-Dotatoc).

Biosynthesis: In biosynthesis, a living organism is grown in a culture medium containing the radioactive tracer, the tracer is incorporated into metabolites produced by the metabolic processes of the organism, and the metabolites are then chemically separated. For example, vitamin B_{12} is labeled with ^{60}Co or ^{57}Co by adding the tracer to a culture medium in which the organism *Streptomyces griseus* is grown. Other examples of biosynthesis include ^{14}C-labeled carbohydrates, proteins, and fats.

Recoil labeling: in a nuclear reaction, when particles are emitted from a nucleus, recoil atoms or ions are produced that can form a bond with other molecules present in the target material. Several tritiated compounds can be prepared in the reactor by the ^{6}Li(n,α)^{3}H reaction. The compound to be labeled is mixed with a lithium salt and irradiated in the reactor.

Figure 11. *Picture of lead shielded "hot cells" and a radiolabeling synthesis module. (Courtesy van Veghel [114]).*

Excitation labeling: Excitation labeling entails the utilization of radioactive and highly reactive daughter ions produced in a nuclear decay process. During β decay or electron capture, energetic charged ions are produced that are capable of labeling various compounds of interest. For example, Krypton-77 decays to ^{77}Br and, if the compound to be labeled is

exposed to ^{77}Kr, then energetic ^{77}Br ions label the compound to form the brominated compound. Similarly, various proteins have been iodinated with ^{123}I by exposing them to ^{123}Xe, which decays to ^{123}I. The yield is considerably low with this method.

In most cases the radiolabeling of molecules with the two most used PET radionuclides (^{11}C and ^{18}F) is introducing the nuclides to readymade precursors by nucleophilic substitution or a leaving group substitution such as triflates, mesylates and tosylates. The longer half-life of ^{18}F allows more complicated and time-consuming chemistry and provides the opportunity to transport ^{18}F-labeled tracers to PET-facilities that are not equipped with a cyclotron. Moreover, multiple subjects can be scanned using the same batch of ^{18}F-labeled tracer and the low maximal positron energy of fluorine-18 (634 keV) results in high resolution PET-images. The latter is an advantage over gallium-68 (^{68}Ga) and iodine-124 (^{124}I), as their emitted high energy positrons (table 5) may cause significant loss of spatial resolution when small structures are to be visualised using high resolution microPET-cameras [115-117]. The more complex cyclotron production of ^{124}I, as well as copper-64 (^{64}Cu) and zirconium-89 (^{89}Zr), (solid targets vs. gas or liquid targets for ^{11}C and ^{18}F), limits their use. The radioisotopes ^{13}N and ^{15}O are, due to their very short half-lives, only available in the chemical forms in which they are produced in the cyclotron target (e.g. ^{13}N-NH_3) or require instant high yield reactions (e.g. ^{15}O-H_2O) [116]. The emergence of ^{68}Ga in nuclear medicine can be explained by its broad availability at a reasonable cost-price via a ^{68}Ge/^{68}Ga generator and thus the non-requirement of an on-site cyclotron [115].

Radiopharmaceuticals targeting specific entities such as receptors or enzymes are often referred to as “tracers” because they are used in a very small (trace) amounts (in micro- to nanograms). To be useful for PET-imaging, the tracer should show high binding affinity (K_d), preferably in the subnanomolar to low nanomolar range, and selectivity for its target. Still, it is often difficult to estimate the required affinity of a tracer, in the perspective of high quality images, since the expression level of a protein usually varies among different tissues and may be up- or down-regulated in pathophysiological conditions [116].

4.2. Positron emission tomography (PET)

Principle of PET

PET is an exciting field of molecular imaging that uniquely explores the biochemical process at the cellular (subcellular) level. It is a non-invasive molecular imaging technique used in

nuclear medicine and is based on the detection of two coincident gamma rays emitted during annihilation of positroniums, formed by collision of positrons with electrons.

PET-radionuclides, characterised by an excess of protons (or lower proton to neurton ratio than their stable isotope), are unstable and decay by conversion of a proton into a neutron and subsequent emission of a positron and neutrino (a chargeless and an almost massless particle). The positron (β^+), which is the positively charged anti-particle of an electron (β^-), travels a short distance (0-10 mm, depending on its characteristic kinetic energy and density of the tissue in which the emission occurs) and combines with an electron in the surrounding tissue to form a positronium that immediately annihilates. Upon annihilation, two gamma rays of each 511 keV are emitted simultaneously in opposite directions (180°) which are detected in a PET camera as a coincident event. This coincident event is used to localize the origin of annihilation with a PET camera and computer algorithm. A PET-camera typically consists of multiple rings of scintillation detectors composed of inorganic crystals, such as sodium iodide doped with thallium [NaI(Tl)] (though they are no longer used in PET cameras and their use is restricted in gamma cameras for planar or SPECT imaging), bismuth germanate (BGO), luthetium oxyorthosilicate doped with cerium (LSO), yttrium oxyorthosilicate doped with cerium (YSO), gadolinium oxyorthosilicate doped with cerium (GSO) and barium fluoride (BaF_2) with each detector connected in a coincidence circuit with a detector located on the opposite side of the ring [109]. The physical properties of the common PET scintillator detectors are given in table 5.

The simultaneous detection of a pair of 511-keV gamma rays by two opposite detectors within the PET-camera indicates that an annihilation event took place somewhere along the imaginary line between those two detectors (figure 12). Only the gamma rays detected within a brief time frame (10-20 ns) are registered and by combining the data from millions of annihilation events a three-dimensional image can be reconstructed using mathematical techniques. In this way, it is possible to visualise the distribution of radioactivity in the body over time and quantify the radioactivity bound to the target [109, 110].

In diagnostic nuclear medicine, PET is considered a very sensitive technique, allowing the detection of picomolar concentrations and thus subpharmacological amounts of radiopharmaceuticals. State-of-the-art clinical PET scanners typically have a spatial resolution of 4-6 mm, however, new systems developed for brain imaging show increased spatial resolution up to 2.5 mm. Small animal microPET scanners achieve a spatial resolution of 1-2

mm. The ability to perform translational research starting from preclinical animal models directly to clinical settings is one of the most unique and powerful features of PET [110, 115]. The technique is applied to gain information on functional state and metabolic activity of organs and tissues through specific binding of radiopharmaceuticals to their target proteins (e.g. receptors, transporters or enzymes), which is a major advantage compared to anatomic imaging techniques such as X-ray computed tomography (CT) that can only provide information on structural changes. Molecular processes such as receptor density and occupancy, transporter and enzyme activity, and gene expression, among many others, can be visualised *in vivo*. This permits to study the role of certain proteins in selected pathologies, to detect diseases before morphological signs appear and to measure therapy response in an early stage. In addition, PET is a powerful tool to study the pharmacodynamic and pharmacokinetic properties (e.g. dose-occupancy relationship and brain uptake) of new therapeutics and, thereby, facilitates drug development.

Table 6. *The physical properties of the common PET scintillator detectors. Adapted from reference [109].*

Property	**NaI(Tl)**	**BGO**	**LSO**	**YSO**	**GSO**	**BaF_2**
Effective Z	50	74	66	34	59	52
Density (g/cm^3)	3.7	7.1	7.4	4.5	6.7	4.9
Scintillation decay time (ns)	230	300	40	70	60	0.6
Photon yield per keV	38	6	29	46	10	2
Relative light output	100	15	75	118	25	5
Linear attenuation coefficient, μ/cm	0.32	0.96	0.87	0.39	0.70	0.44
Energy resolution (% at 511 keV)	6.6	20	10	12.5	8.5	11.4

NaI(Tl): sodium iodide doped with thallium; BGO: bismuth germanate; LSO: luthetium oxyorthosilicate doped with cerium; YSO: yttrium oxyorthosilicate doped with cerium; GSO: gadolinium oxyorthosilicate doped with cerium; BaF_2: barium fluoride; keV: kiloelectron volt; ns: nanosecond; effective Z: the effective atomic number

The latest innovation in the field of nuclear medicine is the development of clinical PET/MR-scanners, housing the two modalities in a single imaging system that assures accurate anatomical designation of PET-images. The combination of other imaging modalities is intensively being explored and technical advancements in the field of multimodal imaging will definitely provide unique opportunities in the future.

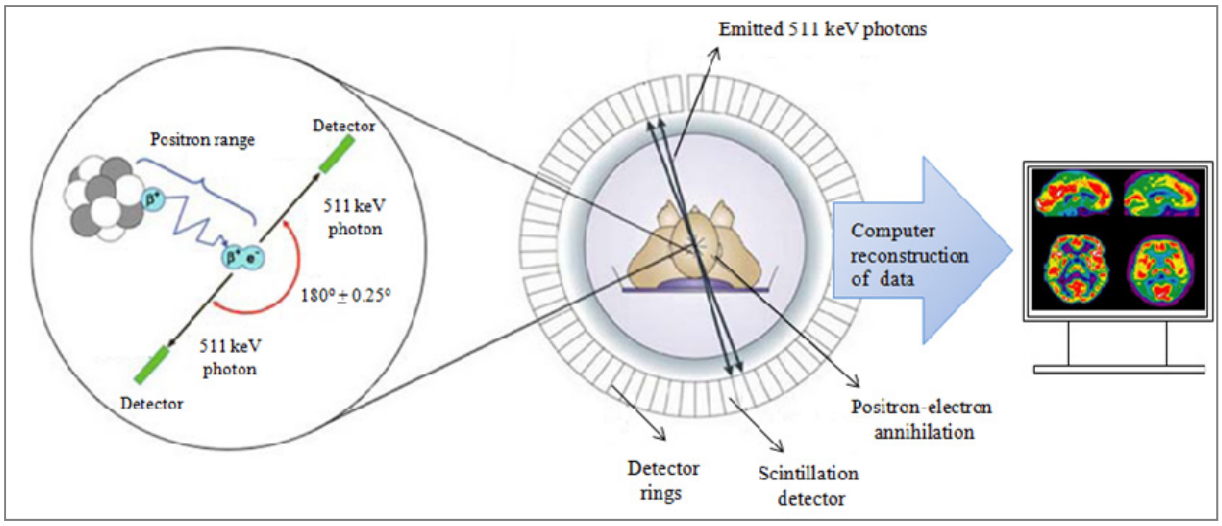

***Figure 12**. Schematic representation of the principle behind PET showing the positron decay and annihilation which produces two gamma rays of 511 keV. The two gamma rays are detected as coincident by two opposite detectors and are processed to generate 3D images. (Courtesy of van Veghel [108]).*

5. Objectives and overview of the thesis

Despite the success enjoyed by the application of several PDE5 inhibitors in the treatment of different diseases, there has not been a successful PET radioligand targeting PDE5 except in one publication which evaluated a carbon-11 labeled tracer ([^{11}C]RAL-01) though specificity of the tracer for PDE5 was not established [102, 106]. Therefore, development of PDE5 specific PET radioligands would allow to quantify and evaluate changes in PDE5 expression, select patients that would benefit from PDE5 inhibitor treatment early during disease progression and assess PDE5 occupancy and optimize dose regimens in patients treated with PDE5 inhibitors.

The main purpose of this research work was the development of PET probe(s) labeled with carbon-11 or fluorine-18 and the biological evaluation in order to select the optimal radioligand with high affinity and specificity for the PDE5 enzyme, ultimately enabling *in vivo* visualization/evaluation of PDE5. A successful PET radioligand(s) with high affinity and specificity for PDE5 would enable to quantify changes in PDE5 expression as a function of disease progression and could, furthermore, be used in clinical studies to quantify the occupancy of PDE5 in heart failure and PAH patients undergoing treatment with PDE5 inhibitors which could be exploited to determine the optimal dose of PDE5 inhibitors that are used in those patients.

During the course of the research, the general stages of new tracer development have been followed more or less: target selection (phosphodiesterase 5 expression in PAH and cardiac hypertrophy); lead selection and optimization (organic synthesis of selected PDE5 inhibitors reported in the literature); radiolabeling (carbon-11 and fluorine-18 production and labeling of precursors); purification (mainly HPLC based); formulation (pH adjustment, sterile filtration, ethanol concentration adjustment); quality control (mainly HPLC based and in some cases high resolution mass spectrometry); *in vitro* tests (mainly autoradiography); and *ex vivo/in vivo* evaluation of tracers in laboratory animals (plasma/brain radiometabolite analysis, biodistribution studies, microPET imaging, toxicity study [112].

Chapter II discusses the most time consuming aspect of radiochemistry in any new tracer development: synthesis of the labeling precursor and non-radioactive standard reference compounds that were used to authenticate the radiolabeled tracers. Non-radioactive standard compound or reference compound is essentially the same as the labeled compound except a stable isotope is used in place of the radioactive isotope and behaves identically to the labeled variant in every way and is used as surrogate to establish *in vitro* binding data, analytical as well as purification procedures by means of HPLC or other purification methods. Besides, the preliminary biological evaluation of the six tracers out of the total nine tracers that have been evaluated during the course of the last four years is discussed. A detailed description of the organic synthesis of precursors and reference compounds, characterization, HPLC analysis data, *in vitro* affinity assay results and biological evaluation data are given in the supporting document for **Chapter II**.

Chapter III is a continuation of the results described in **Chapter II** on the vardenafil derivatives. In this chapter, based on the conclusion of **Chapter II**, further biological evaluation of [^{11}C]**7** is reported. Biodistribution studies in transgenic mice with cardiomyocyte specific PDE5 over-expression (PDE5 TG), blocking studies in PDE5 TG mice as well as microPET imaging in PDE5 TG mice and in rats with monocrotalin induced PAH model, plasma radiometabolite analysis in mice and pigs, and large animal studies are reported. In this chapter, the high affinity and specific binding of [^{11}C]**7** to PDE5 is established.

In **Chapter IV**, a separate class of PDE5 inhibitors with the ability to cross the BBB is discussed. The organic synthesis, radiolabeling, preliminary biological evaluation (biodistribution in NMRI mice and PDE5 TG mice), *in vitro* autoradiography, microPET

imaging in PDE5 TG mice and rats are reported for two ^{11}C and ^{18}F labeled pyridopyrazine derivatives.

Chapter V describes a toxicity study (microdosing approach) of compound **7** (NMVardenafil) in rats. This was performed to move towards first- in-human applications.

A general discussion on the results of the experiments undertaken with future perspectives and limitations of the current study/work are discussed in **Chapter VI**.

Chapter II

Evaluation of PET Radioligands for *in vivo* Visualization of Phosphodiesterase 5 (PDE5)

Rufael Chekol[1]; Olivier Gheysens[2]; Jan Cleynhens[1]; Peter Pokreisz[3]; Greet Vanhoof[4]; Muneer Ahamed[1]; Stefan Janssens[3]; Alfons Verbruggen[1]; Guy Bormans[1]

[1]KU Leuven, Laboratory of Radiopharmacy, Leuven, Belgium

[2]KU Leuven, Department of Imaging and Pathology, Leuven, Belgium and Nuclear Medicine, UZ Leuven, Leuven Belgium

[3]KU Leuven, Departement of Cardiovascular Sciences, Leuven, Belgium and Cardiac Unit, UZ Leuven, Leuven Belgium

[4]C.R.E.A.Te Translational Sciences, Janssen Pharmaceutica, R&D, Beerse, Belgium

Nucl Med Biol. 2014; 41:155-162.

Abstract

Introduction: The cyclic guanosine monophosphate (cGMP) specific phosphodiesterase type 5 (PDE5) is considered to play an important role in various etiologies such as pulmonary arterial hypertension (PAH) and chronic heart failure. This PDE5 modulation represents an important prognostic and/or therapeutic target; however, there is currently no method to non-invasively evaluate the PDE5 expression levels *in vivo*.

Methods: Radiolabeling was achieved by N-alkylation of the corresponding precursors with [^{11}C]methyl trifluoromethanesulfonate ([^{11}C]CH_3OTf) or 2-[^{18}F]fluoroethyl trifluoromethane-sulfonate ([^{18}F]FEtOTf). Biodistribution of radiolabeled tracers was studied in NMRI mice and their specific binding to PDE5 was investigated by comparing their lung retention as the enzyme is abundantly expressed in this organ.

Results: The overall radiochemical yields ranged between 18 and 60 % for labeled radiotracers with radiochemical purity of > 99 %. The highest retention in the lungs at 30 min post injection was observed for vardenafil derivatives [^{11}C]-**7** and [^{18}F]-**11** and the retention of the ethoxyethyl pyrazolopyrimidine derivative [^{11}C]-**37** was moderate. The other investigated compounds [^{11}C]-**8,** [^{11}C]-**14**, [^{11}C]-**21** and [^{11}C]-**33** showed lower retention in lungs in agreement with their lower *in vitro* affinity for PDE5.

Conclusion: Among the different radiolabeled PDE5 inhibitors evaluated in this study, the vardenafil derivatives [^{11}C]-**7** and [^{18}F]-**11** are found to be promising tracers for *in vivo* visualization of PDE5.

1. Introduction

Cyclic adenosine monophosphate (cAMP) and cyclic guanosine monophosphate (cGMP) are ubiquitous second messengers responsible for transducing effects of various extracellular mediators including hormones, light and neurotransmitters [1-3].

The hydrolysis of cyclic nucleotides to their respective linear forms is catalyzed by a superfamily of enzymes known as phosphodiesterases (PDEs). The human genome contains 21 distinct PDE genes that encode 11 PDE protein families (PDE1 through PDE11). Some PDEs specifically hydrolyze cAMP or cGMP while others have mixed specificity. cAMP-specific PDEs include PDE4, 7 and 8 and cGMP-specific PDEs are PDE5, 6 and 9, whereas PDE1, 2, 3, 10 and 11 metabolize both cyclic nucleotides [1].

PDE5 is expressed in vascular smooth muscles, lungs, platelets, corpus cavernosum, and Purkinje fibers in the cerebellum [4]. It plays an important role in the regulation of vascular smooth muscle tone in the pulmonary vasculature, platelet aggregation, neuronal excitability and synaptic plasticity in Purkinje cells, handling of sodium secretion in renal cells and apoptosis [2, 4]. Moreover, PDE5 is considered to play an important role in disease progression such as pulmonary arterial hypertension (PAH), ischemic and dilated cardiomyopathy [2, 5-9]. As such, three PDE5 inhibitors (sildenafil, vardenafil and tadalafil) have been approved by FDA for the treatment of male erectile dysfunction and PAH and several others are in clinical evaluation for use in PAH [10-13]. A number of authors also advocate the use of PDE5 inhibitors to ameliorate cardiac hypertrophic response in chronic heart failure as the enzyme is up-regulated up to 5-fold in patients with ischemic and dilated cardiomyopathy [14-19].

Despite the involvement of PDE5 in several ailments and the success of PDE5 inhibitors in clinical practice, there is currently no method to non-invasively evaluate PDE5 expression levels *in vivo*. With regard to PAH, development of carbon-11 and/or fluorine-18 labeled PDE5 specific probes would enable the quantification of PDE5 availability and occupancy by PDE inhibitors in the pulmonary vasculature and consequently pave the path for determination of optimal doses regimens of PDE5 inhibitors used in the treatment of PAH. In addition, developing a positron emission tomography (PET) probe provides an insight into the extent and severity of PDE5 up-regulation in chronic cardiomyopathy and can potentially predict adverse remodeling and progression towards heart failure.

In recent years there have been several attempts to develop radioligands targeting PDEs with some success [20]. Only one article discusses the attempt to develop a PDE5 radioligand. In this article Jacobsen et al described the development of a PET radioligand [^{11}C]RAL-01 for *in vivo* visualization of PDE5 though PDE5-specific binding could not be demonstrated for the tracer [21]. Here, we discuss the synthesis, radiolabeling and preliminary biological evaluation of different PDE5 inhibitors in mice as a potential radioligands for *in vivo* visualization of PDE5 expression.

2. Results and discussion

2.1. Organic synthesis

Four different families of PDE5 inhibitors were prepared, namely derivatives of vardenafil, sildenafil, 4-benzylaminoquinoline, and ethoxyethylpyrazolopyrimidine derivatives (figures 1, 2, 3, and 4). Precursors **5**, **6**, **13**, **20**, **32**, and **35** were prepared for labeling with carbon-11 and/or fluorine-18 to provide [^{11}C]-**7**, [^{11}C]-**8**, [^{18}F]-**11** and [^{11}C]-**14**, [^{11}C]-**21**, [^{11}C]-**33**, [^{11}C]-**37** (figure 5).

Compounds **7**, **8** and **11** are close analogues of vardenafil, in which the ethyl substituent on the piperazine ring was replaced by a methyl group and 2-fluoroethyl group in **7** and **11**, respectively and the N-ethylpiperazine is replaced with N,1-dimethylpiperidin-4-amine in **8** [22]. Precursors **5**, **6**, and the authentic references **7**, **8** and **11** were prepared according to figure 1 starting from commercially available **1** based on procedures described in literature [23-26].

Sildenafil (**14**) is the first FDA approved PDE5 inhibitor for the treatment of male erectile dysfunction and pulmonary arterial hypertension [22, 27]. Precursor **13** for radiolabeling was prepared according to figure 2 starting from commercially available **12** [26]. Sildenafil (**14**) that was used for authentication was obtained from a commercial source.

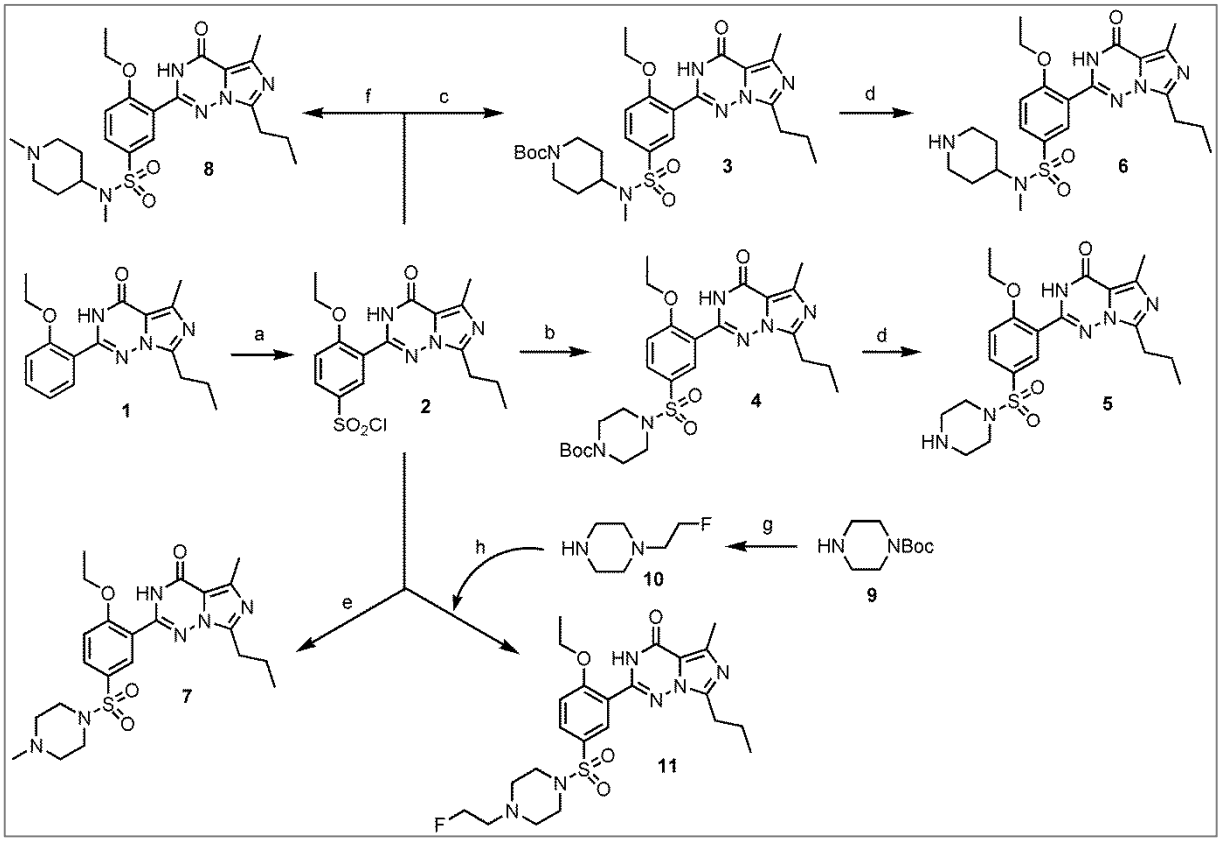

***Figure 1**. Synthesis of vardenafil derivatives (**7**, **8** and **11**).Reaction conditions: (a) HSO_3Cl, 0 °C→RT, 16 h; (b) N-Boc-Piperazine, CH_2Cl_2, 4-DMAP, RT, 16 h; (c) t-Butyl-4-(methylamino)piperidine-1-carboxylate, CH_2Cl_2, 4-DMAP, RT, 5 h; (d) CH_2Cl_2, TFA, 0 °C→RT, 16 h; (e) 1-Methylpiperazine, 4-DMAP, CH_2Cl_2, RT, 16 h; (f) N,1-Dimethylpiperidine-4-amine, 4-DMAP, DIEA, RT, 16 h; (g) 1) FEtBr, DIEA, CH_3CN, 50 °C, 16 h, then reflux, 6.5 h; 2) CH_2Cl_2, TFA, 0 °C→Rt, RT, 2 h; (h) 4-DMAP, RT, 16 h.*

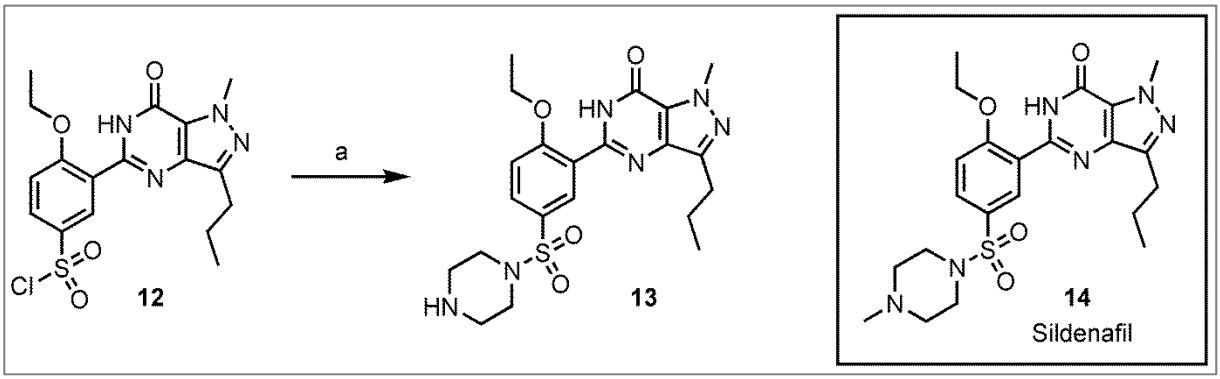

***Figure 2**. Synthesis of precursor (**13**) of sildenafil (**14**). Reaction conditions: (a) Piperazine, THF, RT, 2.5 h.*

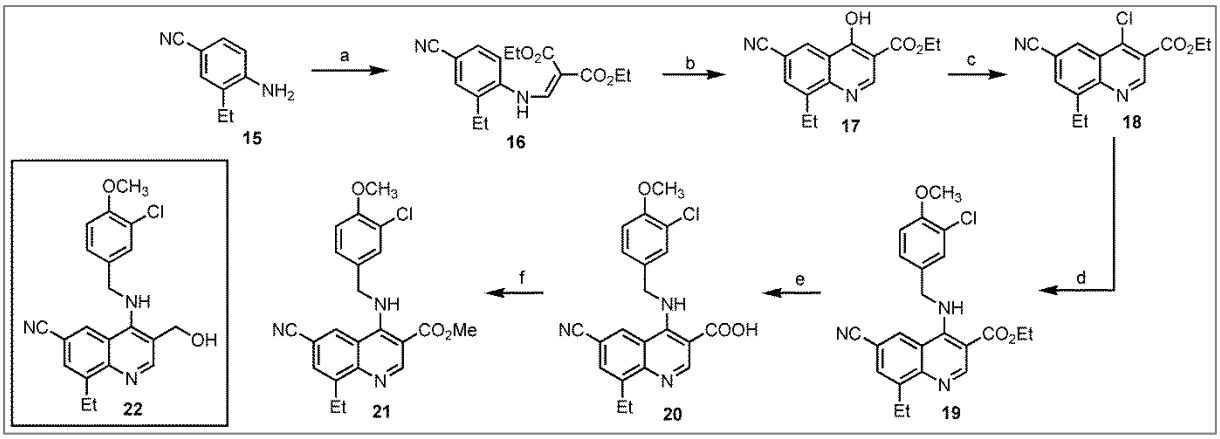

Figure 3. *Synthesis of precursors and reference of 4-benzylaminoquinoline derivative. Reaction conditions: (a) Diethyl ethoxymethylenemalonate, $PhCH_3$, reflux, 6 h; (b) Diphenylether, reflux, 2 h; (c) $POCl_3$, reflux, 48 h; (d) n-Propanol, 3-Chloro-4-methoxybenzyl amine, DIEA, reflux, 2 h; (e) 1 N NaOH/MeOH, RT, 4 h; (f) CH_2Cl_2, MeOH, 4-DMAP, RT, 1 h, then to 0 °C, DCC, 16 h. 4-BAQ (4-aminobenzyl quinoline).*

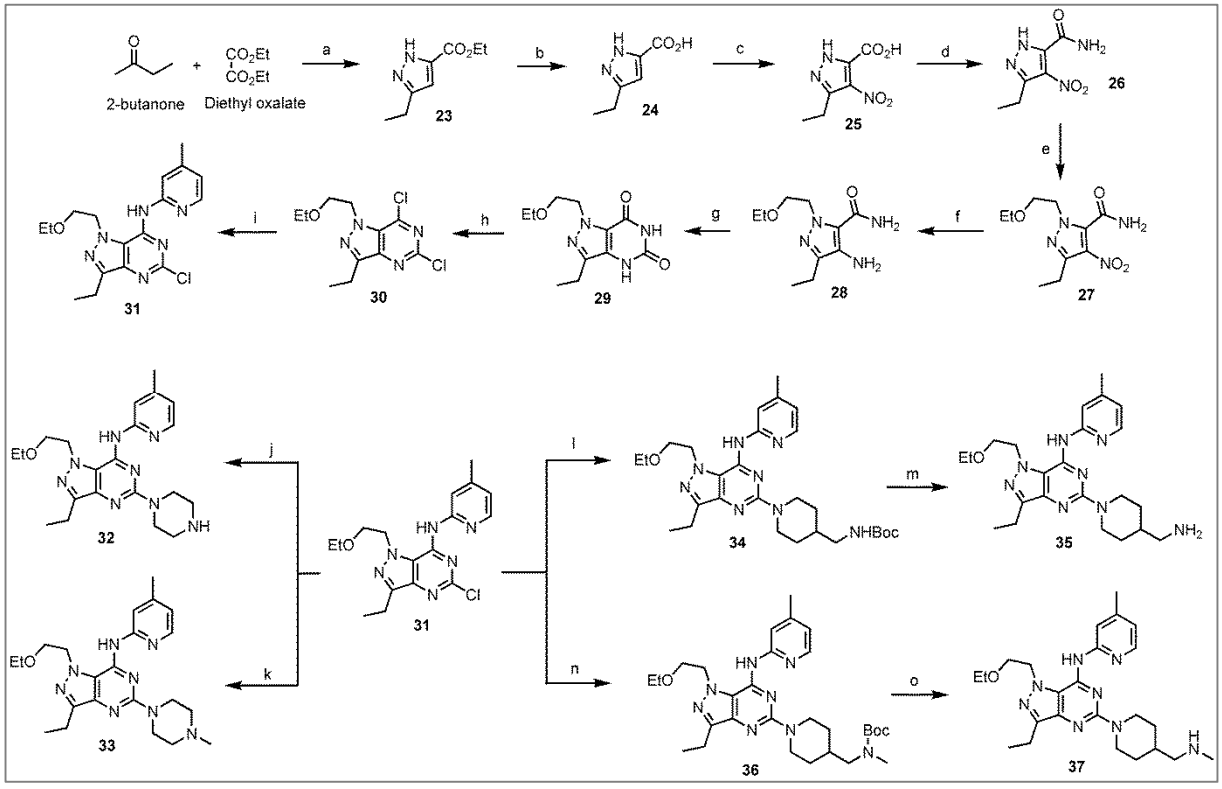

Figure 4. *Synthesis of precursors and reference of ethoxyethyl pyrazolopyrimidine derivatives. Reaction conditions: (a) 1) EtOH, 1 M t-BuOK (in THF), 75 °C, 30 min, 2) 4 °C, N_2H_4, 75 °C, 1 h; (b) THF, MeOH, 1 M LiOH, reflux, 3 h; (c) H_2SO_4 (fuming), HNO_3 (fuming), 0 °C → 50 °C, 30 min, 60 °C, 16 h; (d) $SOCl_2$, N_2, reflux, 3 h, THF, 0 °C, NH_3, 1 h; (e) THF, Triphenylphosphine, 0 °C, 2-EtOEtOH,*

di-tert-Butyl azodicarboxylate, 3.5 h, 0 °C, 6 M HCl, 40 °C, 1 h; (f) EtOH, $Pd(OH)_2$/C, ammoniumformate, 40 min, reflux, 2 h; (g) Carbonyldiimidazol, CH_3CN, 75 °C, 1 h, RT, 2 h, 0 °C, H_2O; (h) Phenylphosphonic dichloride, N_2, 135 °C, 48 h, 0 °C, 3 h, H_2O, THF, 1 M HCl, pH 1; (i) 0 °C, THF, 2-Amino-4-picoline, 1 M Lithium bis(trimethylsilyl)azanide (in THF), 5 °C, 30 min, 10 % citric acid, 5 °C, 1 h; (j) Piperazine, 2-PrOH, 175 °C, 45 min; (k) 1-Methylpiperazine and the rest same as (j); (l) tert-Butylpiperidin-4-yl carbamate and the rest same as (j); (m) CH_2Cl_2, 0 °C, N_2, TFA, 1 h, RT, 1 h; (n) tert-Butyl methylpiperidin-4-ylcarbamate and the rest same as (j); (o) same as (m).

4-Benzylaminoquinoline derivative (**22**) was first reported in 2003 by Bi et al as a selective PDE5 inhibitor with the highest inhibitory activity for PDE5 among its predecessors [11, 12, 28]. **19** along with **22** were among a series of PDE5 inhibitors reported by the same group. A series of compounds (**19**, **20**, **21**, and **22**) were prepared according to figure 3 based on literature reports [28-30]. Synthesis attempts to demethylate **22** to provide the phenolic precursor for radiolabeling were not successful. Therefore, **21** which is a methyl ester analogue of **19** was selected for biological evaluation.

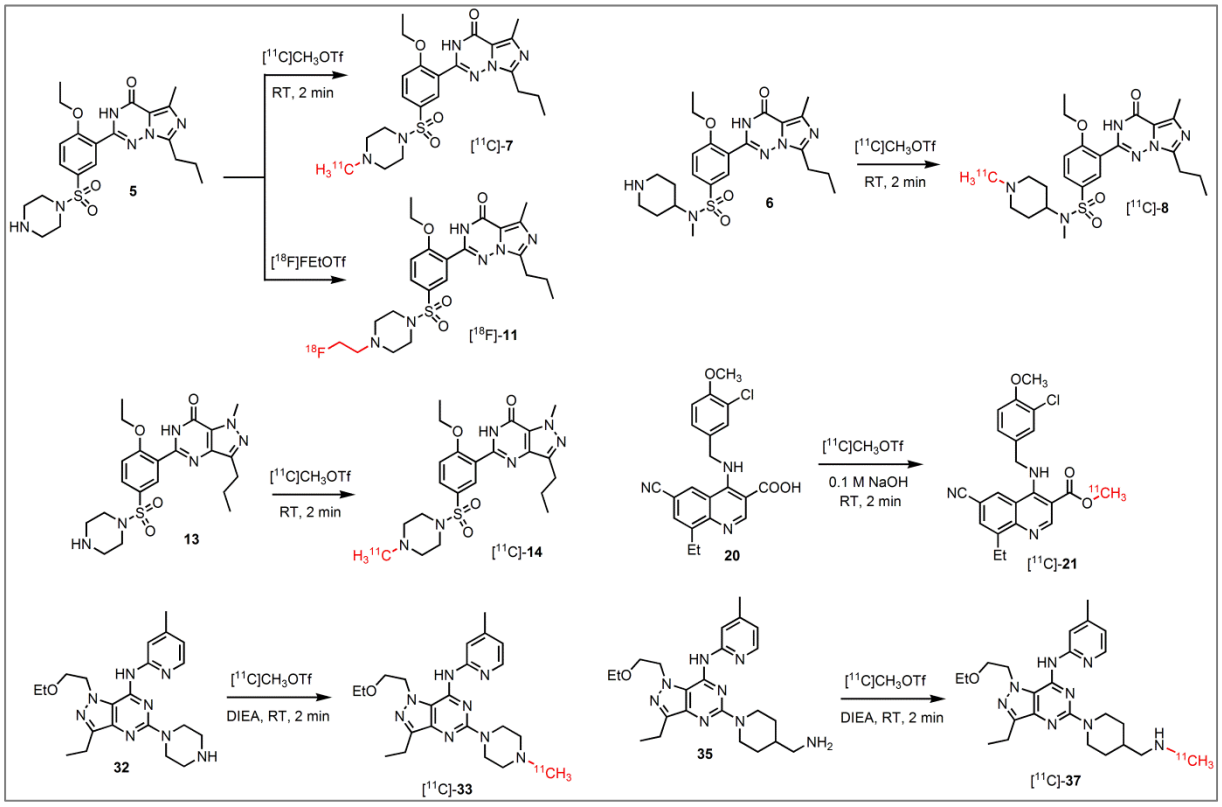

***Figure 5**. Radiosynthesis of PDE5 radioligands.*

Compound **35**, an ethoxyethyl pyrazolopyrimidine derivative reported by Tollefson et al. [31] has the highest PDE5 inhibitory activity (IC_{50} = 7 pM) among the PDE5 inhibitors reported

thus far [11, 12]. We have synthesized two of the derivatives in this group (**33** and **37**) along with the precursors **32** and **35** for carbon-11 radiolabeling according to the literature methods (figure 5) [31-36]. A methyl group was introduced on a primary amine of the 4-(aminomethyl)piperidine moiety of **35** in order to get **37** which resulted in a slightly different compound than the one reported by Tollefson and **37** was used in subsequent biological evaluation.

A detailed description of the synthesis of all compounds, ^{1}H-NMR and HRMS data for precursors and reference compounds are provided in the supporting information.

2.2. In vitro PDE5 inhibitory activity assay

In vitro PDEs inhibitory activity (IC_{50}) was experimentally determined for the different series of compounds. Their PDEs inhibitory activity for selected families (PDE5, PDE6 and PDE11) is given in table 1 (IC_{50} values for all PDE families are given in supporting information).

Vardenafil and its close derivative (**7**) were reported to have an IC_{50} value of 0.7 nM and 0.6 nM *in vitro* PDE5 inhibitory activities, respectively [22] and this value was in line with our *in vitro* PDE5 inhibitory assay for **7** (0.8 nM). The other two vardenafil derivatives (**8** and **11**) also showed PDE5 inhibitory activity in sub nanomolar to lower nanomalar range (1.1 nM and 0.7 nM, respectively).

Table 1. *IC_{50} (µM) values of PDE5 inhibitors for selected PDE families*

Compounds	hPDE5A3	hPDE6AB	hPDE11A4
7	0.0008	0.0031	0.8137
8	0.0011	0.0031	0.9918
11	0.0007	0.0023	0.6979
14	0.0173	0.1175	7.3393
21	0.0081	0.0830	7.7678
33	0.1636	0.3513	3.2574
35	0.0032	0.0008	0.0076
37	0.0032	0.0008	0.0095

The ethoxyethyl pyrazolopyrimidine derivatives (**33** and **35**) were reported to have an IC_{50} value of 0.89 nM and 0.007 nM for PDE5, respectively [31]. **37** was selected for biological evaluation as the parent compound **35** was not suitable for radiolabeling other than at the primary amino site. A methyl group was introduced on a primary amine of the 4-(aminomethyl)piperidine moiety of **35** which resulted in a slightly different compound than the one reported by Tollefson. The IC_{50} value determined for these two compounds (**35** and **37**) in our assay gave identical results (3.2 nM) for both compounds (table 1). But the *in vitro* PDE5 inhibitory activity for **33** was 163 nM; which is a significant deviation from the literature reported value of 0.89 nM.

Other groups of PDE5 inhibitors sildenafil (**14**) and 4-benzylaminoquinoline derivative (**21**) were found to have an *in vitro* PDE5 inhibitory activity much higher than the other PDE5 inhibitors with the exception of **14** and **33**. 4-Benzylaminoquinoline derivative (**22**) was first reported in 2003 by Bi et al. as a selective PDE5 inhibitor with the highest inhibitory activity for PDE5 among its predecessors based on its IC_{50} value (50 pM) [28]. In our *in vitro* assay, **22** was found to have the highest inhibitory activity (0.3 nM) and selectivity for PDE5 among the PDE5 inhibitors evaluated in this study although this value was 16-fold higher than that reported by Bi et al. Its ethylester (**19**) derivative was reported to have an IC_{50} value equivalent to that of vardenafil (0.7 nM) [22, 28]. For **21**, a methylester analogue of **19,** the *in vitro* PDE5 inhibitory activity was found to be 8 nM. This is the third highest IC_{50} value among the PDE5 inhibitors evaluated in this study.

Most of the PDE5 inhibitors evaluated in this study showed a significant *in vitro* PDE5 inhibitor activity in the nanomolar range. However, the experimentally determined values for the PDE5 inhibitors showed a difference from literature reported values except for **7**. This may be due to differences in the assay method.

2.3. Radiosynthesis

Radiolabeling was achieved by the one-step N-alkylation in anhydrous DMF of the amine precursors (**5**, **6**, **13**, **32** and **35**), or esterification of **20** with [^{11}C]methyl trifluoromethanesulfonate ([^{11}C]CH_3OTf) with the use of base (NaOH or DIEA). N-alkylation of **5** with 2-[^{18}F]fluoroethyl trifluoromethanesulfonate (2-[^{18}F]FEtOTf , figure 5) gave the ^{18}F-analog [^{18}F]-**11**. The reaction mixtures were kept at room temperature (RT) for 2 min. All radiotracers were purified by HPLC. The overall radiosynthesis, including alkylation (either with [^{11}C]CH_3OTf or [^{18}F]FEtOTf), HPLC purification, sterile filtration and radiotracer

formulation was completed in 50 to 60 min from end of bombardment for carbon-11 labeling and 60 to 90 min for fluorine-18 labeling.

The incorporation yield (non-decay corrected radiochemical yield, RCY based on HPLC recovered activity) of alkylation with [^{11}C]CH_3OTf or [^{18}F]FEtOTf ranged from 18 to 60 % for the different compounds, and the radiochemical purity after HPLC purification was greater than 99 % for all compounds. The identity of the labeled compounds was confirmed using analytical HPLC by co-injection of the corresponding authentic reference analogues (**7**, **8**, **11**, **14, 21, 33 and 37**). The specific activities of the different radiotracers ranged from 60 GBq/μmol to 209 GBq/μmol (table 2) at the end of formulation of radiotracers for animal administration. Representative radiochromatograms of RP-HPLC purification and identity confirmation with co-injection of tracer solution and non radioactive standard reference compound is given for [^{11}C]**7** in supporting information.

2.4. Biodistribution Studies

As the first step in the evaluation of the suitability of carbon-11 or fluorine-18 labeled tracers for *in vivo* visualization of PDE5, our focus was on the retention of the tracers in the lungs of healthy mice. Abundant expression of PDE5 in the lungs among different species had been established by several authors [4, 10, 37, 38]. Hence, it was expected that a suitable tracer would show high uptake and retention in the lungs. This uptake should also be blocked by pre-treatment with a competitive inhibitor of the enzyme if tracer binding is PDE5 specific.

Comparison of the different radiotracers was made based on the percentage of injected dose (% ID) and standard uptake value (SUV) in different organs and tissues. For each tracer the % ID and SUV (obtained by normalizing the % ID for animal's body weight and the weight of organ of interest) are given in tables 3 and 4. Particular emphasis was given to the tracer distribution in the lungs at 30 min post injection (pi).

Results obtained from the preliminary biological evaluation of the several radiotracers are given in tables 3 and 4. When comparing the lung retention at 30 min pi, [^{11}C]-**7** and [^{18}F]-**11** showed the highest retention followed by a moderate observed retention for [^{11}C]-**8** and [^{11}C]-**37**. The lung retention of [^{11}C]-**14**, [^{11}C]-**21** and [^{11}C]-**33** was low. The tracer concentration in the lung at 30 min pi of [^{11}C]-**7** (8.0±1.9 SUV) and [^{18}F]-**11** (8.9±0.8 SUV) were the highest among all organs (supporting information) with lung-to-blood SUV ratios of 11.2 and 7.9, respectively. This is in agreement with literature findings that PDE5 is abundantly expressed

in the lungs. The *in vitro* low PDE5 inhibitory activity of **14** (sildenafil) in our assay was also reflected in the *in vivo* lower uptake and retention of [^{11}C]-**14** in the lungs of NMRI at 30 min pi compared to [^{11}C]-**7** uptake (tables 3 and 4).

Table 2. *Results of radiochemistry, logD and PSA values of PDE5 tracers*

Radioligand	RCY (%)	Specific activity (GBq/μmol)	logD at pH7.4	PSA (Å^2)
[^{11}C]-**7**	29 (n=6)	77	0.73	112.9
[^{11}C]-**8**	60 (n=1)	209	0.41	112.9
[^{18}F]-**11**	25 (n=3)	60	0.94	112.9
[^{11}C]-**14**	50 (n=3)	145	1.33	113.4
[^{11}C]-**21**	56 (n=4)	155	5.21	84.3
[^{11}C]-**33**	33 (n=2)	57	3.37	80.6
[^{11}C]-**37**	18 (n=2)	61	0.88	89.8

logD at pH 7.4 generated with MarvinSketch 5.5.0.1 software (ChemAxon Ltd), PSA (polar surface area) is software generated (Molinspiration Cheminformatics 2011); GBq (gigabecquerel)

The biodistribution study of [^{11}C]-**21** in NMRI mice at four time points (tables 3, 4 and supporting information) is in agreement with the moderate *in vitro* inhibitory activity for PDE5 with relatively low lung uptake followed by rapid wash-out. The lung uptake of [^{11}C]-**21** at all studied time points (supporting information) was the lowest compared to that of all other tracers evaluated in this study. Plasma radiometabolite analysis of [^{11}C]-**21** at 30 min pi showed that at least 58 % of the activity was still in the form of intact tracer (supporting document). This rules out fast metabolism as the culprit for the observed absence of retention of [^{11}C]-**21** in the lungs.

Together with [^{11}C]-**14** and [^{11}C]-**21**, [^{11}C]-**33** was among those which showed the lowest uptake and retention at 30 min pi. [^{11}C]-**33** also showed a significant wash-out from the lungs from 5.1±1.0 % ID at 2 min to 1.7±0.3 % ID at 30 min pi (table 3 and supporting information). Radiotracers [^{11}C]-**14**, [^{11}C]-**21** and [^{11}C]-**33** showed the lowest in vitro PDE5 inhibitory activity and this corresponds also with their low *in vivo* retention in the lungs (figure 6). Interestingly, retention of [^{11}C]-**37** in the lungs at 30 min pi was high and comparable to that of [^{11}C]-**7** (table 3). Comparison of % ID (4.4±1.2 and 5.9±1.1 for [^{11}C]-**37**

and [^{11}C]-**7**, respectively) and SUVs (6.6±1.5 and 8.0±1.9 for [^{11}C]-**37** and [^{11}C]-**7**, respectively) in the lungs of NMRI mice showed no significant difference in the retention of the two tracers (p = 0.1 and 0.3 for % ID and SUV, respectively). The specificity of [^{11}C]-**37** for PDE5 was subsequently tested with a pre-blocking study (table 5) using the PDE5 specific inhibitor tadalafil [39].

Table 3. *Biodistribution of the various radiolabeled PDE5 inhibitors in NMRI mice at 30 min post injection (n = 4, SD = standard deviation)*

	[a]Percentage of Injected Dose (% ID±SD)						
Organs	[^{11}C]-**7**	[^{11}C]-**8**	[^{18}F]-**11**	[^{11}C]-**14**	[^{11}C]-**21**	[^{11}C]-**33**	[^{11}C]-**37**
kidneys	2.5±0.4	5.6±1.0	3.0±0.6	8.7±6.3	2.2±0.3	4.9±0.4	11.6±1.01
Liver	16.5±2.1	23.2±3.9	8.7±0.4	18.0±1.6	14.2±1.1	20.3±2.9	30.0±0.9
Lungs	5.9±1.0	3.2±0.4	6.4±1.6	1.0±0.1	0.7±0.1	1.7±0.3	4.4±1.2
Heart	0.3±0.0	0.1±0.0	0.5±0.1	0.3±0.0	0.4±0.1	0.4±0.1	0.6±0.0
Intestines	32.3±6.1	39.5±3.2	20.7±3.1	25.5±1.7	31.1±3.1	18.0±1.9	16.7±1.2
Blood	3.3±0.3	1.6±0.2	8.5±0.5	3.7±0.5	2.8±0.1	1.8±0.3	2.8±0.5
Penis	0.1±0.0	0.1±0.0	0.1±0.0	0.1±0.0	0.0±0.0	0.1±0.0	0.0±0.0

*Data are expressed as mean±SD; [a]percentage of injected dose calculated as CPM in organ * 100%/total CPM recovered*

All of the studied compounds showed accumulation in the intestine over a time period and were cleared from plasma mainly *via* the hepatobiliary pathway (supporting information). However, [^{11}C]-**8** showed a higher percentage of activity in the kidneys and urine/bladder (% ID, 5.6±1.0 and 5.2±1.3 respectively, table 3 and supporting information) and this might be attributed to a polar radiometabolite. Though [^{11}C]-**14** and [^{11}C]-**37** showed high percentage of activity in the kidney at 30 min pi (8.7±6.3 and 11.6±1.0 % ID, respectively), these was not accompanied by excretion in the urine (2.3±0.3 and 0.8±0.3 % ID, respectively). This might be due to reabsorption and/or retention of the tracers after glomerular filtration.

Table 4. *Standard uptake values of the various radiolabeled PDE5 inhibitors at 30 min post injection in NMRI mice (n = 4, SD = standard deviation)*

	[a]Standard Uptake Value (SUV±SD)						
Organs	[^{11}C]-**7**	[^{11}C]-**8**	[^{18}F]-**11**	[^{11}C]-**14**	[^{11}C]-**21**	[^{11}C]-**33**	[^{11}C]-**37**
Kidneys	1.3±0.1	3.7±0.6	1.8±0.3	5.0±3.6	1.3±0.1	3.3±0.8	7.4±1.3
Liver	3.5±0.4	4.8±0.9	2.0±0.1	3.5±0.3	3.5±0.3	4.4±0.9	6.4±0.3
Lungs	8.0±1.9	3.8±1.2	8.9±0.8	1.5±0.2	1.0±0.2	2.7±0.4	6.6±1.5
Heart	0.7±0.1	0.3±0.1	1.2±0.1	0.7±0.1	1.1±0.3	0.9±0.1	1.1±0.2
Intestines	3.5±0.6	4.8±0.3	2.2±0.2	3.0±0.2	1.3±0.8	2.5±0.2	2.0±0.2
Blood	0.7±0.3	0.2±0.0	1.2±0.1	0.5±0.1	0.4±0.0	0.3±0.0	0.2±0.0
Muscle	0.4±0.1	0.3±0.0	0.7±0.1	0.5±0.0	0.6±0.0	0.4±0.1	0.5±0.1
Penis	0.7±0.1	0.5±0.1	1.3±0.1	1.0±0.2	0.5±0.1	0.6±0.1	0.3±0.0
L/B[b]	11.2±2.3	16.9±5.1	7.4±0.9	2.9±0.5	2.5±0.4	10.9±2.2	31.8±3.8
H/B[c]	0.9±0.2	1.4±0.1	1.0±0.1	1.4±0.3	2.9±0.8	3.4±0.21	5.2±0.8

*Data are expressed as mean±SD; [a]SUV calculated as (CPM in organ * Weight of mouse)*100% /(total CPM recovered * organ weight); [b]L/B: Lung to Blood ratio; [c]H/B: Heart to Blood ratio*

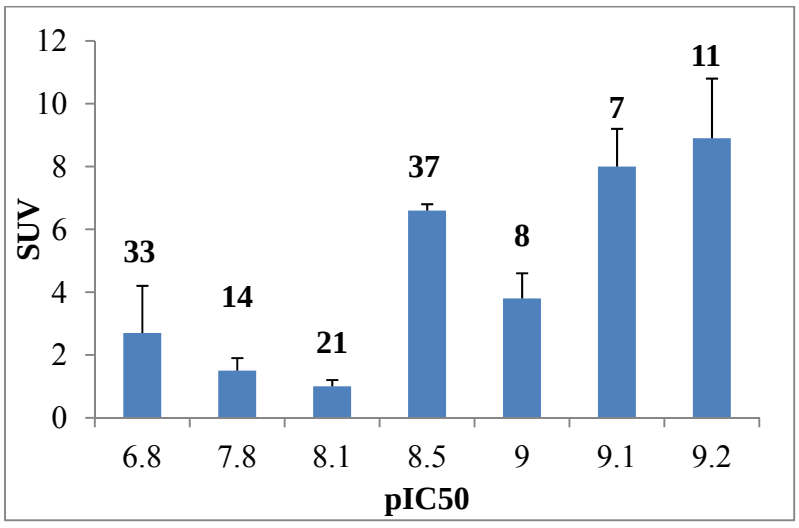

Figure 6*. Lung retention of the different radiolabeled tracers in relation to their in vitro PDE5 activity. pIC50, SUV (standard uptake value).*

Myocardial uptake of any of the evaluated tracers was very limited as expected due to the low expression level of PDE5 in normal conditions in mouse myocardium. None of the radiolabeled compounds showed significant brain uptake as expected from the calculated low logD and high PSA value.

One of the main clinical applications of PDE5 inhibitors is in the treatment of male erectile dysfunction where PDE5 inhibitors inhibit cGMP degradation and maintain penile tumescence. Despite this fact, the maximum observed activity at 30 min pi in the penis was 0.2±0.0 % ID for [^{18}F]-**11**. However intriguing this might seem, the general consensus is that PDE5 is abundantly expressed in the lungs and not in the penis [4, 10, 37, 38] and moreover, there might be a difference in expression level of PDE5 in the penis of humans and mice. As it was not our interest of research we didn't as well pursue this issue any further.

2.5. Blocking study in NMRI mice

Owing to the appealing property (a high lung retention) of [^{11}C]-**7** and [^{11}C]-**37,** a pre-blocking study was performed in order to confirm the specificity of [^{11}C]-**7** and [^{11}C]-**37** binding to PDE5 in the lung. Pre-blocking was conducted in mice with tadalafil, a structurally unrelated PDE5 inhibitor [39]. The results (table 5 and supporting information) show that lung uptake of [^{11}C]-**7** was significantly reduced (> 86 % reduction in % ID and SUV) in tadalafil pre-treated groups ($p < 0.001$) whereas other organs including the heart showed no significant difference in retention compared to the control group. This indicates that binding of [^{11}C]-**7** in the lungs is PDE5 specific.

Pre-treatment of mice with tadalafil in [^{11}C]-**37** injected group resulted in an almost 46 % reduction of retention (both % ID and SUV) of [^{11}C]-**37** in the lungs from 6.6±1.5 to 3.6±0.9 SUV (table 5). Though the reduction was found to be statistically significant ($p = 0.03$), the residual activity in the lungs was much higher than for [^{11}C]-**7**. The lower reduction observed after PDE5 blocking of this tracer might be attributed to higher *in vivo* affinity of [^{11}C]-**37** for PDE5 or off-target binding of the tracer. The former reasoning is supported by the higher lung/blood SUV ratio of [^{11}C]-**37** vs [^{11}C]-**7** (32 vs 11, table 4) but is in contrast to the experimentally determined IC_{50} value (3.2 nM vs 0.7 nM, respectively). The fact that the residual activity after pre-treatment remained high might be the contributing factor for the observed high retention in the lungs of mice despite the moderate *in vitro* PDE5 inhibitory activity (figure 6). Additional experiments will be required to determine the exact cause for the inability to fully block lung retention of [^{11}C]-**37**.

Table 5. *Comparison of pre-blocking effect on the uptake of [^{11}C]-**7** and [^{11}C]-**37** at 30 min post injection in control and tadalafil pre-treated (10 mg/kg, sc, 60 min prior to tracer injection) NMRI mice (n = 4, SD = standard deviation)*

[a]Standard uptake values (SUV±SD)				
[^{11}C]-**7**			[^{11}C]-**37**	
Organ	**Control**	**Tadalafil treated**	**Control**	**Tadalafil treated**
Kidneys	1.3±0.1	1.7±0.3	7.4±1.3	6.2±0.9
Liver	3.5±0.4	4.8±0.4	6.4±0.3	6.4±0.9
Lungs	8.0±2.0	1.0±0.2	6.6±1.5	3.6±0.9
Heart	0.7±0.1	0.7±0.1	1.1±0.2	1.3±0.1
Intestines	3.5±0.6	4.6±0.3	2.0±0.2	2.2±0.3
Blood	0.7±0.3	0.4±0.2	0.2±0.0	0.3±0.0
Muscle	0.4±0.1	0.5±0.1	0.5±0.1	0.9±0.9
Penis	0.7±0.1	0.7±0.17	0.3±0.0	0.6±0.6

*Data are expressed as mean±SD; [a]SUV calculated as (CPM in organ * Weight of mouse)*100% /(total CPM recovered * organ weight)*

3. Conclusion

We have been able to successfully prepare and radiolabel different derivatives of PDE5 inhibitors reported in literature. Although initial biological evaluation of ethoxyethyl pyrazolopyrimidin derivative [^{11}C]-**37** showed favorable properties, further investigation is required to confirm its specificity for PDE5. Initial biological evaluation of [^{11}C]-**14** and [^{11}C]-**20** revealed that these tracers have low affinity for PDE5 and do not possess the property required of a PET tracer for *in vivo* visualization of PDE5. Of all the radiotracers that have been evaluated in this study, the vardenafil derivatives [^{11}C]-**7** and [^{18}F]-**11** are the tracers with the most favorable properties for *in vivo* visualization of phosphodiesterase type 5. The vardenafil derivatives were selected for further biological evaluation in clinically relevant animal models and the results are presented in Chapter III.

4. Experimental section

4.1.Chemistry

All final compounds (precursors and references) were characterized by LC-MS and ^{1}H-NMR. A detailed description of the synthesis of all compounds with their ^{1}H-NMR and HRMS data for precursors and references is provided in the supporting information

4.2. In vitro affinity test

Compounds **7**, **8**, **11**, **14**, **21**, and **37** were dissolved in DMSO to a concentration of 5 mM, and **33** to a concentration of 2 mM. All compounds were profiled on the PDE assay platform, comprising members of each of the 11 described PDE families.

PDE1B1 and PDE11A4 were expressed in human embryonic kidney (HEK) cells from full-length human recombinant clones. Human recombinant phosphodiesterases 2A, 4D3, 5A3, 7A1, 9A1, 10A2 were expressed in Sf9 cells, using a recombinant baculovirus construct containing the full length sequence with a 6xHis sequence following the start Met to allow metal affinity purification of the recombinant protein. Cells were harvested and the phosphodiesterase protein was purified by metal chelate chromatography on Ni-sepharose 6FF (GE Health Care). PDE6AB, PDE3B and PDE8A were purchased as partially purified Sf9 cell lysates (Scottish Biomedical, UK). All enzymes were diluted in 50 mM Tris pH 7.8, 1.7 mM EGTA, 8.3 mM $MgCl_2$, except for PDE9A that was diluted in 50 mM Tris pH 7.8, 5 mM $MnCl_2$ and PDE1B was diluted in 50 mM Tris pH 7.8, 1.7 mM EGTA, 8.3 mM $MgCl_2$ complemented with 624 U/mL calmodulin and 800 µM $CaCl_2$. The affinity of the compounds for the PDEs is measured by a scintillation proximity assay (SPA).

PDE Yttrium Silicate SPA beads allow PDE activity to be measured by direct binding of the primary phosphate groups of non-cyclic AMP or GMP to the beads via a complex iron chelation mechanism. The amount of bound tritiated product ([^{3}H]-AMP or [^{3}H]-GMP) is measured by liquid scintillation counting in a TopCount^{TM} (Perkin Elmer)).

The compounds were dissolved and diluted in DMSO in polystyrene plates to a concentration of 100-fold of the final concentration in the assay. Human recombinant PDE5A3 enzyme solution (10 µl) was added to 20 µl of incubation buffer (50 mM Tris pH 7.8, 8.3 mM $MgCl_2$, 1.7 mM EGTA), 10 µl substrate solution consisting of a mixture of non-tritiated and tritiated substrate (1 µM cGMP, 0.01 µCi ^{3}H-cGMP), and 0.4 µl compound in DMSO in a 384-well

plate, and incubated for 30 min at room temperature. After incubation, the reaction was stopped with 20 µl of stop solution, consisting of PDE SPA beads (17.8 mg beads/mL in 200 mM zinc chloride). To measure the blank value, the enzyme was omitted from the reaction mixture. After sedimentation of the beads for 30 min, the radioactivity was measured in a PerkinElmer TopCount scintillation counter and results were expressed as counts per minute (cpm). The same assay principle was applied for the measurement of the inhibition of other members of the PDE family, with appropriate modifications of enzyme concentration, incubation buffer, substrate solution, incubation time and stop solution. Each experiment was performed in duplicates.

Data were calculated as the percentage of inhibition of total activity measured in the absence of test compound (% control). A best-fit curve is fitted by a minimum sum of squares method to the plot of % control versus compound concentration, from which an IC_{50} value (inhibitory concentration causing 50 % inhibition of hydrolysis) is obtained.

4.3 Radiosynthesis

Carbon-11 was produced in a Cyclone 18/9 cyclotron (IBA, Louvain-la-Neuve, Belgium) via an [$^{14}N(p,\alpha)^{11}C$] nuclear reaction. A mixture of N_2 (95 %) with H_2 (5 %) was irradiated with 18-MeV protons for 30 min to get [$^{11}C]CH_4$ ([$^{11}C]CH_4$). [$^{11}C]CH_4$ was transferred to a home-built synthesis module to convert it to [$^{11}C]CH_3I$ which was then converted to the more reactive [^{11}C]methyl triflate ([$^{11}C]CH_3OTf$) by passing through a silver triflate column (150 x 3 mm) heated at 180 ^{o}C.

[$^{11}C]CH_3OTf$ was streamed with helium through a solution of 250 - 500 µg precursors in DMF at room temperature. The reaction mixture was diluted with buffer and then injected onto HPLC (XBridge™ C18, 5µm, 4.6 x 150 mm; Waters) for purification. Radiotracers were eluted with a mixture of buffer and ethanol (EtOH) at a flow rate of 1 mL/min. The peak corresponding roughly to retention time of reference compound was collected and analyzed by RP-HPLC for purity and identity for biological evaluation. For all evaluation of tracers in animals, the ethanol concentration was diluted with normal saline to a maximum of 10 % and then sterile filtered through a 0.22 µm membrane filter (Millipore Millex GV 13 mm). Chemical and radiochemical purity of tracers were assayed with HPLC (XTerra™ C18, 5 µm, 4.6 mm x 100 mm) eluted with buffer and acetonitrile (ACN) at a flow rate of 1 mL/min, UV detection at 254 nm.

[^{18}F]Fluoride ($^{18}F^-$) was produced in a Cyclone 18/9 cyclotron (IBA) via an [$^{18}O(p,n)^{18}F$] nuclear reaction by bombarding oxygen-18 enriched water ($H_2{}^{18}O$) with 18 MeV protons. [$^{18}F]F^-$ was then passed through a preconditioned, (by successive washing with 10 mL of 0.5 M K_2CO_3 solution and 10 mL of de-ionized water), anion exchange cartridge (SepPak Light Accell plus QMA, Waters) to get rid of the bulk of the $H_2{}^{18}O$. The [$^{18}F]F^-$ was then eluted with 24 mM K_2CO_3/98 mM Kryptofix 2.2.2® (4,7,13,16,21,24-Hexaoxa-1,10-diazabicyclo[8.8.8]-hexacosane) in 750 µl of a mixture of acetonitrile:water (95:5 v/v) into a reaction vial. Any remaining water was removed by azeotropic distillation with acetonitrile. [$^{18}F]F^-$ was converted to 1-bromo-2-[^{18}F]fluoroethane by reaction with 2-bromoethyltriflate at 120 ^oC. The reaction product was passed through a silver triflate column heated at 225 ^oC to convert it to the more reactive 2-[^{18}F]fluoroethyl trifluoromethanesulfonate.

With a stream of helium the 2-[^{18}F]fluoroethyl trifluoromethanesulfonate was bubbled through a solution of 250 - 500 µg precursor in 250 µl DMF at room temperature. The purification, formulation, sterile filtration, and quality control were done in similar conditions as above for carbon-11 labeled tracers.

4.4. Biological evaluation

4.4.1. Biodistribution Studies

For biodistribution study adult NMRI mice, weighing 25 to 40 g were used. Animals were housed in individually ventilated cages in a thermo regulated (22°C), humidity-controlled facility under a 12 h/12 h light/dark cycle, with free access to food and water. All animal experiments were conducted according to the Belgian code of practice for the care and use of animals, after approval from the Animal Ethics Committee, KU Leuven (Ethische Commissie Dier Proeven, KU Leuven, License number: LA1210237).

Biodistribution studies of carbon-11 or fluorine-18 labeled tracers were performed in healthy NMRI mice at 2, 10, 30, and 60 min post injection (n = 4/time point). Mice were anesthetized with 2.5% isoflurane in oxygen at a flow rate of 1 L/min and 5 to 7 MBq of the tracer under study was injected via tail vein and sacrificed by decapitation at the specified time points. Blood and major organs were collected in tarred tubes and weighed. The radioactivity in blood and organs was counted using an automated γ-counter and expressed as a percentage of injected dose (% ID) and standardized uptake value (SUV). For the

calculation of total radioactivity in blood, blood mass was assumed to be 7 % of the body weight.

4.4.2. Blocking study

In order to assess the affinity and specificity of [^{11}C]-**7** and [^{11}C]-**37** for PDE5, a blocking study was performed. In brief, NMRI mice were subcutaneously injected with tadalafil (a structurally unrelated PDE5 inhibitor, TCR, Canada) 10 mg/kg, subcutaneous (sc), 60 minutes prior to tracer administration. Tadalafil solution for injection was prepared in such a way that the final concentration was 1 mg/mL in 10 % dimethylsulfoxide in 40 % (2-hydroxypropyl)-β-cyclodextrin solution and sterile filtered via a 0.22 μm membrane filter (Millipore, Ireland). Biodistribution was then performed as mentioned above and results were expressed as % ID and SUV.

All animal experiments were conducted according to the Belgian code of practice for the care and use of animals, after approval from the Animal Ethics Committee, KU Leuven (Ethische Commissie Dier Proeven, KU Leuven, License number: LA1210237).

4.4.3. Statistics

All calculated results are expressed as mean ± standard deviation (SD). For comparison the Student's t-test was used and $p < 0.05$ was considered statistically significant.

Acknowledgement:

We would like to thank Ann Van Santvoort, Julie Cornels and Ivan Sannen for their technical assistance during animal experiments.

We would also like to express our appreciation for the financial support from *In Vivo* Molecular Imaging Research (IMIR) and Fonds Wetenschappelijk Onderzoek Vlaanderen (FWO).

5. References

[1] Jeon YH, Heo YS, Kim CM, Hyun YL, Lee TG, Ro S, Cho JM. Phosphodiesterase: overview of protein structures, potential therapeutic application and recent progress in drug development. Cell Mol Life Sci 2005; 62:1198-1220.

[2] Tsai EJ, Kass DA. Cyclic GMP signalling in cardiovascular pathophysiology and therapeutics. Pharmacol Ther 2009; 122:216-38.

[3] Fischmeister R, Castro LR, Abi-Gerges A, Rochais F, Jurevicius J, Leroy J, Vandecasteele G. Compartmentation of cyclic nucleotide signaling in the heart: the role of cyclic nucleotide phosphodesterases. Circ Res 2006; 99:816-28.

[4] Lin CS, Lin G, Xin ZC, Lue TF. Expression, distribution and regulation of phosphodiesterase 5. Curr Pharm Des 2006; 12:3439-57.

[5] Kass DA, Champion HC, Beavo JA. Phosphodiesterase type 5 expanding roles in cardiovascular regulation. Circ Res 2007; 101:1084-95.

[6] Nagendran J, Archer SL, Soliman D, Gurtu V, Moudgil et al. Phosphodiesterase type 5 is highly expressed in the hypertrophied human right ventricle, and acute inhibition of phosphodiesterase type 5 improves contractility. Circulation 2007; 116:238-48.

[7] Pokreisz P, Vandenwijngaert S, Bito V, Van den Bergh A, Lenaerts I, Busche C, et al. Ventricular phosphodiesterase-5 expression is increased in patients with advanced heart failure and contributes to adverse ventricular remodeling after myocardial infarction in mice. Circulation 2009; 119:408-16.

[8] Lu Z, Xu X, Hu X, Lee S, Traverse J. Oxidative stress regulates left ventricular PDE5 expression in the failing heart. Circulation 2010; 121:1474-83.

[9] Shan X, Quaile MP, Monk JK, French B, Cappola TP et al. Differential expression of PDE5 in failing and nonfailing human myocardium. Circ Heart Fail 1012; 5:79-86.

[10] Buckley MS, Staib RL, Wicks LM, Feldman JP. Phosphodiesterase-5 inhibitors in management of pulmonary hypertension: Safety, tolerability, and efficacy. Drug Healthc Patient Saf 2010; 2:151-61.

[11] Giovannoni MP, Vergelli C, Graziano A, Dal Piaz V. PDE5 inhibitors and their applications. Curr Med Chem 2010; 17:2564-87.

[12] Bell AS, Palmer MJ, Novel phosphodiesterase type 5 modulators: a patent survey (2008-2010). Expert Opin Ther Pat 2011; 21:1631-41.

[13] Crom KF, Curran MP. Sildenafil: A Review of its Use in Pulmonary Arterial Hypertension. Drug 2008; 68:383-97.

[14] Takimoto E, Champion HC, Li M, Belardi D, Ren S, Rodriguez ER, et al. Chronic inhibition of cyclic GMP phosphodiesterase 5A prevents and reverses cardiac hypertrophy. Nat Med 2005; 11:214-22.

[15] Salloum FN, Ockaili RA, Wittkamp M, Marwaha VR, Kukreja RC; Vardenafil: a novel type 5 phosphodiesterase inhibitor reduces myocardial infarct size following ischemia/reperfusion injury via opening of mitochondrial KATP channels in rabbits. J Mol Cell Cardiol 2006; 40:405-11.

[16] Szabo G, Radovits T, Veres G, Krieger N, Loganathan S, Sandner P, et al. Vardenafil protects against myocardial and endothelial injuries after cardiopulmonary bypass. Eur J Cardiothorac Surg 2009; 36:657-64.

[17] Hassan MAH, Ketat AF. Sildenafil citrate increases myocardial cGMP content in rat heart, decreases its hypertrophic response to isoproterenol and decreases myocardial leak of creatine kinase and troponin T. BMC Pharmco 2005; l5:6-10.

[18] Guazzi M, Vicenzi M, Area R, guazzi MD. PDE5 inhibition with sildenafil improves left ventricular diastolic function, cardiac geometry, and clinical status in patients with stable systolic heart failure: results of a 1-year, prospective, randomized, placebo-controlled study. Circ Heart Fail 2010; 1:8-17.

[19] Lewis GD, Shah R, Shahzad K, Camuso JM, Pappagianopoulos PP, Hung J, et al. Sildenafil improves exercise capacity and quality of life in patients with systolic heart failure and secondary pulmonary hypertension. Circulation 2007; 116:1555-62.

[20] Andres JI, De Angelis M, Alcazar J, Celen S, Bormans G. Recent advances in positron emission tomography (PET) radiotracers for imaging phosphodiesterases. Curr Top Med Chem 2012; 12:1224-36.

[21] Jakobsen S, Kodahl GM, Olsen AK, Cumming P. Synthesis, radiolabelling and *in vivo* evaluation of [^{11}C]RAL-01, a potential phosphodiesterase 5 radioligand. Nucl Med Boil 2006; 33:593-97.

[22] Haning H, Niewohner N, Schenke T, Es-Sayed M, Schmidt G, Lampe T, et al. Imidazo[5,1-f][1,2,4]triazin-4(3H)-ones, a new class of potent PDE 5 inhibitors. Bioorg Med Chem Lett 2002; 12:865-68.

[23] Niewohner U, Haning H, Radtke M, Seidel D, Bischoff E , Karl W. 2-alkoxyphenyl substituted imidazotriazinones. World patent 2002; WO 02.064593 A1.

[24] Niewohner U, Haning H, Schenke T, Schlemmer KH, Keldenich J, Karl W, et al. 2-alkoxyphenyl substituted imidazotriazinones as phosphodiesterase inhibitors. U.S. Patent 2002; 6,362,178 B1.

[25] Siedel D, Brehmer P, Schoof Y, Weinberg U, Niewohner U, Nowakowski M. Syntheis of [^{14}C]-labelled vardenafil hydrochloride and metabolites. J Label Compd Radiopharm 2003; 46:1019-32.

[26] Khan KM, Maharvi GM, Khan MTH, Perveen S, Choudhary MI, Atta-ur-Rahman A facile and improved synthesis of sildenafil (Viagra®) analogs through solid support microwave irradiation possessing tyrosinase inhibitory potentials, their conformational analysis and molecular dynamics simulation studies. Mol Divers 2005; 9:15-26.

[27] Terret NK, Bell AS, Brown D, Ellis P. Sildenafil (Viagra™), a potent and selective inhibitor of type 5 cGMP phosphodiesterase with utility for the treatment of male erectile dysfunction. Bioorg Med Chem Lett 1996; 6:1819-24.

[28] Bi Y, Stoy P, Adam L, He B, Krupinski J, Normandin D, et al. Quinolines as extremely potent and selective PDE5 inhibitors as potential agents for treatment of erectile dysfunction. Bioorg Med Chem Lett 2004: 14: 1577-80.

[30] Bi Y, Yu Guixue, Rotella DP, Macor JE (2003) Quinoline inhibitors of cGMP phosphodiesterase. US patent, US 6576644 B2.

[31] Neise B, Steglich W. Esterification of carboxylic acids with dicyclohexylcarbodiimide/4-dimethylaminopyridine: tert-bytylethyl fumarate. Org Synth Coll Vol 1990; 7:93.

[32] Tollefson MB, Acker BA, Jacobsen EJ, Hughes RO , Walker JK, Foker DN, et al. 1-(2-ethoxyethyl)-1H-pyrazolo[4,3-d]pyrimidines as potent phosphodiesterase 5 (PDE5) inhibitors. Bioorg Med Chem Lett 2010; 20:3120-24.

[33] Harris JL, Storey AR, Wood SA. Crystalline therapeutic agent. World patent 2002; WO 02/10171A1.

[34] Acker BA, Hughes RO, Jacobsen EJ, Hwang-Fun RT, Tollefson MB, Walker JK, et al. Novel pharmaceuticals. World patent 2006; WO 2006/0461135A2.

[35] Matthews JM, Dyatkin AB, Evangelist M, Bauthier DA, Hecker LR, William JH, et al. Synthesis, resolution, and absolute configuration of novel tricyclic benzodiazepines. Tetrahedron: Asymmetry 2004; 15:1259-67.

[36] Skinner PJ, Cherrier MC, Webb PJ, Shin YJ, Gharbaoui T, Lindstrom A, Lindstrom A, et al. Fluorinated pyrazole acids are agonists of the high affinity niacin receptor GPR109a. Bioorg. Med Chem Lett 2007; 17:5620-23.

[36] Tollefson MB. Pyrazolo[4,3-d]pyrimidin-5-yl derivatives used as PDE5 inhibitors. World paten 2007; WO 2007/054778A1.

[37] Lakics V, Karran EH, Boess FG. Quantitative comparison of phosphodiesterase mRNA distribution in human brain and peripheral tissues. Neuropharmacology 2010; 59:367-74.

[38] Corbin JD, Beasley A, Blount MA, Francis SH. High level PDE5: A strong basis for treating pulmonary hypertension with PDE5 inhibitors. Biochem Biophys Research Commun 2005; 334:930-38.

[39] Dungan A, Grondin P, Ruault C, Le Monnier de Gouvile A-C, Coste H, Kirilovsky J, et al. The discovery of tadalafil: A novel and highly selective PDE5 inhibitor. 2: 2,3,6,7,12,12a-hexahydropyrazino[1´,2´:1,6]pyrido[3,4,-b]indole-1,4,-dione analogues. J Med Chem 2003; 46:4533-42.

Chapter II - Supporting information

Chemistry

All final compounds (precursors and references) were characterized by, LC-MS and ^{1}H-NMR. Chemical and radiochemical purity was determined by RP-HPLC and representative chromatograms for compounds **5** and **7** are given in figures 1 and 2.

^{1}H-NMR spectra were recorded on a 400 MHz spectrometer (Bruker AVANCE) and either, deuterated chloroform ($CDCl_3$) or deuterated methanol (MeOD) or deuterated dimethyl sufoxide (DMSO-*d*6) was used as a solvent as indicated. Chemical shifts are reported in parts per million relative to tetramethylsilane ($\delta = 0$). Coupling constants are reported in hertz (Hz). Splitting patterns are defined as follow: s (singlet), br s (broad singlet), d (doublet), q (quartet), dd (double doublet), t (triplet), dt (double triplet), or m (multiplet).

High-performance liquid chromatography (HPLC) analysis was performed on a LaChrom Elite HPLC system (Hitachi) connected to an ultraviolet spectrometer set at 254 nm. For the analysis of radiolabeled compounds, the HPLC eluate (after passage through the UV detector) was led over a 7.62-cm (3-in.) NaI(Tl) scintillation detector connected to a single-channel analyzer (GABI box; Raytest, Straubenhard, Germany). Quantification of radioactivity measurements in biodistribution studies was performed using an automated γ-counter equipped with a 7.62-cm (3-in.) NaI(Tl) well crystal coupled to a multichannel analyzer (1480 Wizard; Wallac, Turku, Finland). The results were corrected for background radiation and decay during counting.

All solvents and chemicals were obtained from commercial sources (Acros Organics, Aldrich or Fluka unless specified otherwise) and used as such without further purification. Purity of all final compounds (precursors and references) was ≥ 95 % and was determined by HPLC.

Vardenafil derivatives

The synthesis of the precursors for radiolabeling and reference compounds were carried out based on procedures described in literature [23-26].

4-Ethoxy-3-(5-methyl-4-oxo-7-propyl-3,4-dihydro-imidazo[5,1-f][1,2,4]triazin-2-yl)benzen-1-sulfonyl chloride (**2**)

2-(2-Ethoxyphenyl)-5-methyl-7-propylimidazo[1,5-f][1,2,4]triazin-4(3H)-one (**1**, 1.0 g, 3.20 mmol, Toronto Research Chemicals Inc,) was added slowly to a solution of chlorosulfonic acid (2.12 mL, 10 eq) at 0 ^{o}C. The reaction mixture was allowed to warm to room temperature (RT), stirred overnight and then poured into ice water (50 mL). After 5 min a white precipitate was formed and stirring was continued for 1 h at RT. The precipitate was filtered off, washed with water and dried under vacuum (0.64 g, first fraction). Further, the filtrate was extracted with CH_2Cl_2 (3 x 10 mL) and dried over $MgSO_4$, evaporation of the solvent gave an additional amount of **2** as colorless foam (0.26 g, second fraction). Yield (combined): (900 mg, 68%)

^{1}H NMR (MeOD, 400 MHz): δ 1.07 (t, 3H, *J* 7.4, CH_3), 1.46 (t, 3H, *J* 7.0, CH_3), 1.87-1.98 (m, 2H, CH_2), 2.76 (s, 3H, CH_3), 3.22 (t, 2H, *J* 7.5, CH_2), 3.31 (q, 2H, *J* 7.0, CH_2), 7.54 (s, 1H, Ar), 8.30-8.32 (m, 2H, Ar). MS: $(M+H)^+$ m/z = 411.1.

4-Ethoxy-N-methyl-3-{5-methyl-4-oxo-7-propyl-3H,4H-imidazo[4,3-f][1,2,4]triazin-2-yl}-N-(Boc-piperidin-4-yl)benzene-1-sulfonamide (**3**)

To a solution of **2** (160 mg, 0.39 mmol) in CH_2Cl_2 (5 mL) at 0 ^{o}C were added 1-*Boc*-4-(methylamino)piperidine (APOLLO Scientific) (0.25 mL, 1.17 mmol, 3 eq) and a catalytic amount of 4-DMAP and the reaction mixture was stirred for 5 h at room temperature. The mixture was diluted with CH_2Cl_2, washed with a saturated solution of ammonium chloride and dried over $MgSO_4$. The solvent was evaporated under reduced pressure and the crude residue was purified on a silica gel column with CH_2Cl_2 as eluent to obtain **3** as colorless oil (170 mg, 74 %).

^{1}H NMR (DMSO-d_6, 400 MHz): δ 7.94 (s, 2H), 7.35 (d, 1H), 4.22 (q, 2H), 3.90 (m, 1H), 3.35 (m, 4H), 2.83 (t, 2H), 2.66 (s, 3H), 2.51 (s, 3H), 1.75 (hex, 2H), 1.44-1.48 (m, 4H), 1.37 (s, 9H), 1.34 (t, 3H), 0.93 (t, 3H). MS: $(M+H)^+$ m/z = 589.1

2-[2-Ethoxy-5-(N-Boc-piperazine-1-sulfonyl)-phenyl]-5-methyl-7-propyl-4a,7-dihydro-3H-imidazo[5,1-f][1,2,4]triazin-2-yl)-4-one (**4**)

A solution of **2** (640 mg, 1.56 mmol) in dichloromethane (10 mL) was added drop-wise to a solution of *N-boc*-piperazine (872 mg, 4.68 mmol, 3 eq) in dichloromethane (2 mL) at RT followed by the addition of a catalytic amount of 4-DMAP. After stirring overnight, a saturated solution of NH_4Cl (20 mL) was added, the organic phase was separated, dried over

$MgSO_4$ and concentrated under reduced pressure. The resulting white residue was recrystallised from diethyl ether to yield **4** (594 mg, 68 %).

^{1}H NMR (DMSO-d_6, 400 MHz): δ 7.88 (s, 2H), 7.4 (d, 1H), 4.3 (q, 2H), 3.42 (m, 2H), 2.80-2.95 (m, 8H), 2.49 (s, 3H), 1.74 (m, 2H), 1.36 (s, 9H), 1.32-1.37 (t, 3H), 0.93 (t, 3H). MS: $(M+H)^+$ m/z = 561.0

2-[2-Ethoxy-5-(piperazine-1-sulfonyl)-phenyl]-5-methyl-7-propyl-4a,7-dihydro-3H-imidazo[5,1-f][1,2,4]triazin-2-yl)-4-one (**5**)

A solution of **4** (482 mg, 0.86 mmol) in a mixture of TFA (1 mL) and CH_2Cl_2 (2 mL) at 0 ^oC was stirred for 2 h at RT. The solvents were removed at reduced pressure and the residue was co-evaporated twice with heptane (2 x 5 mL) to obtained colourless oil, which was then recrystallized from methanol/diethylether mixture to yield **5** as a TFA salt. Yield (395 mg, 80% yield as a TFA salt).

^{1}H NMR (MeOD, 400 MHz): 0.93 (t, 3H, *J* 7.36, CH_3), 1.33 (t, 3H, *J* 6.9, CH_3), 1.73 (q, 2H, *J* 7.44, CH_2), 2.48 (s, 3H, CH_3), 2.76-2.86 (m, 8H, CH_2), 4.21 (q, 2H, *J* 6.84, CH_2), 7.39 (d, 1H, *J* 8.6, Ar), 7.83-7.88 (m, 2H, Ar). HRMS-ESI: calcd for $C_{21}H_{29}N_6O_4S^+$ 461.1971, found 461.1978.

4-Ethoxy-N-methyl-3-{5-methyl-4-oxo-7-propyl-3H,4H-imidazo[4,3-f][1,2,4]triazin-2-yl}-N-piperidin-4-yl)benzene-1-sulfonamide (**6**)

To a solution of **3** (100 mg, 0.17 mmol) in CH_2Cl_2 at 0 ^oC was added TFA (1 mL) in CH_2Cl_2 (4 mL). After overnight stirring at RT, the reaction mixture was evaporated under reduced pressure and the residue was co-evaporated three times with heptane (3 x 10 mL). The obtained oil was dried overnight under vacuum at 60 ^oC, triturated with diethyl ether and stirred overnight at RT. The solvent was carefully removed under reduced pressure and the oily residue dried under vacuum at 60 ^oC for 72 h yielding a white solid (50 mg, 0.1 mmol, 25 %).

^{1}H NMR (DMSO-d_6, 400 MHz): δ 0.72 (t, 3H, *J* 7.4, CH_3), 1.12 (t, 3H, *J* 6.9, CH_3), 1.23-1.29 (m, 2H, CH_2), 1.51-1.63 (m, 4H, $2CH_2$), 2.32 (s, 3H, CH_3), 2.47 (s, 3H, CH_3), 2.66-2.83 (m, 4H, $2CH_2$), 3.03-3.09 (m, 2H, CH_2), 3.84-3.91 (m, 1H, CH), 4.00 (q, 2H, *J* 6.8, CH_2), 7.14 (d, 1H, *J* 8.6, Ar), 7.74-7.78 (m, 2H, Ar), 11.75 (br s, 1H, NH). HRMS-ESI: calcd for $C_{24}H_{35}N_6O_4S^+$ 503.2440, found 503.2442

2-[2-Ethoxy-5-(N-methylpiperazine-1-sulfonyl)-phenyl]-5-methyl-7-propyl-4a,7-dihydro-3H-imidazo[5,1-f][1,2,4]triazin-2-yl)-4-one (**7**)

The procedure was the same as for preparing **4,** except *N*-methylpiperazine (53.3 mg, 0.13 mmol) was used instead of *N-Boc*-piperazine. The title compound was obtained as a white powder (46 mg, 0.1 mmol, 74 %).

^{1}H NMR ($CDCl_3$, 400 MHz): δ 8.44 (d, 1H), 7.88 (dd, 1H), 7.17 (d, 1H), 4.33 (q, 2H), 3.08 (m, 4H), 3.00 (t, 2H), 2.63 (s, 3H), 2.51 (m, 4H), 2.29 (s, 3H), 1.88 (hex, 2H), 1.59 (t, 3H), 1.04 (t, 3H). HRMS-ESI: calcd for $C_{22}H_{31}N_6O_4S^+$ 475.2127, found 475.2132.

4-Ethoxy-N-methyl-3-{5-methyl-4-oxo-7-propyl-3H,4H-imidazo[4,3-f][1,2,4]triazin-2-yl}-N-(1-methylpiperidin-4-yl)benzene-1-sulfonamide (**8**)

To a solution of **2** (160 mg, 0.4 mmol) in 5 mL CH_2Cl_2 at 0 ^oC, a tip of spatula of 4-DMAP and *N*,1-dimethylpiperidin-4-amine (150 mg, 1.17 mmol, APPLO Scientific) were added. The reaction mixture was stirred overnight at room temperature. The mixture was diluted with CH_2Cl_2, washed with saturated ammonium chloride solution and dried over $MgSO_4$. The residue was passed through a silica gel column with 2 % to 7.5 % MeOH/CH_2Cl_2 as the eluent to obtain the title compound as colorless oil which turned to solid upon storage (50 mg, 0.1 mmol, 25 %).

^{1}H NMR (400 MHz, $CDCl_3$): δ 1.02 (t, 3H, *J* 7.4, CH_3), 1.58 (t, 2H, *J* 7.0, CH_3), 1.70-2.05 (m, 8H, $2CH_2$), 2.24 (s, 3H, CH_3), 2.62 (s, 3H, CH_3), 2.78 (s, 3H, CH_3), 2.82-2.87 (m, 2H, CH_2), 2.98 (t, 2H, *J* 7.4, CH_2), 3.78-3.86 (m, 1H, CH), 4.32 (q, 2H, *J* 7.0, CH_2), 7.11 (d, 1H, *J* 8.8, Ar), 7.92 (d, 1H, *J* 6.4, Ar), 8.49 (s, 1H, Ar).

HRMS-ESI: calcd for $C_{24}H_{35}N_6O_4S^+$ 503.2440, found 503.2442.

4-(2-Fluoroethyl)-piperazine bis TFA salt (**10**)

A mixture of 1-boc-piperazine (1.02 g, 5.47 mmol), 1-bromo-2-fluorethane (4.17 g, 32 mmol) and DIEA (41.36 mg, 55.41 mL, 32 mmol) in CH_3CN (10 mL) was heated at 50 ^oC overnight and then refluxed for 6.5 h. The reaction mixture was cooled to RT and the solvent removed at reduced pressure. The residue was treated with 1 M NaOH (6.24 mL), extracted with EtOAc (2 x 20 mL) and dried over $MgSO_4$. Purification was done by silicagel chromatography using a gradient mixture of 0 to 10 % MeOH in CH_2Cl_2 to afford colorless oil (**9**) (1.11 g, 87.4 %). An aliquot of **9** (1 g, 4.31 mmol) was dissolved in CH_2Cl_2 (10 mL) was treated drop wise at 0 ^oC with TFA (5 mL) and stirred at RT for 2 h. The solvent was

removed with under reduced pressure and the residue co-evaporated twice with heptane (2 x 10 mL). To the resultant oil was carefully added diethyl ether with vigorous stirring. A white precipitate was obtained which was filtered under a stream of nitrogen and dried under vacuum (742 mg, 70 % as bis TFA salt). For the next reaction TFA salt of 1-(2-fluoroethyl)piperazine was partitioned between CH_2Cl_2 and saturated Na_2CO_3 solution. The organic layer was separated and the aqueous layer was washed with CH_2Cl_2. The combined organic layers were dried over $MgSO_4$, filtered and the filtrate was concentrated under reduced pressure. A white precipitate was obtained which was filtered off under a steady stream of N_2 and further dried under vacuum

^{1}H NMR (DMSO-d_6, 400 MHz): δ 4.73 (dt, 2H, *J* 4.6 & 47.4, CH_aH_b), 3.23-3.35 (m, 10H, CH_2). MS: $(M+H)^+$ m/z = 133.0

2-[2-Ethoxy-5-(N-2-fluoroethylpiperazine-1-sulfonyl)-phenyl]-5-methyl-7-propyl-4a,7-dihydro-3H-imidazo[5,1-f][1,2,4]triazin-2-yl)-4-one (**11**)

The procedure was the same as for preparing **4** except 1-(2-fluoroethyl)piperazine bis TFA (**10**, 578 mg, 2.35 mmol) and equivalent amount of DEIA was used instead of *N-boc*-piperazine to afford the title compound as white crystals (310 mg, 0.6 mmol, 43 %).

^{1}H NMR ($CDCl_3$, 400 MHz): δ 1.01 (t, 3H, *J* 7.3), 1.58 (t, 3H, *J* 6.9), 1.81-1.90 (m, 2H), 2.62 (s, 3H), 2.98 (t, 2H, *J* 8.1), 4.31 (q, 2H, *J* 6.9), 4.42 (t, 2H, *J* 4.7), 4.54 (t, 2H, *J* 4.7), 7.20 (d, 1H, *J* 8.0), 7.85 (d, 1H, *J* 8.0), 8.51 (s, 1H), 9.69 (br s, 1H). HRMS-ESI: calcd for $C_{24}H_{32}N_6O_4S^+$ 507.2190, found 507.2190.

Sildenafil precursor

The sildenafil precursor for radiolabeling was prepared following the procedure described in literature [26,26].

2-[2-Ethoxy-5-(piperazine-1-sulfonyl)-phenyl]-5-methyl-7-propyl-4a,7-dihydro-3H-imidazo[5,1-f][1,2,4]triazin-2-yl)-4-one (**13**)

of 4-ethoxy-3-(6,7-dihydro-1-methyl-7-oxo-3-propyl-1H-pyrazolo[4,3-d]pyrimidin-5-yl)benzene-1-sulfonyl chloride (**12**, A solution of (181 mg, 0.44 mmol, Toronto Research Chemicals Inc) in THF (15 mL) was treated with piperazine (189.7 mg. 2.2 mmol) in THF (4.4 mL). The mixture was stirred at room temperature for 2.5 h, solvent was removed at reduced pressure, and the residue was washed with cold water (18 mL). The resulting

precipitates were filtered under suction, washed with ice-cold water, drained to dryness (68. 3 mg, 0.15 mmol, 34 %).

^{1}H NMR ($CDCl_3$, 400 MHz): δ 1.02 (t, 3H, *J* 7.3), 1.65 (t, 3H, *J* 7.0), 1.82-1.90 (m, 2H), 2.91-2.96 (m, 6H), 3.03-3.06 (m, 4H), 4.28 (s, 3H), 4.38 (q, 2H), 7.15 (d, 1H, *J* 8.8r), 7.83 (dd, 1H, *J* 2.4 & 8.8r), 8.83 (d, 1H, *J* 2.4), 10.80 (br s, 1H). HRMS-ESI: calcd for $C_{21}H_{29}N_6O_4S^+$ 461.1971, found 461.1962

4-Benzylaminoquinoline derivatives

The precursor and reference compounds were prepared following procedures described by Bi et al [28,29] and Neise et al [30].

2-[(4-Cyano-2-ethylphenylamino)methylene]malonic acid diethyl ester (**16**)

To a solution of 4-amino-3-ethylbenzonitrile (**15**, 14.62 g, 100 mmol, Amfinecom Inc, Illinois, USA) in toluene (120 mL, Fisher Scientific, UK) was added diethyl 2-(ethoxymethylene)malonate (25 mL, 110 mmol, 1.1 eq) and the reaction mixture was refluxed for 6 h. 470 mL of heptane was poured into the reaction mixture, upon which a white precipitate was formed. This was filtered off under reduced pressure, and washed several times with heptane and dried under vacuum overnight (22.4 g, 70.8 mmol, 70.8 %)

^{1}H NMR ($CDCl_3$, 400 MHz): δ 1.26-1.38 (m, 9H, CH_3), 2.70 (q, 2H, *J* 7.5, CH_2), 4.24 (q, 2H, *J* 7.0, CH_2), 4.30 (q, 2H, *J* 7.0, CH_2), 7.26 (t, 1H, *J* 8.4, Ar), 7.48-7.56 (m, 2H, Ar), 8.49 (d, 1H, *J* 13.0, Ar), 11.32 (br d, 1H, *J* 12.7, NH). MS: $(M+H)^+$ m/z = 317

6-Cyano-8-ethyl-4-hydroxyquinoline-3-carboxylic acid ethyl ester (**17**)

Diphenyl ether (100 mL) was kept at vigorous reflux to which **16** (12 g, 37.9 mmol) was added in portions, over a course of one hour. The solution was further refluxed for an hour, cooled to RT and poured into heptane (200 mL). The resulting precipitate was filtered off and washed well with heptane to yield the title compound as a light brown solid (9.8 g, 36.3 mmol, 96 %).

MS: $(M+H)^+$ m/z = 271.0

4-Chloro-6-cyano-8-ethylquinoline-3-carboxylic acid ethyl ester (**18**)

To **17** (9.5 g; 35.2 mmol) was carefully added phosphorous (V) oxychloride ($POCl_3$, 45 mL) and the resulting mixture was refluxed for 48 h. The excess $POCl_3$ was evaporated under reduced pressure and the residue was co-evaporated once with CH_2Cl_2 and twice with toluene.

The resulting brown solid was dissolved in CH_2Cl_2 and treated with NEt_3 until aqueous washings of aliquots had pH > 10. The solution was then filtered through a short path of silica gel with 5 % ethylacetate/heptanes to give the title compound as an off-white solid (6.3 g, 21.8 mmol, 62.1 %).

MS: $(M+H)^+$ m/z = 289.6

4-(3-Chloro-4-methoxy-benzylamino)-6-cyano-8-ethyl-quinoline-3-carboxylic acid ethyl ester (**19**)

To a solution of **18** (2.4 g, 8.3 mmol) in *n*-propanol (40 mL) was added 3-chloro-4-methoxybenzyl amine hydrochloride (2 g, 11.7 mmol, 1.5 eq., ChemiCollect) and DIEA (8 mL, 46 mmol, ≈ 6 eq.). The mixture was refluxed for 2 h under vigorous stirring and thenwas cooled and poured into water (100 mL). The resulting precipitate was filtered, washed with water (100 mL) and ethanol (2 x 10 mL) respectively. The solid was then co-evaporated with ethanol to get the title compound as a white solid (3 g, 7.1 mmol, 86.7 %).

^{1}H NMR ($CDCl_3$, 400 MHz): δ 1.29-1.40 (m, 6H, $2CH_3$), 3.18 (q, 2H, *J* 7.4, CH_2), 3.90 (s, 3H, CH_3), 4.34 (q, 2H, *J* 7.1, CH_2), 4.83 (d, 2H, *J* 5.3, CH_2), 6.94 (d, 1H, *J* 8.4, Ar), 7.22-7.25 (m, 1H, Ar), 7.38 (s, 1H, Ar), 7.63 (s, 1H, Ar), 8.35 (s, 1H, Ar), 9.21 (s, 1H, Ar), 9.57 (br s, 1H, NH). MS: $(M+H)^+$ m/z = 424.7

4-(3-Chloro-4-methoxybenzylamino)-6-cyano-8-ethylquinoline-3-carboxylic acid (**20**, precursor).

A mixture of **19** (1 g, 2.4 mmol) and 12 mL each of THF, MeOH and 1M NaOH was stirred well. The solids gradually dissolved. After complete dissolution (3 h or more) THF and most of the MeOH was evaporated under reduced pressure to leave an aqueous slurry of a white solid. The slurry was acidified to pH 1.5 with HCl, stirred well for 1 h, and then filtered and washed well with water. Co-evaporation twice to dryness with absolute ethanol afforded the title compound as a white chalky solid (720 mg, 1.8 mmol, 77 % yield).

^{1}H NMR ($CDCl_3$, 400 MHz): δ 1.20 (t, 3H, CH_3), 3.06 (q, 2H, *J* 7.4, CH_2), 3.81 (s, 3H, CH_3), 4.90 (s, 2H, CH_2), 7.11 (d, 1H, *J* 8.4, Ar), 7.30 (d, 1H, *J* 8.3, Ar), 7.45 (s, 1H, Ar), 7.83 (s, 1H, Ar), 8.61 (s, 1H, Ar), 8.93 (s, 1H, Ar). HRMS-ESI: calcd for $C_{21}H_{19}ClN_3O_3^+$ 396.1115, found 396.1114; HRMS-ESI: calcd for $C_{21}H_{17}ClN_3O_3^-$ 394.0958, found 394.0946

4-(*3-Chloro-4-methoxy-benzylamino)-6-cyano-8-ethylquinoline-3-carboxylic acid methyl ester* (**21**) [30]

A solution of **20** (100 mg, 0.24 mmol) and 4-DMAP (26 mg, 0.208 mmol) in a mixture of 1 mL CH_2Cl_2 and 1 mL MeOH was stirred and cooled in an ice bath to 0 ^oC while dicyclohexylcarbodiimide (DCC, 60 mg, 0.29 mmol) was added over a period of 5 min. After additional 5 min of stirring at 0 ^oC the ice bath was removed and the reaction mixture was stirred overnight at RT. Precipitate of dicyclohexylurea was removed by filtration and the filtrate was washed with two 10 mL portion of 0.5 M HCl and two 10 mL portions of saturated $NaHCO_3$. Additional precipitate of dicyclohexyl was removed by filtration of both layers. The organic solution was dried over $MgSO_4$ and concentrated under reduced pressure. The residue was further purified by passing through silica gel with 5% ethylacetate/heptanes to afford **21** (65 mg, 0.16 mmol, 67 %).

^1H NMR ($CDCl_3$, 400 MHz): δ 1.32 (t, 3H, *J* 7.5, CH_3), 3.18 (q, 2H, *J* 7.4, CH_2), 3.90 (s, 6H, $2CH_3$), 4.83 (d, 2H, *J* 5.4, CH_2), 6.94 (d, 1H, *J* 8.4, Ar), 7.23 (d, 1H, *J* 7.0, Ar), 7.37 (s, 1H, Ar), 7.64 (s, 1H, Ar), 8.35 (s, 1H, Ar), 9.18 (s, 1H, Ar), 9.56 (br s, 1H, NH). HRMS-ESI: calcd for $C_{22}H_{21}ClN_3O_3^+$ 410.1271, found 410.1273

Ethoxyethlypyrazolopyrimidine derivatives

The various ehtoxyethylprazolopyrimidin derivatives including the two precursors for labeling and the references were prepared following procedures described in literature [31-36].

3-Ethyl-1H-pyrazole-5-carboxylic acid ethyl ester (**23**)

To a solution of 2-butanone (3.6 g, 50 mmol) in ethanol (250 mL) was added diethyl oxalate (8.8 g, 60.2 mmol) and *t*-BuOK (1 M solution in THF, 55 mL, 55 mmol, 1.1 eq.). The reaction mixture was heated at 75 °C for 0.5 h and cooled to 4 °C in an ice bath. A solution of hydrazine hydrochloride (6.9 g, 100.7 mmol,) in water (200 mL) was added drop wise and the resulting mixture was heated at 75 °C for 1 h. Solvent was removed under reduced pressure and residue partitioned between water and CH_2Cl_2. The organic layer was separated and dried over $MgSO_4$, filtered and concentrated to provide the title compound as a white solid (5.6 g, 44.1 mmol, 66%).

^1H NMR (400 MHz, $CDCl_3$): δ 1.28 (t, 3H, *J* 7.6), 1.39 (t, 3H, *J* 7.1), 2.72(q, 2H, *J* 7.6), 4.38 (q, 2H, *J* 7.1), 6.63 (s, 1H). MS: $(M+H)^+$ *m/z*= 169.0

3-Ethyl-1H-pyrazole-5-carboxylic acid (**24**)

To a solution of **23** (4.9 g, 38.6 mmol) in THF (270 mL) and methanol (60 mL) was added 1 N LiOH (60 mL, 60 mmol) and the reaction mixture was refluxed for 3 h. The solvent was evaporated to yield a white solid that was taken up in water (60 mL) and washed with toluene (3 x 30 mL). The pH of the water layer was adjusted to 1 with 1 M HCl and extracted with EtOAc (3 x 30 mL). The organic layer was dried over $MgSO_4$, filtered and concentrated. To the residue was added diethyl ether (100 mL) and this suspension was stirred for 1 hour. The white precipitate was filtered off and dried to provide the title compound (2.8 g, 25 mmol, 64.8 %).

^{1}H NMR (400 MHz, DMSO-d_6): δ 1.15 (t, 3H, *J* 7.6), 2.57 (q, 2H, *J* 7.6), 6.48 (s, 1H).

MS: $(M+H)^+$ *m/z*= 141.1.

3-Ethyl-4-nitro-1H-pyrazole-5-carboxylic acid (**25**)

A nitrating agent was prepared as follows: fuming sulphuric acid (4.6 mL) was added drop wise to stirred ice-cooled fuming nitric acid (4.16 mL). The ice bath was removed and the mixture was heated to 50 °C. To this mixture, **24** (3.9 g, 34.8 mmol) was added portion wise over a period 30 min, maintaining the reaction temperature below 60 °C. The resulting solution was heated overnight at 60 °C, cooled and poured into ice, providing a brown solid. This suspension was stirred at 0 °C for 1 h, filtered and dried in a vacuum oven at 50 °C. Yield 2.66 g (14.4 mmol, 41.4 %).

^{1}H NMR (400 MHz, DMSO-d_6): δ 1.22 (t, *J* 9.0, 3H), 2.90 (q, *J* 7.5, 2H).

3-Ethyl-4-nitro-1H-5-carboxamide (**26**)

To a solution of **25** (8.3 g, 44.8 mmol) in (was added) thionyl chloride (40 mL) under N_2 was (The reaction mixture was) refluxed for 3 h. Excess thionyl chloride was removed under reduced pressure vacuum. To remove residual traces of thionyl chloride, THF (2 x 20 mL) was added to the residue and evaporated at a reduced pressure. The acid chloride was suspended in THF (25 mL) and the mixture was cooled in an ice-bath. During 1 h gaseous ammonia was bubbled through the ice-cooled suspension. Water (25 mL) was added and the resulting mixture was evaporated under reduced pressure yielding a white solid. To this solid, water was added and after stirring for 1 h, the precipitate was filtered off and dried in vacuum oven. Yield 6.7 g (36.4 mmol, 81.3 %).

^{1}H NMR (400 MHz, DMSO-d_6): δ 1.21 (t, 3H, *J* 7.6), 2.91 (q, 2H, *J* 7.6), 7.70 (s, 1H), 7.97 (s, 1H). MS: $(M+Na^+)$ *m/z*= 206.3.

1-(2-Ethoxyethyl)-3-ethyl-4-nitro-1H-5-carboxamide (**27**)

To a solution of **26** (6.7 g, 34.6 mmol) in THF (100 mL) was added triphenylphosphine (11.5 g, 43.9 mmol, Janssen Pharmaceutica) and the reaction mixture was cooled to °C. 2-Ethoxyethanol (4.27 mL, 44mmol, Alfa Aesar Chemicals) was added drop wise and then a solution of di-*tert*-butyl azodicarboxylate (10 g, 43.4 mmol) in THF (50 mL) was added over a period of 2.5 h. After an additional stirring for 1 h at 0 °C and 1 h at room temperature, the reaction mixture was again cooled to 0 °C, treated with 6 M HCl (18 mL), slowly warmed up to 40 °C and stirred for 1 h. Most of the solvent was removed under reduced pressure and the residue was partitioned between ethyl acetate and water. The water layer was washed once with ethyl acetate and the combined organic layers were washed with water and brine, dried over $MgSO_4$, filtered and concentrated. The crude product was purified by chromatoghraphy on silica gel with 67 % EtOAc in heptane to give pure **27** (3.04 g, 34.4 %).

MS: ($M+Na^+$) *m/z*= 278.8.

1-(2-Ethoxyethyl)-3-ethyl-4-amino-1H-5-carboxamide (**28**)

To a solution of **27** (1.2 g, 4.5 mmol) in ethanol (22 mL), 10 % $Pd(OH)_2/C$ (200 mg) was added. Ammonium formate (1.4 g, 22 mmol) was added in 4 portions in a time span of 40 min. The mixture was refluxed for 2 h, cooled, filtered and concentrated. The dark red liquid was purified by column chromatography on silica gel with EtOAc/hepatane mixture to provide 687 mg (3.1 mmol, 69 %) of the title compound.

MS: ($M+Na^+$) *m/z*= 248.7.

1-(2-Ethoxyethyl)-3-ethyl-1H-pyrazolo[4,3-d]pyrimidine-5,7(4H,6H)-dione (**29**)

A mixture of **28** (1.1 g, 4.3 mmol) and carbonyldiimidazole (1.1 g, 6.7 mmol, Janssen Pharmaceutica) in acetonitrile (5 mL) was heated at 75 °C during 1 h and stirred at room temperature for 2 h. The reaction mixture was cooled in an ice bath and water (50 mL) was added. The formed precipitate was filtered off, washed with water, dried in a vacuum oven at 60 °C and used in the next step without further purification. Yield: 780 mg (3 mmol, 68 %).

MS: ($M-H^+$) *m/z*= 250.4.

5-7-Dichloro-1-(2-Ethoxyethyl)-3-ethyl-1H-pyrazolo[4,3-d]pyrimidine (**30**)

To a mixture of **29** (1.0 g, 4.8 mmol) and phenylphosphonic dichloride (7.8 g, 40 mmol) was heated under N_2 with stirring at 135 °C for 48 h. The reaction mixture was cooled, slowly

poured in an ice-water mixture and stirred for 3 h. The precipitate was filtered off, rinsed with water and suspended in a mixture of ethyl acetate (30 mL) and water (30 mL). The suspension was first acidified (pH 1-2) by addition of 1 M HCl and then neutralized by the addition of 10 % $NaHCO_3$ (pH 7). The organic layer was separated, washed with water and brine, dried over $MgSO_4$, filtered and concentrated. The residue was purified by column chromatography on silica gel with 9% EtOAc in heptane to provide 797 mg (2.8 mmol, 65%) of the title compound as colourless oil.

^{1}H NMR (400 MHz, $CDCl_3$): δ 1.05 (t, *J* 7.0, 3H), 1.40 (t, *J* 7.6, 3H), 3.02 (q, *J* 7.6, 2H), 3.42 (q, *J* 7.2, 2H), 3.81 (t, *J* 5.9, 2H), 4.80 (t, *J* 5.9, 2H). MS: $(M+H)^+$ *m/z*= 289.7.

5-Chloro-1-(2-ethoxyethyl)-3-ethyl-N-(4-methylpyridin-2-yl)-1H-pyrazolo[4,3-d]pyrimidin-7amine (**31**).

To an ice cold solution of **30** (757 mg, 2.6 mmol) in THF (7 mL) was added 2-amino-4-picoline (563 mg, 5.22 mmol) and 1M lithium bis(trimethylsilyl)amide in THF (2 x 2.6 mL, 5.2 mmol) at a temperature below 5 °C. The reaction mixture was stirred at 5 °C for 30 min, then the THF was evaporated under reduced pressure and the residue was neutralized by adding a solution of 10 % citric acid solution. The mixture was further stirred at 5 °C for 1 h, water was added and the resulting precipitate was filtered off, washed with water and dried in a vacuum oven at 50 °C yielding a yellow solid (816 mg, 2.3 mmol, 88.5 %).

^{1}H NMR (400 MHz, $CDCl_3$): δ 1.16 (t, 3H, *J* 7.0, CH_3), 1.37 (t, 3H, *J* 7.6, CH_3), 2.4 (s, 3H, CH_3), 2.96 (q, 2H, *J* 7.6, CH_2), 3.62 (q, 2H, *J* 6.9, CH_2), 3.90 (t, 2H, *J* 4.5, CH_2), 4.70 (br s, 2H, CH_2), 6.83 (s, *J* 4.5, 1H, Ar), 8.17 (d, *J* 4.5, 1H, Ar), 8.31 (s, 1H, Ar). MS: $(M+H)^+$ *m/z*= 361.16.

1-(2-Ethoxyethyl)-3-ethyl-N-(4-methylpyridin-2-yl)-5-(-piperazine-1-yl)-1H-pyrazolo[4,3-d]pyrimidin-7-amine (**32**, precursor).

A suspension of **31** (18 mg, 0.06 mmol) and piperazine (22 mg, 0.3 mmol) in 2-propanol (0.4 mL) in a reaction vial was heated for 45 min on an oil bath at 175 °C. The reaction mixture was cooled, concentrated and purified by passing through silica gel with CH_2Cl_2/MeOH/(25 %)NH_4OH (190/9/1) as the eluant. The fractions with the pure product were combined and solvent removed under reduced pressure. The obtained oil was dissolved in diethyl ether (10 mL) and treated with a solution of 4M HCl in methanol (0.5 mL). A yellow precipitate was formed, filtered off and dried in a vacuum oven. Yield: 12 mg (0.03 mmol, 48 %).

HRMS-ESI: calcd for $C_{21}H_{31}N8O^+$ 411.2621, found 411.2624.

1-(2-Ethoxyethyl)-3-ethyl-N-(4-methylpyridin-2-yl)-5-(4-methylpiperazine-1-yl)-1H-pyrazolo[4,3-d]pyrimidin-7-amine (**33**, reference)

The title compound was prepared following the procedure for the preparation of **32**, but replacing piperazine by *N*-methylpiperazine. Final purification was done using HPLC. (XTerra Prep RP18, 5 µM, 7.8 x 150 mm; Gradient: Water/ACN: 95 → 5 % over 20 minutes) semi-prep, gradient elution H_2O-ACN)

Yield: 8 mg (0.02 mmol, 36 %).HRMS-ESI: calcd for $C_{22}H_{33}N8O^+$ 425.2777, found 425.2770

Tert-butyl(1-(7-(4-methylpyridin-2-ylamino)-1-(2-ethoxyethyl)-3-ethyl-1H-pyrazolo[4,3-d]pyrimidin-5-yl)piperidin-4-yl)methylcarbamate (**34**)

A suspension of compound **31** (18 mg, 0.05 mmol) and *tert*-butyl (piperidin-4-yl)methylcarbamate (56 mg, 0.3 mmol, APOLLO Scientific) in 2-propanol in a reaction vial was heated at 175 °C for 45 min. After evaporation of the solvent under reduced pressure, the residue was purified by column chromatography on silica gel with gradient mixtures of ethylacetate and heptane as the eluant. Yield: 20 mg (0.04 mmol, 80 %) as yellow oil.

^{1}H NMR (400 MHz, $CDCl_3$): δ 1.13 (t, *J* 7.0, 3H), 1.25 (br s, 2H), 1.32 (t, *J* 7.6, 3H), 1.39 (s, 9H), 1.70 (d, *J* 11.7, 2H), 2.35 (s, 3H), 2.75-2.93 (m, 6H), 3.56 (q, *J* 7.0, 2H), 3.80 (t, *J* 4.6, 2H), 4.58-4.62 (m, 4H), 6.92 (d, 1H), 8.09 (s, 1H), 8.19 (d, *J* 5.0, 1H), 9.6 (s, 1H)

MS: $(M+H)^+$ *m/z*= 538.4.

5-(4-(Aminomethyl)piperidin-1-yl)-1-(2-ethoxyethyl)-3-eethyl-N-(4-methylpyridin-2-yl)-1H-pyrazolo[4,3-d]pyrimidin-7-amine (**35**, precursor)

Compound **34** (14 mg, 0.03 mmol) was suspended in CH_2Cl_2 (1 mL) and cooled to 0 °C under N_2, TFA (0.5 mL) was added drop-wise and the solution was stirred for 1 h and further at RT for 1 h. The reaction mixture was concentrated under reduced pressure; the residue was dissolved in toluene (1 mL), then concentrated again under reduced pressure and dried in vacuum oven. Yield: 10 mg (0.2 mmol, 87.7 %).

^{1}H NMR (400 MHz, DMSO-d_6): δ 1.08 (t, *J* 7.6, 3H), 1.20-1.36 (m, 7H), 1.84 (d, *J* 12.8, 2H), 2.41 (s, 3H), 2.75-2.90 (m, 4H), 3.02-3.06 (m, 2H), 3.50-3.53 (m, 2H), 3.81 (t, *J* 4.8, 2H), 4.50-4.75 (m, 4H), 7.05 (d, *J* 4.6, 1H), 7.91 (br s, 2H), 8.04 (s, 1H), 8.23 (d, *J* 5.5, 1H).

HRMS-ESI: calcd for $C_{23}H_{35}N_8O^+$ 439.2934, found 439.2939.

Tert-butyl(1-(7-(4-methylpyridin-2-ylamino)-1-(2-ethoxyethyl)-3-ethyl-1H-pyrazolo[4,3-d]pyrimidin-5-yl)piperidin-4-yl)methylmethylcarbamate (**36**)

Following the procedure for the preparation of **34**, but replacing *tert*-butyl (piperidin-4-yl)methylcarbamate by *tert*-butyl (piperidin-4-yl) methylmethylcarbamate provided the crude title compound. Yield 16 mg (0.03 mmol, 58 %).

^{1}H NMR (400 MHz, $CDCl_3$): δ 1.10-1.35 (m, 8H), 1.39 (s, 9H, boc), 1.61-1.67 (m, 2H), 1.90 (br s, 1H, NH), 2.33 (s, 3H, Me), 2.75-2.90 (m, 8H), 3.09 (d, 2H, *J* 7.0), 3.56 (q, *J* 7.0, 2H), 3.80 (t, *J* 4.5, 2H), 4.59-4.66 (m, 4H), 6.92 (d, 1H, *J* 5.0, Ar), 8.09 (s, 1H, Ar), 8.19 (d, 1H, *J* 5.0, Ar), 9.65 (s, 1H, NH). MS: $(M+H)^+$ *m/z*= 553.4.

1-(2-Ethoxyethyl)-3-ethyl-5-(4-((methylamino)methyl)piperidin-1-yl)-N-(4-methylpyridin-2-yl)-1H-pyrazolo[4,3-d]pyrimidin-7-amine (**37**, reference)

Following the procedure for the preparation of compound **35**, but starting from compound **36** provided the crude title compound. Yield 8 mg (0.02 mmol, 90 %)

^{1}H NMR (400 MHz, $CDCl_3$): δ 8.11 (d, 2H, *J* 5.2, Ar), 6.71 (d, 1H, *J* 4.8, Ar), 4.77 (d, 2H, *J* 12.7, CH_2), 4.59 (t, 2H, *J* 4.1, CH_2), 3.86 (t, 2H, *J* 4.1, CH_2), 3.58 (q, 2H, *J* 6.7, CH_2), 2.83-2.95 (m, 6H, $3CH_2$), 2.30 (s, 3H, CH_3), 1.85-1.92 (m, 2H, CH_2), 1.36-1.39 (m, 12H). MS:

HRMS-ESI: calcd for $C_{24}H_{37}N_8O^+$ 453.3090, found 453.3097.

In vitro PDEs inhibitory activity assay

***Table 1**. IC_{50} (µM) values of PDE5 inhibitors for the 11 PDE families*

Compounds		PDE1B1	PDE2A	PDE3B	PDE4D3	PDE5A3	PDE6AB	PDE7A1	PDE8A1	PDE9A	PDE10A2	PDE11A4
7	IC_{50}	0.84	8.80	5.72	6.17	0.0008	0.0031	30.20	30.20	0.81	2.56	0.81
8	IC_{50}	0.37	5.62	3.36	4.96	0.0011	0.0031	30.20	29.19	1.70	1.57	0.99
11	IC_{50}	0.41	9.02	3.68	3.94	0.0007	0.0023	26.04	30.20	0.75	2.32	0.70
14	IC_{50}	2.93	10.00	10.00	8.68	0.017	0.12	30.20	30.20	6.88	7.60	7.34
21	IC_{50}	30.20	2.40	10.00	30.20	0.008	0.08	30.2	30.20	30.20	0.9	7.8
33	IC_{50}	19.95	10.00	10.00	19.95	0.16360	0.3513	19.95	19.95	23.37	7.59	3.26
35	IC_{50}	30.20	9.55	10.00	5.14	0.0032	0.0008	30.20	22.15	30.20	0.47	0.01
37	IC_{50}	30.20	10.00	10.00	4.91	0.0032	0.0008	30.20	30.20	30.20	0.49	0.01

HPLC purification and quality control of labeled compounds

***Table 2**. Purification and analysis of radiotracers*

Radioligand	Mobile phase preparative HPLC (%, buffer in EtOH)	Rt (min)	Mobile phase analytical HPLC (%, buffer in ACN)	Rt (min)
[^{11}C]-**7**	67, 0.01 M Na_2HPO_4 pH 9	14.9	70, 0.01 M Na_2HPO_4 pH 9	10.1
[^{11}C]-**8**	67, 0.01 M Na_2HPO_4 pH 9	17.6	70, 0.01 M Na_2HPO_4 pH 9	9.8
[^{18}F]-**11**	67, 0.01 M Na_2HPO_4 pH 9	16.2	70, 0.01 M Na_2HPO_4 pH 9	12.8
[^{11}C]-**14**	65, 0.01 M Na_2HPO_4 pH 9	16	** 65, 0.01 M Na_2HPO_4 pH 9	6.8
[^{11}C]-**21**	45, 0.01 M NaOAc pH 5.5	10.8	70, 0.01 M NaOAc pH 5.5	7.5
[^{11}C]-**33**	70, 0.05 M NaOAc pH 5.5	16	70, 0.05 M NaOAc pH 5.5	6.3
[^{11}C]-**37**	*70 , 0.01 M Na_2HPO_4 pH 9	22	70, 0.01 M Na_2HPO_4 pH 9	14.9

R_t (retention time), ACN (acetonitrile),
* ACN instead of EtOH
** XTerra®, RP18 3.5 µm, 3 mm x100 mm

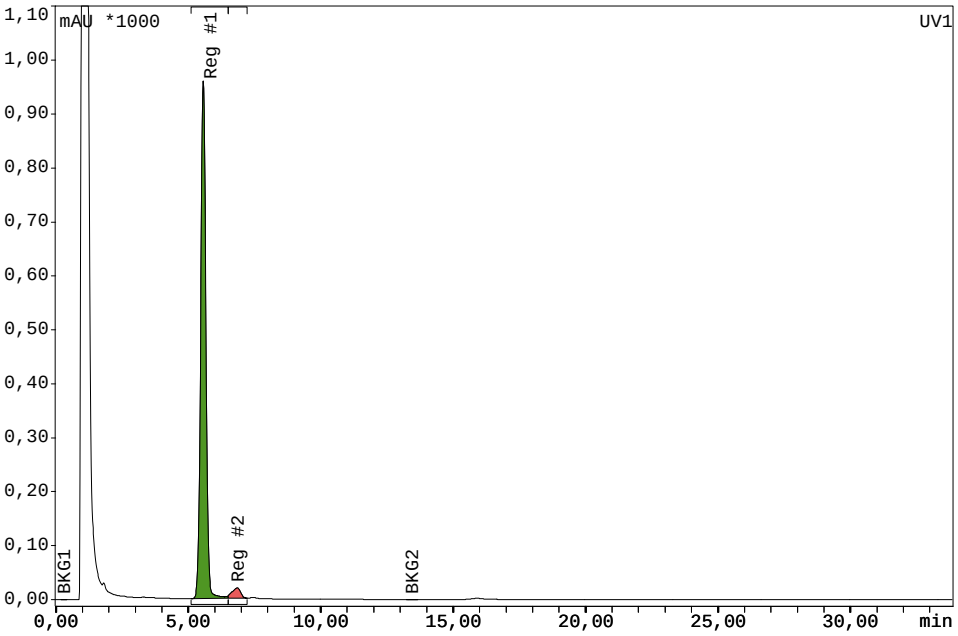

***Figure 1**. Chromatogram of* chemical purity determination of precursor (**5**)

UV1 integration

Substance	R/T	Area	%Area
	min	mAU*s	%
Reg #1	5,57	12925,81	96,83
Reg #2	6,85	423,82	3,17
Sum in ROI		13349,63	

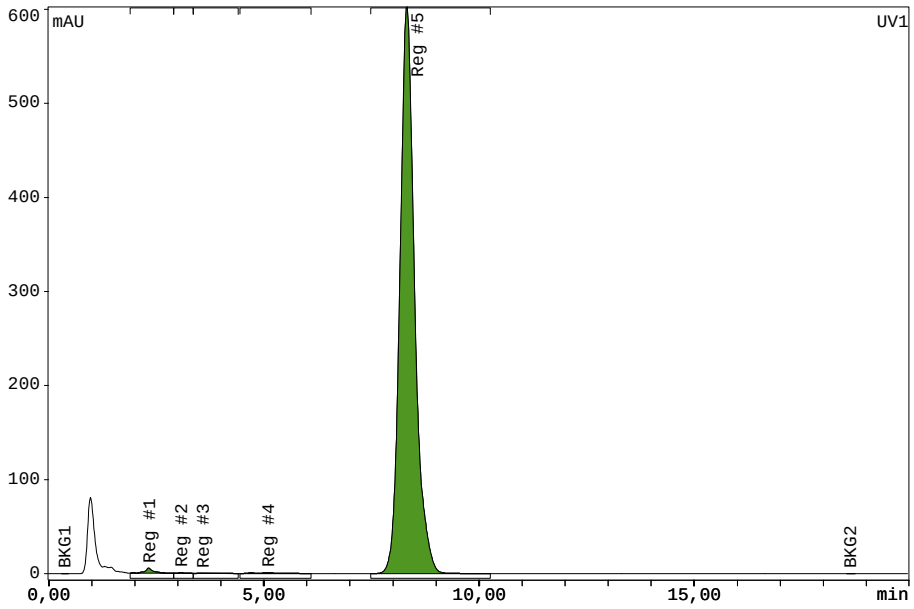

***Figure 2**. Chromatogra of* chemical purity determination of reference (**7**).

UV1 Integeration

Substance	R/T	Area	%Area
	min	mAU*s	%
Reg #1	2,33	73,10	0,51
Reg #2	3,07	4,73	0,03
Reg #3	3,57	9,29	0,06
Reg #4	5,08	37,07	0,26
Reg #5	8,33	14259,10	99,14
Sum in ROI		14383,30	

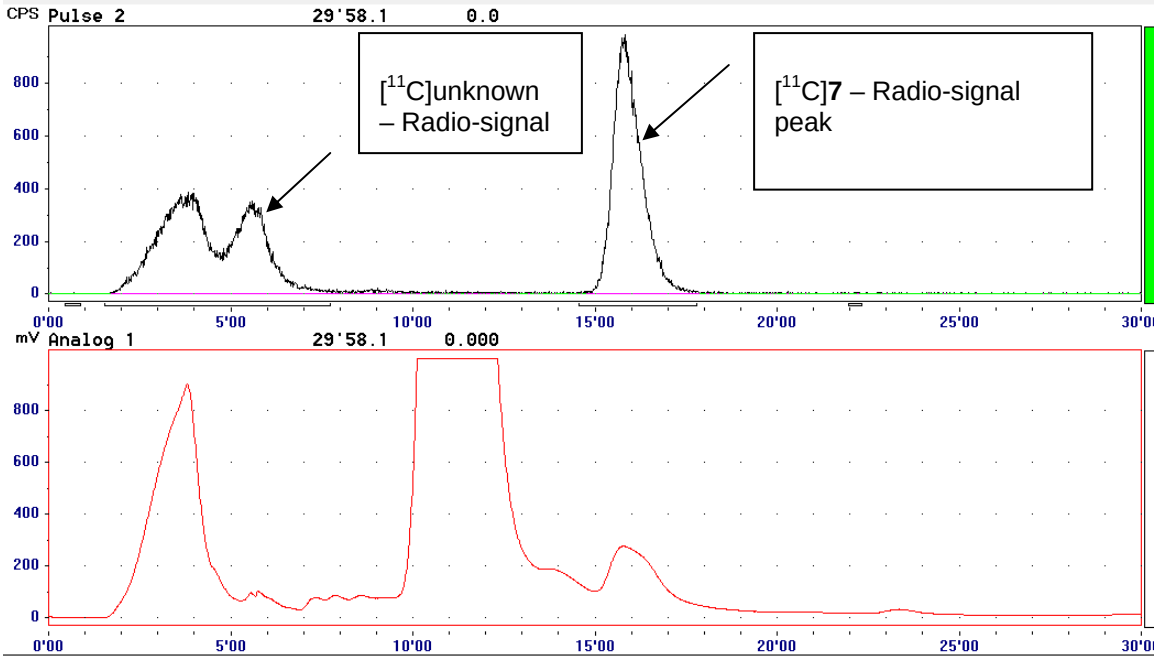

***Figure 3.** Radio-chromatograms of RP-HPLC purification of [^{11}C]**7**.*

Integration ChA

Substance	R/T	Area	%Area
	min	C/S*s	%
Reg #1	3.50	59273.8	53.46
Reg #2	15.49	51596.2	46.54
Sum in ROI		110870.0	

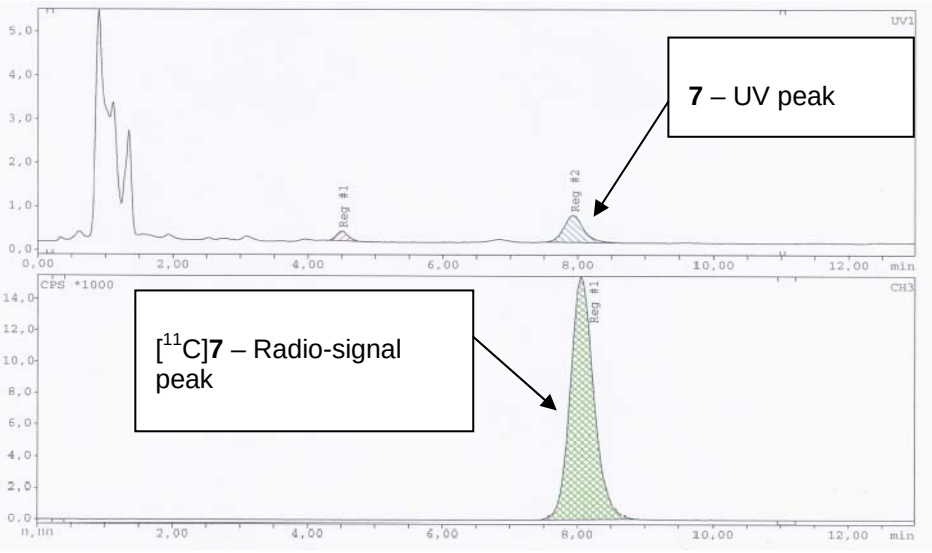

Figure 4. *Radio-chromatograms of RP-HPLC of quality control (chemical and radiochemical purity control) of [^{11}C]**7***

Integration ChA			
Substance	R/T	Area	%Area
	min	C/S*s	%
Reg #1	8.05	374051.6	100
Integration UV1			
Substance	R/T	Area	%Area
	min	mAU*s	%
Reg #1	4.50	0.97	3.16
Reg #2	7.93	29.7	96.84
Sum in ROI		30.67	

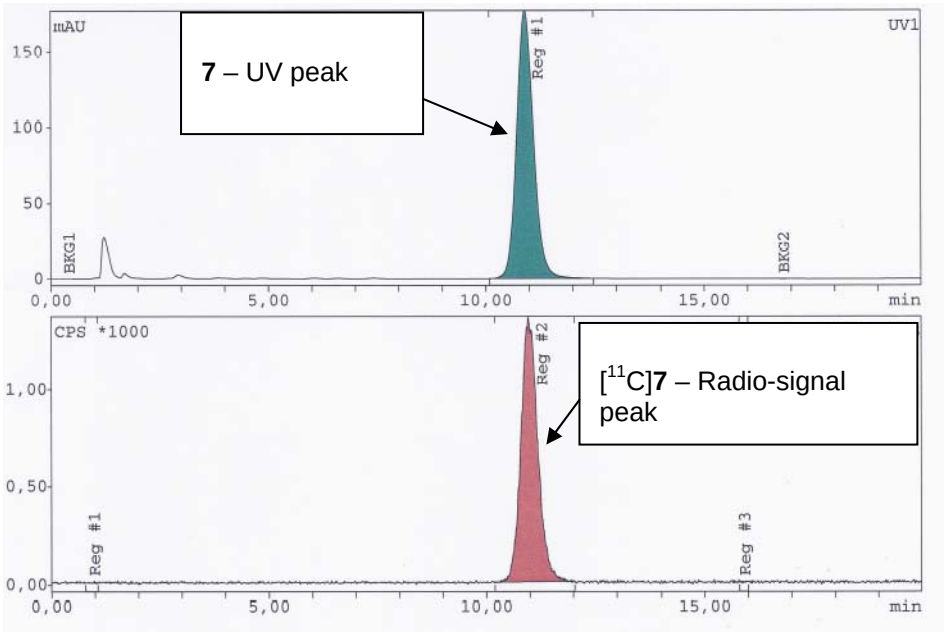

Figure 5. *Radio-chromatograms of RP-HPLC for identity confirmation by co-injection of standard non-radioactive reference* ***7*** *with the isolated radioactive formulation of [*^{11}*C]****7****.*

Integration ChA			
Substance	R/T	Area	%Area
	min	C/S*s	%
Reg #1	10.97	36121.33	100
Integration UV1			
Substance	R/T	Area	%Area
	min	mAU*s	%
Reg #1	10.90	4764.359	100.00

Specific activity determination

The specific radioactivity of the tracer formulation defined as the radioactivity divided by the mass amount was determined by analytical HPLC (QC HPLC system). UV detection was done at the λmax of the authentic reference material.

A UV calibration curve was constructed using three concentrations of the reference material (1, 5 and 10 µg/mL dissolved in the formulation vehicle). 20 µL of each concentration was injected onto HPLC in order to determine the UV absorption corresponding to the injected mass. The experiment was done in triplicate for each concentration. A linear equation was derived from the mass (nmol) – UV response (area under the curve for absorption).

At the end of radiosynthesis, the concentration of the formulation was measured. An aliquot (20 µL) of the formulation was injected onto the QC HPLC system and the corresponding UV absorption was used to back calculate the mass of the compound (both labeled and unlabeled) in 20 µL formulation using the linear response of the calibration curve. The total mass of the compound in total volume of the formulation was determined. With the use of the molecular weight of the reference and the total amount of compound in the formulation, the mole weight was calculated which was subsequently used to calculate the specific activity of the radiotracer solution at the end of formulation.

However, since there might be differences in response of UV detector either due to UV lamp life time (decreased energy) or the use of different HPLC system other than the one used for developing calibration curve, a onetime injection of a known amount (20 µL of a 1 µg/mL or 20 µL of a 10 µg/mL) of reference solution (before QC analysis) was used in order to determine specific activity of subsequent radiolabeling formulation.

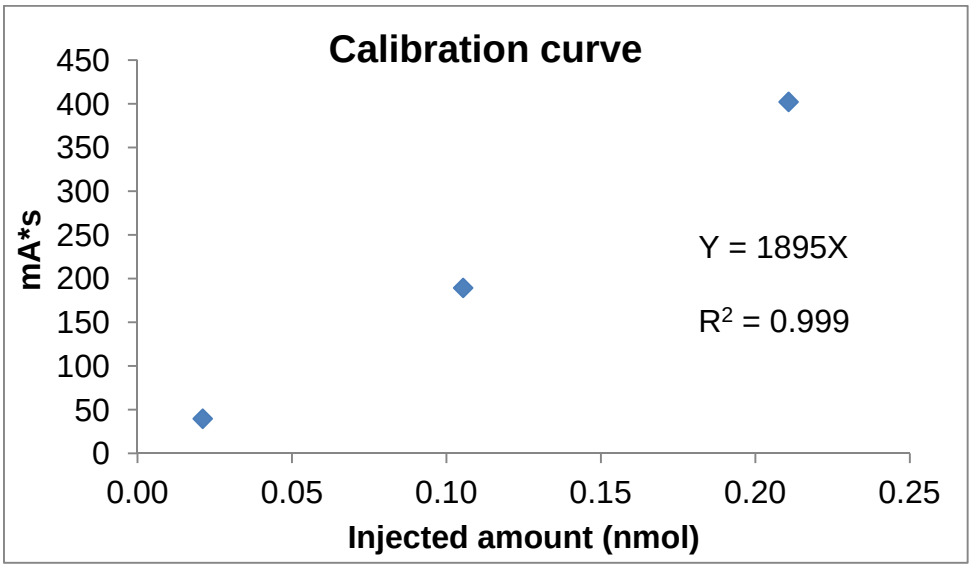

***Figure 6**. Calibration curve developed for NMVardenafil. Each point is a triplicate.*

Example: [^{11}C]NMVardenafil formulation was 621.6 MBq (16.8 mCi) in 7 mL sterile filtered solution at EOS. Injection of 20 µL of tracer formulation onto the analytical QC HPLC system gave absorption of 26.3 mAu*s (area under the curve, AUC). On that same day injection of 20 µL of 10 µg/mL solution of cold NMVardenafil gave absorption of 483.8 mAu*s (AUC). The mass amount in the radioactive formulation was determined using following equation:

$$y = mx \qquad eq\ 1$$

*y is absorption (mAu*s), m is slope (mAu*s/nmol) and x is amount of compound both labeled and unlabeled (nmol) in the injected volume (20 µL)*

We get slop of 1148 mAu*s/nmol for 20 µL of a 10 µg/mL solution of reference compound (474.58 g/mol) and the origin (0,0). Using the slop and 26.3 mAu*s absorption (AUC) for the tracer formulation, the amount of labeled and unlabeled compound will be 22.91 pmol in 20 µL of tracer solution. We get 8.0185 nmol as the total amount of labeled and unlabeled compound in 7 mL formulation. Specific activity is calculated as: radioactivity (GBq) / mass (µmol)

$$SA = Activity/amount\ of\ labeled\ and\ unlabed\ compound \qquad eq\ 2$$

For 621.6 MBq of [^{11}C]NMVardenafil, the specific activity will be 77.5 GBq/µmol at end of formulation.

Biological evaluations of labeled PDE5 inhibitors

Biodistribution – [^{11}C]-7

***Table 3**. Biodistribution of [^{11}C]-**7** in NMRI mice at 2, 10, 30 and 60 min post injection (n = 4 at each time point, SD = standard deviation)*

	percentage of injected Dose (% ID±SD)			
Organs	2min	10min	30min	60min
bladder/urine	0.2±0.0	0.6±0.1	2.2±0.6	2.7±0.1
kidneys	9.2±2.2	5.2±0.4	2.5±0.4	2.8±0.2
liver	22.5±2.5	27.5±1.0	16.5±2.1	20.2±1.5
spleen	0.7±0.1	0.9±0.3	0.4±0.1	0.7±0.2
Pancreas	1.5±0.4	1.3±0.7	0.8±0.2	0.5±0.1
lungs	8.1±0.8	5.8±0.8	5.9±1.0	5.1±0.3
heart	0.9±0.2	0.4±0.1	0.3±0.0	0.4±0.1
intestines	11.0±1.1	18.2±1.5	32.3±6.1	35.4±1.5
stomach	1.6±0.1	2.5±0.6	5.5±2.7	3.5±0.9
cerebrum	0.1±0.0	0.1±0.0	0.2±0.0	0.2±0.0
cerebellum	0.0±0.0	0.0±0.0	0.1±0.1	0.1±0.0
blood	6.2±0.2	5.3±0.4	3.3±0.3	3.3±0.3
Penis			0.1±0.0	

*Data are expressed as mean±SD; percentage of injected dose calculated as CPM in organ * 100%/total CPM recovered*

***Table 4**. Uptake values of [^{11}C]-**7** at 2, 10, 30 and 60 min post injection in NMRI mice (n = 4 at each time point, SD = standard deviation)*

	standard uptake values (SUV±SD)			
	2 min	10 min	30 min	60 min
kidneys	5.7±1.2	3.4±0.4	1.3±0.1	1.6±0.1
liver	4.9±0.7	5.6±0.2	3.5±0.4	4.1±0.3
spleen	2.6±0.4	2.5±0.1	1.4±0.3	1.8±0.3
Pancreas	1.8±0.5	2.1±0.2	1.1±0.2	1.1±0.2
lungs	10.2±2.6	6.6±0.9	8.0±1.9	6.5±1.9
heart	1.9±0.4	0.9±0.1	0.7±0.1	0.7±0.1
intestines	1.3±0.1	2.1±0.2	3.5±0.6	4.0±0.4
stomach	1.1±0.2	1.1±0.3	2.5±0.9	1.3±0.4
Cerebrum	0.1±0.0	0.1±0.0	0.2±0.0	0.2±0.0
cerebellum	0.1±0.0	0.0±0.0	0.2±0.0	0.2±0.1
blood	1.2±0.3	0.7±0.3	0.7±0.3	0.3±0.1
Muscle	0.8±0.3	0.3±0.1	0.4±0.1	0.3±0.0
Penis			0.7±0.1	

*Data are expressed as mean±SD; SUV calculated as (CPM in organ * Weigh of mouse)/(total CPM recovered * Weight of organ)*

Biodistribution – [^{11}C]-8

***Table 5**. Biodistribution of [^{11}C]-**8** in NMRI mice at 2 and 30 min post injection (n = 4 at each time point, SD = standard deviation)*

percentage of Injected Dose (% ID±SD)			Standard uptake value (SUV±SD)	
organ	2 min	30 min	2 min	30 min
bladder/urine	0.5±0.2	5.2±1.3		
kidneys	25.9±3.2	5.6±1.0	16.4±1.3	3.7±0.6
liver	29.0±4.0	23.2±3.9	6.1±1.2	4.8±0.9
spleen	1.16±0.1	0.3±0.1	3.5±0.2	1.0±0.3
Pancreas	0.7±0.2	0.8±0.1	1.4±0.2	1.3±0.1
lungs	4.5±1.1	3.2±0.4	4.4±0.7	3.8±1.2
heart	0.8±0.1	0.1±0.0	1.9±0.2	0.3±0.1
intestines	10.4±1.2	39.5±3.2	1.2±0.1	4.8±0.3
stomach	1.1±0.1	2.5±0.5	0.6±0.1	1.5±0.4
cerebrum	0.0±0.0	0.0±0.0	0.0±0.0	0.0±0.0
cerebellum	0.0±0.0	0.0±0.0	0.1±0.0	0.1±0.0
blood	4.2±0.1	1.6±0.2	0.6±0.0	0.2±0.0
muscle			0.4±0.1	0.3±0.0
penis	0.0±0.0	0.1±0.0	0.3±0.0	0.5±0.1

*Data are expressed as mean±SD; percentage of injected dose calculated as CPM in organ * 100%/total CPM recovered; SUV calculated as (CPM in organ * Weigh of mouse)/(total CPM recovered * Weight of organ)*

Biodistribution – [^{18}F]-11

***Table 6**. Biodistribution of [^{18}F]-**11** in NMRI mice at 2, 30 and 60 min post injection (n = 4 at each time point, SD = standard deviation)*

percentage of Injected Dose (% ID±SD)				Standard uptake value (SUV±SD)		
organ	2 min	30 min	60 min	2 min	30 min	60 min
bladder/urine	0.1±0.1	3.0±0.6	5.3±0.2			
kidneys	13.0±1.5	3.0±0.6	2.0±0.1	7.3±0.8	1.8±0.3	1.2±0.0
liver	17.4±4.3	8.7±0.4	6.5±0.8	4.0±1.2	2.0±0.1	1.5±0.1
spleen	0.8±0.1	0.4±0.1	0.2±0.0	5.5±1.9	2.0±0.1	1.4±0.2
Pancreas	1.0±0.2	0.5±0.1	0.4±0.1	2.0±0.1	0.9±0.1	0.8±0.1
lungs	10.2±1.6	6.4±1.6	3.6±0.6	19.0±2.6	8.9±0.8	4.8±1.3
heart	1.1±0.2	0.5±0.1	0.5±0.1	2.4±0.3	1.2±0.1	1.1±0.1
intestines	11. 7±1.3	20.7±3.1	22.2±1.3	1.2±0.1	2.2±0.2	2.5±0.2
stomach	2.0±0. 5	3.1±0.3	3.8±0.6	1.3±0.4	2.0±0.3	2.6±0.2
cerebrum	0.1±0.1	0.7±0.1	0.8±0.2	0.2±0.1	0.9±0.1	1.1±0.1
cerebellum	0.0±0.0	0.2±0.0	0.2±0.0	0.2±0.1	1.2±0.1	1.6±0.1
blood	9.4±1.6	8.5±0.5	7.8±0.3	1.3±0.2	1.2±0.1	1.1±0.0
muscle				0.8±0.3	0.7±0.1	0.7±0.0
penis	0.0±0.0	0.1±0.0	0.2±0.0	0.5±0.1	1.3±0.1	1.5±0.1

*Data are expressed as mean±SD; percentage of injected dose calculated as CPM in organ * 100%/total CPM recovered; SUV calculated as (CPM in organ * Weigh of mouse)/(total CPM recovered * Weight of organ)*

Biodistribution – [^{11}C]-14

***Table 7**. Biodistribution of [^{11}C]-**14** (sildenafil) in NMRI mice at 2 and 30 min post injection (n = 4 at each time point, SD = standard deviation)*

percentage of Injected Dose (% ID±SD)			Standard uptake value (SUV±SD)	
organ	2 min	30 min	2 min	30 min
bladder/urine	0.2±0.2	2.3±0.3		
kidneys	12.5±3.4	8.7±6.3	9.2±2.2	5.0±3.6
liver	21.2±6.8	18.0±1.6	5.0±1.9	3.5±0.3
spleen	0.2±0.3	0.0±0.0	1.0±1.7	0.0±0.0
Pancreas	1.4±0.3	1.0±0.3	2.2±0.5	1.2±0.2
lungs	4.8±0.9	1.0±0.1	9.5±1.2	1.5±0.2
heart	1.3±0.1	0.3±0.0	3.2±0.2	0.7±0.1
intestines	9.8±2.7	25.5±1.7	1.2±0.3	3.0±0.2
stomach	1.4±0.5	5.8±1.1	0.7±0.3	3.4±1.4
cerebrum	0.1±0.0	0.2±0.0	0.2±0.0	0.3±0.0
cerebellum	0.0±0.0	0.1±0.0	0.2±0.0	0.3±0.1
blood	8.2±0.8	3.7±0.5	1.2±0.1	0.5±0.1
muscle			1.0±0.4	0.5±0.0
penis	0.1±0.0	0.1±0.0	0.5±0.2	1.0±0.2

*Data are expressed as mean±SD; percentage of injected dose calculated as CPM in organ * 100%/total CPM recovered; SUV calculated as (CPM in organ * Weigh of mouse)/(total CPM recovered * Weight of organ)*

Biodistribution – [^{11}C]-21

Table 8. *Biodistribution of [^{11}C]-**21** in NMRI mice at 2, 10, 30 and 60 min post injection (n = 4 at each time point, SD = standard deviation)*

	percentage of Injected Dose (% ID±SD)			
Organs	2min	10min	30min	60min
bladder/urine	0.1±0.0	0.2±0.1	1.2±0.2	2.1±1.4
kidneys	7.3±0.9	2.7±0.2	2.2±0.3	1.6±0.3
liver	51.6±3.8	40.7±3.7	14.2±1.1	20.4±2.6
spleen	0.5±0.10	0.2±0.0	0.3±0.2	0.1±0.0
Pancreas	0.7±0.1	0.9±0.4	0.6±0.2	0.3±0.1
lungs	3.3±0.4	1.0±0.1	0.7±0.1	0.5±0.2
heart	2.1±0.2	0.7±0.1	0.4±0.1	0.2±0.0
intestines	5.6±0.3	12.6±2.8	31.1±3.1	42.6±4.7
stomach	1.2±0.4	1.4±0.4	2.9±2.8	0.8±0.3
cerebrum	0.3±0.0	0.4±0.0	0.3±0.0	0.2±0.0
cerebellum	0.1±0.0	0.2±0.1	0.1±0.0	0.1±0.0
blood	6.1±0.6	2.8±0.2	2.8±0.0	1.6±0.3
penis			0.1±0.0	

*Data are expressed as mean±SD; percentage of injected dose calculated as CPM in organ * 100%/total CPM recovered*

Table 9*. Uptake values of [^{11}C]-**21** at 2, 10, 30 and 60 min post injection in NMRI mice (n = 4 at each time point but at 30 min; n = 7, SD = standard deviation)*

	standard uptake values (SUV±SD)			
	2 min	10 min	30 min	60 min
kidneys	4.7±0.6	1.5±0.1	1.3±0.1	0.9±0.1
liver	11.7±1.9	7.5±1.1	3.5±0.3	4.0±0.6
spleen	1.3±0.4	0.3±0.1	1.0±0.4	0.3±0.1
pancreas	1.3±0.3	1.3±0.4	1.1±0.2	0.4±0.2
lungs	6.1±1.3	1.5±0.1	1.0±0.2	0.7±0.2
heart	5.4±0.9	1.5±0.1	1.1±0.3	0.5±0.0
intestines	0.7±0.2	1.3±0.3	1.3±0.9	4.9±0.6
stomach	0.6±0.2	0.5±0.2	2.6±1.0	0.4±0.1
cerebrum	0.5±0.1	0.5±0.0	0.5±0.1	0.2±0.0
cerebellum	0.5±0.1	0.6±0.1	0.5±0.0	0.2±0.1
blood	1.1±0.4	0.4±0.1	0.4±0.0	0.2±0.1
muscle	0.6±0.2	0.7±0.1	0.6±0.0	0.4±0.1
penis			0.5±0.1	

*Data are expressed as mean±SD; SUV calculated as (CPM in organ * Weigh of mouse)/(total CPM recovered * Weight of organ)*

Plasma radiometabolite analysis – [^{11}C]-21

***Table 10**. Plasma radiometabolite analysis of [^{11}C]-21*

	Metabolite (%)	Intact (%)
2 min	4.6	95.4
30 min	41.5	58.5

Biodistribution – [^{11}C]-33

***Table 11**. Biodistribution of [^{11}C]-**33** in NMRI mice at 2 and 30 min post injection (n = 4 at each time point, SD = standard deviation)*

	percentage of Injected Dose (% ID±SD)		Standard uptake value (SUV±SD)	
organ	2 min	30 min	2 min	30 min
bladder/urine	0.1±0.0	0.9±0.2		
kidneys	14.3±1.9	4.9±0.4	7.8±0.9	3.3±0.8
liver	17.7±2.5	20.3±2.7	4.2±0.6	4.4±0.9
spleen	0.9±0.2	0.6±0.2	3.1±0.1	2.7±0.6
Pancreas	0.8±0.2	1.6±0.5	1.4±0.1	3.1±0.6
lungs	5.1±1.0	1.7±0.3	7.2±0.5	2.7±0.4
heart	1.2±0.4	0.4±0.1	2.5±0.5	0.9±0.1
intestines	8.6±0.1	18.0±1.9	1.1±0.1	2.5±0.2
stomach	1.1±0.1	4.0±0.6	0.9±0.1	3.8±0.8
cerebrum	0.5±0.2	0.2±0.1	0.6±0.2	0.3±0.1
cerebellum	0.2±0.0	0.1±0.0	0.7±0.2	0.3±0.1
blood	3.2±0.4	1.8±0.3	0.5±0.0	0.3±0.0
muscle			0.7±0.2	0.4±0.1
penis	0.0±0.0	0.1±0.0	0.6±0.1	0.6±0.1

*Data are expressed as mean±SD; percentage of injected dose calculated as CPM in organ * 100%/total CPM recovered; SUV calculated as (CPM in organ * Weigh of mouse)/(total CPM recovered * Weight of organ)*

Biodistribution – [^{11}C]-37

***Table 12**. Biodistribution of [^{11}C]-**37** in NMRI mice at 2, and 30 min post injection (n = 4 at each time point, SD = standard deviation)*

percentage of Injected Dose (% ID±SD)			Standard uptake value (SUV±SD)	
organ	2 min	30 min	2 min	30 min
bladder/urine	0.7±0.9	0.8±0.3		
kidneys	18.1±8.4	11.6±1.0	10.9±5.3	7.5±1.3
liver	19.7±9.5	30.0±1.0	4.3±2.2	6.4±0.3
spleen	1.0±0.5	1.5±0.9	3.9±1.8	2.8±0.7
Pancreas	1.1±0.5	1.8±0.4	1.8±0.8	2.3±0.3
lungs	4.5±1.7	4.4±1.2	7.6±3.2	6.6±1.5
heart	1.4±0.5	0.7±0.2	3.5±1.4	1.1±0.2
intestines	6.6±3.5	16.8±1.2	0.7±0.4	2.0±0.2
stomach	1.1±0.7	2.±0.4	0.5±0.2	1.3±0.1
cerebrum	0.1±0.1	0.0±0.0	0.2±0.1	0.1±0.0
cerebellum	0.1±0.1	0.0±0.0	0.3±0.3	0.1±0.0
blood	3.7±0.6	2.8±0.5	0.5±0.1	0.2±0.0
muscle	0.2±0.1	0.1±0.	1.6±1.2	0.5±0.1
penis	0.2±0.2	0.0±0.0	1.7±2.2	0.3±0.0

*Data are expressed as mean±SD; percentage of injected dose calculated as CPM in organ * 100%/total CPM recovered; SUV calculated as (CPM in organ * Weigh of mouse)/(total CPM recovered * Weight of organ)*

Blocking study in NMRI mice

***Table 13**. Comparison of pre-blocking effect on the uptake of [^{11}C]-**7** and [^{11}C]-**37** at 30 min post injection in control and tadalafil pre-treated NMRI mice (n = 4, SD = standard deviation)*

% Injected dose (%ID±SD)*				
	[^{11}C]-**7**		[^{11}C]-**37**	
organ	**Control**	**Tadalafil treated**	**Control**	**Tadalafil treated**
Kidneys	2.5±0.4	3.5±0.5	11.6±1.0	12.5±1.4
Liver	16.5±2.1	22.2±1.6	30.0±0.9	28.6±3.6
Lungs	5.9±1.1	0.8±0.2	4.4±1.2	2.3±0.6
Heart	0.3±0.0	0.3±0.0	0.6±0.0	0.4±0.0
Intestines	32.2±6.1	33.9±1.9	16.7±1.2	16.6±2.0
Blood	3.3±0.3	4.3±0.1	2.8±0.5	1.8±0.2
Muscle	0.1±0.1	0.1±0.0	0.1±0.	0.1±0.1
Penis	0.1±0.0	0.1±0.0	0.0±0.0	0.1±0.0

*Data are expressed as mean±SD; *percentage of injected dose calculated as CPM in organ * 100%/total CPM recovered*

Chapter III

[^{11}C]NMVardenafil: A PET Radioligand for *in vivo* Visualization of Phosphodiesterase Type 5 (PDE5)

Rufael Chekol[1]; Dieter Dauwe[2]; Andrey Postnov[3]; Peter Pokreisz[2]; Michel Koole[4]; Stefan Janssens[2]; Alfons Verbruggen[1]; Guy Bormans[1]; Olivier Gheysens[3]

[1]KU Leuven, Department of Pharmaceutical and Pharmacological Sciences, Laboratory of Radiopharmacy, Leuven, Belgium

[2]KU Leuven, Department of Cardiovascular Sciences, Leuven, Belgium and Department of Cardiology, University Hospital Leuven, Belgium

[3]KU Leuven, Department of Imaging and Pathology, Leuven, Belgium and Nuclear Medicine, University Hospital Leuven, Leuven Belgium

[4] Department of Nuclear Medicine, University Medical Center Groningen, Groningen, The Netherlands

Abstract

Introduction: The cyclic guanosine monophosphate (cGMP) specific phosphodiesterase type 5 (PDE5) is considered to play an important role in a variety of diseases such as pulmonary arterial hypertension (PAH) and chronic heart failure. This PDE5 modulation represents an important prognostic and/or therapeutic target; however, there is currently no method available to non-invasively assess the spatial and temporal changes of PDE5 expression levels *in vivo*. Therefore, we aimed to develop a PDE5-specific PET imaging probes.

Methods: [^{11}C]NMVardenafil (a close analogue of vardenafil) was synthesized and evaluated in transgenic mice with cardiomyocyte-specific PDE5 over-expression (PDE5 TG), monocrotalin (MCT) treated rats and a pig.

Results: [^{11}C]NMVardenafil showed a selective and specific retention in the myocardium of PDE5 TG mice which could significantly be blocked by tadalafil, a structurally unrelated PDE5-specific inhibitor. Rats and pigs showed high tracer retention in the lungs, in agreement with the abundant and constitutive expression of the PDE5 enzyme in this organ. [^{11}C]NMVardenafil retention in lungs of MCT treated rats was not significantly different compared to control rats.

Conclusions: [^{11}C]NMVardenafil showed selective, specific and high affinity binding to PDE5 *in vivo*. [^{11}C]NMVardenafil has been selected as lead candidate for further clinical investigation in patients with pulmonary hypertension or patients with end-stage heart failure awaiting heart transplantation.

1. Introduction

Phosphodiesterase inhibitors have been used for more than two thousand years since the advent of coffee in East Africa but only during the last 60 years these enzymes have been isolated and characterized (1). Phosphodiesterases (PDEs) are a superfamily of intracellular enzymes that catalyze the degradation of cyclic nucleotides (cyclic adenosine monophosphate/cAMP and cyclic guanosine monophosphate/cGMP). There are 11 families of PDEs (PDE1 through PDE11) of which some specifically catalyze the degradation of cAMP (PDE4, PDE7 and PDE8) while others are cGMP specific (PDE5, PDE6 and PDE9) and remaining families catalyze hydrolysis of both cAMP and cGMP with different affinities (2, 3).

Phosphodiesterase 5 (PDE5) is a cGMP-specific esterase that is expressed in vascular smooth muscle cells, lungs, platelets, corpus cavernosum and Purkinje fibers in the cerebellum (2, 3). PDE5 plays an important role in regulating vascular smooth muscle tone in pulmonary vasculature, platelet aggregation, handling of sodium secretion in renal cells, neuronal excitability, synaptic plasticity, neurogenesis and apoptosis (3, 4). In addition, PDE5 is implicated in a number of diseases including pulmonary arterial hypertension (PAH), atherosclerosis, and in ischemic and dilated cardiomyopathy. There is increasing evidence that PDE5 plays a major role during disease progression of heart failure and cardiomyopathy even though PDE5 is not expressed to any significant level in the healthy myocardium (3, 5-10). Recent studies reported significantly increased PDE5 expression in right and left ventricles of patients with pulmonary hypertension or an end-stage phase of ischemic and dilated cardiomyopathy (6-10). In mammalian experimental models, depletion of cGMP by excessive levels of PDE5 aggravated cardiac remodeling and suppressed cardiac contractile reserve after myocardial infarction or induced heart failure (7-10). In addition, preclinical and clinical data suggest that inhibition of PDE5 using vardenafil, a PDE5 inhibitor used for treating erectile dysfunction, reverses pathological remodeling and improves global cardiac function and quality of life (11-13). Therefore, [^{11}C]NMVardenafil was evaluated in transgenic mice with up to 10-fold myocardiocyte-specific PDE5 over-expression (PDE5 TG) in order to assess its uptake and retention in myocardium (7, 10).

Besides its role in cardiomyopathy, abundant expression of PDE5 in the lungs is a strong basis for using PDE5 inhibitors in PAH patients (14). Black and colleagues also reported elevated expression of PDE5 in pulmonary hypertensive lambs (15). PDE5 inhibitors in

general and vardenafil in particular have been shown to be beneficial in alleviating and reversing pulmonary arterial hypertension in rats (16-18).

The development of a PDE5 specific PET radioligand can be of particular interest to assess and quantify spatial and temporal changes in PDE5 expression as a function of disease progression and to quantify PDE5 occupancy during pharmacologic treatment with PDE5 inhibitors. Several radiolabeled tracers based on PDE5 inhibitors were successfully synthesized and investigated by our group for their suitability to non-invasively evaluate PDE5 expression (19). A carbon-11 labeled vardenafil derivative [^{11}C]NMVardenafil (*2-{2-ethoxy-5-[4-(¹¹C)methylpiperazine-1-sulfonyl]phenyl}-5-methyl-7-propyl-3H,4H-imidazo[4,3-f][1,2,4]triazin-4-one*) showed a high PDE5-specific retention in the lungs of wild type mice with 87 % inhibitable PDE5 binding. This tracer showed considerable promise for PET studies of PDE5 binding in the cardiopulmonary system. In this study, we investigated [^{11}C]NMVardenafil in PDE5 TG mice to assess its uptake and retention in the myocardium and in rats with monocrotaline (MCT) induced pulmonary hypertension (20). In addition, *in vivo* biodistribution studies of [^{11}C]NMVardenafil in pigs were performed as translational proof-of-concept.

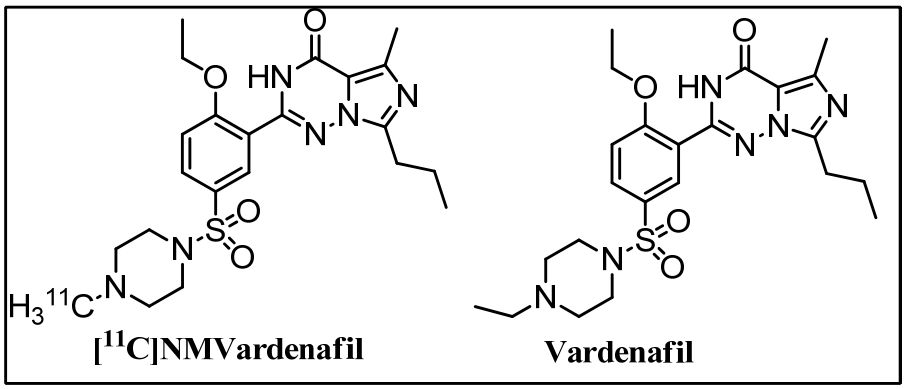

***Figure 1**. Structures of [^{11}C]NMVardenafil and vardenafil.*

2. Results and discussion

2.1. Synthesis and radiolabelling

Synthesis and radiolabeling of [^{11}C]NMVardenafil have been reported previously (19). For all evaluation of tracer in animals, the ethanol concentration in the eluting solution of the radiotracer was diluted to < 10 % with normal saline and sterile filtered. Chemical and radiochemical purity of tracers were analyzed with HPLC and purity of more than 95 % was accepted (supporting information figures 1 and 2).

2.2. Biodistribution

2.2.1. Wild type (C57Bl/6) mice

[^{11}C]NMVardenafil biodistribution was evaluated in transgenic mice with cardiomyocyte-specific PDE5 over-expressing (N = 3) and wild type C57Bl/6 (Bl6) littermates (N = 3). Consistent with reports that PDE5 is abundantly expressed in lungs (14, 16) and in agreement with previous reports of the distribution of the tracer in another murine strain (19); the highest retention of [^{11}C]NMVardenafil was observed in the lungs (8.1±0.7 % ID and 10.2±2.3 SUV_W) of wild type (WT) mice (figure 2 and supporting information).

2.2.2. Transgenic mice with cardiomyocyte specific PDE5 over-expression (PDE5 TG)

To assess specificity of [^{11}C]NMVardenafil for PDE5, biodistribution studies in transgenic mice with cardiomyocyte-specific PDE5 over-expression (PDE5 TG) was studied at 30 min post injection (pi). The PDE5 TG mice are characterized by an up to 9-fold increase in PDE5 protein expression and a 10-fold increase in sildenafil-inhibitable cGMP hydrolytic activity specifically in the cardiomyocytes compared to wild type littermates (7, 10).

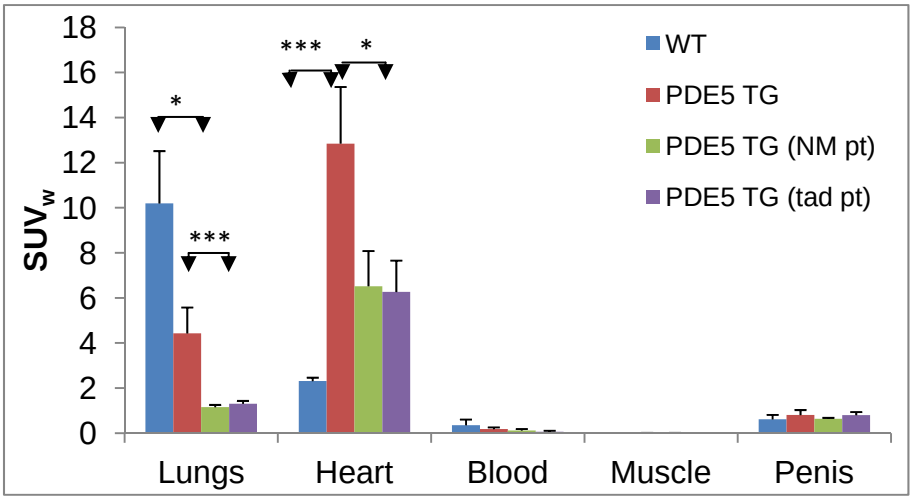

Figure 2. *Biodistribution of [^{11}C]NMVardenafil at 30 min post injection in wild type (WT) mice, PDE5 TG Transgenic mice with cardiomyocyte specific PDE5 over-expression mice (control,); PDE5 TG (NM pt): PDE5 TG mice pre-treated with NMVardenafil (10 mg/kg, SC, 60 min prior to tracer injection); PDE5 TG (tad pt): PDE5 TG mice pre-treated with tadalafil (10 mg/kg, SC, 60 min prior to tracer injection); *(p < 0.05); ***(p < 0.001); SUV_w: standardized uptake value based on weight. N = 3 for each group.*

At 30 min pi, the myocardial retention of [^{11}C]NMVardenafil in PDE5 TG mice was more than 5-fold higher compared to wild type mice (from 1.1±0.0 to 6.1±1.1 % ID, $p < 0.001$) demonstrating selective binding to PDE5. The retention of [^{11}C]NMVardenafil in the lungs of

PDE5 TG mice was reduced by more than 65 % (8.1±0.7 vs. 2.8±0.4 % ID) compared to wild type mice, probably due to a ‘‘stealing’’ effect of the available radiotracer in the plasma by the myocardium.

2.2.3. Blocking study in PDE5 TG mice

To challenge the PDE5 specific binding of [^{11}C]NMVardenafil in PDE5 TG mice, a blocking study was performed by pre-treating PDE5 TG mice (N = 3) with tadalafil, a structurally unrelated competitive PDE5-specific inhibitor, (10 mg/kg) (21) or a self-blocking (N = 3) study with cold NMVardenafil (10 mg/kg) administered subcutaneously (sc), 60 min prior to tracer injection. [^{11}C]NMVardenafil retention in the lungs (figure 2 and Supporting information-tables 1 and 2) was significantly blocked (more than 62 % reduction in % ID for both pre-treated groups, $p < 0.01$ and $p < 0.001$ in NMVardenafil and tadalafil pre-treated mice, respectively). Similarly, myocardial retention was reduced by more than 52 % after self-blocking ($p < 0.05$) and 58 % after tadalafil pre-treatment ($p < 0.05$) compared to non-treated PDE5 TG mice.

The difference in myocardial retention of [^{11}C]NMVardenafil between the NMVardenafil and tadalafil pre-treated groups was not statistically significant ($p = 0.4$). These results demonstrate that binding of [^{11}C]NMVardenafil is PDE5-specific. Moreover, no significant difference in tracer retention in other organs was observed between non-treated mice and mice pre-treated with PDE5 inhibitor supporting our findings that the tracer binds selectively and specifically to PDE5 in lung and myocardial tissue.

2.3. Plasma radiometabolite analysis of [^{11}C]NMVardenafil

2.3.1. Plasma of mice

Mouse plasma (N = 3) was analyzed with reversed phase high pressure liquid chromatography (RP-HPLC) to quantify radiometabolites of [^{11}C]NMVardenafil at 2 and 30 min post tracer injection (table 1). At 2 min pi 81 % of the activity was present as intact radiotracer and this fraction was reduced to 37 % at 30 min pi. The main metabolite is most likely a result of demethylation of the piperazine [^{11}C]methyl-group (figure 1) and it was not expected to contribute to the measured activity in lungs or myocardium (22). Radioactive metabolites detected were more polar than [^{11}C]NMVardenafil as shown by the shorter retention time during RP-HPLC analysis (supporting information-figure 1).

2.3.2. Plasma of pig

Plasma radiometabolites of [^{11}C]NMVardenafil were also quantified in pig arterial plasma samples (N = 1) obtained at 2, 5, 10, 30 and 60 min pi (table 1). The fraction of activity recovered in the form of intact [^{11}C]NMVardenafil ranged from 87 % at 2 min pi to 48 % at 60 min pi. Similar to mice studies, all recovered radiometabolites were more polar than the intact tracer.

Table 1. *Plasma radiometabolite analysis of [^{11}C]NMVardenafil in mice and pig plasma as a function of time post injection.*

	Mice plasma (N = 2)		Pig plasma (N = 1)				
	2 min	30 min	2 min	5 min	10 min	30 min	60 min
Intact tracer (%)	81 - 82	31 – 44	87.3	94.6	74.6	59.5	48.4

2.4. Small-animal PET study

2.4.1. MicroPET imaging in PDE5 TG mice

In vivo biodistribution of [^{11}C]NMVardenafil was evaluated in PDE5 TG mice using dynamic microPET imaging. In addition to biodistribution studies, reversible and specific binding of [^{11}C]NMVardenafil was assessed with chase and blocking experiments with tadalafil. Time-activity curves (TACs) of the myocardium showed a significant uptake and retention in control PDE5 TG mice in agreement with biodistribution results (figure 3).

In contrast to the findings in control PDE5 TG mice, there was no significant tracer retention and accumulation in tadalafil pre-treated mice. The tracer was quickly displaced after intravenous injection of tadalafil in the chase study (figures 3 and 4). These results demonstrate that *in vivo* binding of [^{11}C]NMVardenafil to PDE5 is highly specific and reversible.

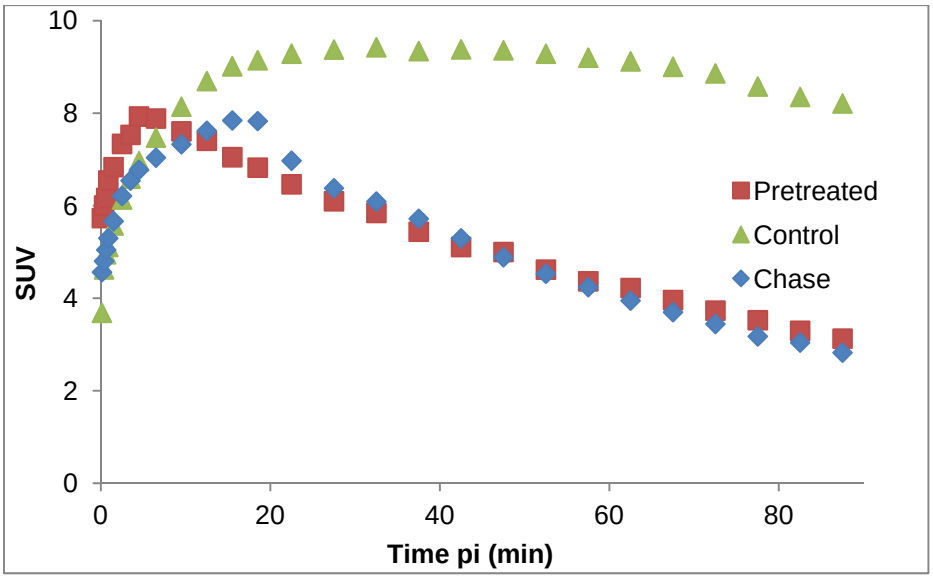

Figure 3. *Time-activity curve of the myocardium in PDE5 TG mice after iv injection of [11C]NMVardenafil (7 MBq). Control (baseline scan); pre-treated: tadalafil 10 mg/kg, sc, 60 min prior to tracer injection; and chase: tadalafil 10 mg/kg, iv, 20 min after start of scan.*

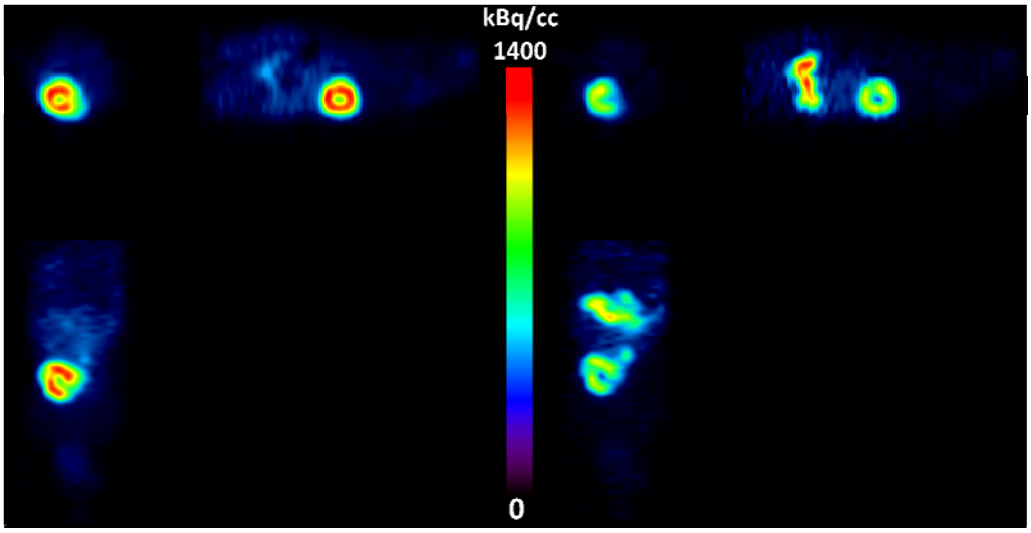

Figure 4*. Left: A summed image of dynamic microPET acquisition from 8 to 20 min after iv injection of [11C]NMVardenafil (7 MBq) in PDE5 TG mice. Right: A summed image of the same dynamic microPET* acquisition from 40 to 50 min after the chase. *Sagittal view (top right), transaxial (top left), and coronal view (bottom).*

2.4.2. MicroPET imaging of MCT induced pulmonary arterial hypertension rat model

[11C]NMVardenafil was evaluated in a MCT induced pulmonary hypertension rat model to monitor changes in PDE5 expression level during disease progression. MCT is an 11-membered macrocyclic pyrrolizidine alkaloid which is oxidized in the rat liver to the reactive metabolite monocrotaline pyrrole (MCTP). In rats, MCTP causes pulmonary vascular

syndrome characterized by proliferative pulmonary vasculitis, pulmonary hypertension and cor pulmonale (23, 24).

The weight of rats was monitored throughout the experiment and served as a non-invasive indicator of disease progression (25). During the first week of isolation, all rats gained proportionally about 3.5 % in weight. In the experimental group (N = 3), two rats initially gained weight in the first week (5.1 % and 8.9 %, respectively), but lost weight in the sixth week (5.4 % and 21 %, respectively) and eventually died. The third MCT treated rat showed a similar pattern as the other MCT treated rat but started gaining weight from the fifth week on till the end of the experiment. In contrast to treated rats, all control rats gained weight till the end of the experiment. Therefore, loss of body weight was taken as indicators of a pre-terminal disease stage (25).

[^{11}C]NMVardenafil-microPET scans of the MCT treated rats were acquired on a weekly basis for eight weeks and TACs for different lung regions are shown in figure 5.

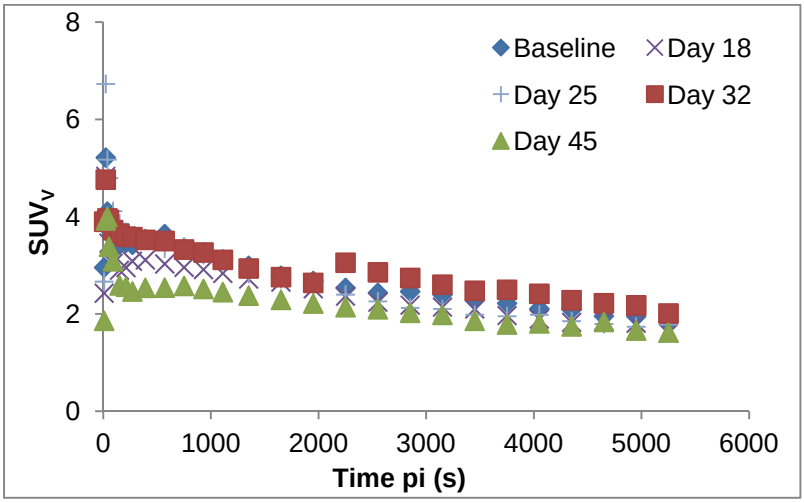

***Figure 5**. MicroPET follow up in MCT treated rats (75 mg/kg, ip). Time-activity curves for lung regions at subsequent imaging time points after injection of [^{11}C]NMVardenafil (37 MBq).*

Rat lung TACs acquired at different time points post MCT treatment showed no significant difference compared to baseline scans or control group. It was concluded from this experiment that [^{11}C]NMVardenafil PET could not detect significant changes in PDE5 expression levels during the 6-weeks follow-up period after MCT treatment. There was no difference in uptake of the tracer between control and MCT pre-treated rats and there is still some controversy about this model and the uncertain correlation between this rat model and clinical features in PAH patients (20).

2.5. Pig PET study

In addition to rodent experiments, *in vivo* biodistribution of [11C]NMVardenafil was also evaluated in a pig (N = 1). Similar to mice biodistribution results, a strong uptake and retention in the lungs was observed, whereas the myocardium was only faintly visible (figure 6, bottom). There was a non-uniform uptake and retention of the tracer in the different lung regions. This might not be surprising taking into consideration the non-uniform distribution of PDE5 in the lungs (mainly distributed in the blood vessels). Whether the non-uniform retention of [11C]NMVardenafil was due to non-uniform PDE5 expression or related to heterogeneous perfusion and/or ventilation (figure 6) or a combination of these needs to be further investigated but, nevertheless, this observation is intriguing. Time-activity curves generated for the different regions of the lungs are given in figure 7.

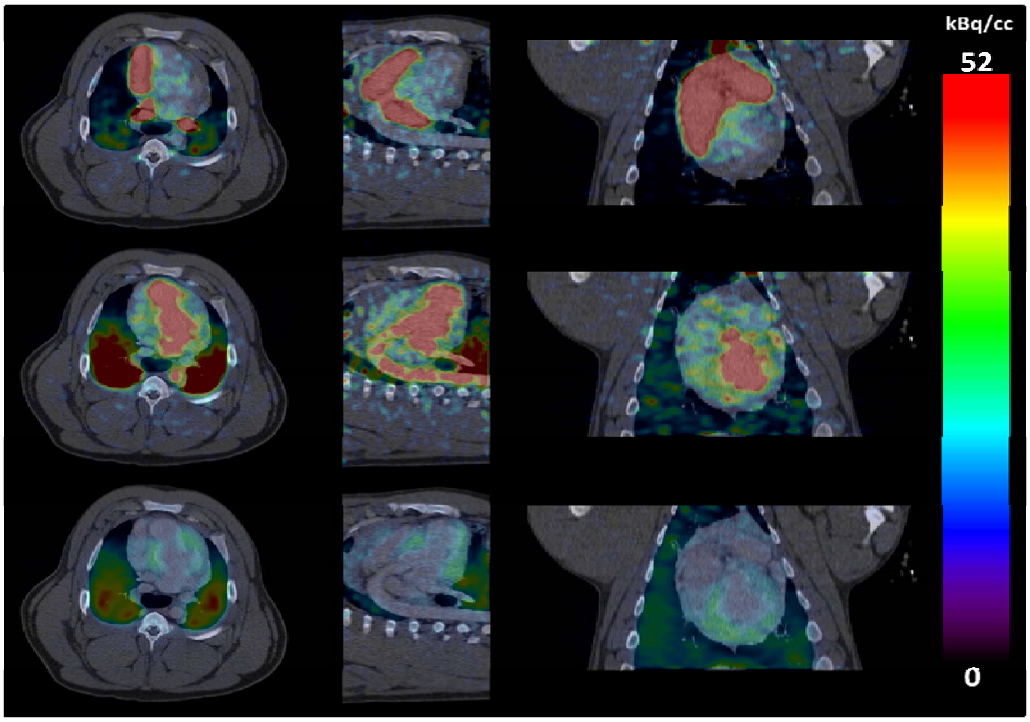

***Figure 6**. Transaxial (left), sagittal (middle), and coronal (right) fused PET-CT images of the lungs and myocardium in a pig model after intravenous administration of [11C]NMVardenafil (370 MBq). Top: Summed image between 6 and 12 s showing first-pass of the tracer with high activity in the right ventricle, pulmonary arteries and to a lesser extent in the dorsal part of the lungs. Middle: summed image between 30 and 36 s showing blood pool activity in the left ventricle and high tracer retention/perfusion in the lungs, mainly in the dorsal regions. Bottom: summed image between 720 and 900 s showing high tracer retention in the lungs and slightly increased tracer uptake in the myocardial wall of the left ventricle.*

The TACs obtained in different lung regions showed a high and significant tracer uptake and retention. The middle and dorsal regions of the lungs showed an initial higher uptake compared to the ventral areas (figure 6) whereas the latter regions showed an initial lower uptake but a steady accumulation was observed to finally reach similar levels of tracer retention (figure 7, TACs of left ventral/Lv and right ventral/Rv). With regard to perfusion and tracer delivery, the lung is quite different from other organs as it receives blood supply from the right ventricle with a much more concentrated tracer bolus after intravenous injection. In addition lung perfusion is coupled to ventilation (26) and density of lung tissue varies according to local content of air during respiration. Anesthesia and mechanical ventilation may further influence local lung ventilation and perfusion making it extremely difficult to explain the heterogeneity of the observed [^{11}C]NMVardenafil kinetics which may however be related to the putative role of PDE5 with regard to hypoxia related vasoconstriction (27). Further investigations are warranted to elucidate the underlying mechanisms of this heterogeneous tracer distribution.

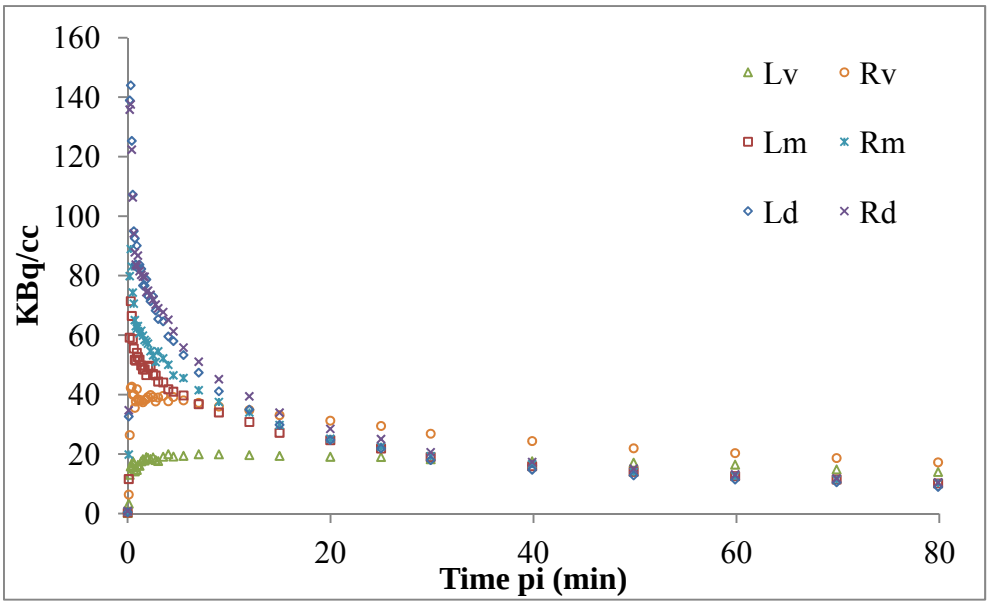

***Figure 7**. TACs reconstructed for lung regions after iv injection of [^{11}C]NMVardenafil (370 MBq). Ld: Left dorsal (blue); Lv: Left ventral (green); Lm: Left middle (red); Rm: Right middle (light blue); Rv: Right ventral (orange); RL: Right dorsal (violet)*

3. Conclusion

A carbon-11 radiolabeled vardenafil derivative ([^{11}C]NMVardenafil) was synthesized and evaluated for its potential to non-invasively image PDE5 expression. Biodistribution and PET imaging studies in PDE5 TG mice and a pig model showed that the tracer binds specifically,

selectively and reversibly to PDE5 in the myocardium and lungs. A small animal PET study in MCT induced pulmonary hypertension model in rats could not show a significant difference in tracer uptake between control and experimental groups. In this study, we demonstrated that [^{11}C]NMVardenafil has high affinity and specificity for PDE5 with promising properties for *in vivo* visualization of PDE5 and assessing receptor occupancy during treatment with PDE5 inhibitors. [^{11}C]NMVardenafil has been selected as lead candidate for further clinical investigation in patients with pulmonary hypertension and end-stage heart failure awaiting heart transplantation. Furthermore, this tracer may show considerable promise to study the role of PDE5 in hypoxia related vasoconstriction *in vivo*.

4. Experimental section

All animal experiments were conducted according to the Belgian code of practice for the care and use of animals, after approval from the Animal Ethics Committee, KU Leuven (Ethische Commissie Dier proeven, KU Leuven, License number: LA1210237).

4.1. Radiosynthesis

Synthesis and radiolabeling of [^{11}C]NMVardenafil have been reported previously (19). For all evaluation of tracer in animals, the ethanol concentration in the eluting solution of the radiotracer was diluted to < 10 % with normal saline and sterile filtered. Chemical and radiochemical purity of tracer were analyzed with HPLC and purity of more than 95 % was accepted (19).

4.2. Biodistribution in mice

Adult wild type C57Bl/6 (Bl6) (KU Leuven Animalium) and PDE5 TG mice (graciously supplied by Cardiology Unit, KU Leuven) weighing 25 to 40 g were used for biodistribution studies. Animals were housed in individually ventilated cages in a thermo regulated (22°C), humidity-controlled facility under a 12 h/12 h light/dark cycle, with free access to food and water. Biodistribution studies of [^{11}C]NMVardenafil were performed in wild type Bl6 and PDE5 TG mice at 30 min post injection (N = 3 per time point). Mice were anesthetized with 2.5 % isoflurane in oxygen at a flow rate of 1 L/min and the radiotracer (5-7 MBq) was injected via tail vein. The mice were sacrificed by decapitation at 30 min pi and blood and major organs were collected and weighed. Radioactivity in blood and organs was counted using an automated γ-counter (Perkin Elmer Wizard 2480, Walthan, USA) and expressed as a

percentage of injected dose (% ID) and standardized uptake value based on weight (SUV_W) where initially the concentration in organ was expressed as activity (KBq) per gram (g) and then adjusted for body weight and total injected dose. For calculating total radioactivity in blood and muscle, weight of blood and muscle was assumed to be 7 % and 40 % of body weight, respectively.

4.3. Blocking study

In order to assess the affinity and specificity of [^{11}C]NMVardenafil for PDE5, a blocking study was performed in PDE5 TG mice (N = 3). In brief, PDE5 TG mice were subcutaneously injected with tadalafil (a structurally unrelated PDE5 inhibitor, TCR, Canada) or cold NMVardenafil (self-blocking) 10 mg/kg, subcutaneous (sc), 60 min prior to tracer administration. Tadalafil or NMVardenafil solution for injection was prepared in such a way that the final concentration was 1 mg/mL in 10 % dimethylsulfoxide in 40 % (2-hydroxypropyl)-β-cyclodextrin solution and sterile filtered through a 0.22 μm filter (Millex®-GV, Millipore, Ireland). Biodistribution study was then performed as described above and results were expressed as % ID and SUV_W.

4.4. Radiometabolites

4.4.1. Plasma radiometabolites analysis in mice

Radiometabolites of [^{11}C]NMVardenafil in plasma of mice were quantified at 2 and 30 min pi (N = 2 per time point). Mice were anaesthetized with pentobarbital (60 mg/kg; ip) and injected with [^{11}C]NMVardenafil (~7.4 MBq) via tail vein. Mice were decapitated at predetermined time points, blood was collected into lithium heparin PST tubes (BD Vacutainer; BD, Franklin Lakes, New Jersey) and stored on ice. After centrifugation (420 x g; 10 min), plasma was separated and analyzed by HPLC on a Chromolith RP C_{18} column (3 mm×100 mm; Merck) eluted with gradient mixtures of CH_3CN (A) and 0.05 M NaOAc pH 5.5 (B) (0-4 min: isocratic 0 % A, 0.5 mL/min; 4-9 min: linear gradient 0 % A to 90 % A, 1 mL/min; 9-12 min: isocratic 90 % A, 1 mL/min; 12-15 min: linear gradient 90 % A to 0 % A, 0.5 mL/min). The non-radioactive reference compound NMVardenafil was co-injected to determine the retention time of the intact parent tracer. The eluate from the UV detector was passed through a 3-in. NaI(Tl) scintillation detector, connected to a single channel analyzer. The eluate from the radiodetector was collected as 1-mL fractions (model 2110 fraction

collector, Bio-Rad, Hercules, CA). The radioactivity in each fraction was measured using an automated gamma counter.

4.4.2. Plasma Radiometabolite Analysis in pigs

After intravenous administration of 370 MBq of [^{11}C]NMVardenafil in an anesthetized pig blood was drawn at 2, 10, 30, 60 and 90 min. Blood was collected in lithium heparin-containing tubes and stored on ice. Subsequently, the blood was centrifuged for 10 min at 3155 x g and the supernatant (plasma) was drawn and spiked with 50 µg of the reference compound (NMVardenafil). The plasma was then analyzed with HPLC according to the procedure mentioned above.

4.5. Small-Animal PET Studies

All rodent imaging experiments were performed on a Focus 220 microPET scanner (Concorde Microsystems, Knoxville, USA). Male PDE5 TG mice were kept under gas anesthesia (2.5% isoflurane in O_2 at a flow rate of 1 L/min) and 90 min dynamic scans were acquired in list mode. Acquisition data were separated into 24 time frames (frame x time: 4 x 15 s, 4 x 60 s, 5 x 180 s, 8 x 300 s and 3 x 600 s min) and reconstructed with MAP. Time–activity curves (TAC) were generated for the heart for each individual scan, using PMOD software (version 3.2; PMOD Technologies, Zurich, Switzerland). The radioactivity concentration in the heart region was expressed as standardized uptake value based on volume (SUV_V) where the concentration in organ was expressed initially as activity (KBq) per volume of interest (mL) and then adjusted for body weight and total injected dose.

4.5.1. MicroPET imaging in PDE5 TG mice

Baseline imaging was performed in PDE5 TG mice and the same mice were used to determine specific binding of the tracer to PDE5 by blocking and chase experiments using the structurally unrelated PDE5-specific inhibitor tadalafil (21). Mice were intravenously injected with 5 to 7 MBq of [^{11}C]NMVardenafil. For the blocking study, mice were pre-treated with 10 mg/kg tadalafil, subcutaneously (sc), 60 min prior to tracer administration whereas for the chase experiment an intravenous (iv) injection of tadalafil 10 mg/kg was given 20 min after the start of PET acquisition. Tadalafil solution for injection was prepared in such a way that the final concentration was 1 mg/mL in 10 % dimethylsulfoxide in 40 % (2-hydroxypropyl)-β-cyclodextrin solution and it was filtered through a 0.22 µm membrane filter.

4.5.2. MicroPET imaging of MCT induced pulmonary arterial hypertension rat model

For microPET imaging, 6 Wistar rats (KU Leuven Animalium) less than 8 weeks old at the start of the experiment were used. All animals underwent a baseline microPET scan and were treated with monocrotaline (MCT) following a baseline scan. For this, 200 mg of MCT was dissolved in 3.3 mL of 1 M HCl and the solution was neutralized with 6.6 mL of 0.5 M NaOH in order to obtain a 20 mg/mL MCT solution (2 % MCT solution). MCT 75 mg/kg was injected intraperitoneally to induce PAH in three rats (6, 23, 25). Consecutive microPET scans of the MCT treated rats were performed on average on a weekly basis for several weeks. The weight of the rats was monitored throughout the experimental period.

4.6. PET-Ct studies in pig

Imaging experiments were performed on a PET scanner (Concorde Microsystems, HiRez Biograph 16, Siemens, Knoxville, USA). A 90-min ECG-gated PET scan was acquired in list mode. A low-dose CT scan was conducted for attenuation correction. A domestic pig (N = 1), weighing 40 kg was pre-anesthetized with an intramuscular injection of 8 mg/kg tiletamine/zolazepam (Zoletil 100®, Virbac) and 2.5 mg/kg xylazine hydrochloride (Xyl-M 2%®, VMD). Continuation of anaesthesia was performed using a continuous infusion of propofol (10 mg/kg/h)(Diprivan 2%®, Astra Zeneca) and remifentanil (0.3 µg/kg/min)(Ultiva®, GSK). After intubation, pig was ventilated with a 1:1 mixture of air and oxygen. Denudation of the carotid artery was performed and an 8 F sheet was introduced, after which pig was anticoagulated with an initial bolus of 10,000 IU unfractionated heparin (Heparine LEO®, Leo). Continuous ECG and invasive blood pressure monitoring was registered during the whole procedure. Regular blood gas analyses were performed in order to optimize the ventilatory settings.

Statistics

All calculated results are expressed as mean ± standard deviation (SD). For comparison the Student's t-test was used and $p < 0.05$ was considered statistically significant.

Acknowledgement:

We would like to thank Ann Van Santvoort (KU Leuven, MoSAIC), Julie Cornels and Ivan Sannen (KU Leuven, Laboratory of Radiopharmacy), Melissa Swinnen (KU Leuven, Cardiology) for her expertise on Echo, TAC mice and cardiac hypertrophy, Ellen Caluwe and Hilde Gillijns (KU Leuven, Clinical Cardiology) for their technical assistance in generating

TAC/LAD mice and Kwinten Porters (Nuclear Medicine, UZ Leuven) for his technical assistance during pig PET scanning.

We also express our appreciation for the financial support from *In Vivo* Molecular Imaging Research (KU Leuven, IMIR) and Fonds Wetenschappelijk Onderzoek Vlaanderen (FWO, Flanders)

5. References

1. Corbin JD, Francis SH. Molecular biology and pharmacology of PDE-5-inhibitor therapy for erectile dysfuncition. J Androl. 2003;24:S38-S41.
2. Lin CS, Lin G, Xin ZC, Lue TF. Expression, distribution and regulation of phosphodiesterase 5. Curr Pharm Des. 2006;12:3439-3457.
3. Tsai E J, Kass D A. Cyclic GMP signalling in cardiovascular pathophysiology and therapeutics. Pharmacol Ther. 2009;122:216-238.
4. Puzzo D, Sapienza S, Arancio O, Palmeri A. Role of phosphodiesterase 5 in synaptic plasticity and memory. Neuropsychiatr Dis Treat. 2008;2:371-387.
5. Kass DA, Champion HC, Beavo JA. Phosphodiesterase type 5 expanding roles in cardiovascular regulation. Circ Res. 2007;101:1084-1095.
6. Nagendran J, Archer SL, Soliman D, et al. Phosphodiesterase type 5 is highly expressed in the hypertrophied human right ventricle, and acute inhibition of phosphodiesterase type 5 improves contractility. Circulation. 2007;116:238-248.
7. Pokreisz P, Vandenwijngaert S, Bito V, et al. Ventricular phosphodiesterase-5 expression is increased in patients with advanced heart failure and contributes to adverse ventricular remodeling after myocardial infarction in mice. Circulation. 2009;119:408-416.
8. Lu Z, Xu X, Hu X, Lee S, Traverse J. Oxidative stress regulates left ventricular PDE5 expression in the failing heart. Circulation. 2010;121:1474-483.
9. Shan X, Quaile MP, Monk JK, et al. Differential expression of PDE5 in failing and nonfailing human myocardium. Circ Heart Fail. 1012;5:79-86.
10. Vandenwijngaert S, Pokreisz P, Hermans H, et al. Increased cardiac myocyte PDE5 levels in human and murine pressure overload hypertrophy contribute to adverse LV remodeling. PLoS One. 2013;8:e58841.

11. Takimoto E, Champion HC, Li M, et al. Chronic inhibition of cyclic GMP phosphodiesterase 5A prevents and reverses cardiac hypertrophy. Nat Med. 2005;11:214-222.
12. Salloum FN, Ockaili RA, Wittkamp M, Marwaha VR, Kukreja RC; Vardenafil: a novel type 5 phosphodiesterase inhibitor reduces myocardial infarct size following ischemia/reperfusion injury via opening of mitochondrial KATP channels in rabbits. J Mol Cell Cardiol. 2006;40:405-411.
13. Szabo G, Radovits T, Veres G, Krieger N, Loganathan S, Sandner P, et al. Vardenafil protects against myocardial and endothelial injuries after cardiopulmonary bypass. Eur J Cardiothorac Surg. 2009;36:657-664.
14. Corbin JD, Beasley A, Blount MA, Francis SH. High level PDE5: A strong basis for treating pulmonary hypertension with PDE5 inhibitors. Biochem Biophys Research Commun. 2005;334:930-938.
15. Black SM, Sanchez LS, Mata-Greenwood E, Bekker JM, Steinhorn RH, Fineman JR. sGC and PDE5 are elevated in lambs with increased pulmonary blood flow and pulmonary hypertension. Am J Physiol Lung Cell Mol Physiol. 2001;281:L1051-7.
16. Buckley MS, Staib RL, Wicks LM, Feldman JP. Phosphodiesterase-5 inhibitors in management of pulmonary hypertension: Safety, tolerability, and efficacy. Drug Healthc Patient Saf. 2010;2:151-161.
17. Crom KF, Curran MP. Sildenafil: A Review of its Use in Pulmonary Arterial Hypertension. Drug. 2008;68:383-397.
18. Fan YF, Zhang R, Jiang X, Wen L, Wu DC, Liu D, Yuan P, Wang YL, Jing ZC. The phosphodiesterase-5 inhibitor vardenafil reduces oxidative stress while reversing pulmonary arterial hypertension. Cardiovasc Res. 2013;99:395-403.
19. Stenmark KR, Meyrick B, Galie N, Mooi WJ, McMurtry IF. Animal models of pulmonary arterial hypertension: the hope for etiological discovery and pharmacological cure. Am J Physiol Lung Cell Mol Physiol. 2009;297: L1013–L1032.
20. Chekol R, Gheysens O, Cleynhens J, Pokreisz P, Vanhoof G, Ahamed M, Janssens S, Verbruggen A, Bormans G. Evaluation of PET radioligands for *in vivo* visualization of phosphodiesterase 5 (PDE5). Nuc Med Biol. 2014;41:155-162.
21. Dungan A, Grondin P, Ruault C, Le Monnier de Gouvile A-C, Coste H, Kirilovsky J, et al. The discovery of tadalafil: A novel and highly selective PDE5 inhibitor. 2:

2,3,6,7,12,12a-hexahydropyrazino[1′,2′:1,6]pyrido[3,4,-b]indole-1,4,-dione analogues. J Med Chem. 2003;46:4533-4542.

22. Ku HY, Shon JH, Liu KH, Shin JG, Bae SK. Liquid chromatography/tandem mass spectrometry method for the simultaneous determination of vardenafil and its major metabolite, N-desethylvardenafil, in human plasma: application to a pharmacokinetic study. J Chromatogr B Analyt Technol Biomed Life Sci. 2009;877:95-100.
23. Wilson DW, Segall HJ, Pan LC, Lamé MW, Estep JE, Morin D. Mechanisims and pathology of monocrotaline pulmonary toxicity. Crit Rev Toxicol. 1992;22:307-325.
24. Lamé MW, Jones AD, Wilson DW, Segall HJ. Monocrotaline pyrolle targets proteins with and without cysteine residues in the cytosol and membranes of human pulmonary artery endothelial cells. Proteomics. 2005;5:4398-4413.
25. Werchan PM, Summer WR, Gerdes AM, McDonough KH. Right ventricular performance after monocrotaline-induced pulmonary hypertension. Am J Physiol. 1989;256:H1328-336.
26. Melsom MN, Kramer-Johansen J, Flatebø T, Müller C, Nicolaysen G. Distribution of pulmonary ventilation and perfusion measured simultaneously in awake goats. Acta Physiol Scand. 1997;159:199-208.
27. Herrera EA, Ebensperger G, Krause BJ, Riquelme RA, Reyes RV, et al. Sildenafil reverses hypoxic pulmonary hypertension in highland and lowland newborn sheep. Pediatr Res. 2008;63:169-175.

Chapter III – Supporting Information

Biodistribution study in Bl6 mice, PDE5 TG mice and PDE5 TG mice pre-treated with PDE5 specific inhibitors

Table 1. *Biodstribution of [^{11}C]NMVardenafil at 30 min post injection in wild type (Bl6) mice, PDE5 TG mice and pre-treated PDE5 TG mice. N = 3 for each group.*

	Control group (% ID±SD)		**PDE5 TG Pre-treated (% ID±SD)**	
	Bl6 mice	PDE5 TG mice	NMVardenafil pre-treated	Tadalafil pre-treated
urine	0.1±0.1	1.1±0.9	1.6±0.1	1.4±1.2
kidneys	6.3±0.7	2.6±0.5	2.4±0.2	2.7±0.7
liver	17.7±3.7	16.0±3.4	18.6±0.8	16.8±2.0
spleen	0.7±0.2	0.5±0.1	0.4±0.1	0.4±0.1
pancreas	1.7±0.3	1.1±0.2	0.8±0.3	0.7±0.1
lungs	8.1±0.7	2.8±0.5	0.8±0.4	1.1±0.2
heart	1.1±0.1	6.1±1.1	2.9±0.4	2.5±0.5
intestines	11.5±1.7	30.7±4.9	32.3±1.9	30.0±2.7
stomach	1.9±0.6	2.4±0.3	1.9±0.4	3.3±0.4
cerebrum	0.1±0.0	0.3±0.0	0.3±0.0	0.3±0.0
cerebellum	0.0±0.0	0.1±0.0	0.1±0.0	0.1±0.0
blood	6.9±0.2	4.4±0.9	3.7±0.1	4.7±0.6
muscle	44.8±6.0	16.8±1.8	17.8±1.8	19.2±3.9
penis	0.1±0.0	0.1±0.0	0.1±0.0	0.1±0.0

Pre-treatment: NMVardenafil or tadalafil, 10 mg/kg, sc, 60 min prior to tracer administration in both cases; % ID: percent injected dose; SD:standard deviation.

***Table** 2. Standardized uptake at 30 min pi in Bl6 and PDE5 TG mice and PDE5 TG mice pre-treated with NMVardenafil or tadalafil (average±SD, N = 3).*

	Control group (SUV_W±SD)		**PDE5 TG Pre-treated (SUV_W±SD)**	
	Bl6 mice	PDE5 TG mice	NMVardenafil pre-treated	tadalafil pre-treated
kidneys	5.1±0.7	2.0±0.4	1.8±0.2	1.8±0.3
liver	3.8±0.9	4.1±0.6	4.4±0.3	4.7±0.2
spleen	3.0±0.9	2.0±0.3	1.9±0.3	1.7±0.3
Pancreas	2.6±0.4	1.7±0.1	1.8±0.3	1.4±0.2
lungs	10.2±2.3	4.4±1.1	1.2±0.1	1.3±0.1
heart	2.3±0.1	12.8±2.5	6.5±1.6	6.3±1.4
intestines	1.5±0.2	3.8±0.6	3.8±0.1	4.3±0.4
stomach	1.3±0.4	2.4±0.2	1.2±0.3	2.5±0.8
Cerebrum	0.1±0.0	0.3±0.0	0.2±0.0	0.4±0.0
cerebellum	0.1±0.0	0.2±0.0	0.2±0.0	0.4±0.0
blood	0.4±0.3	0.2±0.1	0.1±0.1	0.1±0.0
Muscle	0.0±0.0	0.0±0.0	0.0±0.0	0.0±0.0
Penis	0.6±0.2	0.8±0.2	0.6±0.0	0.8±0.1

Pre-treatment: NMVardenafil or tadalafil, 10 mg/kg, sc, 60 min prior tracer administration in both cases; SUV_W: Standardized uptake based on weight.

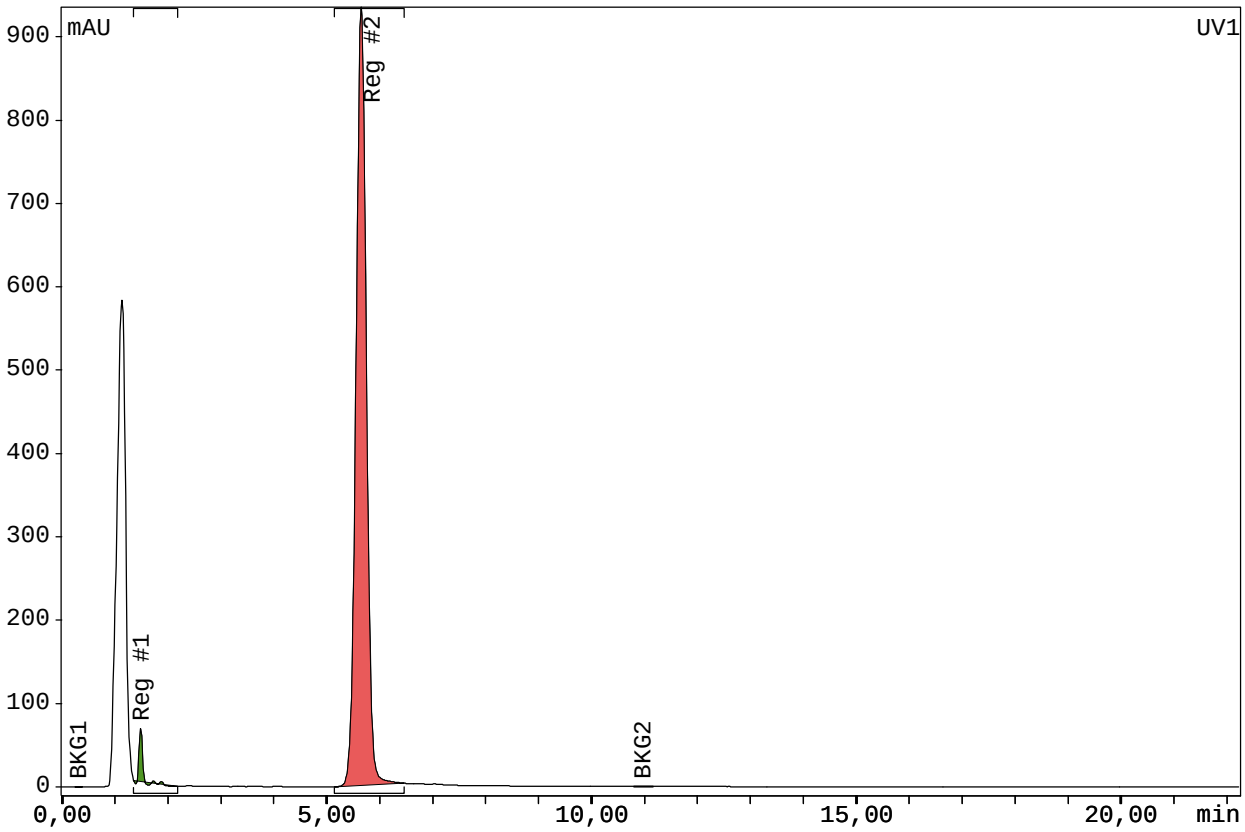

***Figure 1**. Chemical purity determination of the precusor solution for radiolabeling of [^{11}C]**7**.*

Column: XTerra C18 5 µm, 4.6 x100 mm

Detection UV: 254 nm, Flow rate: 1 ml/min

Mobile phase: Isocratic: mixture of hydrogenmonophosphate buffer and ACN (70:30 v/v)

Integration UV1

Substance	Retention time (min)	Area (C/S*s)	% Area
Reg #1	1.48	254.54	1.98
Reg #2	5.65	12575.57	98.02
Sum in ROI		12830.11	

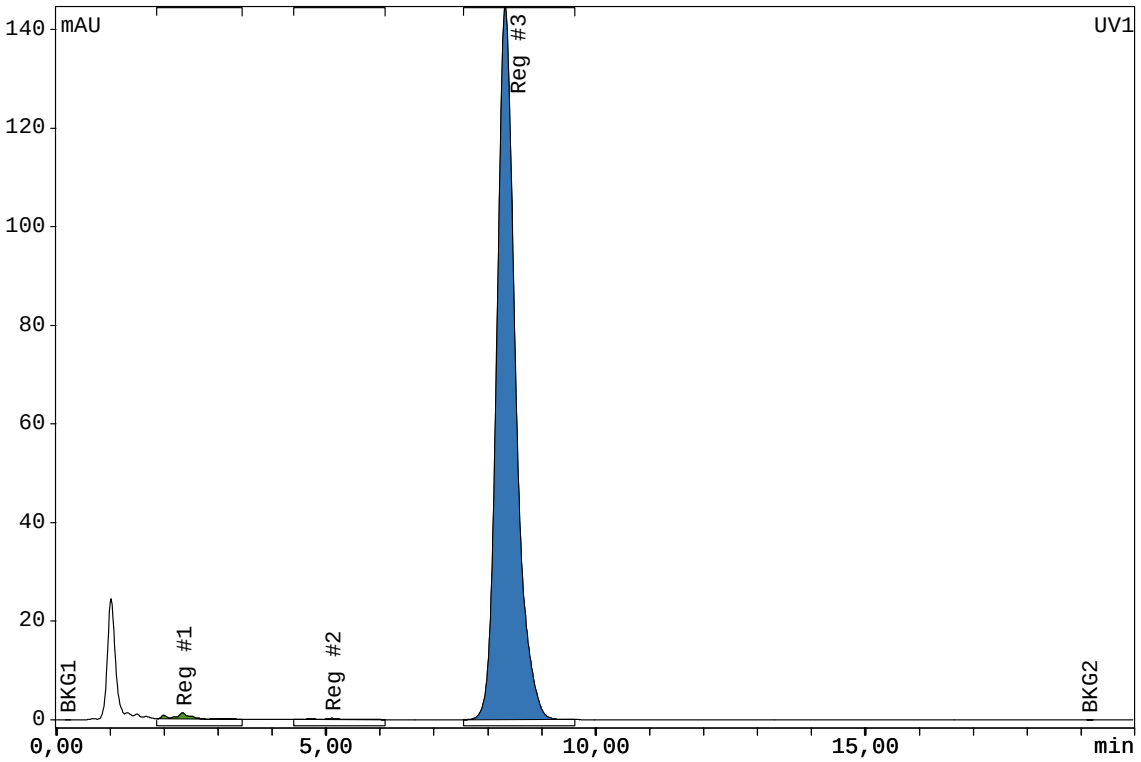

***Figure 2**. Chemical purity determination of the reference compound **7** (NMVardenafil).*

QC of NMVardenafil formulation (250 µg/ml in DMSO)

Injection volume: 20 µl

Column XTerra C18 5 µm, 4.6x100 mm

Detection UV: 254 nm; Flow rate: 1 ml/min

Mobile phase: Isocratic: A mixture of 0.01M Na_2HPO_4 (pH 9) and ACN (70:30 v/v)

Integration UV1

Substance	Retention time (min)	Area (C/S*s)	% Area
Reg #1	2.35	25.455	0.73
Reg #2	5.12	7.932	0.23
Reg #3	8.33	3464.756	99.05
Sum in ROI		3498.144	

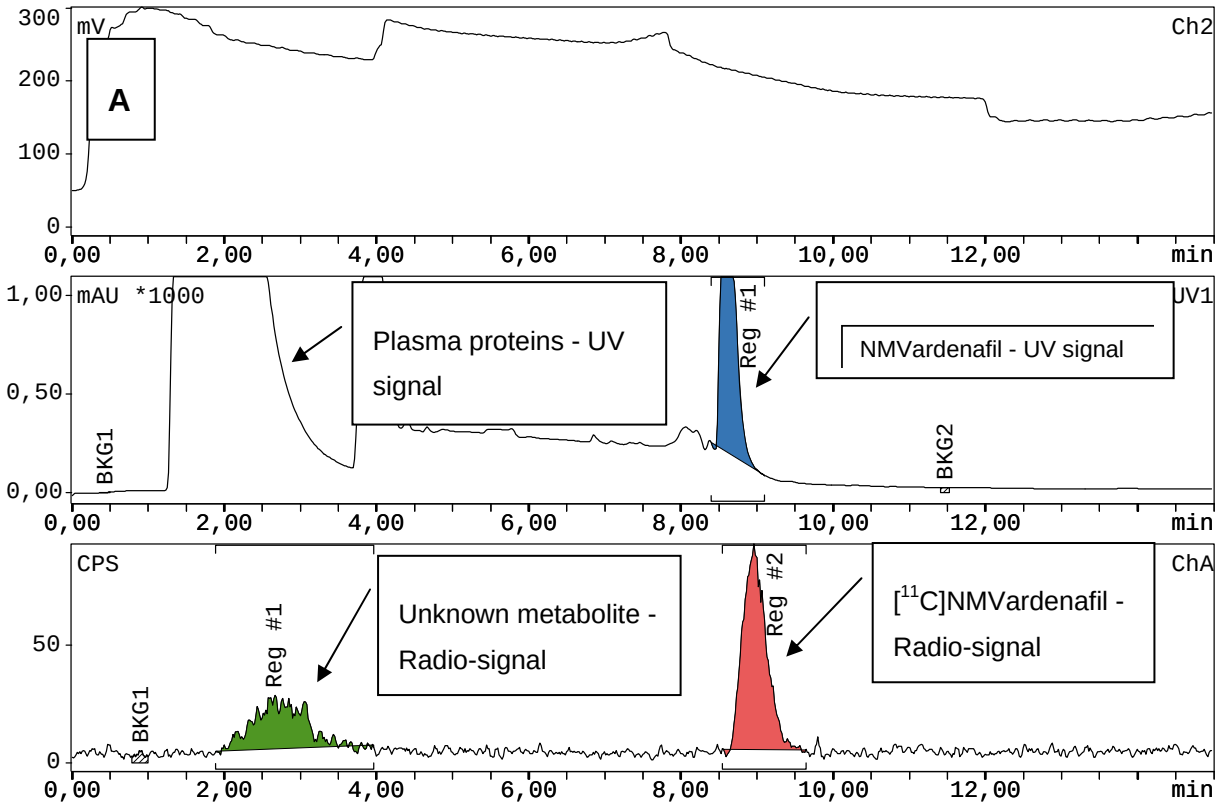

***Figure 3**. Radio-chromatogram of mouse plasma analysis 2 min post [^{11}C]NMVardenafil injection spiked with cold NMVardenafil.Mouse was injected with 7.5 MBq of [^{11}C]NMVardenafil. Recovered activity after HPLC run was more than 84 %*

Integration ChA (Radiosignal)

Substance	Retention time (min)	Area (C/S*s)	% Area
Reg #1	2.63	4532.40	18.00
Reg #2	8.95	20640.20	89.99

Integration UV1

Substance	Retention time (min)
Reg #1	8.67

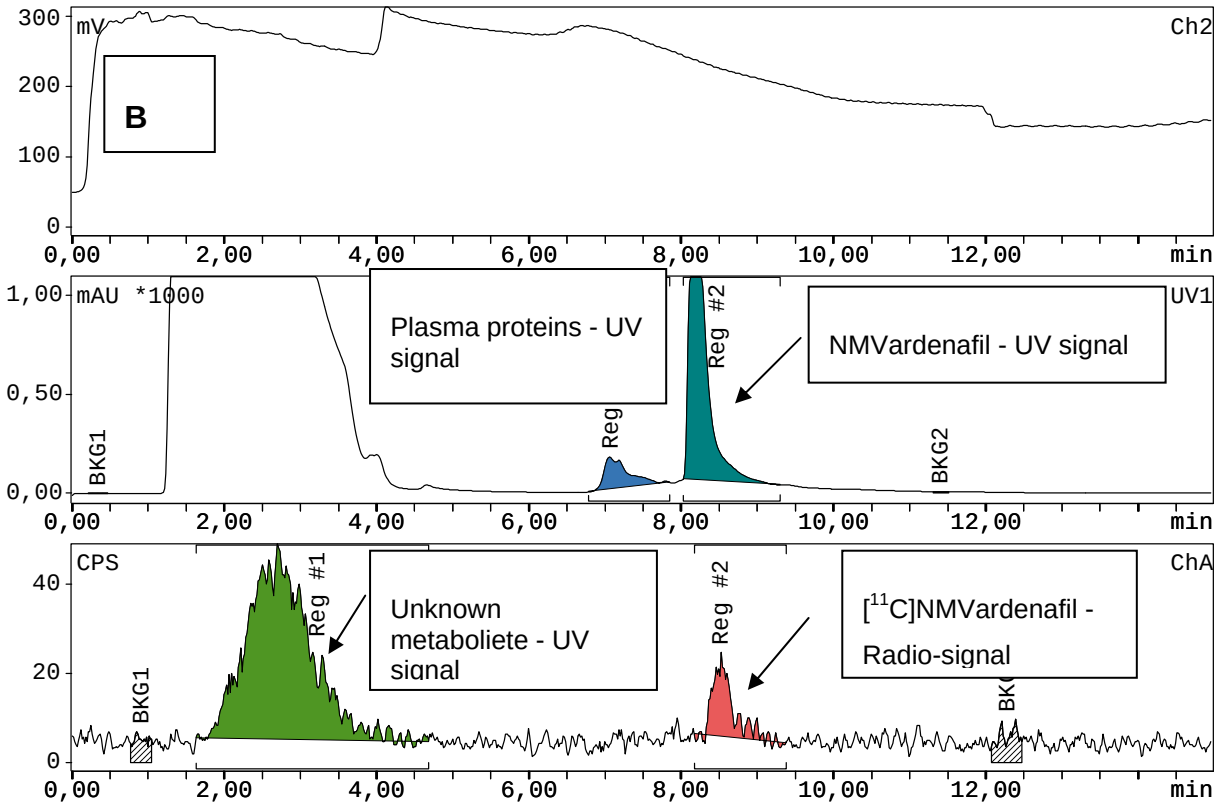

***Figure 4**. Radio-chromatogram of mouse plasma analysis 30 min post [^{11}C]NMVardenafil injection spiked with cold NMVardenafil Mouse was injected with 7.5 MBq of [^{11}C]NMVardenafil. Recovered activity after HPLC run was more than 80 %*

Integration ChA

Substance	Retention time (min)	Area (C/S*s)	% Area
Reg #1	2.72	20164.50	69.16
Reg #2	8.52	8991.00	30.84

Integration UV1

Substance	Retention time (min)
Reg #1	7.07
Reg #2	8.23

Chapter IV

Radiolabeled Pyridopyrazinone Derivatives for PET Imaging of Phosphodiesterase-5A (PDE5A)

Rufael Chekol[1]; Olivier Gheysens[2]; Muneer Ahamed[1]; Jan Cleynhens[1]; Peter Pokreisz[3]; Greet Vanhoof[4]; Stefan Janssens[3]; Alfons Verbruggen[1]; Guy Bormans[1]

[1]KU Leuven, Department of Pharmaceutical and Pharmacological Sciences, Laboratory of Radiopharmacy, Leuven, Belgium

[2]KU Leuven, Department of Imaging and Pathology, Leuven, Belgium and Nuclear Medicine, UZ Leuven, Leuven, Belgium

[3]KU Leuven, Department of Cardiovascular Sciences, UZ Leuven, Leuven, Belgium

[4]Discovery Sciences, Janssen Pharmaceutica, R&D, Beerse, Belgium

Abstract

Introduction: The cyclic guanosine monophosphate (cGMP) specific phosphodiesterase type 5 (PDE5) plays an important role in various pathologies including pulmonary arterial hypertension and cardiomyopathy. PDE5 represents an important therapeutic and/or prognostic target; however, there is currently no method available to non-invasively assess PDE5 expression and occupancy levels *in vivo*. The purpose of this study was to evaluate pyridopyrazinone derivatives as PDE5 specific PET tracers.

Methods: Radiolabeled tracers were prepared by N-alkylation of the amine precursor with [^{11}C]methyl trifluoromethanesulfonate or [^{18}F]F^- substitution of a tosylate precursor to yield [^{11}C]**12** ([^{11}C])RPP07B and [^{18}F]**17** ([^{18}F]FRPP07), respectively. Biodistribution studies, autoradiography and *in vivo* small animal PET scanning were performed to determine the distribution and specificity of the tracers for PDE5.

Results: Biodistribution studies of both tracers in control mice revealed the highest uptake in the lungs whereas very strong uptake was observed in the myocardium of transgenic mice with cardiomyocyte-specific PDE5 over-expression at 30 min post-injection. Binding specificity *in vivo* was demonstrated by a blocking study in which mice were pre-treated with a structurally unrelated PDE5 inhibitor (tadalafil). Dynamic microPET images in rats revealed that both tracers show relatively homogenous brain distribution; however *in vitro* autoradiography could not demonstrate specific binding to PDE5 in brain tissue.

Conclusion: [^{11}C]**12** and [^{18}F]**17** were successfully synthesized and showed specific binding to PDE5. Both tracers are promising for *in vivo* visualization of PDE5, but microPET studies showed that [^{18}F]**17** appears to be superior with respect to its kinetics. Both compounds are highly brain penetrant but retention in brain is a PDE5 independent process.

1. Introduction

Phosphodiesterase type 5 (PDE5) is a member of the phosphodiesterase superfamily that specifically catalyzes and metabolically inactivates the second messenger cyclic guanosine monophosphate (cGMP). PDE5 is expressed in vascular smooth muscle cells, lungs, platelets, corpus cavernosum and Purkinje fibers in the cerebellum. PDE5 exerts potent effects on vascular tone in the corpus cavernosum and pulmonary vasculature and plays an important role in platelet aggregation, handling of sodium secretion in renal cells and apoptosis.[1,2] PDE5 is also implicated in a number of diseases including pulmonary arterial hypertension (PAH), ischemic and dilated cardiomyopathy.[2,3-8] Expression of PDE5 in the human brain is still a subject of debate; nonetheless, there is a general consensus that PDE5 is expressed in the cerebellum (Purkinje cells) and in the hippocampal interneurons (in a scattered manner) of rodents. The cGMP-PDE5 signaling pathway in rodent brain is considered to play a role in early memory consolidation stages of object information, neuronal excitability, synaptic plasticity and neurogenesis.[9,10]

Currently four PDE5 inhibitors (sildenafil, vardenafil, tadalafil and avanafil) have been approved for treating male erectile dysfunction and some of them are approved for PAH.[11-13] A number of authors also advocate the use of PDE5 inhibitors in cardiovascular diseases including heart failure and myocardial infarction since up-regulation of PDE5 in the myocardium has been observed in these conditions.[4,5,14-19] In addition to aforementioned clinical indications, PDE5 inhibitors were also shown to improve early memory consolidation of object information in rodents and to improve functional recovery after stroke in rats.[20,21] However, it remains to be determined whether the distribution and physiological role of PDE5 in the human brain is similar to that observed in rodents. Based on preclinical evidence, there might be a role for PDE5 inhibitors to improve functional recovery after stroke in patients but further investigation is needed.[4,19,20]

Despite the involvement of PDE5 in several disorders and the success of PDE5 inhibitors in clinical practice, there is currently no method to non-invasively evaluate PDE5 expression and occupancy levels *in vivo*. Therefore, development of specific PDE5 PET radioligands would allow to quantify and evaluate changes in PDE5 expression, identify patients that would benefit from PDE5 inhibitors early during disease progression and assess PDE5 occupancy and optimize dose regimens in patients treated with PDE5 inhibitors.

In recent years, several attempts have been made to develop radioligands targeting PDEs with variable success.[22] Jacobsen et al described the development of a PET radioligand, [^{11}C]RAL-01, for *in vivo* visualization of PDE5 though PDE5-specific binding could not be demonstrated.[23] Our group also published a preliminary biological evaluation of a number of radiolabeled tracers targeting PDE5.[24] In this article, [^{11}C]-**7** ([^{11}C]NMVardenafil) was shown to be a selective and specific radiotracer with 87 % inhibitable PDE5 binding in the lungs of NMRI mice. However, none of the tracers were shown to have any significant retention in the brain.

Here, we discuss the synthesis, radiolabeling and preliminary biological evaluation of derivatives of a novel PDE5 inhibitor, 3-(4-(2-hydroxyethyl)piperazin-1-yl)-7-(6-methoxypyridin-3-yl)-1-(2-propoxyethyl)pyrido[3,4-b]pyrazin-2(1H)-one (**PF-5**), reported in literature, as potential radioligands for *in vivo* visualization of PDE5.[25]

2. Results and discussion

2.1. Organic synthesis

14 (**RPP07**) was first reported in 2010 by Hughes et al as a selective and brain penetrant PDE5 inhibitor.[25] Compounds **10** and **18** were also among a series of PDE5 inhibitors reported by the same group and we developed two close derivatives of **14** as potential PET radioligands (scheme 1) for *in vivo* visualization of PDE5.

Compounds **12** and **17** are close analogues of **14** in which the 2-hydroxyethyl substituent on the piperazine ring of **14** was replaced by methyl and 2-fluoroethyl in **12** and **17**, respectively. Compounds **2** to **6** were prepared starting from commercially available **1** according to literature.[25] Treatment of the dione (**6**) with thionyl chloride and DMF at reflux for 16 h yielded chloroimidate **7** (59 % yield).[26] Reaction of **7** with *tert*-butyl piperazine-1-carboxylate or 2-(piperazin-1-yl)ethanol followed by standard Suzuki coupling with 6-methoxypyridin-3-ylboronic acid resulted in **9** and **14**, respectively with good overall yield (60 %). Standard deprotection of **9** with TFA and tosylation of **14** with tosyl chloride in the presence of triethylamine and trimethylammonium chloride[27] furnished precursors **10** and **15** for radiolabeling with carbon-11 and fluorine-18, respectively. The standard non-radioactive references **12** (**RPP07B**) and **17** (**FRPP07**) were prepared by reacting the chloroimidate (**7**) with 1-methylpiperazine or 1-(2-fluoroethyl)piperazine followed by Suzuki coupling with 6-methoxypyridin-3-ylboronic acid.

A detailed description of the synthesis of all compounds, ^{1}H-NMR and HRMS data for intermediates, precursors and non-radioactive standard reference compounds is provided in supporting information.

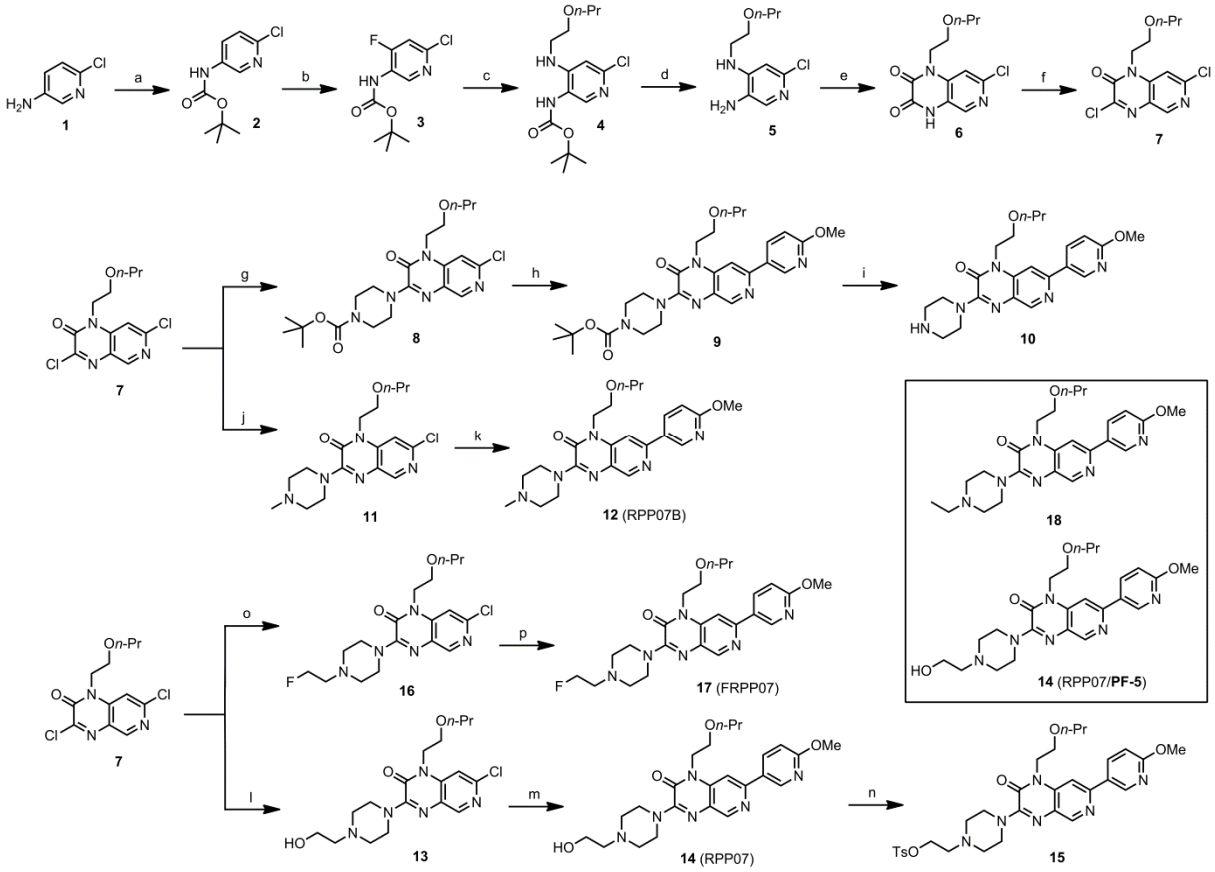

***Scheme 1**. Organic synthesis of pyridopyrazinone derivatives **10** and **15** (precursors) and **12** and **17** (references). Reactions conditions: (a) 1,4-dioxane, $(Boc)_2O$, 27 h, reflux; (b) TMEDA, n-BuLi, Et_2O,- 60 → -10 °C, 2 h; then N-fluorobenzenesulfonimide (NFSI), THF -60 → 0 °C, 1 h, 58 %; (c) 2-propoxyethanamine, EtOH, reflux, 22 h, 70 %; (d) 4 M HCl, 1,4-dioxane, room temp, 16 h, 87 %; (e) MeOC(O)C(O)Cl, i-Pr_2NEt, CH_2Cl_2, 0 °C → room temp, 4 h; then PhMe, 105 °C; (f) PhMe, $SOCl_2$, DMF, 130 °C, 59 % (for steps e and f); (g) tert-butyl piperazine-1-carboxylate, Et_3N, THF, room temp, 4 h, 83 %; (h) 6-methoxypyridin-3-ylboronic acid, $(Ph_3P)_4Pd$ (0), Na_2CO_3, 1,4-dioxane-EtOH, reflux, 16 h, 61 %; (i) TFA, CH_2Cl_2, 0 °C → room temp, 16 h, 60 %; (j) same as (g) except 1-methylpiperazine, 78 %; (k) same as (h), 65 %; (l) same as (g) except 1-(2-hydroxyethyl)piperazine, 71 %; (m) same as (h), 59 %; (n) $(Et)_3N$, $(Me)_3N.HCl$, CH_2Cl_2, 4-methylbenzene-1-sulfonyl chloride, 0 °C → room temp, 16 h, 38 %; (o) same as (g) except 1-(2-fluoroethyl)piperazine, 69 %; (p) same as (h), 50 %.*

2.2. In vitro PDE5 inhibitory activity assay

In vitro PDE5 inhibitory activity (IC_{50}) was determined for **10**, **12**, **14** and **17**. Their IC_{50} values for selected families of phosphodiesterases (PDE5, PDE6 and PDE11) are given in table 1. IC_{50} values for all other PDE families are given in supporting information-table 1.

The pyridopyrazinone derivatives (**10**, **14** and **18**) were reported to have an IC_{50} of 3.28, 0.2, and 0.22 nM *in vitro* PDE5 inhibitory activities, respectively.[25] In our assay **10**, **12**, **14** and **17** were found to have a PDE5 inhibitory activity in the lower nanomolar range. However, in our assay the inhibitors (**10**, **12**, and **14**) showed a lower *in vitro* PDE5 inhibitory activity than previously reported.[24]

Table 1. *[a]IC50 (nM) values of PDE5 inhibitors for selected PDE families*

Compounds	hPDE5A3	hPDE6AB	hPDE11A4
10	16	ND	ND
10[b]	3.28	167.28	8068
12	6.60	3170	2100
14	1.95	1600	800
14[b]	0.20	31.60	492
17	6.45	ND	ND
18[b]	0.22	43.56	1082.40

[a]IC_{50} values are averages of duplicates; [b]reported IC_{50} values for selected PDEs without subtype specification (Hughes et al[25]); ND: Not determined.

2.3. Radiosynthesis

Radiolabeling with carbon-11 was achieved by one-step N-alkylation of 0.5 mg of the amine precursor (**10**) in anhydrous DMSO with [^{11}C]methyl trifluoromethanesulfonate ([^{11}C]CH_3OTf) in the presence of base (Cs_2CO_3) and the reaction mixture was heated at 90 °C for 2 min (scheme 2). Radiolabeling with fluorine-18 was achieved by [^{18}F]F^- substitution for tosylate of **15** (0.5 mg in DMSO, scheme 2) and the reaction mixtures were heated at 90 °C for 15 min. The crude reaction mixtures were purified by HPLC in both cases. The overall radiosynthesis, HPLC purification, sterile filtration and radiotracer formulation were completed in 50 to 60 min from end of bombardment.

The incorporation yield (non-decay corrected radiochemical yield/RCY, based on HPLC recovered activity) was 20 % and 31 % for [^{11}C]**12** and [^{18}F]**17**, respectively, and the radiochemical purity after HPLC-purification was greater than 99 % for both compounds (table 2 and supporting information-table 2). Chemical and radiochemical purity of more than 95 % was accepted.

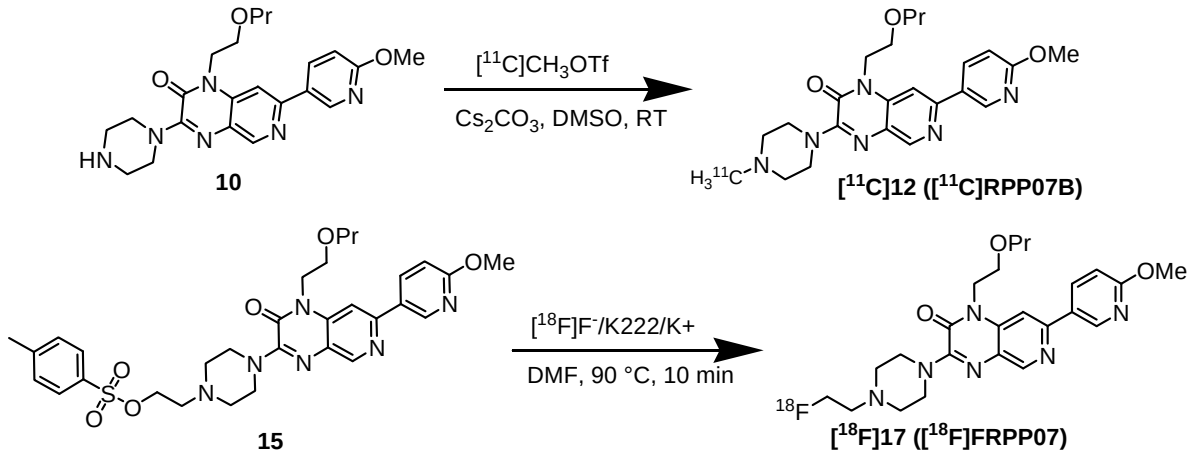

Scheme 2**. Radiolabeling of [^{11}C]**12** and [^{18}F]**17

The identity of the labeled compounds was confirmed by co-injection of the corresponding standard non-radioactive reference analogues (**12** and **17**) on HPLC (supporting information-figure 2). The specific activities were determined after HPLC purification and were found 67 GBq/µmol for [^{11}C]**12** and 91 GBq/µmol for [^{18}F]**17** (table 2) at the time of tracers formulation (detailed description of determination of specific activity can be found in the supporting information for Chapter II).

Table 2**. Results of radiochemistry, logD and PSA values of [^{11}C]**12** and [^{18}F]**17.

Radioligand	RCY (%)	Purity (%)	[a]SA	[b]logD	[c]PSA
[^{11}C]**12**	20±13 (n = 11)	> 99	67	1.29	85.6
[^{18}F]**17**	31±2 (n = 4)	> 99	91	1.69	85.6

Purity determined by RP-HPLC; [a]SA (specific activity in gigabecquerel per micromole; GBq/µmol), [b]logD at pH 7.4 generated with MarvinSketch 5.5.0.1 software (ChemAxon Ltd), [c]PSA (polar surface area in Å^2) is software generated (Molinspiration Cheminformatics, 2011).

2.4. Biodistribution Studies

2.4.1. Biodistribution in NMRI mice

The pyridopyrazinone derivatives ([^{11}C]**12** and [^{18}F]**17**) were initially evaluated by assessing their uptake and retention in the lungs of NMRI mice (N = 4) because abundant expression of PDE5 in the lungs among different species has been reported by several authors.[1,11,27-29] Hence, it was expected that a tracer with high affinity for PDE5 would show high uptake and retention in the lungs. Both tracers were also evaluated in transgenic mice with myocardiocyte specific PDE5 over-expression (PDE5 TG, N = 3) in which a significant myocardial retention was expected. The specificity of the binding of the tracers to PDE5 both in the lungs of control mice and myocardium of PDE5 TG mice was challenged by pre-blocking studies where mice were pre-treated with tadalafil (a structurally unrelated competitive PDE5 inhibitor)[30] prior to tracers administration. In the pre-treatment group, significant reductions in the retention of the tracers in the lungs of control mice and myocardium of PDE5 TG mice were expected if binding of tracers was PDE5 specific.

Results of biodistribution experiments with both radiotracers were expressed as percentage of injected dose (% ID) and as standardized uptake value based on weight (SUV_W, obtained by normalizing the % ID for the animal's body weight and the weight of organ of interest). Both [^{11}C]**12** and [^{18}F]**17** showed initial distribution to the major organs including kidneys, liver, and lungs (supporting information-tables 3 and 4). The urinary excretion of both tracers was negligible during the first 30 min post injection (pi) but the uptake and retention in the kidneys for [^{11}C]**12** was almost twice that of [^{18}F]**17** (supporting information-table 3). Despite this difference in kidney retention, the urinary excretion of both tracers was similar up to 30 min pi. However, microPET imaging showed accumulation of [^{11}C]**12** in the bladder.

The lung uptake and retention of [^{11}C]**12** and [^{18}F]**17** was relatively high at 30 min pi for both tracers and also remained high at 60 min pi for [^{18}F]**17** (supporting information-table 3). The relative concentration of [^{11}C]**12** and [^{18}F]**17** in the lungs was the highest at all studied time points (supporting information-table 4). The initial uptake of [^{11}C]**12** in the lungs was high but declined fast and at 30 min pi, only 20 % of the % ID at 2 min pi was retained whereas at 30 min pi 30 % of the % ID at 2 min pi was retained for [^{18}F]**17**. This could be due to a higher binding affinity of [^{18}F]**17** for PDE5 than [^{11}C]**12** in the lungs or a slower clearance of [^{18}F]**17** from plasma. However, plasma radiometabolite analysis showed a faster metabolism and consequently faster clearance for [^{18}F]**17** than for [^{11}C]**12** (table 3). Nevertheless, both

radiotracers showed a relatively rapid decline of the activity in the lungs at 10 min compared to 2 min: 66 % and 47 % reduction for [^{11}C]**12** and [^{18}F]**17**, respectively (supporting information-tables 3 and 4). This relatively fast decline in retention, compared to another tracer [^{11}C]**7** that was evaluated by our group (which showed a 28 % and 27 % reduction at 10 min and 30 min compared to 2 min pi, respectively and an increase in lung-to-blood activity ratio),[24] might be due to faster dissociation kinetic properties of the tracers or extensive metabolism. The latter is supported at least in the case of [^{18}F]**17** by the fact that only 7 % of the activity in plasma at 30 min pi was due to the intact radiotracer (table 3).

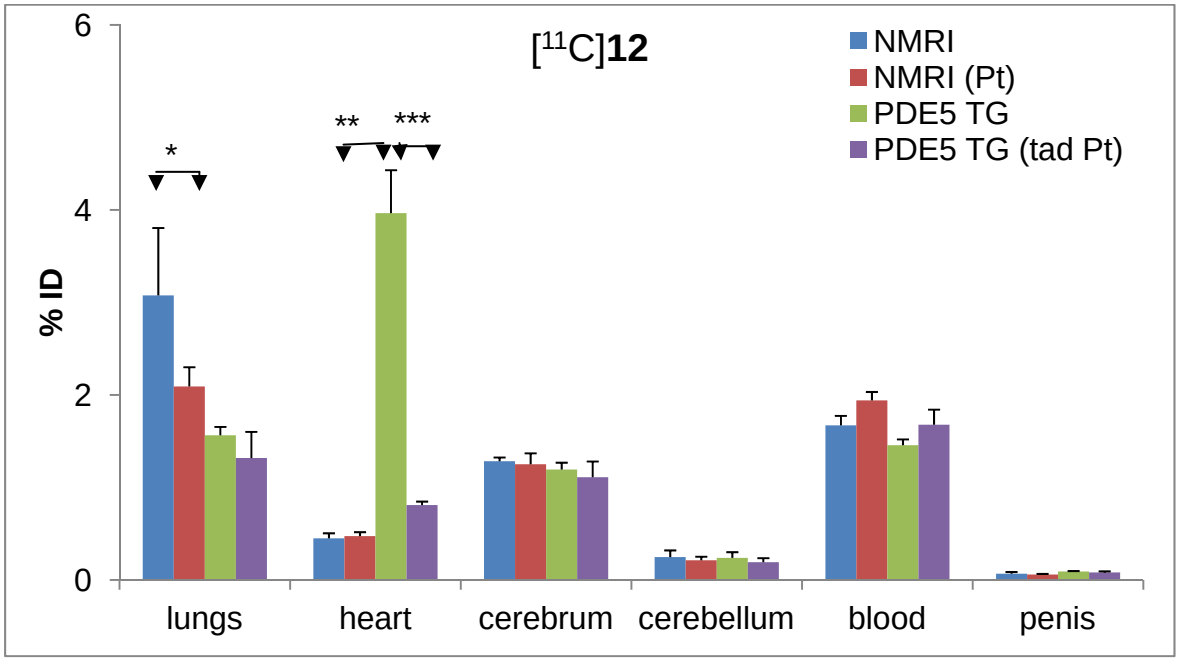

***Figure 1**. Biodistribution results of [^{11}C]**12** in NMRI mice (NMRI, N = 4), pre-treated [NMRI (Pt, N = 4)], PDE5 TG mice (N = 3) and pre-blocking (PDE5 TG (Pt), N = 3] at 30 min pi. Pre-treatment was with tadalafil, 10 mg/kg, sc, 60 min prior to tracer administration. % ID: percentage injected dose. *(p < 0.01); **(p < 0.001); ***(p < 0.0001).*

The high lung-to-blood SUV_W (19) at 30 min pi for [^{11}C]**12** in NMRI mice is in agreement with reports in the literature that PDE5 is abundantly expressed in lungs (supporting information-table 4). Although [^{18}F]**17** showed relatively high lung-to-blood ratio of 4 at 30 min pi in NMrI mice, it was almost one-fifth of [^{11}C]**12**'s lung-to-blood ratio (supporting information-table 4). This was due to the relative high blood SUV_W value of [^{18}F]**17** (0.8±0.1), four-fold compared to that of [^{11}C]**12** (0.2±0.0), and mild reduction in lung retention of [^{18}F]**17** (3.8±1.1 vs 2.8±1.0 SUV_W for [^{11}C]**12** and [^{18}F]**17**, respectively, supporting information-table 4) at 30 min pi. The relatively high blood % ID for [^{18}F]**17** both in the control and PDE5 TG mice (figure 2) could be due to metabolism. This caused a

concern as the activity measured in the lungs of mice injected with [^{18}F]**17** could be radioactive metabolites in the lung vasculature and this was assessed by pre-blocking study (section on pre-blocking).

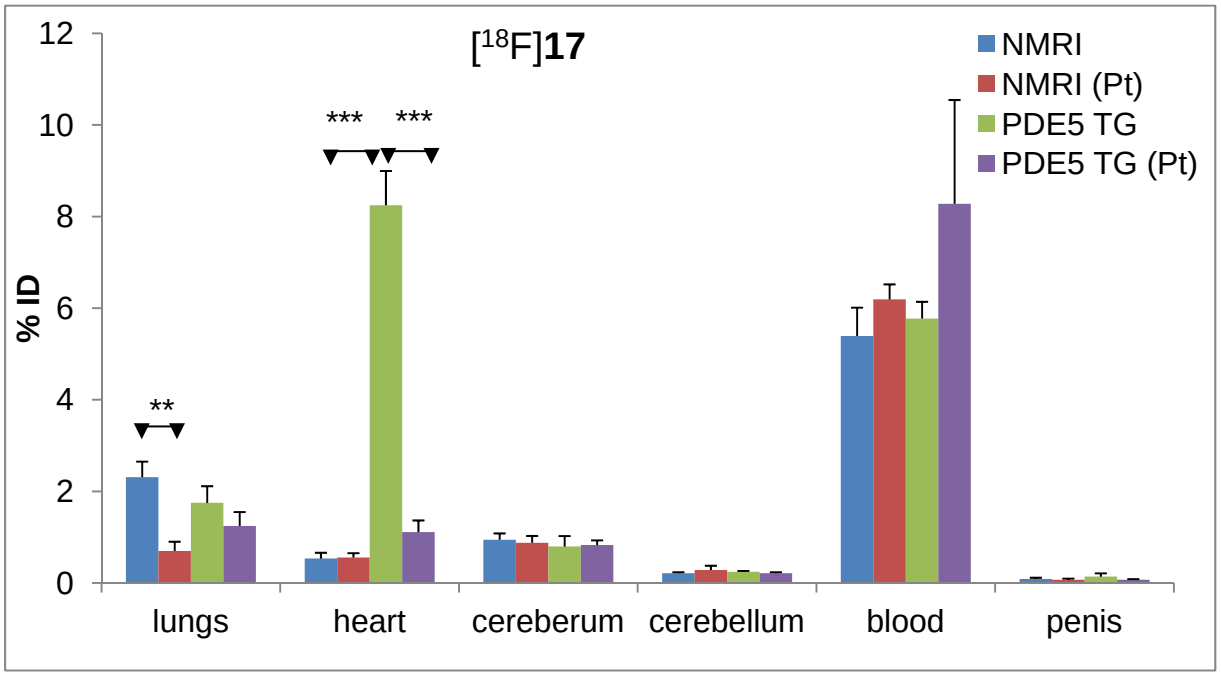

***Figure 2**. Biodistribution results of [^{11}C]**17** in NMRI mice (NMRI, N = 4), pre-treated [NMRI (Pt, N = 4)], PDE5 TG mice (N = 3) and pre-blocking (PDE5 TG (Pt), N = 3) at 30 min pi. Pre-treatment was with tadalafil, 10 mg/kg, sc, 60 min prior to tracer administration. % ID: percent injected dose.). **(p < 0.001); ***(p < 0.0001).*

Both tracers were cleared from plasma mainly *via* the hepatobiliary pathway and showed progressive accumulation in the intestines as a function of time (supporting information-tables 3 and 4). Myocardial uptake and retention of both tracers were very limited which was expected based on the low expression levels of PDE5 in healthy myocardium. Interestingly, unlike for most radiolabeled PDE5 tracers we have evaluated so far[23] uptake of [^{11}C]**12** and [^{18}F]**17** in the brain was relatively high. Retention in the cerebrum and cerebellum was higher for [^{11}C]**12** (4.0±0.9 and 1.5±0.1 SUV_Ws at 2 and 30 min pi, respectively) than for [^{18}F]**17** (2.4±0.3 and 0.9±0.1 SUV_Ws at 2 and 30 min pi, respectively).

One of the main clinical applications of PDE5 inhibitors is treatment of male erectile dysfunction where PDE5 inhibitors are used to inhibit cGMP degradation and maintain penile tumescence. Despite this fact, the maximum observed SUV_W in the penis for both tracers was

relatively low (SUV_W < 0.9, supporting information-table 4). This is not surprising since the expression of PDE5 in lung tissue is significantly higher than in the penis.[10,11,28,29]

2.4.2. Biodistribution in PDE5 TG mice

A biodistribution study in transgenic mice (N = 3), characterized by an up to 10-fold increase in PDE5 protein expression in the myocardiocyte and a 10-fold increase in sildenafil-inhibitable cGMP hydrolysis compared to wild type littermates, was performed at 30 min pi.

Myocardial uptake in PDE5 TG mice was almost 10-fold and 16-fold higher (% ID) for [^{11}C]**12** and [^{18}F]**17**, respectively compared to control mice (figures 1 and 2). This strengthens our initial claim that retention of both radiotracers in the lungs was PDE5-specific. Despite lower retention/uptake of [^{18}F]**17** than [^{11}C]**12** in lungs of control mice, evaluation of [^{18}F]**17** in PDE5 TG showed a two-fold (% ID) and three-fold (SUV_W) higher uptake in the myocardium than [^{11}C]**12** at 30 min pi. In contrast, SUV_W values in lung tissue of PDE5 TG mice for [^{11}C]**12** and [^{18}F]**17** were almost 50 % ($p < 0.05$) and 24 % ($p = 0.09$) lower, respectively compared to the control mice. This might be explained by the ‘‘stealing effect’’ of the myocardium and lower availability of circulating tracer.

In PDE5 TG mice, [^{18}F]**17** showed high blood concentration at 30 min pi (5.8±0.4 % ID, supporting information-table 5). The contribution of the radioactivity in the blood to myocardial retention and the specific binding of [^{18}F]**17** to PDE5 was assessed by pre-treating PDE5 TG mice with tadalafil.

2.5. Blocking study in control and PDE5 TG mice

The specific binding of [^{11}C]**12** and [^{18}F]**17** to PDE5 in the lungs of NMRI mice (N = 4) and myocardium of PDE5 TG mice (N = 3) was assessed by a pre-blocking biodistribution study where mice were pre-treated with tadalafil 10 mg/kg, sc, 60 min prior to tracer administration.

The results showed that there was a mild (32 %, $p < 0.05$) and marked (70 %, $p < 0.001$) reduction in % ID in the lungs of control mice for [^{11}C]**12** and [^{18}F]**17**, respectively (supporting information-table 5). However, the SUV_W values of [^{11}C]**12** in the lungs of non-treated and pre-treated NMRI mice showed no significant difference. This could be partly due to the significantly different ($p < 0.01$) average body weights between the two group 29.8±1.8 g and 35.7±1.5 g for non-treated and pre-treated groups, respectively. [31]

The myocardium of the PDE5 TG mice showed a marked 80 % ($p < 0.001$) and 87 % ($p < 0.0001$) reduction in the retention of [^{11}C]**12** and [^{18}F]**17** based on % ID, respectively. The reduction in the retention of the tracers in the lungs of PDE5 TG mice was mild and 16 % and 30 % of [^{11}C]**12** and [^{18}F]**17** were PDE5 specific inhibitable-binding (both not statistically significant), respectively. This could be explained by an already depleted inhibitable pool in the lungs of PDE5 TG mice by the ‘‘stealing effect’’ of the myocardium. The blocking study both in the control and PDE5 TG mice showed that despite the high lung-to-blood ratio observed for [^{18}F]**17**, more than 70 % of the activity in the lungs of control mice and 87 % in the myocardium of PDE5 TG mice were PDE5-specific inhibitable binding.

2.6. Plasma and brain radiometabolite analysis

Plasma and brain extracts were analyzed with HPLC to quantify the fraction of radiometabolites of [^{11}C]**12** and [^{18}F]**17** at 2 and 30 min pi (tables 3 and 4). At 2 min pi more than 94 % and 71 % of the activity recovered in the plasma were in the form of [^{11}C]**12** and [^{18}F]**17** respectively. However, at 30 min pi only 30 % of the activity recovered in the plasma was in the form of intact [^{11}C]**12**. Despite structural similarity between the two radiotracers, [^{18}F]**17** showed extensive metabolism and less than 7 % of activity in the plasma was in the form of intact radiotracer at 30 min pi. Defluorination of [^{18}F]**17** was not observed as this could have been reflected in the bone uptake. In addition, microPET imaging of [^{18}F]**17** did show any significant bone uptake (figure 6).

Table 3*. Plasma radiometabolite analysis of [^{11}C]**12** and [^{18}F]**17** in mice.*

	[^{11}C]**12** (%±SD)		[^{18}F]**17** (%±SD)	
	2 min (n = 2)	30 min (n = 3)	2 min (n = 2)	30 min (n = 3)
Intact tracer	92.9 - 90.4	32 - 29.5	71.4 - 68.8	7.1 - 5.4

Apparently, the polar radiometabolites detected in the plasma did not cross the blood brain barrier to any significant level for both radiolabeled molecules at 2 and 30 min pi as most of the activity in the brain was in the form of intact tracer (table 4). None of the tracers underwent major metabolism in the brain since the relative percentage of activity in the form of metabolite(s) was < 10 % for both tracers (supporting information figure 3).

***Table 4**. Brain radiometabolite analysis of [^{11}C]**12** and [^{18}F]**17** in mice expressed as percentage.*

	[^{11}C]**12** (%)		[^{18}F]**17** (%)	
	2 min (n = 2)	30 min (n = 2)	2 min (n = 2)	30 min (n = 2)
Intact tracer	98.7 - 99.7	91.3 - 92.7	99.1 – 99.7	90.7 – 93.8

2.7. MicroPET imaging

2.7.1. Myocardial uptake

In vivo tracer kinetics of [^{11}C]**12** and [^{18}F]**17** were studied in PDE5 TG mice and in rats. Binding specificity and reversibility of [^{11}C]**12** and [^{18}F]**17** was assessed in PDE5 TG mice by chasing and blocking experiments using the structurally unrelated PDE5 inhibitor tadalafil.[30]

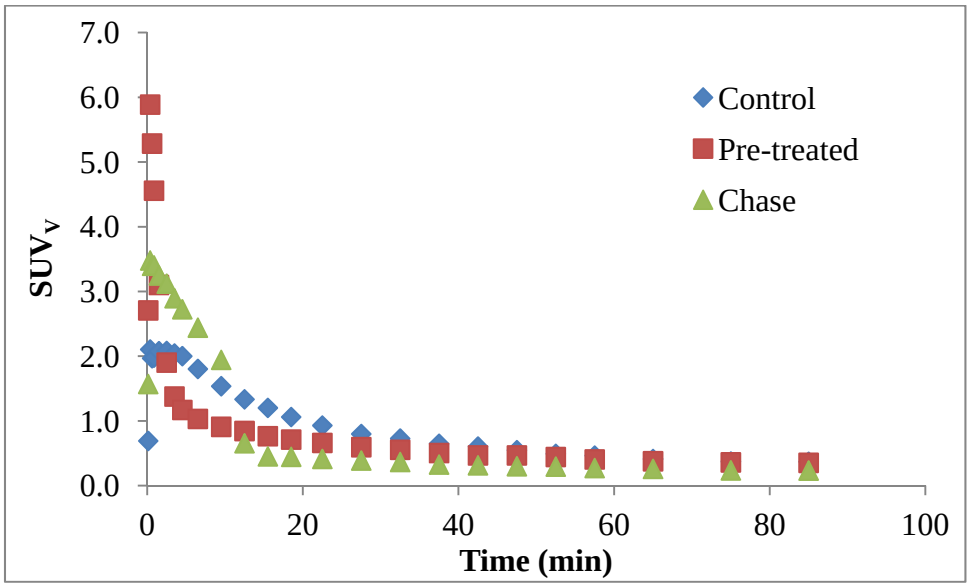

***Figure 3**. Time activity curves of the myocardium after IV injection of [^{11}C]**12** (7 MBq) in PDE5 TG mice (control), PDE5 TG mice pre-treated with tadalafil (10 mg/kg, sc, 60 min prior to tracer injection) and PDE5 TG mice chased with tadalafil (10 mg/kg, iv, 10 min after injection of tracer). SUV$_V$: standardized uptake value based on volume.*

The baseline scan showed a significant uptake and retention in the myocardium for both tracers albeit with relatively fast kinetics particularly for [^{11}C]**12** (figures 3 and 5). [^{18}F]**17** showed an almost 3-fold higher maximum SUV$_V$ value compared to [^{11}C]**12** (6.7 vs 2.3). Myocardial SUV$_V$ values for [^{18}F]**17** stayed within the range of 6.1 and 5.7 for 14 min (from 1.5 to 15.5 min post tracer injection). It is likely that a transient equilibrium was reached

within this 14-minutes time window specifically between 3.5 and 9.5 min post tracer injection as the average concentration of [^{18}F]**17** remained at 6.7±0.2 SUV_V in the six minutes window. However, [^{11}C]**12** showed rather fast kinetics and brief (transient) equilibrium between 2.5 and 4.5 min where the concentration remained around 2.2±0.2 SUV_V. In tadalafil pre-treated PDE5 TG mice the uptake was completely abolished in the myocardium for both tracers (figures 3 and 5).

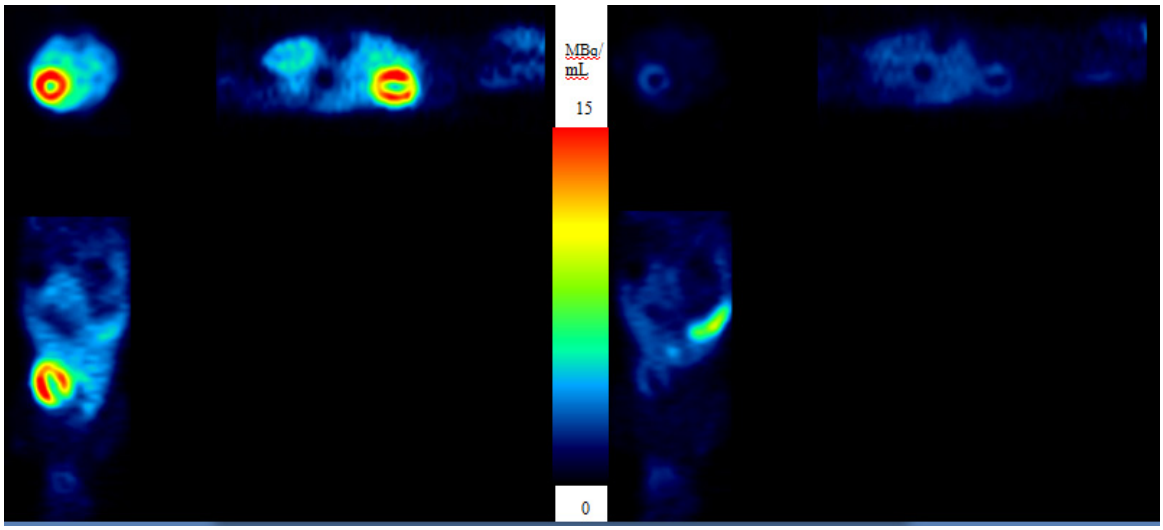

***Figure 4**. MicroPET images of PDE5 TG mice after injection of [^{11}C]**12** (7 MBq). Left: A summed image of dynamic microPET acquisition between 0 s and 660 s (60 s after tadalafil injection) in chase mouse. Right: A summed image of dynamic microPET acquisition between 840 s and 1500 s in the same chase mouse.*

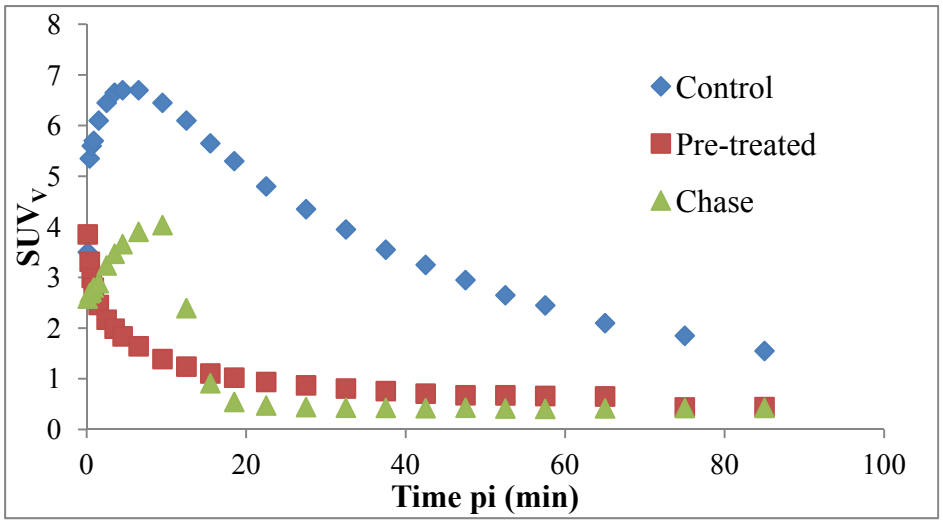

***Figure 5**.Time activity curves of the myocardium after IV injection of [^{18}F]**17** (7 MBq) in PDE5 TG mice (control); PDE5 TG mice pre-treated with tadalafil (10 mg/kg, sc, 60 min prior to tracer) and PDE5 TG*

mice chased with tadalafil (10 mg/kg, iv, 10 min post tracer injection). SUV_V: standardized uptake value based on volume.

In the chase mice, the myocardium was clearly visible in the early summed images (figures 4 and 6, left panel) but myocardial retention decreased very rapidly after tadalafil iv administration due to the displacement of tracers from myocardial regions by tadalafil (figures 4 and 6, right panel). Tracer displacement is also illustrated by the TAC curves of the chase experiment (green triangles) showing a marked decline immediately after tadalafil administration (figures 3 and 5). These microPET studies demonstrated that both [^{11}C]**12** and [^{18}F]**17** have high *in vivo* affinity and specificity for PDE5 and bind reversibly to this enzyme. However, [^{18}F]**17** appears superior in that the ratio of the TAC of base line scan to pre-treamnet scan is higher than that of [^{11}C]**12** (supporting information-figure 2).

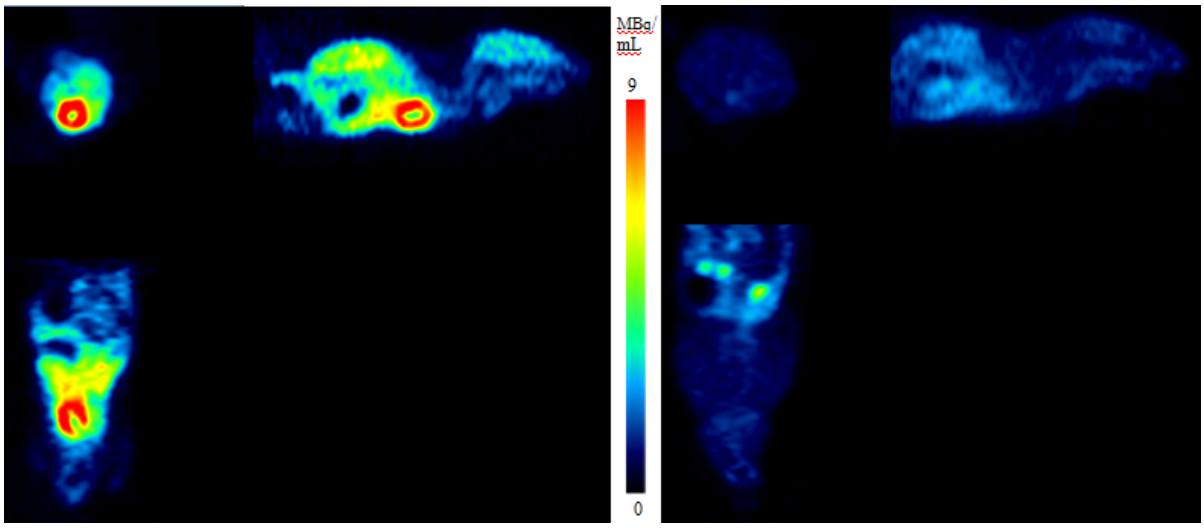

***Figure 6**. MicroPET images in PDE5 TG mice after injection of [^{18}F]**17** (7 MBq): Left: A summed image of dynamic microPET acquisition between 0 s and 660 s (60 s after tadalafil injection) in chase mouse. Right: A summed image of dynamic microPET acquisition between 840 s and 1500 s in the same chase mouse.*

2.7.2. Brain uptake

Dynamic microPET imaging was also performed in Wistar rats to evaluate the kinetics and binding properties of [^{11}C]**12** (figure 7) and [^{18}F]**17** in the brain (figure 8). MicroPET images showed that both tracers crossed the blood brain barrier (BBB) and were retained in the brain with a relatively homogenous distribution. Nonetheless, *in vivo* binding specificity of [^{11}C]**12** and [^{18}F]**17** in brain could not be demonstrated due to the unavailability of a structurally unrelated PDE5 inhibitor that crosses the BBB or brain specific PDE5 over-expressing

rat/mouse model. Despite this lack, a self-blocking study with cold **17** in rats showed no significant blocking (figures 7 and 8). In addition, *in vitro* autoradiography was performed in order to assess binding specificity of [^{11}C]**12** and [^{18}F]**17** to PDE5 in the brain by incubating both tracers with different PDE5 specific and non-specific inhibitors.

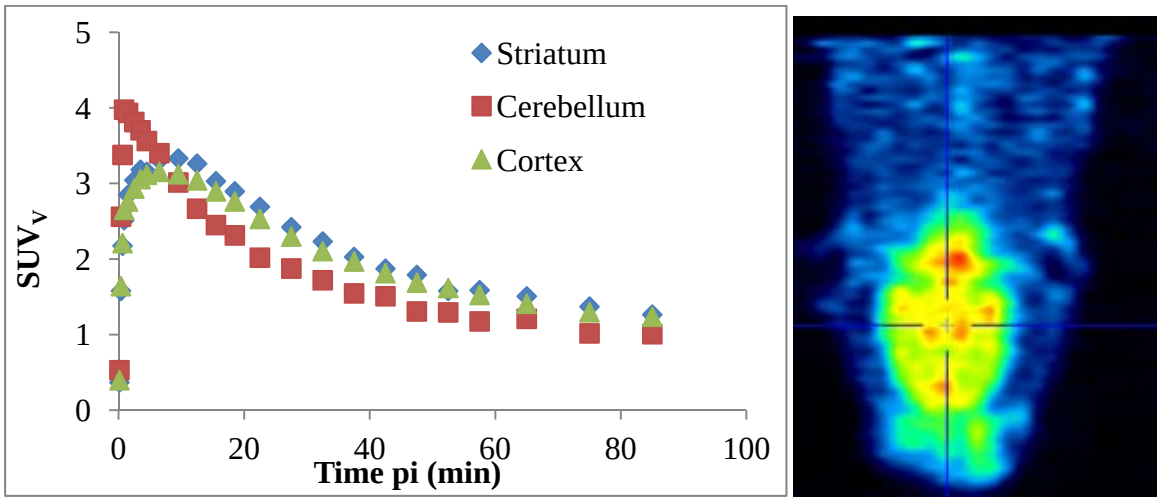

Figure 7. *Left: Time activity curves of different brain regions after IV injection of [^{11}C]**12** (37 MBq) in Wistar rats (N = 2). Right: Representative image of the brain after IV injection of [^{11}C]**12**.*

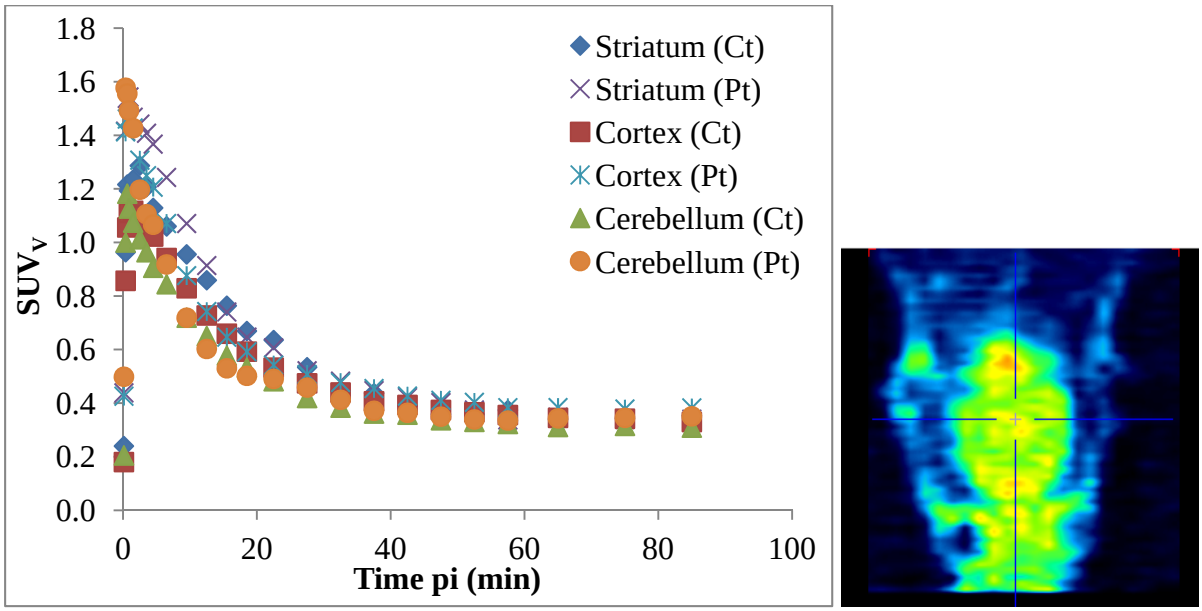

Figure 8*. Left: Time activity curves of different brain regions after IV injection of [^{18}C]**17** (37 MBq) in Wistar rats (N = 2); Ct: Control; Pt: Pre-treated (**17**, 10 mg/kg, sc, 60 min prior to tracer administration). Right: Representative image of the brain after IV injection of [^{18}F]**17**.*

2.8. In vitro autoradiography

Rat brain slices were used for *in vitro* autoradiography (figure 9). The slices were incubated with 370 kBq [^{11}C]**12** or [^{18}F]**17** alone or in the presence of different competitive PDE5

inhibitors (20 µM of each of NMVardenafil, tadalafil, **14**, or **12**, and 1 mM of 3-isobuty-1-methylxanthin/IBMX). IBMX is a non-selective phosphodiesterase inhibitor with the exception of PDE8 and PDE9 with *in vivo* PDE inhibitory activity (IC_{50}) ranging 2 µM from to 50 µM.[32-35]

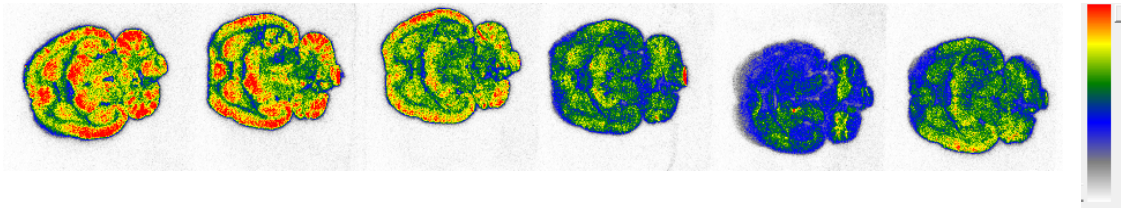

370 kBq [^{11}C]**12**	**7**	tadalafil	**14**	**12**	IBMX	
210902	204542	193394	157283	121014	159634	DLU/mm^2
100 %	93 %	87 %	73 %	55 %	74 %	% max reg.

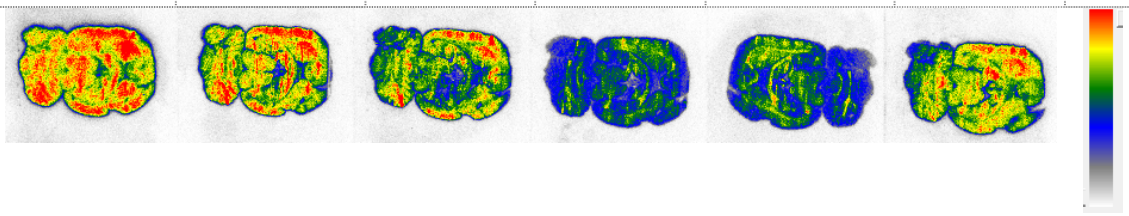

370 kBq [^{18}F]**17**	**7**	tadalafil	**14**	**17**	IBMX	
215700 DLU/mm^2	1980748	1746769	1293653	1336039	1840207	DLU/mm^2
100 %	88 %	83 %	62 %	65 %	87 %	% max reg.

***Figure 9**. Autoradiogram of rat brain slices incubated with [^{11}C]**12** (top) and [^{18}F]**17**(bottom) in the presence of different PDE inhibitors; DLU: Digital light unit; % max reg.:activity as percentage of maximum region (tracer only incubated slice as 100 % in both cases).*

Autoradiography with [^{11}C]**12** and [^{18}F]**17** revealed a uniform distribution of both tracers throughout the grey matter. The radioactivity concentration in the autoradiograms was expressed as digital light unit (DLU)/mm^2. The maximum blocking of [^{11}C]**12** and [^{18}F]**17** was observed in slices incubated with cold **12** or **17**, respectively and to a lesser extent by **14** and IBMX (figure 9). However, the PDE5 specific inhibitors (NMVardenafil[24] and tadalafil[30]) did not significantly block binding of [^{11}C]**12** and [^{18}F]**17**. Based on reported low levels and restricted expression of PDE5 in the cerebellum[1,9,10,28], non-significant reduction in self-pre-

treated rats (microPET), and lack of significant reduction of binding of both radiotracers in rat brain slices incubated with PDE5 specific inhibitors (autoradiography), it was concluded that *in vitro* binding and *in vivo* brain retention of [^{11}C]**12** and [^{18}F]**17** were not PDE5-specific. Further studies are warranted to determine the cellular binding site of [^{11}C]**12** and [^{18}F]**17** in brain.

3. Conclusion

We have successfully radiolabeled two close analogues of a pyridopyrazinone derivative (**PF-5)**; a compound which was initially reported as a brain penetrant PDE5 specific inhibitor. *In vitro* PDE5 inhibitory activity assay showed a higher IC_{50} value than reported. However, initial biological evaluation of [^{11}C]**12** and [^{18}F]**17** showed that both tracers have high and specific binding to PDE5 in the lungs of healthy mice where abundant expression of PDE5 have been described. Their *in vivo* specific binding to PDE5 was established in PDE5 TG mice in which the myocardial uptake could significantly be blocked by pre-treating the mice with a structurally unrelated PDE5 specific inhibitor tadalafil. Our study could not substantiate reported binding specificity of the tracers to PDE5 in the brain as the self-blocking study did not result in any significant reduction in brain uptake. Our preliminary biological evaluation confirmed the high affinity and binding specificity of [^{11}C]**12** and [^{18}F]**17** to PDE5 with the latter having higher affinity and specificity for PDE5. Therefore, [^{18}F]**17** can potentially be used to quantify and evaluate changes in PDE5 expression, select patients that would benefit from PDE5 inhibitor treatment early during disease progression and assess PDE5 occupancy and optimize dose regimens in patients treated with PDE5 inhibitors. Nonetheless, further experiments in a clinically relevant animal model and humans are required to evaluate the suitability of these radiotracers for the aforementioned applications.

4. Experimental section

4.1. Chemistry

A detailed description of the synthesis of all compounds with their ^{1}H-NMR and HRMS data for precursors and references is provided in the supporting information.

4.2. In vitro affinity assay

Compounds **10**, **12**, **14** and **17** were dissolved in DMSO to a concentration of 5 mM. Compounds were profiled on the PDE assay platform, comprising members of each of the 11 described PDE families.

PDE1B1 and PDE11A4 were expressed in human embryonic kidney (HEK) cells from full-length human recombinant clones. Human recombinant phosphodiesterases 2A, 4D3, 5A3, 7A1, 9A1, 10A2 were expressed in Sf9 cells, using a recombinant baculovirus construct containing the full length sequence with a 6xHis sequence following the start Met to allow metal affinity purification of the recombinant protein. Cells were harvested and the phosphodiesterase protein was purified by metal chelate chromatography on Ni-sepharose 6FF (GE Healthcare). PDE6AB, PDE3B and PDE8A were purchased as partially purified Sf9 cell lysates (Scottish Biomedical, UK). All enzymes were diluted in a mixture containing 50 mM Tris pH 7.8, 1.7 mM EGTA and 8.3 mM $MgCl_2$, except for PDE9A that was diluted in a mixture of 50 mM Tris pH 7.8, 5 mM $MnCl_2$. PDE1B was diluted in a mixture of 50 mM Tris pH 7.8, 1.7 mM EGTA, 8.3 mM $MgCl_2$ complemented with 624 U/ml calmodulin and 800 µM $CaCl_2$. The affinity of the compounds for the PDEs was measured by a scintillation proximity assay (SPA).

PDE yttrium silicate SPA beads allow PDE activity to be measured by direct binding of the primary phosphate groups of non-cyclic AMP or GMP to the beads via a complex iron chelation mechanism. The amount of bound tritiated product ([^{3}H]-AMP or [^{3}H]-GMP) is measured by liquid scintillation counting in a TopCount^{TM} instrument (Perkin Elmer).

The compounds were dissolved in DMSO in polystyrene plates to a concentration of 100-fold of the final concentration in the assay. Human recombinant PDE5A3 enzyme solution (10 µl) was added to 20 µl of incubation buffer (50 mM Tris pH 7.8, 8.3 mM $MgCl_2$, 1.7 mM EGTA), 10 µl substrate solution consisting of a mixture of non-tritiated and tritiated substrate (final concentration 1 µM cGMP, 370 Bq/0.01 µCi ^{3}H-cGMP), and 0.4 µl compound in DMSO in a 384-well plate, and the mixture was incubated for 30 min at room temperature. After incubation, the reaction was stopped with 20 µL of stop solution, consisting of PDE SPA beads (17.8 mg beads/ml in 200 mM zinc chloride). To measure the blank value, the enzyme was omitted from the reaction mixture. After sedimentation of the beads for 30 min, the radioactivity was measured in a PerkinElmer TopCount scintillation counter and results were expressed as counts per minute (cpm). The same assay principle was applied for the

measurement of the inhibition of other members of the PDE family, with appropriate modifications of enzyme concentration, incubation buffer, substrate solution, incubation time and stop solution. Each experiment was performed in duplicate.

Data were calculated as the percentage of inhibition of total activity measured in the absence of test compound (% control). A best-fit curve was fitted by a minimum sum of squares method to the plot of percent control versus compound concentration, from which an IC_{50} value (inhibitory concentration causing 50 % inhibition of hydrolysis) is obtained.

4.3. Radiosynthesis

Carbon-11 was produced in a Cyclone 18/9 cyclotron (IBA, Louvain-la-Neuve, Belgium) via an $^{14}N(p,\alpha)^{11}C$ nuclear reaction. A mixture of N_2 (95 %) with H_2 (5 %) was irradiated with 18-MeV protons for 30 min to get [^{11}C]methane ([^{11}C]CH_4). [^{11}C]CH_4 was transferred to a home-built synthesis module to convert it to [^{11}C]CH_3I which was then converted to the more reactive [^{11}C]methyl triflate ([^{11}C]CH_3OTf) by passing through a silver triflate column (150 x 3 mm) heated at 180 ^{o}C.

[^{11}C]CH_3OTf was streamed with helium through a solution of 250 - 500 µg precursor in DMSO. The reaction mixture was heated at 90 °C for 2 min, cooled and diluted with buffer. The crude reaction mixture was purified by HPLC (XBridge™ C18 column, 5µm, 4.6 mm x 150 mm; Waters) using as the mobile phase a mixture of 0.05 M sodium acetate pH 5.5 (0.05 M NaOAc pH 5.5) and ethanol (EtOH), 63:37 % v/v at a flow rate of 1 mL/min. The peak of interest was collected and analyzed for purity and identity for biological evaluation. For evaluation of the tracers in animals, the ethanol containing HPLC eluate was diluted with normal saline to a maximum concentration of 10 % ethanol and then sterile filtered through a 0.22-µm membrane filter (Millipore Millex GV 13 mm). Chemical and radiochemical purity of tracers were assayed with HPLC (XTerra™ C18 column, 5 µm, 4.6 mm x 100 mm) eluted with a mixture of acetate buffer (0.05 M, pH 5.5) and acetonitrile (ACN), 70:30 v/v at a flow rate of 1 mL/min, UV detection at 254 nm.

[^{18}F]Fluoride ($^{18}F^-$) was produced in a Cyclone 18/9 cyclotron (IBA) via an $^{18}O(p,n)^{18}F$ nuclear reaction by bombarding oxygen-18 enriched water ($H_2{}^{18}O$) with 18-MeV protons. [^{18}F]F^- was then passed through a preconditioned (by successive washing with 10 ml of 0.5 M K_2CO_3 solution and 10 mL of de-ionized water) anion exchange cartridge (SepPak Light Accell plus QMA, Waters) to get rid of the bulk of the $H_2{}^{18}O$. The [^{18}F]F^- was then eluted

with a mixture of 24 mM K_2CO_3/98 mM Kryptofix 2.2.2® (4,7,13,16,21,24-hexaoxa-1,10-diazabicyclo[8.8.8]-hexacosane) in 750 µl of a mixture of ACN:water (95:5 v/v) into a reaction vial. Any remaining water was removed by azeotropic distillation with ACN. An amount of 250 - 500 µg of the tosyl precursor in DMSO was added to the [^{18}F]F$^-$ containing vial and the mixture was heated at 90 ^{o}C for 15 min. The purification, formulation, sterile filtration, and quality control were done in similar conditions as for carbon-11 labeled compounds.

4.4. Biological evaluation

All animal experiments were conducted according to the Belgian code of practice for the care and use of animals, after approval from the Animal Ethics Committee, KU Leuven (Ethische Commissie Dierproeven, KU Leuven, License number: LA1210237).

Biodistribution study

For biodistribution studies adult NMRI mice (N = 4) and/or transgenic mice with cardiomyocyte specific PDE5 over-expression (PDE5 TG, N = 3), weighing 25 to 40 g were used. Animals were housed in individually ventilated cages in a thermo-regulated (22 °C), humidity-controlled facility under a 12 h/12 h light/dark cycle, with free access to food and water.

Biodistribution studies of carbon-11 or fluorine-18 labeled tracers was performed in healthy NMRI mice at 2, 10, 30, and 60 min post injection (N = 4 animals/time point). The biodistribution study in PDE5 TG mice (N = 3) was performed at 30 min pi. Mice were anesthetized with 2.5 % isoflurane in oxygen at a flow rate of 1 L/min and 7 MBq of [^{11}C]**12** or 740 KBq of [^{18}F]**17** was injected via a tail vein. The animals were sacrificed by decapitation at the specified time points. Blood and major organs were collected in tarred tubes and weighed. The radioactivity in blood and organs was counted using an automated γ-counter and expressed as a percentage of injected dose (% ID) and standardized uptake value based on weight (SUV_W) where initially the concentration in organ was expressed as activity (KBq) per gram (g) and then adjusted for body weight and total injected dose.. For the calculation of total radioactivity in blood, muscle and bone, weight of blood was assumed to be 7 %, bone to be 12 % and muscle to be 40 % of body weight.

Blocking study in control and PDE5 TG

In order to assess the affinity and specificity of [^{11}C]**12** and [^{18}F]**17** for PDE5, a blocking study was performed in control and PDE5 TG mice. In brief, mice were subcutaneously injected with tadalafil (TCR, Canada) 10 mg/kg, subcutaneous (sc), 60 min prior to tracer administration. Tadalafil solution for injection was prepared in such a way that the final concentration was 1 mg/mL in 10 % dimethylsulfoxide in 40 % (2-hydroxypropyl)-β-cyclodextrin solution and sterile filtered through a 0.22 μm filter (Millex®-GV, Millipore, Ireland). Biodistribution study was then performed as described above and results were expressed as % ID and SUV_W.

4.5. Radiometabolites analysis

4.5.1. Plasma radiometabolites analysis

Radiometabolites of [^{11}C]**12** and [^{18}F]**17** in plasma of mice (N = 2) at 2 and 30 min pi were quantified. Mice were anesthetized with 2.5 % isoflurane in oxygen at a flow rate of 1 L/min and injected with 7.4 MBq [^{11}C]**12** or [^{18}F]**17** via a tail vein. The mice were decapitated at the desired time point, blood was collected into lithium heparin-containing tubes (4.5-mL lithium heparin PST tubes, BD Vacutainer; BD, Franklin Lakes, New Jersey) and stored on ice. After centrifugation (420 x g; 10 min) of the blood, plasma was separated and analyzed by RP-HPLC on a Chromolith RP C18 column (3 mm × 100 mm; Merck) eluted with gradient mixtures of CH_3CN (A) and 0.05 M NaOAc pH 5.5 (B) (0-4 min: isocratic 0 % A, 0.5 mL/min; 4-9 min: linear gradient 0 % A to 90 % A, 1 mL/min; 9-2 min: isocratic 90 % A, 1 mL/min; 12-15 min: linear gradient 90 % A to 0 % A, 0.5 mL/min). The non-radioactive reference compound **12** or **17** was co-injected to identify the peak of the intact parent tracer. The eluate from the UV detector was passed through a 3-in. NaI(Tl) scintillation detector, connected to a single channel analyzer. The eluate from the radiodetector was collected as 1-mL fractions (model 2110 fraction collector, Biorad, Hercules, CA). The radioactivity in each fraction was measured using an automated gamma counter.

4.5.2. Brain radiometabolites analysis

Radiometabolites of [^{11}C]**12** or [^{18}F]**17** in brain of mice were quantified at 2 and 10 min after iv injection of the tracer (n=2 per time point). Mice were sacrificed by decapitation at the desired time point. Brain was isolated and homogenized in acetonitrile. The crude mixture was filtered through a syringe filter (0.2-μm nylon Acrodisc 13, Acrodisc Syringe Filters,

PALL Life Sciences). The filtrate was spiked with 5 µL of a 1 mg/mL solution of cold **12** or **17** and analyzed on HPLC (Xbridge™ RP C18 5 µm column, 4.6 mm × 150 mm; UV detection at 254 nM, eluted with a mixture of ACN and 0.05 M NaOAc pH 5.5, 32:68 v/v, at a flow rate of 1 mL/min).

4.6. Small-animal PET studies

Dynamic microPET imaging experiments were performed on a Focus 220 microPET scanner (Concorde Microsystems) where male PDE5 TG mice were used as animal model. During scanning, animals were kept under gas anesthesia (2.5 % isoflurane in O_2 at a flow rate of 1 L/min). Dynamic 90-min scans were acquired in list mode. Acquisition data were separated into 24 time frames (frame x time: 4 x 15 s, 4 x 60 s, 5 x 180 s, 8 x 300 s and 3 x 600 s) and reconstructed with maximum a posteriori (MAP) estimation. Time-activity curves (TAC) were generated for the myocardium region for each individual scan, using PMOD software (version 3.1; PMOD Technologies). The radioactivity concentration in the heart region was expressed as standardized uptake value based on volume (SUV_V) where the concentration in organ was expressed initially as activity (KBq) per volume of interest (mL) and then adjusted for body weight and total injected dose..

Base line imaging, blocking and chase experiments were performed in PDE5 TG mice. Tadalafil was used for pre-treatment and chase. Mice were injected with 7 MBq of formulation of [^{11}C]**12** or [^{18}F]**17** via a tail vein. For blocking studies mice were pretreated with 10 mg/kg tadalafil, subcutaneously, 60 min prior to tracer administration and for chase studies mice were given tadalafil 10 mg/kg, iv, 10 min after the start of PET acquisition. Tadalafil, which is a specific PDE5 inhibitor with subnanomolar IC_{50} value[30], was prepared in such a way that the final concentration was 1 mg/ml in 10 % dimethylsulfoxide in 40 % (2-hydroxypropyl)-β-cyclodextrin solution and the solution was sterile filtered via a 0.22-µm membrane filter.

A baseline microPET imaging was also performed in two Wistar rats after iv injection of [^{11}C]**12** or [^{18}F]**17** to assess the tracers' distribution in the brain.

4.7. In vitro autoradiography

Rat brain slices of 20 µm thick serial sections mounted on slides were used for *in vitro* autoradiography studies. Brain slices were incubated with 400 µL of 370 kBq/mL solution of [^{11}C]**12** or [^{18}F]**17** alone (control), or in the presence of 1 mM IBMX, 20 µM tadalafil, 20 µM

NMVardenafil[24], 20 μM **14**, 20 μM cold **12** or **17** for 30 min. Then, the slices were rinsed twice (2×5 min) with 50 mM Tris-HCl pH 7.4 containing 0.3 % BSA at 4 °C. After a quick dip in water at room temperature, the slices were dried.

Autoradiograms were obtained by exposing the slices for 30 min to a high-performance phosphor screen (Canberra Packard, Meriden, CT, USA). The images were analyzed with Optiquant software (Canberra Packard) and the radioactivity concentration in the autoradiograms was expressed in digital light units (DLU) per square millimeters.

4.8. Statistics

All calculated results are expressed as mean ± standard deviation (SD). For comparison the Student's t-test was used and $p < 0.05$ was considered statistically significant.

Acknowledgement:

We would like to thank Ann Van Santvoort, Julie Cornels, Jana Hemelaers and Ivan Sannen for their technical assistance during animal experiments.

We would also like to express our appreciation for the financial support from *In Vivo* Molecular Imaging Research (IMIR) and Fonds Wetenschappelijk Onderzoek Vlaanderen (FWO).

5. References

[1] Lin, C. S.; Lin, G.; Xin, Z. C.; Lue, T. F. Expression, distribution and regulation of phosphodiesterase 5. Curr. Pharm. Des. **2006**, 12, 3439-3457.

[2] Tsai, E. J.; Kass, D. A. Cyclic GMP signalling in cardiovascular pathophysiology and therapeutics. Pharmacol. Ther. **2009**, 122, 216-238.

[3] Kass, D. A.; Champion, H. C.; Beavo, J. A. Phosphodiesterase type 5 expanding roles in cardiovascular regulation. Circ. Res. **2007**, 101, 1084-1095.

[4] Nagendran, J.; Archer, S. L.; Soliman, D.; Gurtu, V.; Moudgil, R.; Haromy, A. Phosphodiesterase type 5 is highly expressed in the hypertrophied human right ventricle, and acute inhibition of phosphodiesterase type 5 improves contractility. Circulation. **2007**, 116, 238-248.

[5] Pokreisz, P.; Vandenwijngaert, S.; Bito, V.; Van den Bergh, A.; Lenaerts, I.; Busch, C.; Marsboom, G.; Gheysens, O.; Vermeersch, P.; Biesmans, L.; Liu, X.; Gillijns, H.; Pellens,

M.; Van Lommel, A.; Buys, E.; Schoonjans, L.; Vanhaecke, J.; Verbeken, E.; Sipido, K.; Herijgers, P.; Block, K. D.; Janssens, S. P. Ventricular phosphodiesterase-5 expression is increased in patients with advanced heart failure and contributes to adverse ventricular remodeling after myocardial infarction in mice. Circulation. **2009**, 119, 408-416.

[6] Vandenwijngaert S.; Pokreisz P.; Hermans H.; Gillijns H.; Pellens M.; Bax A.; Coppiello G.; Oosterlinck W.; Balogh A.; Papp Z.; Bouten V.; Bartunek J.; D'hooge J.; Luttun A.; Verbeken E.; Herregods C.; Herijgers P.; Bloch D.; Janssens S. Increased cardiac myocyte PDE5 levels in human and murine pressure overload hypertrophy contribute to adverse LV remodeling. PLoS One. 2013, 8:e58841.

[7] Lu, Z.; Xu, X.; Hu, X.; Lee, S.; Traverse, J. H.; Zhu, G.; Fassett, J.; Tao, Y.; Zhang, P.; dos Remedios, C.; Pritzker, M.; Hall, J. L.; Garry, D. J. Chen, Y. Oxidative stress regulates left ventricular PDE5 expression in the Failing Heart. Circulation. **2010**, 121, 1474-1483.

[8] Shan, X.; Quaile, M. P.; Monk, J. K.; French, B.; Cappola, T. P.; Margulies, K. B.; Differential expression of PDE5 in failing and nonfailing human myocardium. Circ. Hear. Fail. **2012**, 5, 79-86.

[9] Puzzo, D.; Sapienza, S.; Arancio, O.; Palmeri A. Role of phosphodiesterase 5 in synaptic plasticity and memory. Neuropsychiatr. Dis. Treat. **2008**, 2, 371-387.

[10] Prickaerts, J.; Sik, A.; Van Staveren, W. C.; Koopmansm, G.; Steinbushm, H. W.; Van der Staay, F. J.; de Vente, J.; Blokland, A. Phosphodiesterase type 5 inhibition improves early memory consolidation of object information. Neurochem. Int. **2004**, 45, 915-928.

[11] Buckley, M. S.;, Staib, R. L.; Wicks, L. M.; Feldman, J. P. Phosphodiesterase-5 inhibitors in management of pulmonary hypertension: Safety, tolerability, and efficacy. Drug. Healthc. Patient. Saf. **2010**, 2, 151-161.

[12] Giovannoni, M. P.; Vergelli, C.; Graziano, A.; Dal Piaz, V. PDE5 inhibitors and their applications. Curr. Med. Chem. **2010**, 17, 2564-2587.

[13] Crom, K. F.; Curran, M. P.; Abman, S. H.; Channick, R. N.; Heresi, G. A.; Rubin, L. J.; Torbicki, A. Sildenafil: A Review of its Use in Pulmonary Arterial Hypertension. Drug. **2008**, 68, 383-397.

[14] Takimoto, E.; Champion, H. C.; Li, M.; Belardi, D.; Ren, S.; Rodriguez, E. R.; Bedja, D.; Gabrielson, K. L.; Wang, Y.; Kass, D. A. Chronic inhibition of cyclic GMP

phosphodiesterase 5A prevents and reverses cardiac hypertrophy. Nat. Med. **2005**, 11, 214-222.

[15] Salloum, F. N.; Ockaili, R. A.; Wittkamp, M.; Marwaha, V. R.; Kukreja, R. C. Vardenafil: a novel type 5 phosphodiesterase inhibitor reduces myocardial infarct size following ischemia/reperfusion injury via opening of mitochondrial KATP channels in rabbits. J. Mol. Cell. Cardiol. **2006**, 40, 405-411.

[16] Szabo, G.; Radovits, T.; Veres, G.; Krieger, N.; Loganathan, S.; Sandner, P.; Karck, M. Vardenafil protects against myocardial and endothelial injuries after cardiopulmonary bypass. Eur. J. Cardiothorac. Surg. **2009**, 36, 657-664.

[17] Hassan, M. A. H.; Ketat, A. F. Sildenafil citrate increases myocardial cGMP content in rat heart, decreases its hypertrophic response to isoproterenol and decreases myocardial leak of creatine kinase and troponin T. BMC. Pharmcol. **2005**, 15, 6-10.

[18] Guazzi, M.; Vicenzi, M.; Area, R.; Guazzi, M. D. PDE5 inhibition with sildenafil improves left ventricular diastolic function, cardiac geometry, and clinical status in patients with stable systolic heart failure: results of a 1-year, prospective, randomized, placebo-controlled study. Circ. Heart. Fail. **2010**, 1, 8-17.

[19] Lewis, G. D.; Shah, R.; Shahzad, K.; Camuso, J. M.; Pappagianopoulos, P. P.; Hung, J.; Tawakol, A.; Gerszten, R. E.; Systrom, D. M.; Bloch, K. D.; Semigran, M. J. Sildenafil improves exercise capacity and quality of life in patients with systolic heart failure and secondary pulmonary hypertension. Circulation. **2007**, 116, 1555-1562.

[20] Menniti, F. S.; Ren, J. M.; Coskran, T. M.; Liu, J.; Morton, D.; Siestsma, D. K.; Som, A.; Stephenson, D. T.; Tate, B. A.; Finklestein, S. P. Phosphodiesterase 5A inhibitors improve functional recovery after stroke in rats: optimized dosing regimen with implication for mechanism. J. Pharmacol. Exp. Ther. **2009**, 3, 842-850.

[21] Menniti, F. S.; Ren, J. M.; Sietsma, D. K.; Som, A.; Nelson, F. R.; Stephenson, D. T.; Stephenson, D. T.; Tate, B. A.; Finklestein, S. P. A non-brain penetrant PDE5A inhibitor improves functional recovery after stroke in rats. Restor. Neurol. Neurosci. **2012**, 4, 283-289.

[22] Andres, J. I.; De Angelis, M.; Alcazar, J.; Celen, S.; Bormans, G. Recent advances in positron emission tomography (PET) radiotracers for imaging phosphodiesterases. Curr. Top. Med. Chem. **2012**, 12, 1224-1236.

[23] Jakobsen, S.; Kodahl, G. M.; Olsen, A. K.; Cumming, P. Synthesis, radiolabelling and *in vivo* evaluation of [^{11}C]RAL-01, a potential phosphodiesterase 5 radioligand. Nucl. Med. Biol. **2006**, 33, 593-597.

[24] Chekol, R.; Gheysens, O.; Cleynhens, J.; Pokreisz, P.; Vanhoof, G.; Ahamed, M.; Janssens, S.; Verbruggen, A.; Bormans, G. Evaluation of PET radioligands for *in vivo* visualization of phosphodiesterase 5 (PDE5). Nuc. Med. Biol. **2014**, 41, 155-162.

[25] Hughes, R. O.; Rogier, D. J.; Jacobsen, E. J.; Walker, J. K.; Macinnes, A.; Bond, B.R.; Zhang, L. L.; Yu, Y.; Zheng, Y.; Rumsey, J. M.; Walgren, J. L.; Curtiss, S. W.; Fobian, Y. M.; Heasley, S. E.; Cubbage, J. W.; Moon, J. B.; Brown, D. L.; Acker, B. A.; Maddux, T. M.; Tollefson, M. B.; Mischke, B. V.; Owen, D. R.; Freskos, J. N.; Molyneaux, J. M.; Benson, A. G.; Blevis-Bal, R. M. Design, synthesis, and biological evaluation of 3-[4-(2-hydroxyethyl)piperazin-1-yl]-7-(6-methoxypyridin-3-yl)-1-(2-propoxyethyl)pyrido[3,4-b]pyrazin-2(1H)-one, a potent, orally active, brain penetrant inhibitor of phosphodiesterase 5 (PDE5). J. Med. Chem. **2010**, 6, 2656-2660.

[26] Loev, B.; Musser, J. H.; Brown, R. E.; Jones, H.; Kahen, R.; Huang, F. C.; Khandwala, A.; Sonnino-Goldman, P.; Leibowitz, M. J. 1,2,4-Triazolo[4,3-a]quinoxaline-1,4-diones as antiallergic agents. J. Med. Chem. **1985**, 3, 363-366.

[27] Yoshida, Y.; Sakakura, Y.; Aso, S.; Okada, N.; Okada, S.; Tanabe, Y. Practical and Efficient Methods for Sulfonylafion of Alcohols Using Ts(Ms)CI / Et3N and Catalytic Me_3N.HCI as Combined Base: Promising Alternative to Traditional Pyridine. Tetrahedron. **1999**, 55, 2183-2192.

[28] Lakics, V.; Karran, E. H.; Boess, F. G. Quantitative comparison of phosphodiesterase mRNA distribution in human brain and peripheral tissues. Neuropharmacology. **2010**, 59, 367-374.

[29] Corbin, J. D.; Beasley, A.; Blount, M. A.; Francis, S. H. High level PDE5: A strong basis for treating pulmonary hypertension with PDE5 inhibitors. Biochem. Biophys. Research. Commun. **2005**, 334, 930-938.

[30] Daugan, A.; Grondin, P.; Ruault, C.; Le Monnier de Gouville, A. C.; Coste, H.; Linget, J. M.; Kirilovsky, J.; Hyafil, F.; Labaudinière, R. The discovery of tadalafil: A novel and highly selective PDE5 inhibitor. 2: 2,3,6,7,12,12a-hexahydropyrazino[1´,2´:1,6]pyrido[3,4,-b]indole-1,4,-dione analogues. J. Med. Chem **2003**, 46, 4533-4542.

[31] Keyes, W Jr. SUV: standard uptake or silly useless value? J. Nucl. Med. **1995**, 36, 1836-1839.

[32] Soderling, S. H.; Beavo, J. A. Regulation. of cAMP and cGMP signalling: new phosphodiesterases and new function. Curr. Opin. Cell. Biol. **2000**, 12, 174-179.

[33] Haning, H.; Niewohner, N.; Schenke, T.; Es-Sayed, M.; Schmidt, G.; Lampre, T.; Bischoff, E. Imidazo[5,1-f][1,2,4]triazin-4(3H)-ones, a new class of potent PDE 5 inhibitors. Bioorg. Med. Chem. Lett. **2002**, 12, 865-868.

[34] Essayan, D. M. Cyclic nucleotide phosphodiesterases. J. Allergy. Clin. Immunol. **2001**, 108, 671-680.

[35] Beavo, J. A.; Rogers, N. L.; Crofford, O. B.; Hardman, J. G.; Sutherland, E. W.; Newman, E. V. Effects of xanthine derivatives on lipolysis, and on adenosine 3',5'-monophosphate phosphodiesterase activity. Mol. Pharmacol. **1970**, 6, 597-603.

Chapter IV – Supporting Information

Chemistry

All final compounds (precursors and references) and intermediates were characterized by LC-HRMS and ^{1}H-NMR.

^{1}H-NMR spectra were recorded on a 400 MHz spectrometer (Bruker AVANCE). Deuterated chloroform ($CDCl_3$) or deuterated methanol (MeOD) or deuterated dimethyl sufoxide (DMSO-d_6) were used as solvent as indicated. Chemical shifts are reported in parts per million relative to tetramethylsilane ($\delta = 0$). Coupling constants are reported in hertz (Hz). Splitting patterns are defined as follow: s (singlet), br s (broad singlet), d (doublet), q (quartet), dd (double doublet), t (triplet), dt (double triplet), or m (multiplet).

The mass spectra were recorded on a **Bruker maXis** UHR-TOF mass spectrometer with LC–MS, Dionex 3000RS UHPLC (**maXis**, **Bruker**-Daltonik, Bremen, Germany).

High-performance liquid chromatography (HPLC) analysis was performed on a LaChrom Elite HPLC system (Hitachi) connected to a UV-spectrometer set at 220 nm. For the analysis of radiolabeled compounds, the HPLC eluate (after passage through the UV detector) was led over a 7.62-cm (3-in.) NaI(Tl) scintillation detector connected to a single-channel analyzer (GABI box; Raytest, Straubenhard, Germany). Quantification of radioactivity measurements in biodistribution studies was performed using an automated γ-counter equipped with a 7.62-cm (3-in.) NaI(Tl) well crystal coupled to a multichannel analyzer (1480 Wizard; Wallac, Turku, Finland). The results were corrected for background radiation and decay during counting. All solvents and chemicals were obtained from commercial sources (Acros Organics, Aldrich or Fluka unless specified otherwise) and used as such without further purification. Purity of all final compounds (precursors and references) was ≥ 95 % and was determined by HPLC.

(6-Chloro-pyridin-3-yl)-carbamic acid tert-butyl ester (**2**).

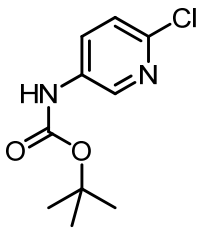

2

A solution of 6-Chloro-pyridin-3-ylamine (**1**, 15.7 g, 122.1 mmol, APOLLO Scientific Limited) and di-tert-butyldicarbonate (32.68 g, 148.8 mmol) in 1,4-dioxane (150 mL) was stirred at reflux for 20 hours. Additional di-tert-butyldicarbonate (5.0 g, 15.7 mmol) was added and the reaction was stirred at reflux for 7 hours. The reaction mixture was cooled and solvent evaporated at reduced pressure. The residue was re-dissolved in ethyl acetate (EtOAc) and poured into water. The layers were separated and the aqueous layer was extracted with ethyl acetate. The combined organic layers were washed with brine, dried over magnesium sulfate, and solvent was removed at reduced pressure to give brown oil. The residue was passed through a column of silica gel with 10 % EtOAc/heptane. **2** ((6-Chloro-pyridin-3-yl)-carbamic acid tert-butyl ester was obtained as off white light powder. (24.7 g, 108 mmol, 88.5 % yield). ^{1}H NMR (MeOD, 400 MHz): δ 1.40 (s, 9H, Boc), 7.21 (d, 1H, *J* 8.7, Ar), 7.82 (d, 1H, *J* 8.5, Ar), 8.28 (s, 1H, Ar). HRMS-ESI: calcd for $C_{10}H_{14}ClN_2O_2^+$ 229.0738, found 229.0731.

(6-Chloro-4-fluoro-pyridin-3-yl)-carbamic acid tert-butyl ester (**3**).

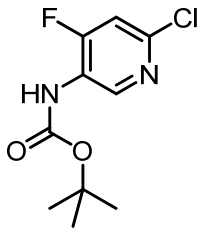

3

To a -63 °C solution of **2** (7.0 g, 30.6 mmol) and TMEDA (10.9 mL, 73.2 mmol) in diethyl ether (196 mL) under nitrogen was added a 1.6M n-butyl lithium solution in hexane (54 mL, 87 mmol) over a period of 30 minutes while maintaining the temperature of the reaction between -60 °C to -50 °C. The reaction was stirred at -60 °C for an additional 10 minutes after the addition was complete then warmed to -10 °C and stirred at -25 ° to -10 °C for 2.0 hours. The reaction was cooled to -60 °C and a solution of *N*-fluorodibenzenesulfonimide (15 g, 47.6 mmol) in THF (45 mL) was added while keeping the temperature below -50 °C. It precipitated on addition and stirring became difficult. The reaction was then allowed to slowly warm to 0 °C over 1 hour. The reaction was quenched with saturated ammonium chloride solution (112 mL). The layers were separated and the aqueous layer was extracted with ethyl acetate (2 x 50 mL). The combined organic layers were washed with brine, dried over $MgSO_4$, and solvent was removed at reduced pressure to give an oily brown solid. The residue was passed through a column of silica gel with 5 % ethyl acetate/ heptane. **3** was obtained as a

yellow solid. (4.44 g, 18 mmol, 58 % yield). ^{1}H NMR (MeOD, 400 MHz): δ 1.43 (s, 9H, Boc), 7.26 (d, 1H, *J* 9.8, Ar), 8.76 (s, 1H, Ar). HRMS-ESI: calcd for $C_{10}H_{13}ClFN_2O_2^+$ 247.0644, found 247.0644.

[6-Chloro-4-(2-propoxy-ethylamino)-pyridin-3-yl]-carbamic acid tert-butyl ester (**4**).

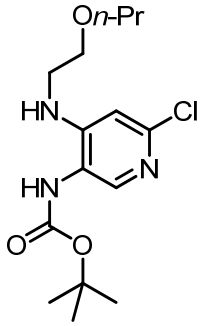

4

A solution of **3** (4.5 g, 18.2 mmol) and 2-n-propoxyethylamine (4.4 mL, 36.5 mmol) in ethanol (45 mL) was stirred at reflux for 22 hours. The reaction was cooled to room temperature and solvent was removed at reduced pressure to give a yellow solid which was triturated with heptane and filtered to give **4** as a white solid. (4.2 g, 12.7 mmol, 70 % yield). ^{1}H NMR ($CDCl_3$, 400 MHz): δ 0.92 (t, 3H, *J* 7.4, CH_3), 1.45 (s, 9H, *t*-Bu), 1.56-1.60 (m, 2H, CH_2), 3.26-3.31 (m, 2H, CH_2), 3.36-3.45 (m, 2H, CH_2), 3.60-3.64 (m, 2H, CH_2), 5.09 (br s, 1H, NH), 5.85 (br s, 1H, NH), 6.50 (s, 1H, Ar), 7.89 (s, 1H, Ar). HRMS-ESI: calcd for $C_{15}H_{25}ClN_3O_3^+$ 330.1579, found 330.1583

6-Chloro-N4-(2-propoxy-ethyl)-pyridine-3,4-diamine (**5**).

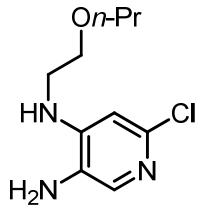

5

A solution of **4** (6.2 g, 18.8 mmol) in 1,4-dioxane (18 mL) was treated with 4 M HCl in 1,4-dioxane (88 mL) and stirred at room temperature overnight. Solvent was evaporated and the residue was partitioned between ethyl acetate and saturated sodium bicarbonate solution. The layers were separated and the aqueous layer was extracted with ethyl acetate. The combined organic layers were washed with brine, dried over magnesium sulfate, and solvent was

removed at reduced pressure to give **5** as dark brown oil. (3.74 g, 87 % yield). ^{1}H NMR ($CDCl_3$, 400 MHz): δ 0.93 (t, 3H, *J* 7.4, CH_3), 1.57-1.64 (m, 2H, CH_2), 2.75-2.96 (br s, 2H, NH_2), 3.29 (q, 2H, *J* 5.0, CH_2), 3.44 (t, 2H, *J* 6.6, CH_2), 3.67 (t, 2H, *J* 5.1, CH_2), 4.67-4.73 (br s, 1H, NH), 6.44 (s, 1H, Ar), 7.63 (s, 1H, Ar). HRMS-ESI: calcd for $C_{10}H_{17}ClN_3O^+$ 230.1055, found 230.1066

7-Chloro-1-(2-propoxy-ethyl)-1,4-dihydro-pyrido[3,4-b]pyrazine-2,3-dione (**6**).

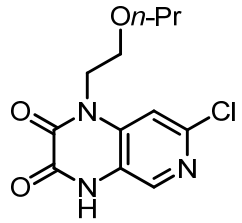

6

A 0 °C solution of **5** (3.74 g, 16.3 mmol) and diisopropylethylamine (6.1 mL, 34.3 mmol) in dichloromethane (134 mL) was treated with methyl chlorooxoacetate(1.5 mL, 15.6 mmol), allowed to warm to room temperature and stirred for four hours. The reaction was diluted with dichloromethane and washed with saturated sodium bicarbonate solution, dried over magnesium sulfate, and solvent was removed at reduced pressure. The residue was dried in a vacuum overnight. The residue was dissolved in toluene (40 mL) and refluxed for eight hours. The reaction mixture was cooled to room temperature and was used in the subsequent reaction as such.

3,7-Dichloro-1-(2-propoxyethyl)pyrido[3,4-b]pyrazin-2(1H)-one (**7**) [25].

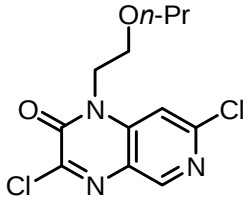

7

An aliquote of **6** from previous step was cooled down, and then thionyl chloride (1.63 mL, 22.7 mmol), DMF (1.63 mL) and additional 65 mL toluene were added. The reaction mixture was stirred at 130 °C for 16 hours and filtered while hot. The solvent was removed at reduced pressure to give a brown solid. This was passed through a column of silica gel with dichloromethane to give **7** as light yellow solid. (2.9 g, 9.6 mmol, 59 % yield). ^{1}H NMR ($CDCl_3$, 400 MHz): δ 0.74 (t, 3H, *J* 7.4, CH_3), 1.37-1.45 (m, 2H, CH_2), 3.28 (t, 2H, *J* 6.5,

CH_2), 3.72 (t, 2H, *J* 4.9, CH_2), 4.33 (t, 2H, *J* 4.9, CH_2), 7.50 (s, 1H, Ar), 8.67 (s, 1H, Ar). HRMS-ESI: calcd for $C_{12}H_{14}Cl_2N_3O_2^+$ 302.0463, found 302.0469.

tert-Butyl 4-(7-chloro-1,2-dihydro-2-oxo-1-(2-propoxyethyl)pyrido[3,4-b]pyrazin-3-yl)piperazine-1-carboxylate (**8**)

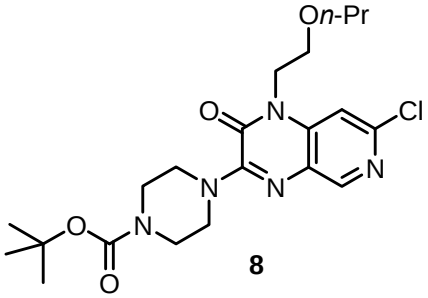

8

A solution of **7** (321 mg, 1.06 mmol), *tert*-butyl piperazine-1-carboxylate (269 mg, 1.45 mmol) and triethylamine (435 µL, 1.94 mmol) in THF (5 mL) was stirred at room temperature for 4 hours. The solvent was removed at reduced pressure and the residue was partitioned between ethyl acetate and water. The layers were separated and the aqueous layer was extracted with ethyl acetate. The combined organic layers were washed with brine, dried over $MgSO_4$ and concentrated at reduced pressure to give a yellow solid. This was passed through a column of silica gel eluted with 5 % MeOH in CH_2Cl_2 to give **8** as a light yellow solid. (384 mg, 0.85 mmol, 83% yield). ^{1}H NMR ($CDCl_3$, 400 MHz): δ 0.84 (t, 3H, *J* 7.2, CH_3), 1.27-1.35 (m, 2H, CH_2), 1.47 (s, 9H, boc), 3.35 (t, 2H, *J* 5.8, CH_2), 3.52-3.59 (m, 4H, $2CH_2$), 3.74 (t, 2H, *J* 5.8, CH_2), 3.92-4.01 (m, 4H, $2CH_2$), 4.32 (t, 2H, *J* 5.0, CH_2), 7.33 (s, 1H, Ar), 8.46 (s, 1H, Ar). HRMS-ESI: calcd for $C_{21}H_{31}ClN_5O_4^+$ 452.2059, found 452.2088

tert-Butyl 4-(1,2-dihydro-7-(5-methoxypyridin-2-yl)-2-oxo-1-(2-propoxyethyl)pyrido[3,4-b]pyrazin-3-yl)piperazine-1-carboxylate (**9**)

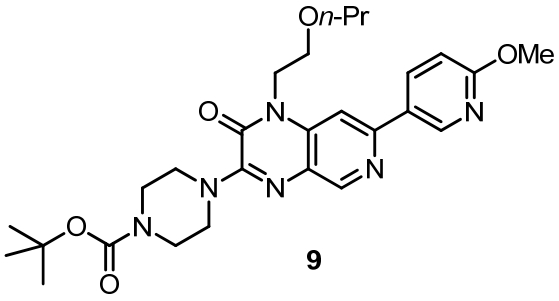

9

A solution of **8** (514 mg, 1.14 mmol) in 1,4-dioxane (5.4 mL) was treated with tetrakis(triphenylphosphine) palladium(0) (128 mg, 0.11 mmol) and stirred 5 min at RT. A warm solution of 2-methoxy-5-pyridineboronic acid (151.2 mg, 1 mmol, Frontier Scientific)

in ethanol (1 mL) and 2.0 M Na_2CO_3 (5.5 mL) were added. The mixture was refluxed during 16 h, filtered hot through celite and concentrated under reduced pressure. The residue was partitioned between ethyl acetate and water and the layers were separated. The aqueous layer was extracted with ethyl acetate (3x). The combined organic layers were washed with brine, dried over $MgSO_4$, concentrated under reduced pressure and passed through a column of silica gel eluted with 5% MeOH/ CH_2Cl_2 to yield **9** as a light yellow solid. (354 mg, 0.7 mmol, 61 % yield). ^{1}H NMR ($CDCl_3$, 400 MHz): δ 0.76 (t, 3H, *J* 7.2, CH_3), 1.48 (s, 9H, *t*-Bu), 3.35 (t, 2H, *J* 6.4, CH_2), 3.53-3.60 (m, 2H, CH_2), 3.76 (t, 2H, *J* 4.9, CH_2), 3.94-3.99 (m, 2H, CH_2), 3.98 (s, 3H, CH_3), 4.40 (t, 2H, *J* 4.8, CH_2), 6.83 (d, 1H, *J* 8.6, Ar), 7.25 (s, 1H, Ar), 7.63 (s, 1H, Ar), 8.23 (d, 1H, *J* 8.4, Ar), 8.75 (s, 1H, Ar). HRMS-ESI: calcd for $C_{27}H_{37}N_6O_5^+$ 525.282, found 525.2853

7-(5-Methoxypyridin-2-yl)-3-(piperazin-1-yl)-1-(2-propoxyethyl)pyrido[3,4-b]pyrazin-2(1H)-one (**10**).

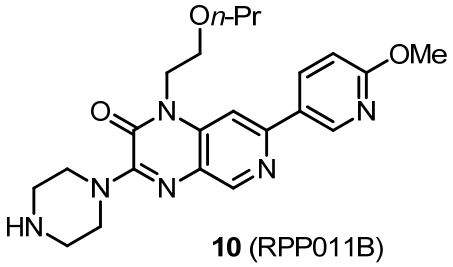

10 (RPP011B)

To a solution of **9** (354 mg, 0.7 mmol) in CH_2Cl_2 (2 mL) at 0 °C, TFA was added dropwise. The reaction mixture was brought to RT over an hour and stirred for 16 h. The reaction mixture was diluted with CH_2Cl_2 and quenched with a saturated Na_2CO_3 solution. The organic layer was separated and the aqueous layer was washed once more with CH_2Cl_2. The combined organic layers were washed with brine, dried over $MgSO_4$, concentrated under reduced pressure and passed through a column of silica gel eluted with 5 to 10 % MeOH/ CH_2Cl_2 to yield **10** as brown oil. (160 mg, 0.4 mmol, 55 % yield). ^{1}H NMR ($CDCl_3$, 400 MHz): δ 0.92 (t, 3H, *J* 7.1, CH_3), 1.58-1.65 (m, 2H, CH_2), 3.31-3.34 (m, 4H, CH_2), 3.52-3.57 (m, 2H, CH_2), 3.93-3.97 (m, 2H, CH_2), 4.12 (s, 3H, CH_3), 4.23-4.27 (m, 2H, CH_2), 4.61-4.65 (m, 2H, CH_2), 5.05-5.11 (m, 2H, CH_2), 7.00 (d, 1H, *J* 8.5, Ar), 7.87 (s, 1H, Ar), 8.36 (s, 1H, Ar), 8.73 (d, 1H, *J* 8.4, Ar), 8.85 (s, 1H, Ar). HRMS-ESI: calcd for $C_{22}H_{29}N_6O_3^+$ 425.2301, found 425.2308

7-Chloro-3-(4-methylpiperazin-1-yl)-1-(2-propoxyethyl)pyrido[3,4-b]pyrazin-2(1H)-one (**11**).

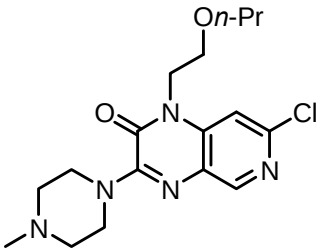

11

The procedure was the same as for preparation of **8** starting from **7** (181 mg, 0.6 mmol) except that 1-methylpiperazine (86 mg, 0.47 mmol) was used instead of *N-boc*-piperazine to afford the title compound as brown solid (171 mg, 0.47 mmol, 78 % yield). ^{1}H NMR ($CDCl_3$, 400 MHz): δ 0.83 (t, 3H, *J* 7.9, CH_3), 1.23-1.29 (m, 2H, CH_2), 1.45-1.53 (m, 2H, CH_2), 2.33 (s, 3H, CH_3), 2.54-2.57 (m, 4H, $2CH_2$), 3.34 (t, 2H, *J* 7.9, CH_2), 3.70-3.75 (t, 2H, *J* 7.8, CH_2), 3.95-4.03 (m, 4H, CH_2), 4.29 (t, 2H, *J* 7.8, CH_2), 7.32 (s, 1H, Ar), 8.46 (s, 1H, Ar). HRMS-ESI: calcd for $C_{17}H_{25}ClN_5O_2^+$ 366.1691, found 439. 366.1750

7-(5-Methoxypyridin-2-yl)-3-(4-methylpiperazin-1-yl)-1-(2-propoxyethyl)pyrido[3,4-b]pyrazin-2(1H)-one (**12**).

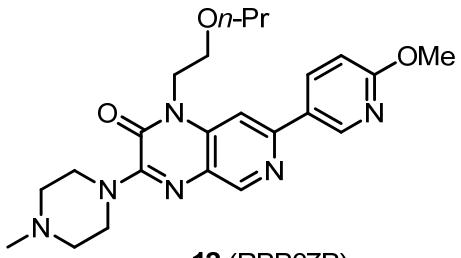

12 (RPP07B)

The procedure was the same as for preparation of **9** starting from **11** (171 mg, 0.47 mmol) and 2-methoxy-5-pyridineboronic acid (71.8 mg, 0.47 mmol) to afford the title compound as brown solid (136 mg, 0.31 mmol, 65 % yield). ^{1}H NMR ($CDCl_3$, 400 MHz): δ 0.76 (t, 3H, *J* 7.4, CH_3), 1.52-1.46 (m, 2H, CH_2), 2.35 (s, 3H, CH_3), 2.56-2.60 (m, 4H, *J* 4.9, CH_2), 3.35 (t, 2H, *J* 6.6, CH_2), 3.77 (t, 2H, *J* 5.4, CH_2), 3.98 (s, 3H, CH_3), 3.97-4.04 (m, 2H, CH_2), 4.40 (t, 2H, *J* 5.4, CH_2), 6.82 (d, 1H, *J* 8.6, Ar), 7.62 (s, 1H, Ar), 8.22 (dd, 1H, *J* 2.4 & 8.6, Ar), 8.72-8.76 (m, 2H, Ar). HRMS-ESI: Calculated for $C_{23}H_{31}N_6O_3^+$ 439.2458, found 439.2464

7-chloro-3-(4-(2-hydroxyethyl)piperazin-1-yl)-1-(2-propoxyethyl)pyrido[3,4-b]pyrazin-2(1H)-one (**13**).

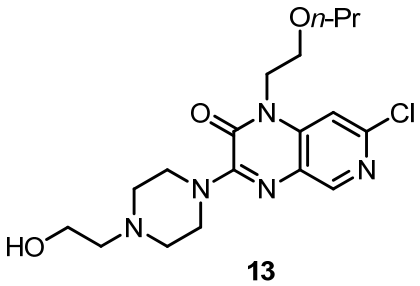

13

The procedure was the same as for preparation of **8** starting from **7** (315 mg, 1.4 mmol) except 1-(2-hydroxyethyl)piperazine (184.3 mg, 1.42 mmol) was used instead of *N-boc*-piperazine to afford the title compound as light yellow solid (392 mg, 1 mmol, 71 % yield). ^{1}H NMR ($CDCl_3$, 400 MHz): δ 0.83 (t, 3H, *J* 7.4, CH_3), 1.46-1.53 (m, 2H, CH_2), 2.61 (t, 2H, *J* 5.1, CH_2), 2.66 (t, 4H, *J* 4.5, $2CH_2$), 3.35 (t, 2H, *J* 6.4, CH_2), 3.67 (t, 2H, *J* 5.1, CH_2), 3.73 (t, 2H, *J* 5.2, CH_2), 4.02 (br m, 4H, $2CH_2$), 4.30 (t, 2H, *J* 5.2, CH_2), 7.33 (s, 1H, Ar), 8.45 (s, 1H, Ar).HRMS-ESI: calcd for $C_{18}H_{27}ClN_5O_3^+$ 396.1797, found 396.1810.

3-(4-(2-Hydroxyethyl)piperazin-1-yl)-7-(6-methoxypyridin-3-yl)-1-(2-propoxyethyl)pyrido[3,4-b]pyrazin-2(1H)-one **(14).**

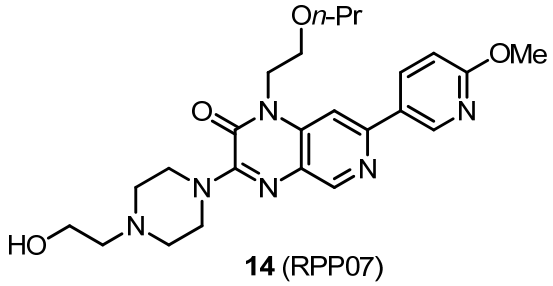

14 (RPP07)

The procedure was the same as for preparation of **9** starting from **13** to afford the title compound as brown solid. ^{1}H NMR ($CDCl_3$, 400 MHz):δ 0.72 (t, 3H, *J* 7.4, CH_3), 1.38-1.47 (m, 2H, CH_2), 2.56 (t, 2H, *J* 5.3, CH_2), 2.59-3.61 (m, 2H, CH_2), 3.31 (t, 2H, *J* 6.7, CH_2), 3.63 (t, 2H, *J* 5.3, CH_2), 3.73 (t, 2H, *J* 5.2, CH_2), 3.93 (s, 3H, CH_3), 3.92-3.97 (m, 2H, CH_2), 4.36 (t, 3H, *J* 5.1, CH_3), 6.77 (d, 1H, *J* 8.6, Ar), 7.55 (s, 1H, Ar), 7.60 (s, 1H, Ar), 8.17 (dd, 1H, *J* 2.2 & 8.7, Ar), 8.70 (s, 1H, Ar). HRMS-ESI: calcd for $C_{24}H_{33}N_6O_4^+$ 469.2563, found 469.2563

2-(4-(1,2-Dihydro-7-(6-methoxypyridin-3-yl)-2-oxo-1-(2-propoxyethyl)pyrido[3,4-b]pyrazin-3-yl)piperazin-1-yl)ethyl 4-methylbenzenesulfonate (**15**).

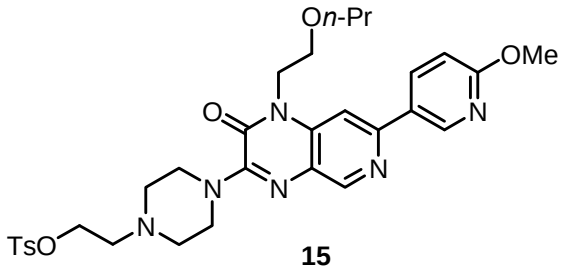

15

To a solution of **14** (100 mg, 0.21 mmol), triethylamine (75 µL, 2.5 eq) and trimethylammonium chloride (20.4 mg, 0.2 mmol, 1 eq) in CH_2Cl_2 (2 mL) at 0 °C, was added dropwise to 4-methylbenzene-1-sulfonyl chloride (61 mg, 0.32 mmol, 1.5 eq) in 2 mL CH_2Cl_2. The reaction mixture was brought to RT and stirred for 16 hours. The solvent was removed at reduced pressure and the crude mixture was passed through silica gel eluted with 2.5 % MeOH in CH_2Cl_2 to give **15** as yellow solid. (50 mg, 0.08 mmol, 38 % yield). ^{1}H NMR ($CDCl_3$, 400 MHz): δ 0.77 (t, 3H, *J* 7.4, CH_3), 1.22-1.24 (m, 2H, CH_2), 1.43-1.52 (m, 2H, CH_2), 2.72 (s, 3H, CH_3), 2.82 (t, 2H, *J* 6.7, CH_2), 3.60 (t, 2H, *J* 6.6, CH_2), 3.66 (t, 2H, *J* 6.7, CH_2), 3.78 (t, 2H, *J* 5.6, CH_2), 3.99 (s, 3H, CH_3), 4.05 (q, 2H, *J* 6.8, CH_2), 7.14 (d, 1H, *J* 8.6, Ar), 7.74-7.78 (m, 2H, Ar), 8.75 (s, 1H, Ar). HRMS-ESI: calcd for $C_{31}H_{39}N_6O_6S^+$ 623.2652, found for tosyl removed $[C_{24}H_{33}N_6O_4]^+$ 469.2558

4-(2-Fluoroethyl)-piperazine.

A mixture of 1-boc-piperazine (1.02 g, 5.47 mmol), 1-bromo-2-fluoroethane (4.17 g, 32 mmol) and DIEA (41.36 mg, 55.41 mL, 32 mmol) in CH_3CN (10 mL) was heated overnight at 50 ^{o}C and then refluxed for 6.5 h. The reaction mixture was cooled to RT and the solvent removed at reduced pressure. The residue was treated with 1 M NaOH (6.24 mL), extracted with EtOAc (2 x 20 mL) and dried over $MgSO_4$. The crude mixture was passed through silica gel eluted with a gradient mixture of 0 to 10 % MeOH in CH_2Cl_2 to afford colorless oil (**9**) (1.11 g, 87.4 %). An aliquot of **9** (1 g, 4.31 mmol) was dissolved in CH_2Cl_2 (10 mL), the reaction mixture was treated dropwise at 0 ^{o}C with TFA (5 mL) and stirred at RT for 2 h. The solvent was removed under reduced pressure and the residue partitioned between CH_2Cl_2 and saturated Na_2CO_3 solution. The organic layer was separated and the aqueous layer waswashed with CH_2Cl_2. The combined organic layers were dried over $MgSO_4$, filtered and the filtrate was concentrated under reduced pressure. A white precipitate was obtained which was filtered

off under a steady stream of N_2 and further dried under vacuum (506 mg, 3.8 mmol, yield: 70 %).^{1}H NMR (DMSO-d_6, 400 MHz): δ 4.73 (dt, 2H, *J* 4.6 & 47.4, CH_aH_b), 3.23-3.35 (m, 10H, CH_2). MS: $(M+H)^+$ m/z = 133.0

7-Chloro-3-(4-(2-fluoroethyl)piperazin-1-yl)-1-(2-propoxyethyl)pyrido[3,4-b]pyrazin-2(1H)-one (**16**).

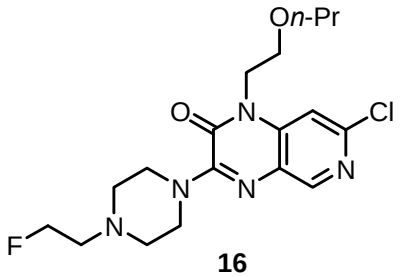

16

The procedure was the same as for preparation of **8** starting from **7** (109 mg, 0.36 mmol) except that 4-(2-fluoroethyl)-piperazine (476 mg, 3.6 mmol) was used instead of *N-boc*-piperazine to afford the title compound as a light yellow solid (100 mg, 0.25 mmol, 69 % yield). ^{1}H NMR ($CDCl_3$, 400 MHz): δ 0.85 (t, 3H, *J* 7.4, CH_3), 1.48-1.56 (m, 2H, CH_2), 2.65-2.75 (m, 4H, CH_2), 2.80 (t, 1H, *J* 4.7, CH), 3.66 (t, 2H, *J* 5.2, CH_2), 3.75 (t, 2H, *J* 5.2, CH_2), 4.01-4.15 (m, 4H, CH_2), 4.32 (t, 2H, *J* 5.2, CH_2), 4.56 (t, 1H, *J* 4.7, CH), 4.68 (t, 1H, *J* 4.7, CH), 7.34 (s, 1H, Ar), 8.48 (s, H, Ar). HRMS-ESI: calcd for $C_{18}H_{26}ClFN_5O_2^+$ 398.1754, found 398.1747

3-(4-(2-Fluoroethyl)piperazin-1-yl)-7-(6-methoxypyridin-3-yl)-1-(2-propoxyethyl)pyrido[3,4-b]pyrazin-2(1H)-one (**17**).

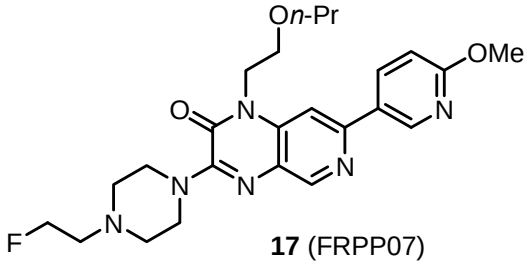

17 (FRPP07)

The procedure was the same as for preparation of **9** starting from **16** (73 mg, 0.2 mmol) and 2-methoxy-5-pyridineboronic acid (31 mg, 0.2 mmol) to afford the title compound as an off white solid (50 mg, 0.11 mmol, 50 % yield). ^{1}H NMR ($CDCl_3$, 400 MHz): δ 0.79 (t, 3H, *J* 7.4, CH_3), 1.24-1.26 (m, 2H, CH_2), 1.48-1.54 (m, 2H, CH_2), 2.70-2.72 (m, 4H, CH_3), 2.82 (t, 2H, *J* 6.5, CH_2), 3.38 (t, 2H, *J* 6.6, CH_2), 3.80 (t, 2H, *J* 6.6, CH_2), 3.99 (s, 3H, CH_3), 4.07 (t, 2H, *J*

6.2, CH_2), 4.43 (t, 2H, *J* 6.5, CH_2), 4.57 (t, 1H, *J* 6.6, CH), 4.70 (t, 1H, *J* 6.6, CH), 6.83-6.87 (m, 2H, Ar), 7.65 (s, 1H, Ar), 8.25 (m, 1H, Ar), 8.78 (s, 1H, Ar). HRMS-ESI: calcd for $C_{24}H_{32}FN_6O_3^+$ 471.2520, found 471.2526.

In vitro PDEs inhibitory activity assay of 12 and 17

Table 1. *IC_{50} (µM) values of PDE5 inhibitors for the 11 PDE families*

	14	**12**	**17**
hPDE1B1	0.016	30	ND
hPDE2A	10.00	10	ND
hPDE3B	10.00	10	ND
hPDE4D3	20.2	28.0	ND
hPDE5A3	0.00195	0.00660	0.00645
hPDE6AB	1.60	3.17	ND
hPDE7A1	30	30	ND
hPDE8A1	30	30	ND
hPDE9A	30	30	ND
hPDE10A2	5.9	8.4	ND
hPDE11A4	0.80	2.10	ND

ND: Not determined

HPLC purification and quality control of labeled compounds

Table 2. Purification and analysis of radiotracers

Radioligand	Mobile phase preparative HPLC (%, buffer in EtOH)	Rt (min)	Mobile phase analytical HPLC (%, buffer in ACN)	Rt (min)
[^{11}C]-**12**	67, 0.05 M NaOAc pH 5.5	16.5	70, 0.05 M NaOAc pH 5.5	10.1
[^{18}F]-**17**	63 , 0.05 M NaOAc pH 5.5	26.0	68, 0.05 M NaOAc pH 5.5	17.1

R_t (retention time), RCY (radiochemical yield, non decay corrected), ACN (acetonitrile), EtOH (ethanol)

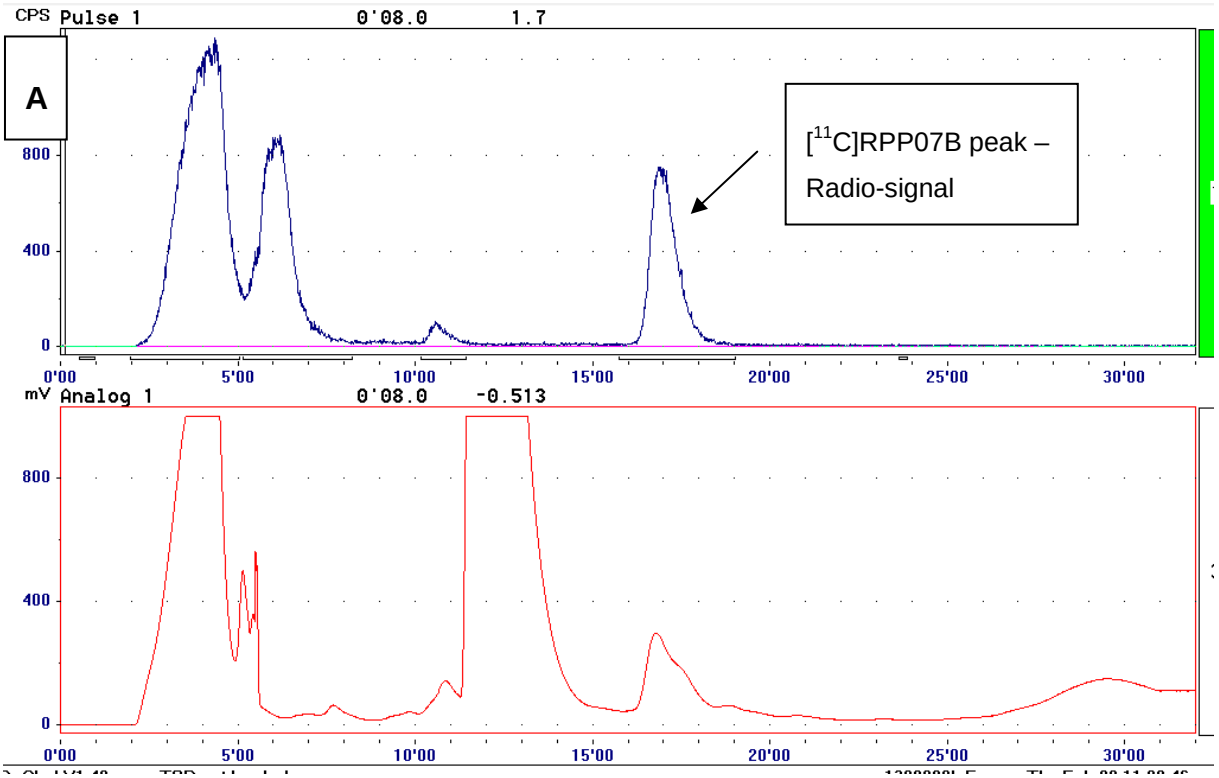

Integration C:\Gina Star data research\RPPS-22052012\RPP07BRA N REF-1-12022014, R

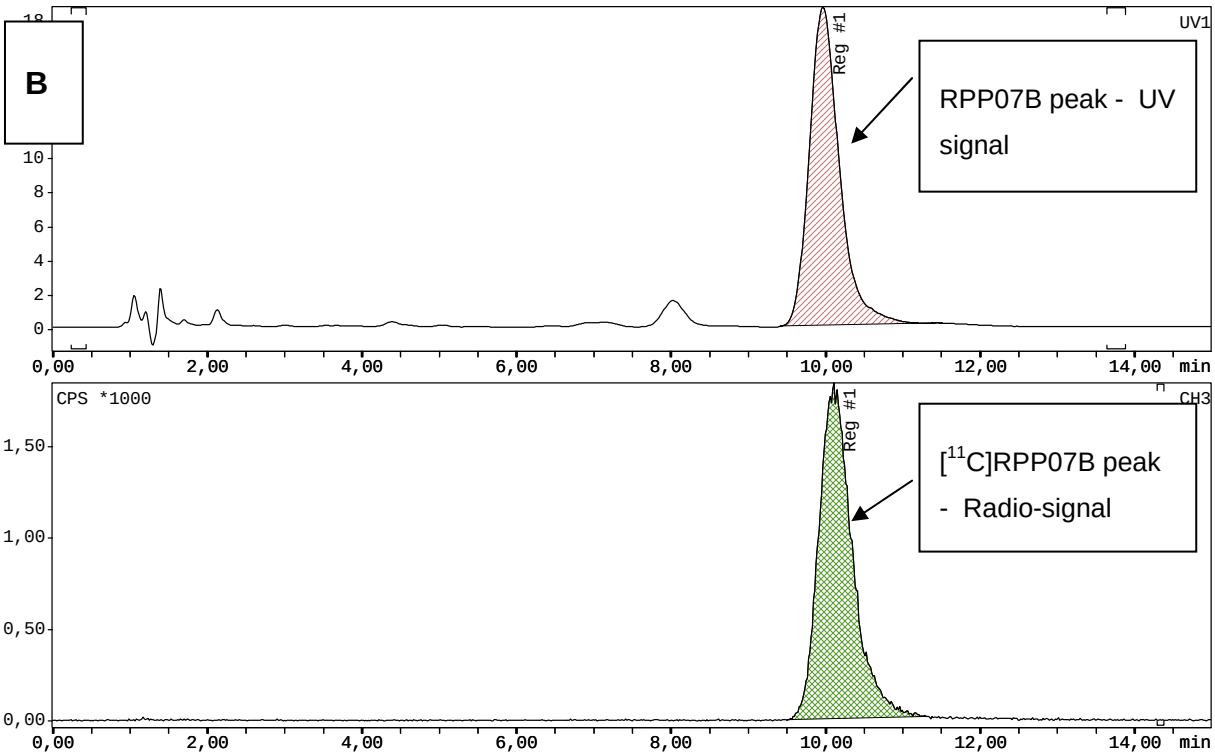

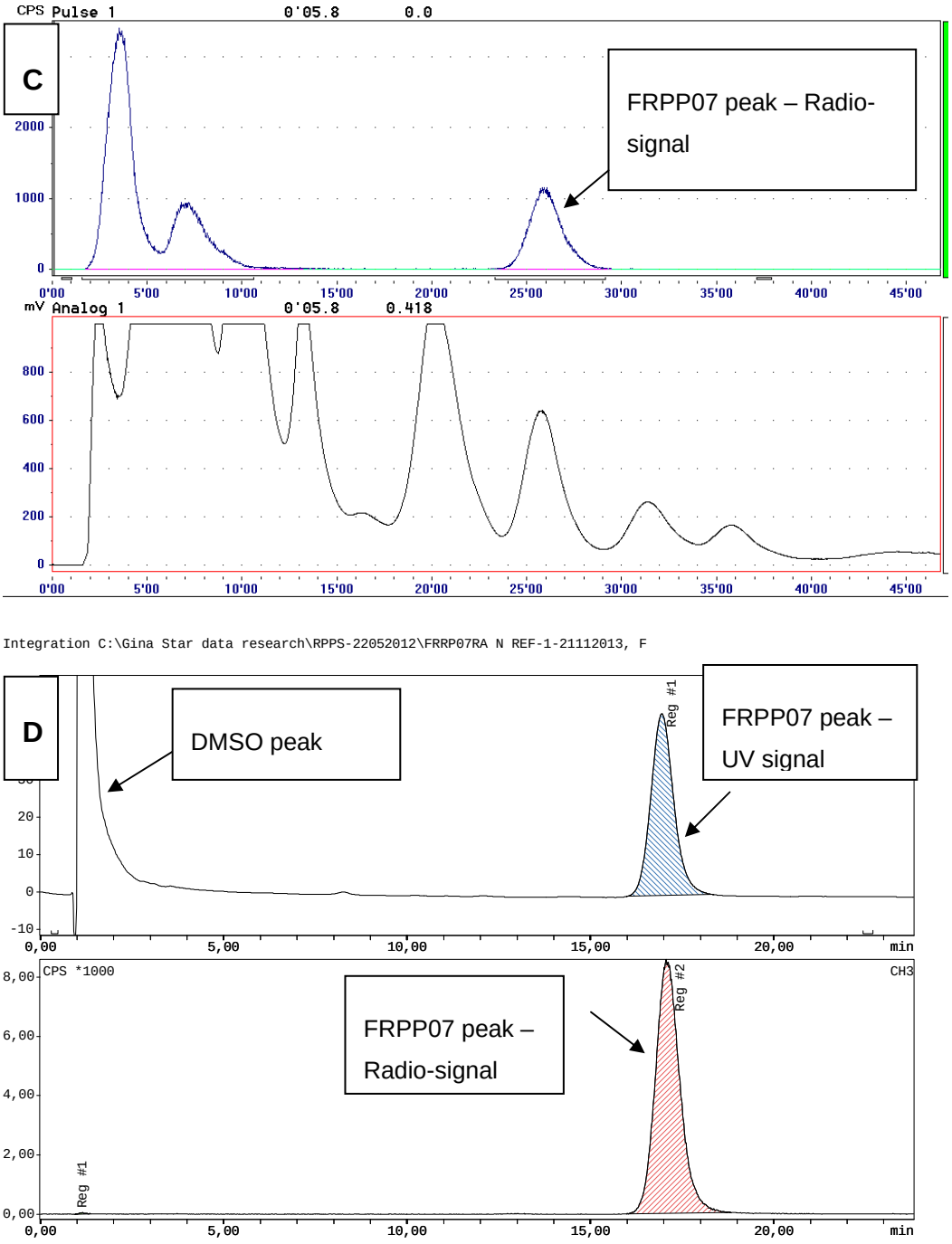

Figure 1. *Radio-chromatograms of RP-HPLC purification of [^{11}C]**12** (**A**) and [^{18}F]**17** (**C**) and identity confirmation by co-injection of standard non-radioactive references **12** and **17** with the isolated radioactive formulation of [^{11}C]**12** (**B**) and [^{18}F]**17** (**D**), respectively.*

Biological evaluations of [^{11}C]12 and [^{18}F]17

Table 3. Biodistribution study of [^{11}C]**12** and [^{18}F]F**12** in NMRI mice at several time points post injection (N = 4 at each time point, SD = standard deviation)

[a]Percentage of Injected Dose (% ID±SD)

	[^{11}C]**12**			[^{18}F]F**17**			
Organs	2 min	10 min	30 min	2 min	10 min	30 min	60 min
Urine	0.2±0.2	0.6±0.2	0.5±0.3	0.2±0.1	0.4±0.2	0.8±0.5	1.4±0.3
Kidneys	9.9±1.9	6.5±1.1	4.4±0.4	6.1±0.8	3.5±0.4	2.5±0.5	2.3±0.2
Liver	13.3±2.4	16.8±2.2	16.8±1.8	14.1±2.1	13.0±0.5	9.0±1.6	7.4±0.7
Spleen	0.9±0.1	1.1±0.2	0.7±0.1	0.5±0.1	0.4±0.1	0.3±0.1	0.3±0.1
Pancreas	1.0±0.0	1.3±0.2	1.2±0.3	1.0±0.4	1.0±0.2	0.9±0.1	0.6±0.1
Lungs	15.2±1.9	5.1±0.6	3.1±0.6	7.7±0.7	4.1±0.2	2.3±0.3	2.6±0.4
Heart	1.2±0.1	0.6±0.1	0.5±0.0	1.2±0.1	0.7±0.1	0.5±0.1	0.5±0.1
Intestines	10.2±1.4	13.6±0.9	21.1±1.4	10.3±1.6	12.6±1.0	14.1±1.1	15.8±1.8
Stomach	1.1±0.2	3.2±0.7	5.0±0.6	1.9±0.5	3.2±0.4	5.2±1.5	9.5±0.5
Cerebrum	3.2±0.6	2.2±0.2	1.3±0.0	1.9±0.2	1.4±0.1	0.9±0.1	0.7±0.1
Cerebellum	0.8±0.3	0.4±0.1	0.2±0.1	0.5±0.1	0.3±0.0	0.2±0.0	0.2±0.1
Blood	2.8±0.2	1.9±0.3	1.7±0.1	5.7±0.6	4.5±0.5	5.4±0.5	5.4±0.7
Muscle	19.1±10.1	30.0±4.3	15.4±8.9	45.5±6.7	29.2±1.9	25.6±4	24.0±2.5
Penis	0.1±0.0	0.1±0.0	0.1±0.0	0.1±0.0	0.1±0.0	0.1±0.0	0.1±0.0
Bone				5.7±1.4	8.4±1.2	7.4±1.0	7.6±1.1
Brain	4.0±0.9	2.6±0.3	1.5±0.1	2.4±0.3	1.7±0.1	1.2±0.1	0.9±0.1

*Data are expressed as mean±SD; [a]percentage of injected dose calculated as CPM in organ * 100%/total CPM recovered*

Table 4. Biodistribution study of [^{11}C]**12** and [^{18}F]F**12** in NMRI mice at several time points post injection (N = 4 at each time point, SD = standard deviation)

[a]Standard uptake values SUV_W±SD)

	[^{11}C]**12**			[^{18}F]F**17**			
Organs	2 min	10 min	30 min	2 min	10 min	30 min	60 min
Kidneys	6.1±0.7	3.9±0.5	2.6±0.1	3.1±1.8	2.3±0.0	1.5±0.4	1.3±0.1
Liver	2.4±0.3	3.6±0.6	3.1±0.4	1.9±1.1	2.4±0.1	1.7±0.2	1.3±0.2
Spleen	2.3±0.3	3.4±0.7	1.8±0.2	2.3±1.3	2.3±0.2	1.2±0.3	0.9±0.2
Pancreas	1.4±0.2	2.3±0.2	1.6±0.3	1.6±1.0	1.9±0.0	1.4±0.2	0.9±0.1
Lungs	15.1±3.0	6.3±0.7	3.8±1.	10.9±6.7	5.5±1.0	2.8±1.0	2.9±0.5
Heart	2.5±0.3	1.5±0.0	0.9±0.1	2.1±1.2	1.8±0.1	1.3±0.2	1.0±0.1
Intestines	1.0±0.1	1.5±0.1	2.1±0.1	0.9±0.5	1.5±0.1	1.6±0.1	1.6±0.2
Stomach	0.6±0.2	1.6±0.8	1.6±0.3	0.6±0.4	1.6±0.6	2.7±0.7	3.5±0.2
Cerebrum	2.9±0.6	2.8±0.4	1.2±0.0	2.2±0.2	1.7±0.1	1.1±0.2	0.8±0.1
Cerebellum	3.0±0.7	2.1±0.3	0.9±0.1	3.0±0.3	2.1±0.1	1.4±0.3	0.9±0.1
Blood	0.4±0.0	0.3±0.0	0.2±0.0	0.8±0.1	0.6±0.1	0.8±0.1	0.8±0.1
Muscle	0.5±0.3	0.7±0.1	0.4±0.2	1.1±0.2	0.7±0.0	0.5±0.3	0.6±0.1
Penis	0.5±0.1	0.7±0.1	0.6±0.2	0.5±0.2	0.8±0.1	0.9±0.0	0.8±0.1
Bone				0.5±0.1	0.7±0.1	0.6±0.1	0.6±0.1
Lung/Blood	38	21	19	14	9	4	4

*Data are expressed as mean±SD; [a]SUV_W calculated as (CPM in organ * Weight of mouse)*100% /(total CPM recovered * organ weight)*

Table 5. Biodistribution of [^{11}C]**12** and [^{18}F]F**12** in NMRI mice pre-treated with tadalafil, PDE5 TG mice, PDE5 TG mice pre-treated with tadalafil at 30 min post injection (N = 3, SD = standard deviation)

	[a]% Injected Dose (% ID±SD)					
	[^{11}C]12			**[^{18}F]17**		
Organs	NMRI mice (Pre-treated)	PDE5 TG	PDE5 TG (Pre-treated)	NMRI mice (Pre-treated)	PDE5 TG	PDE5 TG (Pre-treated)
Urine	3.1±1.5	3.7±0.4	7.5±0.9	1.4±0.6	1.1±0.5	1.1±0.2
Kidneys	4.3±0.7	4.0±0.7	5.1±1.0	4.7±0.9	1.7±0.1	3.6±0.1
Liver	16.4±1.1	13.6±1.4	14.3±2.9	8.3±0.5	6.9±0.6	8.4±1.8
Spleen	0.6±0.1	1.0±0.1	0.8±0.0	0.3±0.0	0.2±0.1	0.4±0.2
Pancreas	1.2±0.2	1.4±0.4	1.2±0.3	0.8±0.2	0.5±0.1	0.7±0.4
Lungs	2.1±0.2	1.6±0.1	1.3±0.3	0.7±0.2	1.7±0.3	1.2±0.3
Heart	0.5±0.0	4.0±0.4	0.8±0.0	0.6±0.1	8.2±0.6	1.1±0.3
Intestines	18.1±2.9	22.3±2.1	15.5±2.6	12.5±1.1	13.6±1.9	13.2±0.9
Cerebrum	1.2±0.1	1.2±0.1	1.1±0.2	0.9±0.1	0.8±0.2	0.8±0.1
Cerebellum	0.2±0.0	0.2±0.1	0.2±0.0	0.3±0.1	0.2±0.0	0.2±0.0
Blood	1.9±0.1	1.5±0.1	1.7±0.2	6.2±0.3	5.8±0.4	8.3±2.3
Muscle	25.3±0.6	23.1±2.5	28.5±9.1	25.3±2.3	25.2±0.3	30.8±3.5
Penis	0.1±0.0	0.1±0.0	0.1±0.0	0.1±0.0	0.1±0.1	0.1±0.0
Bone				5.2±2.3	8.0±0.7	9.0±0.9

*Data are expressed as mean±SD; [a]percentage of injected dose calculated as CPM in organ * 100%/total CPM recovered*

Table 6. Biodistribution of [^{11}C]**12** and [^{18}F]F**12** in NMRI mice pre-treated with tadalafil, PDE5 TG mice, PDE5 TG mice pre-treated with tadalafil at 30 min post injection (N = 3, SD = standard deviation)

	[a]Standardized uptake values (SUV_W±SD)					
	[^{11}C]12			**[^{18}F]17**		
Organs	NMRI mice (Pre-treated)	PDE5 TG	PDE5 TG (Pre-treated)	NMRI mice (Pre-treated)	PDE5 TG	PDE5 TG (Pre-treated)
Kidneys	2.8±0.4	2.6±0.4	3.4±0.5	2.5±0.2	1.4±0.1	2.5±0.2
Liver	3.8±0.3	3.0±0.3	3.4±0.5	2.3±0.1	1.7±0.1	2.3±0.1
Spleen	2.3±0.3	3.8±0.5	4.7±0.1	3.8±1.5	1.2±0.2	3.8±1.2
Pancreas	1.9±0.4	2.1±0.3	2.0±0.3	2.7±0.9	1.0±0.1	2.7±0.7
Lungs	3.4±0.7	1.9±0.3	2.2±0.6	1.8±0.1	1.9±0.3	1.8±0.1
Heart	1.1±0.1	7.5±0.9	1.8±0.2	4.0±0.7	21.4±1.7	4.0±0.6
Intestines	1.7±0.3	2.5±0.2	2.1±0.5	2.0±0.2	1.6±0.2	2.0±0.1
Cerebrum	1.3±0.1	1.1±0.1	1.3±0.2	1.4±0.1	0.9±0.0	1.4±0.1
Cerebellum	0.9±0.0	0.7±0.1	0.9±0.1	2.7±0.3	0.9±0.1	2.8±0.3
Blood	0.3±0.0	0.2±0.0	0.2±0.0	1.2±0.3	0.8±0.0	1.2±0.3
Muscle	0.6±0.0	0.6±0.1	0.7±0.2	0.8±0.1	0.6±0.0	0.8±0.1
Penis	0.7±0.1	1.0±0.0	0.8±0.2	1.4±0.8	1.0±0.0	0.9±0.1
Bone				0.7±0.1	0.7±0.1	0.7±0.1
Heart/Blood		35.7±4.5	7.7±0.1		26.1±4.1	3.4±1.2

*Data are expressed as mean±SD; [a]SUV_W calculated as (CPM in organ * Weight of mouse)*100% /(total CPM recovered * organ weight)*

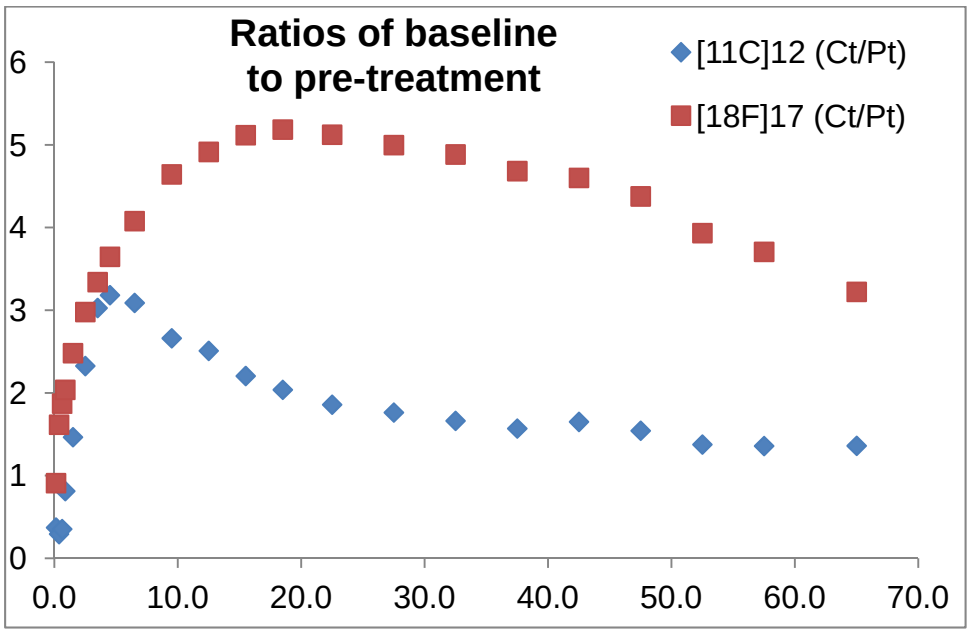

Figure 2. *Ratios between the time-activity curves of the base line and pre-treatment for [^{11}C]**12** and [^{18}F]**17**. [^{11}C]**12** (Ct/Pt): Time-activity-curves ratios between base line (Ct) and pre-treatment for [^{11}C]**12**; [^{18}F]**17** (Ct/Pt): ime-activity-curves ratios between base line (Ct) and pre-treatment for [^{18}F]**17**.*

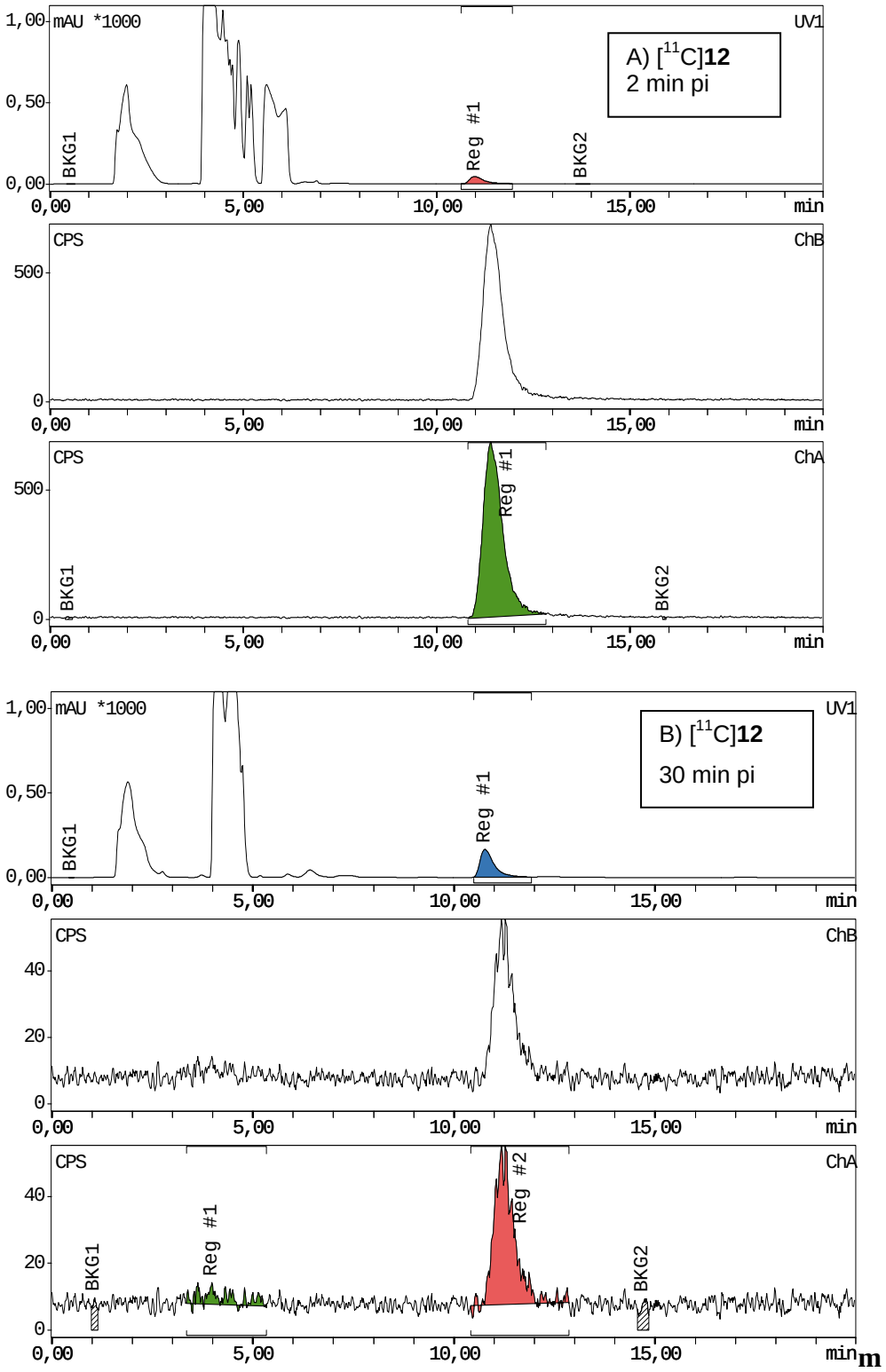

Figure 3. *Radio-chromatograms of brai*n radiometabolite analysis *[[11]C]**12*** co-injected with cold **12** with *RP-HPLC at 2 and 30 min pi.*

Chapter V

A Single Dose Toxicity Study of NMVardenafil to Establish Pharmacological Safety of [^{11}C]NMVardenafil for Application in Humans to Visualize PDE5 with PET

Rufael Chekol[1]; Olivier Gheysens[2]; Alfons Verbruggen[1]; Guy Bormans[1]

[1]KU Leuven, Department of Pharmaceutical and Pharmacological Sciences, Laboratory of Radiopharmacy, Leuven, Belgium

[2]KU Leuven, Department of Imaging and Pathology, Leuven, Belgium and Nuclear Medicine, University Hospital Leuven, Leuven Belgium

Abstract

Vardenafil is a potent phosphodiesterase type 5 (PDE5) inhibitor approved for treatment of male erectile dysfunction. [^{11}C]NMVardenafil, a close analogue of vardenafil, has been evaluated in animal models and showed selective and specific binding to PDE5 with promising properties for *in vivo* visualization of PDE5 with positron emission tomography (PET). Therefore, we have selected [^{11}C]NMVardenafil as candidate for further clinical investigation in selected end-stage heart failure patients awaiting heart transplantation. Although vardenafil has been approved by the European Medicines Agency (EMA) to treat male erectile dysfunction in humans, it is required to establish the safety of the new derivative for first-in-human use according to the 'Note for guidance on non-clinical safety studies for the conduct of human clinical trials and marketing authorization for pharmaceuticals (CPMP/ICH/286/95) to support clinical trials with a single 'microdose'.

A single dose toxicity study of NMVardenafil was conducted in rats according to the recommendation of the International Conference on Harmonization (ICH) Topic 3 guideline on Non-clinical Safety Studies for the Conduct of Human Clinical Trials for Pharmaceuticals. Necropsy, hematology and clinical chemistry parameters were fully investigated to determine the safety of NMVardenafil.

In this study, sporadic variations were detected that were statistically significant in some cases both in the control group and test group treated with NMVardenafil for some hematology and biochemical parameters. Nevertheless, systematic, consistent and treatment-related effects were not observed.

1. Introduction

Vardenafil has been shown to be a potent and selective inhibitor of phosphodiesterase type 5 (PDE5), an enzyme responsible for the degradation of cyclic guanosine monophosphate (cGMP). Vardenafil has been approved by FDA and EMA for treatment of male erectile dysfunction. The adult male recommended dose of vardenafil ranges between 5 mg and 20 mg. At the highest clinically recommended dose (20 mg orally) the peak plasma concentration is around 34 nM [1]. Vardenafil has been evaluated in a comprehensive series of toxicological studies, including *in vitro* and *in vivo* genetic toxicology assays, single-dose studies in mice and rats using both oral and intravenous routes of administration, repeated-dose studies in mice, rats, and dogs, reproductive and developmental studies in rats and rabbits, and life-time carcinogenicity studies in rats and mice [1, 2]. No adverse effects were observed in mice treated with up to 37 mg/kg (males) or 51 mg/kg (females) for 14 weeks. After a 24-month daily treatment the no adverse effect level (NOAEL) was established at an oral dose of 15 mg/kg (male rat) and 10 mg/kg oral (female rat), respectively. Vardenafil was tested in dogs at a 10 mg/kg oral dose and no adverse effect on blood pharmacological parameters, central neverous system (CNS), psychomotor activity, respiration, blood glucose, gastrointestinal function, renal function or coagulation was reported [1, 2]. The NOAEL for vardenafil in a study of dogs treated for 12 months was 3 mg/kg/day orally.

NMVardenafil is a close analogue of vardenafil differing by only a methylene group (figure 1). Despite the fact that vardenafil had been approved by the European Medicines Agency (EMA) to treat male erectile dysfunction in humans; it is required to establish the safety of the new derivative for first-in-human use according to ‘Note for guidance on non-clinical safety studies for the conduct of human clinical trials and marketing authorization for pharmaceuticals (CPMP/ICH/286/95) to support clinical trials with a single ‘microdose’ [3]. EMA's ‘Position paper on non-clinical safety studies to support clinical trials with a single microdose’ requires conducting an extended single dose toxicity study before the commencement of the use of the radioligands in humans [4].

Non-clinical safety studies to support the conduct of human clinical trials for pharmaceuticals have also been internationally harmonised by the International Conference on Harmonization (ICH) as outlined in ICH Topic 3: Note for Guidance on Non-clinical Safety Studies for the Conduct of Human Clinical Trials for Pharmaceuticals [3]. In this document, the recommended method to support human clinical trials of a single dose of a pharmacologically

active compound is based on the principles of 'microdose'. A microdose is defined as less than 1/100th of the dose calculated to yield pharmacological effect of the test substance based on primary pharmacodynamic data obtained in *in vitro* and *in vivo* (typically doses in, or below, the low microgram range) and at a maximum dose of ≤ 100 µg. An example of such a clinical trial is the early characterization of a substance's pharmacokinetic-/distribution properties or receptor selectivity profile using positron emission tomography (PET) imaging or other sensitive analytical techniques [3].

The method we followed for evaluation of the toxicity of NMVardenafil was an extended single-dose toxicity study as recommended in the ICH M3 document and this includes a control group, and a sufficient number of treatment groups to allow the establishment of the safety of NMVardenafil with a large safety window compared to the dose employed in PET. The dose of non-radioactive (cold) NMVardenafil for administration in the toxicity study was calculated based on the specific activity of [^{11}C]NMVardenafil and the possible maximum radioactive dose to be administered to humans and using a safety factor of 1000. Since the intended route of [^{11}C]NMVardenafil administration in humans is intravenous, this route alone in animal testing was considered sufficient. The study period for the extended single-dose toxicity study was 14 days and included an interim sacrifice on day 2 (day of dosing defined as day 1). The extended single-dose toxicity study was designed to obtain information on hematology and clinical chemistry at two time points (day 1 and day 2 or day 14) and histopathology on day 2 or day 14.

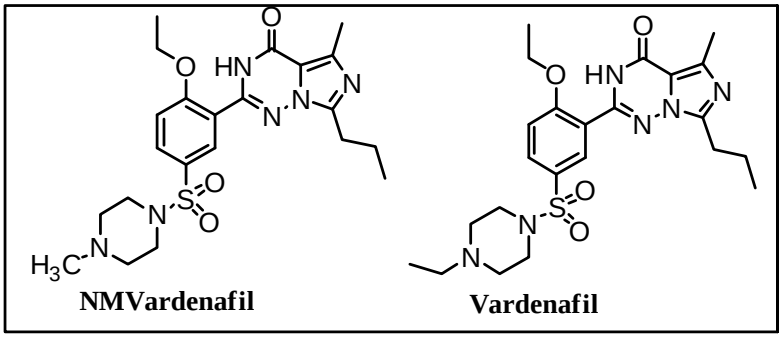

***Figure 1**. Structures of NMVardenafil and vardenafil.*

In the ICH M3 document, two different microdose approaches are described. The first approach involves a total dose of not more than 100 µg that can be divided among up to five doses in any subject. This could be useful to investigate target receptor binding or tissue distribution in a PET study. The second microdose approach involves not more than 5 administrations of a maximum of 100 µg per administration (a total of 500 µg per subject).

We followed a non-clinical safety study of Approach 1 (table 1) in order to support human clinical trials of a single dose of [^{11}C]NMVardenafil.

Table 1. *Non-clinical Studies to Support Exploratory Clinical Investigations: Approach 1*

Clinical:		**Non Clinical:**		
dose to be administered	Start and maximum doses	Pharmacology	General toxicity studies	Genotoxicity/other
Total dose ≤ 100 µg; maximum of 5 administrations (no inter-dose interval limitations) AND Total dose ≤ 1/100th NOAEL and 1/100th pharmacologically active dose (scaled on mg/kg for i.v. and mg/m^2 for oral)	Maximal and starting doses can be the same but not exceed 100 µg	*In vitro* target / receptor profiling should be conducted Appropriate characterization of pharmacology in a pharmacodynamically relevant species should be available to support human dose selection.	Extended single dose toxicity study[a] in one species, usually rodent, by intended route of administration with toxicokinetic profile or via the i.v. route. A limit dose of 10 mg/kg in rats (~6000 times the 100 µg clinical dose on a mg/kg comparison basis) can be used	Genotoxicity studies are generally not conducted, but any studies or SAR[b] assessments conducted should be included in the clinical trial application. For highly radioactive agents, appropriate pharmacokinetics and dosimetry estimates should be submitted

[a]*Generally, extended single dose study dosings fully evaluate hematology, clinical chemistry, necropsy data and histopathology in 10 rodents/sex/group for all groups on day 2 and 5 rodents/sex/group on day 14 in the group that is planned to support the clinical dose;* [b]*SAR: stuctue activity relationship.*

The objective of the experiment was to fully evaluate hematology, clinical chemistry, necropsy and histopathology data in ten rats/sex/group (in both control and treatment groups) on day 2 and five rats/sex/group on day 14 based on the ICH Topic M3 recommendation.

2. Experimental Section

2.1. Synthesis of NMVardenafil

The synthesis of NMVardenafil was previously reported [5]. The identity and purity of the synthesized compound were confirmed by 1H-NMR, HRMS and HPLC.

2.2. Extended toxicity study

All animal experiments were conducted according to the Belgian code of practice for the care and use of animals, after approval from the Animal Ethics Committee, KU Leuven (Ethische Commissie Dierproeven, KU Leuven, License number: LA1210237 and 212-2013).

An extended single dose toxicity study with interim sacrifice on day 2 was carried out in male and female Wistar rats. Wistar rats less than 8 weeks old at the start of the experiment and weighing 200-400 g were used. Initially rats were housed in individually ventilated cages in a thermo regulated (22 °C), humidity-controlled facility under a 12 h/12 h light/dark cycle, with free access to food and water. Then they were kept in metabolic cages in isolation for three to seven days and physically monitored for any abnormality.

2.3. Preparation of dose formulation

NMVardenafil sterile solution for injection was prepared by dissolving NMVardenafil in 10 % dimethyl sulfoxide (DMSO) in 40 % (2-hydroxypropyl)-β-cyclodextrin (β-CD) solution and filtering the solution through a sterile 0.22-μm membrane filter (MILLEX®-GV, Millipore) to get a 250 μg/mL NMVardenafil solution for injection.

The vehicle for injection was prepared in such a way that the final solution was similar in composition to the NMVardenafil formulation (10 % DMSO in 40 % β-CD) except the active pharmaceutical ingredient (NMVardenafil) and the solution was sterile filtered via a 0.22-μm membrane filter.

2.4. Verification of formulation

The stability and identity of NMVardenafil formulation for injection used in the toxicity studies were analyzed using reversed-phase HPLC methods. The conditions were as follows: XBridge™ C18 column (5 μm, 4.6 mm x 150 mm; Waters); isocratic mobile phase (0.05 M Na_2HPO_4 and EtOH, 67:33 v/v at a flow rate of 1 mL/min); UV detector at 254 nm; and ambient temperature.

2.5. Dose calculation

The specific activity (number of disintergrations per second per amount of substance of the sample at the end of formulation) of [^{11}C]NMVardenafil was determined to be 77 GBq/μmol [5]. For an adult dose of 370 MBq, the amount of substance (both labeled and unlabeled NMVardenafil) is:

$$\text{amount of NMVardenafil} = \frac{\text{Dose}}{\text{Specific activity}} = \frac{370\ \text{MBq}}{77\ \text{GBq}/\mu\text{mol}}$$

A dose of 370 MBq thus corresponded to 4.8 nmol of NMVardenafil (2.28 µg). Based on this, it was assumed that the maximum amount of radiolabeled tracer and cold NMVardenafil that may possibly be given with a safety margin to an average healthy adult male (70 kg) is 10 µg. A safety factor of 1000 was used to calculate the dose of NMVarenafil for injection in rats (maximum dose to an adult male would be 10 µg x 1000/70 kg or 143 µg/kg).

2.6. Dosing procedure

Sixty rats were divided in to four groups: 20 rats (control group) and 20 rats (treatment group) for interim sacrifice on day 2 and 10 rats (control group) and 10 rats (treatment group) for day 14 sacrifice. Control groups were given vehicle and treatment groups were given NMVardenafil 143 µg/kg via a tail vein on day 1.

2.7. Observation protocol

All animals in this study were observed regularly for signs of mortality, morbidity, injury, and availability of food and water. Individual body weights were determined and recorded during the experimental period on the first day of quarantine, day 1 and day 2 (for interim sacrificed groups) and first day of quarantine, day 1, day 2, day 8 and day 14 for the groups sacrificed on the 14th day. Each group had an equal number of female and male rats.

Urine analysis was performed before administration of vehicle or NMVardenafil and on the day of sacrifice. Urine was tested for pH and presences of glucose, ketones, leucocytes, nitrite, proteins, blood, and hemoglobin with a urine test kit (Roche Combur 7 Test Strips kit, Brussels, Belgium).

2.8. Clinical hematology and chemistry

Blood was collected for hematology (500 µl in a micro tube with EDTA, Sarstedt, Essen, Belgium) and clinical chemistry (400 µl in heparin tubes, BD Microtainer PST ™ LH Tubes, Ermbodegem, Belgium) before administration of vehicle or NMVardenafil and on the day of sacrifice. After collecting the blood it was well mixed gently and for clinical chemistry it was centrifuged at 4 °C at 420 g for 10 min. Supernatant (plasma) was drawn and transferred to Inpeco (Inpeco, Switzeerland) tubes. The samples were sent to Laboratoriumgeneeskunde UZ Leuven for analysis. Whole blood was analyzed for hematocrit (Hct), red blood cells (RBC) count, mean corpuscular volume (MCV), mean corpuscular hemoglobin (MCH), mean

corpuscular hemoglobin concentration (MCHC), red blood cell distribution width (RDW), white blood cells (WBC) count, platelets count and mean platelets volume (MPV). Plasma was analyzed for sodium (Na^+), potassium (K^+), chloride (Cl^-), bicarbonate (HCO_3^-), anion gap, urea, creatinine, albumin, aspartate transaminase (AST), and alanine transaminase (ALT).

2.9. Clinical pathology/necropsy

Rats were sacrificed on day 2 or day 14 and organs of interest (penis, kidneys, pancreas, spleen, liver, heart, lungs and brain) were harvested and stored in 5 % formaldehyde solution and sent to the Department of Pathology (UZ Leuven) for histopathology examination.

3. Statistical procedure

Means and standard deviations for body weight, hematological and biochemical parameters were calculated. One-way ANOVA was used for statistical evaluation of data pooled from the control and treatment groups. Moreover, when significance was detected both Tukey's post test and the paired Student's t-test (for within group comparison) and unpaired Student's t-test (for between group comparison) were used. The statistical significance level was set at $p < 0.05$.

4. Results

4.1. Death, abnormalities, and feeding

No deaths or clinical abnormalities for any male or female animals were observed during the experimental period. Administration of NMVardenafil did not cause any significant changes in daily water and food consumption in treated females and males compared with control groups.

4.2. Weights of rats

Weight of rats was monitored during the course of the experiment. The average weight and the percentage gain/loss of weight are given in tables 2 and 3 for the two day and 14 day groups. It was observed that keeping the rats in metabolic cages (MC) had a stress effect on the rats and this was reflected in some of the rats losing weight in the first few days of quarantine (in some cases up to 15 % weight loss over four days).

During the four days quarantine period (prior to dosing) female rats were kept in MCs, the weight loss was 4.5±3.8 % on average in the control group and 0.5±2.5 % loss in the test

group and this difference between the groups was statistically significant ($p < 0.01$). In the male control groups the average weight loss during the quarantine period was 4.6±5.1% vs 1.0±2.8 % in the test group with statistical significance between the groups ($p < 0.01$). The lack of water and food was ruled out during the experimental period.

Table 2. *Average weight in gram and average percentage gain or loss of weight of rats during the experimental period (Acute toxicity group – two days).*

Description		Qrt day	WD1	% Qrt vs D1	WD2	% D1 vs D2	% Qrt vs D2
Control group-Day 2	F	238±8	227±10	-4.5±3.8	232±12	1.8±2.3	**-3.0±5.0**
	M	410±28	390±24	-4.6±5.0	391±26	0.2±1.5	**-4.5±5.0**
Treatment group-Day 2	F	243±7	241±10	-0.5±2.5	245±8	1.4±2.0	**0.8±2.1**
	M	258±8	261±10	1.0±2.8	268±7	3.1±3.1	**4±2.0**

Qrt: Quarantine; D: day; Qrt day: average weights of rats on quarantine day; WD1: average weight of rats on day 1; WD2: average weight of rats on day 2; % Qrt vs D1: percentage weight gain/loss between qrt day and day 1; % Qrt vs D2: percentage weight gain/loss between qrt day and day 2; % D1 vs D2: percenatage weight gain/loss between day1 and day 2.

It was hypothesized that keeping rats in metabolic cages (MC) had a possible stress effect on rats due to limitation of mobility and new environment. The statistically significant difference observed in the weight loss between control and test group could only be explained due to the stress effect as there was no systematic difference during the quarantine period till the day of vehicle or NMVardenafil injection.

This seems plausible as the longer rats were kept in MCs the lower the rate of weight loss. At the end of the 14-day experimental period all the control female rats gained weight (36±9 %) and the test group gained on average 16±12 %, this was a significant difference ($p < 0.05$) between day 1 and day 14. However, one female rat in the test group lost weight (4.2 %, supporting information (tables 1-4). The male rats showed no statistically significant difference ($p = 0.35$) with a weight gain of 37±9 % and 42±6 % on average for control and test group during the 14 days, respectively.

Table 3. *Average weight in grams and average percentage gain or loss of weight of rats during the experimental period (Acute toxicity group – 14 days).*

Description		WD1	WD2	% D1 vs D2	WD8	% D2 vs D8	WD14	D8 vs D14	% D1 vs D14
Control group-Day 14	F	186±8	187±7	1.1±1.5	210±10	12±3.	252±15	20±7	**36±9**
	M	250±4	256±7	2.6±1.0	299±29	17±10	343±22	15±5	**37±9**
Treatment group-Day 14	F	189±4	186±3	0.2±0.8	206±11	11±5	215±20	4±9	**16±12**
	M	260±5	261±5	0.7±0.5	315±12	21±3	368±20	17±3	**42±6**

Qrt: Quarantine; D: day; Qrt day: average weights of rats on quarantine day; W D1: average weight of rats on day 1; W D2: average weight of rats on day 2; % Qrt vs D1: percenatage weight gain/loss between qrt day and day 1; % Qrt vs D2: percenatage weight gain/loss between qrt day and day 2; % D1 vs D2: percenatage weight gain/loss between day1 and day 2; % D2 vs D8: percenatage weight gain/loss between day 2 and day 8; % D8 vs D14: percenatage weight gain/loss between day 8 and day 14; % D1 vs D14: percenatage weight gain/loss between day1 and day 2.

4.3. Histopathology

Histopathology examination was done for a number of organs including, pancreas, spleen, kidney, liver, heart, lungs and penis (males). The organs were examined for histopathologic lesions, necrosis, and apoptosis. Except for a liver of one male rat treated with NMVardenafil, there was no lesion or necrosis related to treatment both in females and male rats. The liver function test of the rat with ischemic necrosis; however showed normal values and the rat had a normal body weight. Weight 270 g (group average 268±7.3 g), aspartate transaminase (AST) 66 IU/L (group average 68.4±4.3), and alanine transaminase (ALT) 49 IU/L (group average 49.8±3.2) at the day of sacrifice. The remaining blood chemistry results were also close to the group mean values.

4.4. Hematology

The hematological findings in females and males are presented in tables 4 to 7. The results are divided into control and treatment groups (day 2 sacrificed and day 14 sacrificed). These groups were further divided into two based on sex (female and males). Comparison was made between day 1 and day 2 on data pooled from control and treatment groups (one-way ANOVA) and when significance was observed within group comparison (paired Student's t-test) was performed to check for individual's variability. Besides, between groups (control versus treatment groups) comparison was also performed.

The mean values of females both on day 1 and day 2 in treated and control groups were within the reference range (table 4) before the dosing started. However, there was statistically significant difference for Hct, RBC, MCHC, and MPV (table 4). Within group comparison in the control group between day 1 and day 2 showed a significant difference for Hct ($p < 0.01$), RBC count ($p < 0.001$), MCV ($p < 0.001$), MCH ($p < 0.05$), and MCHC ($p < 0.001$) (supporting information table 5).

Table 4. *Mean and p values (ANOVA) for the control group and treatment groups (female rats, N=10). Comparison was made on data from day 1 and day 2.*

	control group		**treatment group**		**p values**
Females day 2	day 1	day 2	day 1	dayday 2	
Hct	0.43±0.02	0.41±0.03	0.43±0.01	0.40±0.01	0.0005
RBC count	7.9±0.25	7.3±0.51	7.7±0.16	7.4±0.27	0.0010
MCV	55.2±1.43	55.6±1.56	55.6±1.75	54.9±1.81	0.6129
MCH	19.1±0.69	18.8±0.65	19.1±0.58	18.8±0.52	0.7045
MCHC	34.7±0.41	33.9±0.50	34.3±0.27	34.3±0.33	0.0014
RDW	11.6±0.44	11.7±0.50	11.8±0.50	12.0±0.44	0.1781
WBC count	10.3±3.30	12.3±3.30	11.5±3.40	11.6±3.05	0.9998
Platelets count	606.1±69.1	576.2±143.8	602.0±87. 6	587.9±107.5	0.8803
MPV	7.6±0.14	7.6±0.16	7.9±0.25	7.7±0.16	0.0026

Table 5. *Mean and p values (ANOVA) for the control group and treatment groups (male rats, N=10 per group). Comparison was made on data from day 1 and day 2*

	control group		**treatment group**		**p values**
Males day 2	day 1	day 2	day 1	day 2	
Hct	0.39±0.10	0.34±0.06	0.43±0.03	0.44±0.03	0.0085
RBC count	7.0±1.63	6.3±1.08	7.4±0.66	7.3±0.52	0.1634
MCV	55.1±0.99	53.3±1.81	59.0±1.89	60.2±2.15	0.0001
MCH	18.8±0.78	17.8±0.99	20.2±0.46	19.9±0.60	0.0001
MCHC	34.0±0.85	33.3±1.35	34.3±0.47	33.1±0.81	0.9567
RDW	13.1±0.14	12.6±0.50	12.9±0.69	12.6±0.49	0.6332
WBC count	8.2±3.96	8.4±1.47	7.8±2.50	8.3±1.50	0.9728
Platelets count	242.0±121.62	309.8±93.64	679.4±70.17	622.5±125.84	0.0001
MPV	7.7±0.28	7.5±0.17	7.8±0.20	7.8±0.29	0.9900

Within group comparison in the treatment group between day 1 and day 2 also showed a significant difference for Hct ($p < 0.001$), RBC ($p < 0.001$), MCV ($p < 0.001$), MCH ($p < 0.05$), red blood cell distribution width (RDW, $p < 0.01$) and mean platelets volume (MPV, $p < 0.001$) (supporting information table 5). However, the absolute difference between the means of day 1 and day 2 (table 4) is very small.

The mean values of males both on day 1 and day 2 in control and treated groups were within the reference range (table 5) before and after dosing of vehicle or test compound. Statistical analysis showed a difference for Hct, MCV, MCH and platelets count in the male population on day 1 and day 2. Nonetheless, further investigation within the group variation showed that only Hct ($p < 0.05$) and MCV ($p < 0.01$) for the control group and MCV ($p < 0.05$), MCHC ($p < 0.05$) and RDW ($p < 0.05$) for the test group were statistically different (supporting information table 6).

Table 6*. Mean and p values (ANOVA) for the control group and treatment groups (female rats, N=5). Comparison was made on data from day 1 and day 14.*

	control group		**treatment group**		**p values**
Females day 14	day 1	day 14	day 1	day 14	
Hct	0.45±0.01	0.45±0.01	0.44±0.03	0.45±0.01	0.4817
RBC count	7.4±0.28	7.6±0.18	7.9±0.53	8.3±0.41	0.0206
MCV	58.0±0.68	58.2±0.73	56.0±1.89	54.2±2.07	0.0044
MCH	19.4±0.15	19.1±0.31	18.8±0.72	18.8±0.49	0.2978
MCHC	33.4±0.25	32.9±0.68	33.6±0.57	34.8±0.55	0.0001
RDW	12.1±0.41	12.1±0.40	12.5±0.47	12.0±0.69	0.6004
WBC count	10.4±1.43	10.4±1.98	11.5±2.11	12.3±1.32	0.8228
Platelets count	601.3±246.75	763.6±121.07	828.6±138.64	790.4±101.61	0.2465
MPV	7.5±0.22	7.6±0.27	7.4±0.12	7.5±0.22	0.6239

Hematology results for females showed that there was a statistical difference between day 1 and day 14 for RBC count, MCV, and MCHC (table 6). But within group comparison for the control and test groups showed that only MPV ($p < 0.05$) for control and MCV ($p = 0.05$) showed a significant difference between day 1 and day 14 (supporting information table 7).

The mean values of males both on day 1 and day 14 in treated and control groups were within the reference range (table 7) before and after dosing of vehicle or test compound. Nevertheless, comparison on data from day 1 and day 14 for the groups showed a significant

difference for Hct, RBC, MCV and MCHC. Upon further investigation the difference was found to be due to the variability of Hct ($p = 0.05$), RBC ($p = 0.05$), MCV ($p = 0.05$) and RDW ($p = 0.01$) in the control and MCV ($p < 0.01$) in the test group between day 1 and day 14 (supporting information table 8).

Table 7. *Mean and p values (ANOVA) for the control group and treatment groups (male rats, N=5). Comparison was made on data from day 1 and day 14.*

	control group		**treatment group**		**p values**
Males day 14	day 1	day 14	day 1	day 14	
Hct	0.42±0.02	0.45±0.02	0.42±0.01	0.43±0.02	0.0581
RBC count	7.0±0.20	7.6±0.24	7.2±0.09	7.6±0.29	0.0004
MCV	60.0±1.16	58.5±1.76	58.1±1.58	56.3±1.13	0.0081
MCH	19.5±0.25	19.1±0.58	19.0±0.46	18.7±0.41	0.0897
MCHC	32.4±0.31	32.5±0.42	32.7±0.46	33.2±0.19	0.0192
RDW	13.3±0.46	12.8±0.54	13.6±0.33	13.2±0.51	0.1436
WBC count	13.6±2.22	15.4±4.20	14.1±1.97	14.3±3.89	0.9989
Platelets count	723.2±50.56	707.2±72.95	759.6±41.39	737.0±94.67	0.6672
MPV	7.6±0.30	7.6±0.18	7.6±0.11	7.6±0.23	0.9255

4.5. Clinical chemistry

The clinical chemistry results are presented in tables 8 to 11. The mean values for the acute toxicity in control and test groups in female rats on day 1 and day 2 were within the reference range (table 8) except for potassium and ALT levels. Potassium concentration was lower and ALT level higher than the reference range in all groups but not significantly different in any of the groups on any day. Urea level was significantly different. Bicarbonate level on day 2 showed a significant deviation from day 1 in the control group ($p < 0.05$). None of the biochemical parameters in the treatment group showed a significant deviation after dosing (supporting information table 9).

The potassium and ALT level for the male groups in the acute toxicity study were out of reference range. In addition, sodium concentration and chloride (for control group), and anion gap, bicarbonate level (treatment group) were out of reference range. Between groups comparison (unpaired t-test) on day 1 for males gave significantly different chemistry values except for potassium, urea and ALT (supporting information table 10). Moreover, the weight of the two groups on day 1 differed significantly (390.2±23.6 g versus 260.5±9.8 g for control

and test groups respectively, $p < 0.0001$). Therefore, any difference that could be observed on day 2 between the two groups did not have any clinical significance as the two groups were different at the start of the study. Due to limited number of metabolic cages, the test male group were kept in individually ventilated cages for longer days than the control group. This could be the reason for the observed difference in weight as male rats are known to gain weight very rapidly during their early developmental age. The paired t-test for the control group showed a difference between day 1 and day 2 only for bicarbonate concentration. The results for the test group showed a significant difference between day 1 and day 2 for a number of chemistry parameters (sodium, chloride, bicarbonate, anion gap, and creatinine). However, the maximum percentage change observed was (-) 8 % for bicarbonate, followed by 3 % for albumin and less than 2 % for the remaining of significantly different parameters. Except biocaerbonate, the other parameters are within the total allowable variation (table 15).

Table 8. *Mean and p values (ANOVA) of chemistry results for the control group and treatment groups (female rats, N=10). Comparison was made on data from day 1 and day 2.*

	control group		**treatment group**		**p values**
Females day 2	day 1	day 2	day 1	day 2	
Sodium	144.7±1.84	144.5±1.08	145.8±2.99	145.7±1.55	0.5937
Potassium	4.2±0.39	4.5±0.46	4.3±0.60	4.1±0.21	0.4261
Chloride	99.8±1.50	99.7±1.71	101.6±3.24	102.6±1.36	0.0667
Bicarbonate	18.2±1.31	21.3±1.74	20.4±3.21	20.4±0.99	0.3518
Anion gap	31.2±2.23	28.0±2.42	28.1±2.73	26.9±1.26	0.0704
Urea	28.8±8.67	30.4±8.32	32.7±5.68	36.1±5.95	0.0001
Creatinine	0.27±0.03	0.26±0.02	0.26±0.02	0.26±0.01	0.7091
Albumin	44.9±1.64	42.9±1.36	44.0±2.87	43.6±3.20	0.6729
AST	70.8±7.56	67.8±7.26	81.3±25.97	77.1±12.66	0.4882
ALT	48.2±14.64	45.0±16.32	57.5±22.01	58.4±19.31	0.5057

The clinical chemistry results for the female groups of extended toxicity study were out of reference range for potassium and ALT level in both control and treatment groups (table 10). Sodium, potassium and albumin level were significantly different (table 10). The paired t-test showed that differences were caused by the variation in values on day 14 in the control group but there was no significant variability in the treatment group (supporting information table 11). Comparison between female control and test group on day 1 showed some difference

(bicarbonate, anion gap and albumin) and on day 14 (sodium, chloride, bicarbonate, anion gap and albumin). Nonetheless, the day 14 difference between the groups could not be attributed to the test compound as the two groups showed differences on day 1 and also the day 14 results of the control group was different from day 1.

Table 9*. Mean and p values (ANOVA) of chemistry results for the control and treatment groups (male rats, N=10). Comparison was made on data from day 1 and day 2.*

	control group		**treatment group**		**p values**
Males day 2	day 1	day 2	day 1	day 2	
Sodium	152.6±2.01	149.8±2.15	141.5±0.68	144.3±0.58	0.0001
Potassium	4.7±0.31	5.7±1.65	4.5±0.59	4.6±0.19	0.0835
Chloride	107.4±1.72	104.7±2.77	100.7±1.55	102.1±0.92	0.0001
Bicarbonate	19.7±1.15	21.9±1.01	25.9±2.12	23.7±1.06	0.0001
Anion gap	30.1±1.22	28.9±1.88	19.4±1.42	23.0±0.82	0.0001
Urea	36.0±7.44	36.6±5.53	39.6±8.26	41.2±6.10	0.0001
Creatinine	0.33±0.03	0.28±0.06	0.23±0.09	0.23±0.02	0.0100
Albumin	42.4±3.24	43.0±2.08	38.5±1.11	39.6±0.75	0.0001
AST	78.4±5.32	107.6±50.26	68.7±8.67	68.4±4.33	0.0111
ALT	63.1±14.44	72.3±11.27	50.1±6.66	49.8±3.15	0.0001

Table 10. *Mean and p values (ANOVA) of chemistry results for the control and treatment groups (female rats, N=5). Comparison was made on data from day 1 and day 14.*

	control group		**treatment group**		**p values**
Females day 14	day 1	day 14	day 1	day 14	
Sodium	145.9±.35	150.3±2.52	142.9±2.17	143.3±0.88	0.0040
Potassium	4.8±0.38	4.1±0.41	4.3±0.22	4.6±0.35	0.0327
Chloride	102.3±1.77	106.2±2.12	94.6±13.08	100.6±1.28	0.1438
Bicarbonate	20.1±0.67	19.9±1.01	23.0±0.18	22.2±1.03	0.7278
Anion gap	28.4±1.84	28.1±0.70	23.9±1.12	25.1±0.72	0.0575
Urea	38.0±5.40	37.4±3.14	34.0±0.00	40.6±4.92	0.1175
Creatinine	0.22±0.01	0.30±0.10	0.23±0.02	0.24±0.02	0.1807
Albumin	46.2±1.63	46.9±1.44	43.8±1.32	43.8±2.22	0.0364
AST	76.0±11.30	75.0±26.28	74.8±12.07	68.0±4.05	0.8840
ALT	55.4±9.73	65.4±12.69	55.8±3.87	61.6±8.40	0.3820

The clinical chemistry results for the 14-day study in males showed out of reference range values for some parameters (potassium and ALT level) for both control and test groups. Anion gap also was out of reference range for the test group. Among all groups, a significant difference was observed for sodium, chloride, albumin and AST level between day 1 and day 14 measurements (table 11). The control male group showed a significant difference for sodium ($p = 0.01$), chloride ($p = 0.05$), anion gap ($p = 0.01$) and urea ($p = 0.05$) between day 1 and day 14 (supporting information table 12). However, only the anion gap ($p = 0.05$) and urea value ($p = 0.05$) of the test groups showed a significant difference on day 14. Since these differences were also observed in the control group, the effect was not attributed to the test compound.

Table 11. *Mean and p values (ANOVA) of chemistry results for the control and treatment groups (male rats, N=5). Comparison was made on data from day 1 and day 14.*

	control group		**treatment group**		**p values**
Males day 14	day 1	day 14	day 1	day 14	
Sodium	145.1±1.79	150.0±0.92	141.6±1.56	143.1±0.57	0.0001
Potassium	5.1±0.20	5.2±0.60	4.9±0.26	4.8±0.39	0.3788
Chloride	102.6±0.90	105.4±1.39	100.4±1.62	99.9±1.39	0.0001
Bicarbonate	21.2±0.66	21.6±1.08	23.4±0.68	22.9±1.18	0.4900
Anion gap	26.4±0.64	28.3±0.62	22.7±0.62	24.9±0.96	0.1258
Urea	32.4±2.88	44.2±6.06	30.8±5.02	36.8±4.15	0.9957
Creatinine	0.20±0.01	0.23±0.05	0.20±0.00	0.21±0.00	0.3060
Albumin	41.1±1.49	42.3±1.10	40.8±0.87	40.0±0.71	0.0327
AST	73.0±2.00	69.2±7.40	77.8±3.49	64.6±8.80	0.0325
ALT	62.0±7.58	62.6±13.87	66.8±3.77	71.5±5.68	0.3880

5. Discussion and conclusion

An extended toxicity study in Wistar rats was performed based on the 'microdose' principle. Tables 12 and 13 list the respective reference ranges for the hematology and clinical chemistry parameters compiled from three sources [6-9].

There are some issues associated with the use of published ‘normal’ values that first need to be addressed so that the results of the current study can be interpreted properly. ‘Normal’ values are affected by the type of the rat species (strain), food, and housing conditions. As our pre-dosing data show, the ‘normal’ values also vary within a cohort of animals. Consequently,

the reference ranges should only be used as a point of reference. Therefore, reference ranges should never be relied upon as the sole means of making judgments concerning the biological importance of a test material–related effect [6]. Furthermore, because reported normal values vary widely, 'values outside of the reference range also do not necessarily indicate an abnormal condition and values within the reference range do not necessarily signify a normal condition' [6]. Occasionally, very small statistically significant differences occur between control and treated groups in toxicology studies, and unfortunately, the mechanism for the difference is usually not apparent (emphasis here). Although the mechanism for the difference cannot be pin pointed with certainty, it is possible to identify some experimental conditions/manipulations and instrument related issues that could potentially affect the variability within same groups or between different groups.

Table 12*. Hematology parameters reference region from different sources for rats aged less than 6 months.*

		CRL[7]		**Dirikolu L et al**[6]	
Parameters	unit	Females	Males	Females	Males
Hct	%	34-42	32-40	42.3±1.3	41.2±1.7
RBC count	10^{12}/L	6.2-7.6	5.8-7.1	7.7±0.3	7.1±.3
MCV	fL	52-59	53-59	55.1±1.6	58.3±1.5
MCH	pg	19-21	18-22	19.5±0.6	20.4±0. 7
MCHC	g/dL	34-39	33-41	35.4±0.2	35.0±0.5
RDW	%				
WBC count	10^9/L	4.2-9.7	5.1-12.2	10.5±2.3	14.6±4.3
Platelates count	10^9/L	700	700		
MPV	fL				

[7]CRL: Charles Rivers Laboratories adapted from reference [7];[6]adapted from reference [6]

During the course of the experiment, repeated pricking was necessary in some rats to access a tail vein and at the same time massaging of the tail was done in order to have sufficient volume of blood (1 mL). These two handling procedures could potentially result in micro-clotting (as blood was collected in droplets) and hemolysis. Micro-clotting has potential effects on RBC count, platelets count, Hct, ALT and AST in two ways. A first possibility is that micro-clot(s) could be counted as aggregates and this could potentially result in lower number of platelets without affecting the RBC count and the second effect is through blockage of blood analysis instruments by micro-clot which results in a variable RBC count which also affects the Hct [Davy Kieffer, Clinical Laboratory, UZ Leuven, *personal communication*]. Hemolysis affects the RBC count and consequently the Hct value together

with platelets counts. In the case of a decrease in platelet count without any accompanying decrease in RBC count, micro-clotting is the potential culprit for the variation. Repeated needle pricking could also be a stimulus for inflammation and initiation of clotting and this could potentially affect blood parameters such as WBC count or platelets count.

Table 13. *Clinical chemistry parameters reference region from different sources for rats of less than 6 month.*

		CRL[7]		**Dirikolu L et al[6]**		**Boehm et al[8]**	
Parameters	unit	F	M	F	M	F	M
Na^+	mmol/L	140-147	140-146	142.8±1.6	141.1±1.2	135-157	131-142
K^+	mmol/ L	5.8-7.3	6.1-7.7	5.4±0.5	6.1±0.4	4.3-5.6	3.9-6.5
Cl^-	mmol/ L	99-108	99-106	101.3±1.4	98.0±1.0		
HCO_3^-	mmol/ L			21.0±2.8	26.8±1.3		
Anion	mEq/L			24.9±2.8	22.4±1.8		
Urea	mg/dL					41.3-67.9	24.0-55.9
Creatinine	g/ L			0.3±0.1	0.2±0.0		
Albumin	g/dL	36-46	30-44	47.6±1.8	44.7±0.9		
AST	U/ L	47-88	37-94			61-153	50-96
ALT	U/ L	8-37	4-44	36.4±6.4	36.3±5.2	23-67	24-49

[7]CRL: Charles Rivers Laboratories adapted from reference [7]; [6]adapted from reference [6]; [8]adapted from reference [8]; Na^+: Sodium, K^+: potassium; Cl^-: chloride; HCO_3^-, bicarbonate; Anion: Anion gap

The other potential issue that could introduce variability in observed results is instrument related. The blood analysis instruments (Sysmex XE-5000, Sysmex Europe, Hoeilaart, Belgium) used were dedicated for analysis of human blood/plasma samples and calibrated accordingly. Most laboratory animal hematology and chemistry samples are analyzed by dedicated instruments such as Coulter Counter (Model ZBI-6). This difference could potentially result in variation between the reference range in our results (a notable example being platelets count). The other possible difference arising from the type of instrumentation is the measurement method of blood parameters. Hematocrit is a good example here. In our blood analysis, the Hct was directly measured where as in other instruments like the Coulter Counter (Model ZBI-6), Hct is calculated from MCV and RBC count which can potentially introduce variability. Calibration of instruments is done every 3 months and there could be deviation in instrument measurement between calibrations. All these source of variations (both biological and instrument with and among laboratories) lead to the development of guidelines on "Optimal specification for total error, imprecision, and bias, derived from intra - and inter-individual biologic variations" (tables 14 and 15) [10, 11]. Therefore, it was

expected that all these factors add up and could result in statistically but not clinically significant difference in observed values.

Another potential confounding factor that could introduce variability in observed hematological data is stress effect and sampling technique [9, 12]. The effect of stress is highly variable, dependent on individuals, sex, age, and time. The complex nature of the effect of stress on hematological data introduces a highly random and difficult to predict noise in the observed results which could potentially result in a significant difference between or within groups.

Table 14. *Hematological desirable specifications for imprecision, inaccuracy, and total allowable error, calculated from data on within-subject and between-subject biologic variation [9].*

Analyte	**Biological variation**		**Desirable specification**		
	CVw	CVg	I (%)	B (%)	TE (%)
Hct	2.7	6.41	1.35	1.74	3.97
RBC count	3.2	6.3	1.6	1.7	4.4
Hemoglobin	2.85	6.8	1.43	1.84	4.19
Mean corpuscular volume (MCV)	1.4	4.85	0.7	1.26	2.42
Mean corpuscular hemoglobin (MCH)	1.4	5.2	0.7	1.35	2.5
Mean corpuscular hemoglobin concentration (MCHC)	1.06	1.2	0.53	0.4	1.27
Red cell distribution wide (RDW)	3.5	5.7	1.8	1.7	4.6
Leukocytes count	11.4	21.3	5.73	6.05	15.49
Platelets count	9.1	21.9	4.6	5.9	13.4
Mean platelet volume (MPV)	4.3	8.1	2.15	2.29	5.84

CVw = within-subject biologic variation (coefficient of variation); CVg = between-subject biologic variation (coefficient of variation); I = desirable specification for imprecision; B = desirable specification for inaccuracy; TE = desirable specification for allowable total error

Therefore, all these factors need to be taken into account for interpretation of data and the percentage variation in mean values should be considered together with the statistical test in order to reach a clinically sound conclusion.

The rationale behind using ANOVA as a statistical tool was that if the rats for the experiment were taken from the same population then hematology and biochemical parameters should not be significantly different among the control and test group unless in case of a pronounced effect of vehicle and/or test compound. However, when a significant difference was detected; both Tukey's post test and within group comparison (paired t-test) was further employed to identify the source of variation.

5.1. Histopathology/necropsy

Since the liver is the primary organ that detoxifies toxins, a liver function test is an important indicator of the safety of NMVardenafil. There is no evidence for liver damage or impaired liver function in the test group except for one rat which showed ischemic liver necrosis on histopathological analysis. Nonetheless, in this rat the results of all liver function tests and the maintained body mass indicated no *in vivo* liver damage while the rat was alive and therefore necrosis is expected to have occurred after dissection. This could arise if the storage conditions during transportation were not optimal (for example if the liver was not completely submerged in the formaldehyde solution). *In vitro* ischemic liver necrosis due to handling of organ samples during storage and transportation is a frequent phenomenon in histopathology examination (Raphael Sciot, Department of Imaging and Pathology, personal communication). Other than the single incidence of potentially *in vitro* liver necrosis, there was no evidence for the organ toxicity of NMVardenafil.

Table 15*. Biochemical desirable specifications for imprecision, inaccuracy, and total allowable error, calculated from data on within-subject and between-subject biologic variation [9].*

Analyte	**Biological variation**		**Desirable specification**		
	CVw	CVg	I (%)	B (%)	TE (%)
Sodium	0.6	0.7	0.3	0.23	0.7
Potassium	4.6	5.6	2.3	1.81	5.6
Chloride	1.2	1.5	0.6	0.5	1.
Sodium Bicarbonate	4.8	4.7	2.4	1.7	5.6
Anion gap	9.5	10.1	4.8	3.5	11.3
Urea	12.1	18.7	6.05	5.57	15.55
Creatinine	5.95	14.7	2.98	3.96	8.8
Albumin	3.2	4.75	1.6	1.43	4.0
Aspartate aminotransferase (AST)	12.3	23.1	6.15	6.54	16.69
Alanine aminotransferase (ALT)	19.40	41.6	9.7	11.48	27.48

CVw = within-subject biologic variation (coefficient of variation); CVg = between-subject biologic variation (coefficient of variation); I = desirable specification for imprecision; B = desirable specification for inaccuracy; TE = desirable specification for allowable total error

5.2. Hematology

Reference ranges for hematology values are obtained from Dirikolu et al [6] and Charles River Laboratories [7]. Reliable strain, age and sex matched reference ranges could not be

found for RDW, platelets count and MPV. Hence, means of within and between groups were compared to derive any inference.

On the first day of the experiment, almost 1 mL of blood was drawn before dosing for hematology and chemistry analysis. This was almost 6 % of the whole blood volume for an average 227 g weighing rat. Hence, it was anticipated that this might have an effect on the hematology analysis results such as RBC count and hemoglobin measured on the subsequent day. Consequently, these could have further impact on blood parameters that implicitly or explicitly depend on RBC count or hemoglobin level such as Hct, MCV, MCH and MCHC.

Although hematology results showed statistically significant differences on day 2 within female control and test groups, none of the mean values were out of reference ranges. However, WBC count showed the highest coefficient of variation in control groups both on day 1 and day 2 (30.8 % and 26.8 %, respectively). The test groups also showed similar variability in WBC count as that of the control group with 29.7 % and 26.4 % coefficient of variation for day 1 and day 2, respectively. The slightly higher variability both in control and test groups on day 1 could potentially be due to acute metabolic cage stress effect. For both the control and test group of female rats, there was a general trend that the day 2 values (Hct, RBC, MCV, MCH, and MCHC) were lower than the day 1 values. This could be due to the effect of blood drawn on day 1 or to a natural biological variability. Both control groups and test group rats were pooled from the same general population of rats, therefore, the hematology results of control and test groups were compared (unpaired Student's t-test). The results showed that there was no significant difference between control and test group on day 1 except for MPV ($p < 0.001$). Also on day two there was no significant difference between the two groups except for MCHC ($p < 0.05$). The comparison between the two groups showed that even before dosing there was a sporadic variation. Hence, it was deduced that there was no statistically significant difference that could be attributed to the test compound.

The hematological findings in males of interim sacrificed groups did not show any consistent treatment-related effects and all hematology results were in the reference region. One-way ANOVA of WBC count for control and test groups on day 1 and day 2 showed no statistical difference ($p = 0.97$) between samples taken on different days and among different groups.

The hematology results for both control and treatment female groups on day 14 were in the reference region except for Hct of both groups. The averages of Hct for all groups are, nevertheless, within the allowed total variability of 3.97 % (Table 14). In addition, one-way

ANOVA on all Hct data samples from the control and test group showed no statistically significant difference ($p = 0.4817$). Therefore, there is no evidence that the hematological findings in females show any consistent treatment-related effects on day 14. The hematology results of day 1 and day 14 showed no treatment-related effects in the male groups and all the results were in the reference region. The control group showed sporadic variability on day 14 compared to day 1, albeit all results were in the reference region except the Hct and this was also in the allowable variability region.

5.3. Clinical chemistry

Reference ranges for clinical chemistry values were compiled from Dirikolu et al [6], Charles River Laboratories [7] and Boehm et al [8]. Reliable strain, age and sex matched reference ranges could not be found for bicarbonate, anion gap, urea and creatinine. Hence, means of within and between groups were compared to derive any inference.

Clinical chemistry analysis of plasma showed that all groups had mean potassium level lower than and mean ALT level higher than reference regions given by Charles Rivers Laboratories. This might be due to several factors such as genetic shift from the initial Wistar rats colony or feedings (example dietary choline deficiency). Within group comparison for the control did not show any statistically significant differences except for the ALT level in the female control group of day 14. Therefore, any changes observed for the potassium and ALT level was not associated with the test compound.

Biochemical results of the female groups (on day 2) showed no treatment-related variation, but the means of potassium level and ALT in both control and treatment groups were out of the reference range. Since within group comparison did show significant difference for both groups, the variability in potassium level was not treatment-related. NMVardenafil treated male rats showed sporadic variation for some parameters though the means stayed within the reference region.

In the 14 day study groups both female and male control rats showed significant difference between day 1 and day 14 for some chemistry results, however, this pattern was not repeated in the test group except for the anion gap and urea for test male groups. We could not explain the cause for the variation in means for the control group.

In conclusion, although there have been statistically significant differences both within and across groups for some hematology and biochemical parameters, no systematic, consistent

and treatment-related effects were observed. The results of the biological parameters evaluated in this study in order to establish the safety of NMVardenafil are highly variable and dependent on several factors including but not limited to age, sex, stress, weight, experimental handling and, instrument allowed total variability in precision. In addition, hematological results show both intra-and inter-individual variability and any statistically significant difference might be clinically not relevant and/or significant. Taking into account the fact that the amount of NMVardenafil which has to be used in humans for a clinical trial with [^{11}C]NMVardenafil is less than a thousandth of the dose used for this toxicity study on weight basis, any kind of pharmacological toxicity is not anticipated.

6. References

[1] Available at http://www.ema.europa.eu/docs/en_GB/document_library/EPAR_-_Scientific_Discussion/human/000475/WC500039990.pdf. Accessed on 29/11/2013

[2] Levitra® product monograph. Available at http://www.bayer.ca/files/LEVITRA-PM-ENG-11DEC2012-158556.pdf. Accessed on 10/11/2013.

[3] EMA. Note for guidance on non-clinical safety studies for the conduct of human clinical trials and marketing authorization for pharmaceuticals. CPMP/ICH/286/95. Available at http://www.ema.europa.eu/docs/en_GB/document_library/Scientific_guideline/2009/09/WC500002941.pdf. Accessed 13/12/2011

[4] EMA. Position paper on non-clinical safety studies to support clinical trials with a single microdose. CPMP/SWP/2599/02, January 2003.

[5] Chekol R, Gheysens O, Cleynhens J, Pokreisz P, Vanhoof G, Ahamed M, Janssens S, Verbruggen A, Bormans G. Evaluation of PET radioligands for *in vivo* visualization of phosphodiesterase 5 (PDE5). Nuc Med Biol. 2014; 41:155-162.

[6] Dirikolu L, Chakkatch T, Bal-Kell S, Elamma C, Schaeffer D. Subchronic toxicity (90 days) of StemEnhance™ in Wistar rats. Nutr Diet Suppl 2011; 3:19-30.

[7] Baseline hematology and clinical chemistry values for Charles River Wistar Rats – (CRL:(WI)BR) as a function of sex and age. Charles River Laboratories Technical Bulletin 1998. Available from: http://www.criver.com/sitecollectiondocuments/rm_rm_r_hematology_crl_wi_br_sex_age.pdf. Accessed October 2013.

[8] Boehm O, Zur B, Koch A, Tran N, Freyenhagen R, Hartmann M, Zacharowski K. Clinical chemistry reference database for Wistar rats and C57/BL6 mice. Biol Chem 2007; 388:547-54.

[9] Lewi PJ, Marsboom RP. Toxicology reference data for the Wistar rat. Arch Toxicol Suppl 1982; 5:271-6.

[10] Desirable Specifications for Total Error, Imprecision, and Bias, derived from intra- and inter-individual biologic variation. Available at http://www.westgard.com/biodatabase1.htm. Accessed on 07/01/2014.

[11] Fraser CG, Petersen PH, Ricos C, Haeckel R. Proposed quality specifications for the imprecision and inaccuracy of analytical systems for clinical chemistry. Eur J Clin Chem Clin Biochem 1992; 30:311-7.

[12] Upton PK, Morgan DJ. The effect of sampling technique on some blood parameters in the rat. Lab Anim 1975; 9:85-91.

Chapter V – Supporting Information

Table 1. Weight (g) of rats and the percentage gain or loss during the experimental period. Control group of the interim sacrifice.

	Qrt day	**Day 1**	**[a]% gain/loss**	**Day 2**	**[b]% gain/loss**	**[c]% gain/loss**
rat 1	240	239	-0.4	240	0.4	**0.0**
rat 2	219	211	-3.7	218	3.3	**-0.5**
rat 3	246	240	-2.4	249	3.8	**1.2**
rat 4	240	213	-11.3	205	-3.8	**-14.6**
rat 5	242	222	-8.3	231	4.1	**-4.5**
rat 6	250	227	-9.2	234	3.1	**-6.4**
rat 7	240	232	-3.3	239	3.0	**-0.4**
rat 8	235	235	0.0	238	1.3	**1.3**
rat 9	237	226	-4.6	228	0.9	**-3.8**
rat 10	233	228	-2.1	233	2.2	**0.0**
rat 11	397	398	0.3	401	0.8	**1.0**
rat 12	390	378	-3.1	381	0.8	**-2.3**
rat 13	421	423	0.5	422	-0.2	**0.2**
rat 14	435	394	-9.4	405	2.8	**-6.9**
rat 15	440	423	-3.9	426	0.7	**-3.2**
rat 16	410	382	-6.8	378	-1.0	**-7.8**
rat 17	450	380	-15.6	385	1.3	**-14.4**
rat 18	365	343	-6.0	335	-2.3	**-8.2**
rat 19	416	401	-3.6	396	-1.2	**-4.8**
rat 20	375	380	1.3	381	0.3	**1.6**

Qrt: Quarantine, [a]percentage weight gain or loss between quarantine day and day 1, [b]percentage weight gain or loss between day 1 and day 2, [c]the overall percentage weight gain or loss between quarantine day and day 2; rats 1 to 10 are female and rats 11 to 20 are male.

Table 2. Weight (g) of rats and the percentage gain or loss during the experimental period. Treatment groups of the interim sacrifice.

	Qrt day	**Day 1**	**[a]% gain/loss**	**Day 2**	**[b]% gain/loss**	**[c]% gain/loss**
rat 1	244	235	-3.7	243	3.4	**-0.4**
rat 2	251	250	-0.4	251	0.4	**0.0**
rat 3	237	231	-2.5	238	3.0	**0.4**
rat 4	256	255	-0.4	258	1.2	**0.8**
rat 5	237	232	-2.1	239	3.0	**0.8**
rat 6	243	236	-2.9	234	-0.8	**-3.7**
rat 7	243	249	2.5	251	0.8	**3.3**
rat 8	244	255	4.5	250	-2.0	**2.5**
rat 9	231	230	-0.4	240	4.3	**3.9**
rat 10	240	241	0.4	242	0.4	**0.8**
rat 11	254	261	2.8	270	3.4	**6.3**
rat 12	260	268	3.1	271	1.1	**4.2**
rat 13	258	257	-0.4	258	0.4	**0.0**
rat 14	260	245	-5.8	270	10.2	**3.8**
rat 15	255	257	0.8	271	5.4	**6.3**
rat 16	240	250	4.2	254	1.6	**5.8**
rat 17	267	275	3.0	277	0.7	**3.7**
rat 18	271	273	0.7	277	1.5	**2.2**
rat 19	260	265	1.9	267	0.8	**2.7**
rat 20	255	254	-0.4	268	5.5	**5.1**

Qrt: Quarantine, [a]percentage weight gain or loss between quarantine day and day 1, [b]percentage weight gain or loss between day 1 and day 2, [c]the overall percentage weight gain or loss between quarantine day and day 2; rats 1 to 10 are female and rats 11 to 20 are male.

Table 3. Weight (g) of rats and the percentage gain or loss during the experimental period. Control group of day 14.

	Day 1	Day 2	[a]% gain/loss	Day 8	[b]% gain/loss	Day 14	[c]% gain/loss	[d]% gain/loss
rat 1	177		1.130	201	12.291	243	20.896	37.288
rat 2	178	183	2.809	204	11.475	255	25.000	43.258
rat 3	192	190	-1.042	204	7.368	246	20.588	28.125
rat 4	190	191	0.526	222	16.230	276	24.324	45.263
rat 5	192	196	2.083	221	12.755	238	7.692	23.958
rat 6	246	250	1.626	313	25.200	362	15.655	47.154
rat 7	255	263	3.137	322	22.433	350	8.696	37.255
rat 8	253	263	3.953	305	15.970	343	12.459	35.573
rat 9	246	250	1.626	249	-0.400	305	22.490	23.984
rat 10	248	254	2.419	307	20.866	353	14.984	42.339

[a]percentage weight gain or loss between day 1 and day 2, [b]percentage weight gain or loss between day 2 and day 8, [c]percentage weight gain or loss between day 8 and day 14, [d]the overall percentage weight gain or loss between day 1 and day 2; rats 1 to 5 are female and rats 6 to 10 are male.

Table 4. Weight (g) of rats and the percentage gain or loss during the experimental period. Treatment group of day 14.

	Day 1	Day 2	[a]% gain/loss	Day 8	[b]% gain/loss	Day 14	[c]% gain/loss	[d]% gain/loss
rat 1	185	187	1.081	223	19.251	237	6.3	28.1
rat 2	192	191	-0.521	208	8.901	184	-11.5	-4.2
rat 3	183	185	1.093	194	4.865	213	9.8	16.4
rat 4	184	183	-0.543	203	10.929	227	11.8	23.4
rat 5	185	185	0.000	203	9.730	212	4.4	14.6
rat 6	265	268	1.132	325	21.269	384	18.2	44.9
rat 7	259	262	1.158	322	22.901	380	18.0	46.7
rat 8	253	255	0.791	301	18.039	356	18.3	40.7
rat 9	264	264	0.000	326	23.485	382	17.2	44.7
rat 10	257	258	0.389	303	17.442	340	12.2	32.3

[a]percentage weight gain or loss between day 1 and day 2, [b]percentage weight gain or loss between day 2 and day 8, [c]percentage weight gain or loss between day 8 and day 14, [d]the overall percentage weight gain or loss between day 1 and day 2; rats 1 to 5 are female and rats 6 to 10 are male.

Clinical hematology

The results are divided into control group (sacrificed day 2 or day 14) and Treatment groups (sacrificed day 2 or day 14). These groups were further divided into two, based on sex (female vs male). Comparison was made within group on data obtained on day 1 before administration

of vehicle or NMVardenafil and day 2 (or day 14) after administration of vehicle or NMVardenafil (paired t-test).

Between groups comparison (unpaired t-test) was made on data of the control and test group on the first day (day 1) and on the day of sacrifice (day 2 or day 14).

Table 5. p values for the control group and treatment groups (female rats, N=10). Comparison was made on data between day 1 and day 2.

Females day 2		Within group comparison		Between groups comparison	
		control group	treatment group	Day 1	Day 2
Hct		0.002	0.000	0.399	0.597
RBC count		0.001	0.000	0.124	0.983
	MCV	0.000	0.000	0.307	0.401
	MCH	0.014	0.002	0.729	1.000
	MCHC	0.001	0.834	0.061	0.026
	RDW	0.279	0.002	0.331	0.089
WBC count		0.115	0.846	0.628	0.595
Platelets count		0.210	0.413	0.778	0.839
	MPV	0.177	0.000	0.001	0.681

Table 6. p values for the control group and treatment groups (male rats, N=10 per group). Comparison was made on data between day 1 and day 2.					
Males day 2		Within group comparison		Between groups comparison	
		control group	treatment group	Day 1	Day 2
Hct		0.044	0.566	0.082	0.002
RBC count		0.101	0.851	0.965	0.035
	MCV	0.008	0.001	0.001	0.000
	MCH	0.072	0.030	0.000	0.000
	MCHC	0.781	0.006	0.026	0.742
	RDW	0.157	0.004	0.801	0.966
WBC count		0.886	0.665	0.883	0.525
Platelets count		0.425	0.044	0.000	0.011
	MPV	0.822	0.421	0.007	0.085

Table 7. p values for the control group and treatment groups (female rats, N=5). Comparison was made on data between day 1 and day 14.					
Females day 14		Within group comparison		Between groups comparison	
		control group	treatment group	Day 1	Day 14
Hct		0.784	0.658	0.770	0.561
RBC count		0.172	0.342	0.136	0.016
	MCV	0.562	0.030	0.077	0.006
	MCH	0.108	0.898	0.164	0.302
	MCHC	0.188	0.073	0.463	0.002
	RDW	0.865	0.108	0.260	0.771
WBC count		0.985	0.539	0.422	0.149
Platelets count		0.406	0.533	0.147	0.743
	MPV	0.034	0.528	0.441	0.575

Table 8. p values for the control group and treatment groups (male rats, N=5). Comparison was made on data between day 1 and day 4.					
Males day 14		Within group comparison		Between groups comparison	
		control group	treatment group	Day 1	Day 14
Hct		0.013	0.207	0.969	0.169
RBC count		0.012	0.056	0.033	0.825
	MCV	0.040	0.010	0.058	0.046
	MCH	0.129	0.211	0.065	0.243
	MCHC	0.721	0.138	0.354	0.012
	RDW	0.009	0.178	0.411	0.312
WBC count		0.401	0.848	0.738	0.674
Platelets count		0.456	0.573	0.248	0.592
	MPV	1.000	0.305	0.589	0.882

Clinical chemistry

Table 9. p values of chemistry results for the control group and treatment groups (female rats, N=10). Comparison was made on data between day 1 and day 2.				
Females day 2	Within group comparison		Between groups comparison	
	control group	treatment group	Day 1	Day 2
Sodium	0.692	0.956	0.476	0.141
Potassium	0.079	0.391	0.759	0.035
Chloride	0.943	0.512	0.255	0.004
Bicarbonate	0.027	1.000	0.325	0.213
Anion gap	0.233	0.200	0.140	0.252
Urea	0.692	0.156	0.245	0.148
Creatinine	0.621	0.910	0.446	0.393
Albumin	0.176	0.644	0.504	0.684
AST	0.317	0.592	0.400	0.156
ALT	0.532	0.920	0.412	0.207

Table 10. p values of chemistry results for the control and treatment groups (male rats, N=10). Comparison was made on data between day 1 and day 2.

Males day 2	Within group comparison		Between groups comparison	
	control group	treatment group	Day 1	Day 2
Sodium	0.083	0.000	0.000	0.000
Potassium	0.178	0.751	0.439	0.058
Chloride	0.098	0.003	0.000	0.019
Bicarbonate	0.001	0.005	0.000	0.004
Anion gap	0.128	0.000	0.000	0.000
Urea	0.884	0.594	0.388	0.138
Creatinine (IDMS-trac.)	0.084	0.840	0.019	0.026
Albumin	0.685	0.001	0.005	0.000
AST	0.201	0.906	0.021	0.034
ALT	0.222	0.897	0.030	0.000

Table 11. p values of chemistry results for the control and treatment groups (female rats, N=5). Comparison was made on data between day 1 and day 14.

Females D14	Within group comparison		Between groups comparison	
	control group	treatment group	Day 1	Day 14
Sodium	0.021	0.759	0.098	0.001
Potassium	0.071	0.258	0.040	0.074
Chloride	0.046	0.382	0.277	0.002
Bicarbonate	0.639	0.317	0.000	0.012
Anion gap	0.752	0.375	0.007	0.000
Urea	0.836	0.055	0.233	0.305
Creatinine (IDMS-trac.)	0.191	0.460	0.561	0.266
Albumin	0.056	0.981	0.050	0.049
AST	0.905	0.272	0.888	0.613
ALT	0.037	0.109	0.941	0.631

Table 12. p values of chemistry results for the control and treatment groups (male rats, N=5). Comparison was made on data between day 1 and day 14.

Males day 14	Within group comparison		Between groups comparison	
	control group	treatment group	Day 1	Day 14
Sodium	0.007	0.099	0.012	0.000
Potassium	0.597	0.441	0.348	0.220
Chloride	0.037	0.567	0.031	0.000
Bicarbonate	0.610	0.160	0.001	0.156
Anion gap	0.008	0.027	0.000	0.001
Urea	0.036	0.019	0.554	0.085
Creatinine (IDMS-trac.)	0.300	0.058	0.347	0.365
Albumin	0.105	0.092	0.726	0.005
AST	0.322	0.061	0.029	0.428
ALT	0.946	0.131	0.241	0.280

Chapter VI

General Discussion and Future Perspectives

1. Overview of radiolabeled PDE5 inhibitors

Phosphodiesterases are a superfamily of intracellular enzymes that are involved in the degradation of second messenger cyclic nucleotides (cAMP and cGMP). Phosphodiesterase 5 (PDE5) is a cGMP-specific phosphodiesterase present for example in, smooth muscle cells and pulmonary vasculature. PDE5 is implicated in a number of pathologies including pulmonary arterial hypertension and heart failure/cardiomyopathies. Since the first discovery and approval of the PDE5-specific inhibitor sildenafil for treatment of male erectile dysfunction, many more PDE5 specific inhibitors have been reported and a few more (vardenafil, avanafil and tadalafil) have been approved for human use.

Despite the apparent role of PDE5 in a multitude of diseases, there have not been many reports on developing imaging probes labeled with short lived radionuclides to non-invasively assess and visualize PDE5 expression levels in PDE5-related pathophysiological processes.

Molecular imaging is a rapidly emerging field, providing non-invasive quantitative and reproducible information on fundamental biological processes in intact living subjects. Fundamental biomedical research benefits considerably from advances in molecular imaging and technologies such as microMRI and microPET can be easily translated to the clinics and may provide clinical benefit through improved patient care. Integrating molecular imaging and molecular medicine in combination with system-biology approaches to better understand disease complexity, is very promising to provide predictive, preventive and personalized or patient-centered medicine that will transform healthcare in the future. Therefore, developing PDE5-specific PET radioligands would allow to quantify and evaluate changes in PDE5 expression, select patients that would benefit from PDE5 inhibitors early during disease stages and assess PDE5 occupancy and optimize dose regimens in patients treated with PDE5 inhibitors.

In order to achieve this goal, several PDE5 specific inhibitors that have been reported in the literature were selected, synthesized, radiolabeled and evaluated in animal models. The structure of different PDE5 inhibitors that have been selected for radiolabeling and further investigation in this dissertation are given in figure 1. These nine radiolabeled compounds can be grouped into four clusters based on core structural similarities: pyrazolopyrimidinone (sildenafil ([^{11}C]**14**), [^{11}C]**33** and [^{11}C]**37**), imidazotriazine (NMVardenafil ([^{11}C]**7**), [^{11}C]**8** and [^{18}F]**11**), benzyl amino-quinolin ([^{11}C]**21**) and pyridopyrazinones ([^{11}C]**12** and [^{18}F]**17**).

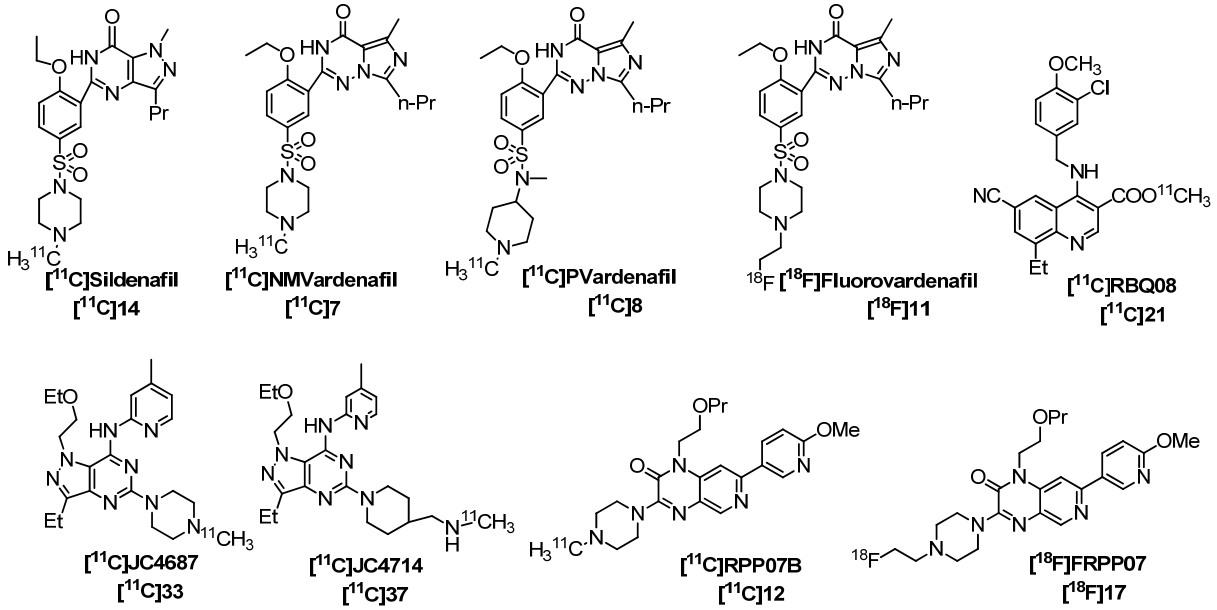

***Figure 1**. Structures of radiolabeled PDE5 inhibitors.*

Selection of PDE5 inhibitors for radiolabeling and biological evaluation was based on reported *in vitro* PDE5 inhibitory activity (IC_{50}), selectivity (specificity) for PDE5, ease of synthetic pathways of precursors and references, and amenability for radiolabeling with carbon-11 or fluorine-18.

Precursors and standard non-radioactive compounds (reference compounds), were successfully synthesized and the latter were sent to Janssen Pharmaceuticals (Beerse, Belgium) to determine their *in vitro* PDE5 inhibitory activity. The *in vitro* PDE5 inhibitory activity of most compounds showed deviations from values reported in the literature except for **7** which showed similar IC_{50} values (table 1).

Carbon-11 was produced in a cyclotron as $[^{11}C]CH_4$ and was converted to the more reactive [^{11}C]methyl iodide and subsequently [^{11}C]methyl triflate. Labeleing was achieved by standard nucleophilic substitution. Fluorine-18 was produced in a cyclotron as $[^{18}F]F^-$. $[^{18}F]F^-$ was used in the tosyl substitution to get [^{18}F]**17**. But converted to 2-[^{18}F]fluoroethyl bromide and subsequently to 2-[^{18}F]fluoroethyl triflate which was used in nucleophilic substitution to produce [^{18}F]**11**.

The radiochemical yield for [^{11}C]**7**, [^{11}C]**8**, [^{11}C]**14**, [^{11}C]**21**, [^{11}C]**33**, [^{11}C]**37** were acceptable for biological evaluation. The labeling of [^{11}C]**12** was not reproducible and consistent and this was reflected in the high standard deviation (20±13). The labeleing of [^{18}F]**11** was not also reproducible. The labeling of [^{18}F]**17** yielded the highest absolute activity upto 6 GBq per

batch. The crude reaction mixture was purified by RP-HPLC in all cases and subsequently formulated for animal experimentation. However, [^{11}C]**37** was further purified with C-18 cartridge in order to get rid of the acetonitrile in the eluting mobile phase and re-formulated. Before animal experimentation, the (radio)chemical purity of the radiolabeled formulation was determined with analytical RP-HPLC. The identity of the radiolabeled compound was confirmed by co-injection with the non-radioactive standard.

Table 1. *Experimental results for different radiolabeled tracers. IC_{50} (nM), lung uptake (SUV±SD, n = 4), blocking (% reduction), heart retention in PDE5 TG mice (SUV±SD, n = 4).*

		IC_{50}[a]	IC_{50}[b]	Lungs[c]	Block[d]	Heart[e]	[f]fold	[g]L/B
Tracers	**other names**	nM	nM	SUV	%	SUV		
[^{11}C]-**7**	[^{11}C]NMVardenafil	0.6	0.8	5.9±1.0	87	12.8±2.1	18.3	11
[^{11}C]-**8**	[^{11}C]PVardenafil	NA	1.1	3.2±0.4	ND	ND	ND	17
[^{18}F]-**11**	[^{18}F]Fluorovardenafil	NA	0.7	6.4±1.6	ND	ND	ND	7
[^{11}C]-**14**	[^{11}C]Sildenafil	3.5	17.3	1.0±0.1	ND	ND	ND	3
[^{11}C]-**21**	[^{11}C]RBQ08	NA	8.1	0.7±0.1	ND	ND	ND	2
[^{11}C]-**33**	[^{11}C]JC4687	0.89	163.6	1.7±0.3	ND	ND	ND	11
[^{11}C]-**37**	[^{11}C]JC4714	0.7	3.2	4.4±1.2	45	3.6±0.9	3.3	32
[^{11}C]-**12**	[^{11}C]RPP07B	NA	6.6	3.1±0.6	32	7.5±0.9	8.3	19
[^{18}F]-**17**	[^{18}F]FRPP07	NA	6.5	2.3±0.3	70	21.4±1.7	16.5	4

[a]IC_{50}: literature reported value for non labeled cold compounds; [b]IC_{50}: values in our assay for non labeled cold compounds; [c]lung retention in healthy mice at 30 min pi (SUV±SD); [d]percentage reduction of lung retention at 30 min pi in healthy mice due to pre-treatment with tadalafil (10 mg/kg, sc); [e]heart retention in PDE5 TG mice at 30 min pi (SUV±SD); [f]percentage increase in uptake of tracers in the myocardium of PDE5 TG mice compared to control at 30 min pi (based on SUV); [g]L/B: lung to blood radioactivity ratio (based on SUV); ND: not determined; NA: not available.

Initial biological evaluation of radiolabeled tracers was investigated in healthy NMRI mice at several post injection (pi) time points (at least at 2 and 30 min pi for all tracers and in some cases additional studies were performed at 10 and 60 min pi). Their retention/uptake in the lungs at 30 min pi was considered indicator of tracers' binding to PDE5 because this enzyme is abundantly expressed in lung tissue. Comparison of retention between different tracers, animal models and conditions (treated and non-treated groups) was made on retention of tracers at 30 min pi. The 30 mi pi was selected because it avoids the early perfusion effect and

it was considered long enough to allow radioligands reach maximal retention. In addition, the selection was partly based on the microPET results of [^{11}C]**7** where the tracer reaches dynamic equilibrium only after 25 min. Only when tracers retention in the lungs of NMRI mice was found to be relatively high, binding specificity of the tracers to PDE5 was assessed by pre-saturating the enzyme (pre-blocking study) with a known structurally unrelated PDE5 specific inhibitor (tadalafil was generally used for this purpose).

Comparison of lung retention of several radiolabeled tracers at 30 min pi showed that the highest retention in the lungs was observed for vardenafil derivatives [^{11}C]**7** and [^{18}F]**11** followed by [^{11}C]**37,** [^{11}C]**8**, and [^{11}C]**12**. [^{18}F]**17** retention in lungs was only moderate whereas other investigated compounds [11C]**14**, [11C]**21** and [11C]**33** showed low retention in lungs which is in agreement with their lower PDE5 *in vitro* inhibitory activity (table 1). However, further investigation of binding of radioligands to PDE5 in the lungs of tadalafil pre-treated mice showed mild for [^{11}C]**12** (32 %), moderate for [^{11}C]**37** (45 %), and marked for [^{11}C]**17** (70 %) and [^{11}C]**7** (87 %) reduction in lung retention based on % injected dose (% ID). The limited reduction of lung retention for [^{11}C]**12** and [^{11}C]**37** can be due to non-specific binding of the tracers to cellular compartment or tissues, but further investigation is required to confirm this hypothesis. The *in vivo* lung retention of the different tracers largely paralleled the *in vitro* PDE5 inhibitory activity (figure 2).

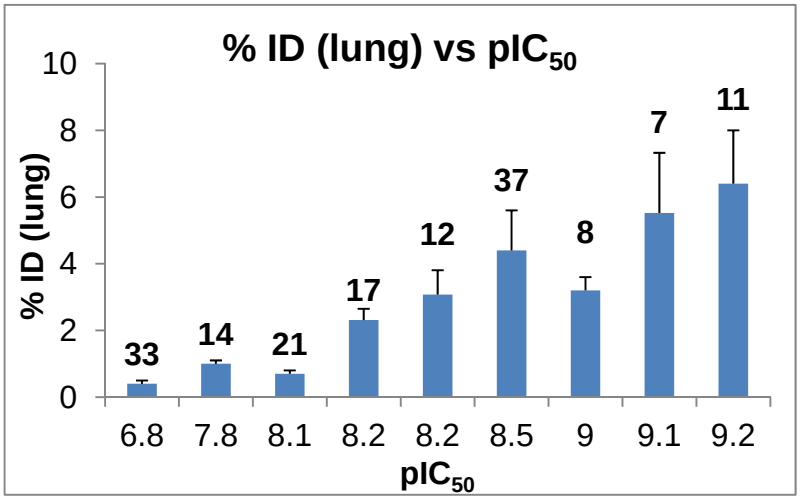

***Figure 2**. Lung retention of different radiolabeled tracers in healthy NMRI mice in relation to their in vitro PDE5 inhibitory activity. pIC_{50} (= $-logIC_{50}$), % ID (% injected dose). For the corresponding names of the numbers, please refer to Appendix at the end of this chapter.*

Some of the more promising tracers ([^{11}C]**7**, [^{11}C]**12**, [^{18}F]**17** and [^{11}C]**37**) were further evaluated in transgenic mice with cardiomyocyte-specific PDE5 over-expression (PDE5 TG) to firmly assess their affinity and specificity for the PDE5 enzyme. The mice were generated at the Department of Cardiovascular Sciences, KU Leuven (*Collaboration with Professor Stefan Janssens*) and graciously supplied to us. The PDE5 TG mice are characterized by an up to 10-fold increase in PDE5 protein expression and a 10-fold increase in sildenafil-inhibitable cGMP hydrolysis specifically in the cardiomyocytes of these mice compared to wild type littermates. Therefore, it was anticipated that any difference observed in the retention of radiotracers administered to the PDE5 TG mice would arise from the increased myocardial (bovine) PDE5 expression level. However, there are no reports describing the difference in affinity of PDE5 inhibitors for bovine and mouse PDE5 as the catalytic core is a highly conserved region across species.

In PDE5 TG mice, [^{11}C]**7** and [^{18}F]**17** showed the highest increase in myocardial retention (18-fold and almost 17-fold, respectively) compared to the retention in wild type (WT) mice at 30 min pi. Similar to previous results, [^{11}C]**12** (8-fold) and [^{11}C]**37** (3-fold) showed only moderately increased myocardial retention in PDE5 TG mice (figure 3, left). In contrast to myocardial uptake, the retention of the tracers in the lungs of PDE5 TG mice decreased significantly (figure 3, right) compared to WT mice: [^{11}C]**37** (60 %), [^{11}C]**12** (50 %), [^{11}C]**7** (45 %), and [^{18}F]**17** (32 %) based on SUV. It was hypothesized that the reduction in lung retention in PDE5 TG mice was due to the ‘‘stealing effect’’ of the high myocardial uptake and lower availability of circulating tracer in the blood.

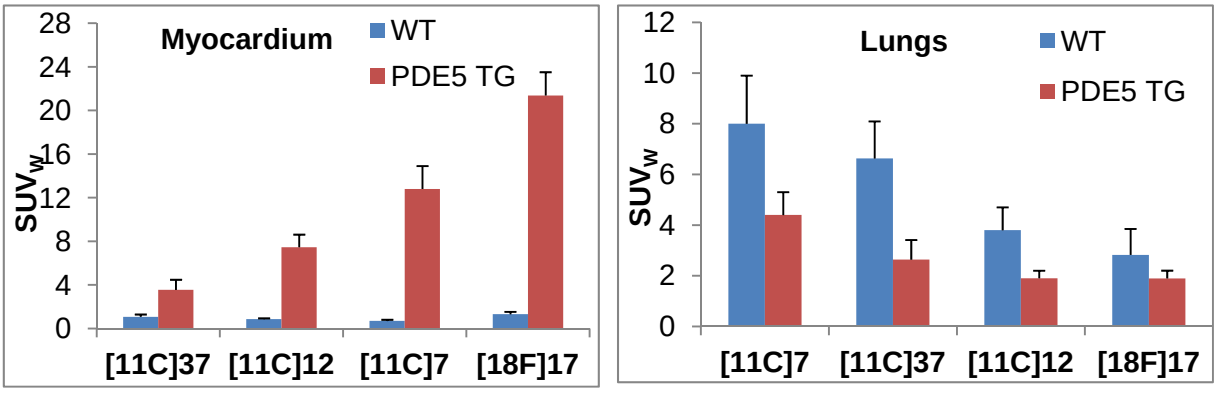

Figure 3. *Left: The myocardium of the PDE5 TG mice showed a marked increase in retention compared to WT mice. Right: The lungs of PDE5 TG mice showed a marked reduction in retention compared to WT mice. SUV (standardized uptake value).*

Thus far, we have discussed invasive methods to evaluate the affinity and specificity of different radiolabeled tracers for PDE5. However, the objective of this research work was to develop radioligands suitable for *in vivo* visualization of PDE5 with positron emission tomography (PET). PET is a non-invasive molecular imaging technique used in nuclear medicine to explore the biochemical process at molecular levels. Therefore, the suitability of the different radioligands for PET imaging was evaluated in different animal models. For this purpose, dynamic microPET imaging of all synthesized radiotracers was performed in PDE5 TG mice. To address specific and reversible binding of the radiolabeled tracers to PDE5, mice were treated with tadalafil prior to administration of the tracers or given tadalafil intravenously (iv) at a specific time (10, 20 or 30 min) after tracer administration, respectively. Tadalafil was chosen for both pre-treatment and chase studies because it is structurally unrelated to the radioligands we have evaluated, hence minimizing the chance of having similar off-target binding patterns.

In the microPET dynamic studies, it was anticipated that a PDE5-specific radioligand would show significantly enhanced accumulation in the myocardium of PDE5 TG mice compared to WT mice. In contrast, tadalafil pre-treated mice should show a significant decrease in tracer accumulation whereas chase experiments were expected to result in displacement of the radioligand from PDE5 catalytic site by the presence of high concentrations of tadalafil if radioligand binding was PDE5 specific and reversible. Radiolabeled tracers with low affinity for PDE5 were not expected to show any significant accumulation in the myocardium of PDE5 TG mice.

Dynamic microPET imaging results of [^{11}C]**7** and [^{11}C]**37** are shown in figure 4. The radioactivity concentration in the myocardium as a function of time after tracer administration was expressed as standardized uptake value (SUV). The time–activity curves (TAC) for the myocardial region after administration of [^{11}C]**37** showed that there was no significant accumulation in PDE5 TG mice (figure 4, left). This is a typical TAC demonstrating low tracer binding due to a too low ratio of PDE5 expression (B_{max}) and tracer binding affinity (K_d). The TACs reconstructed for [^{11}C]**14**, [^{11}C]**8**, [^{11}C]**21** and [^{11}C]**33** were similar to the TAC of [^{11}C]**37** (figure 4, left).

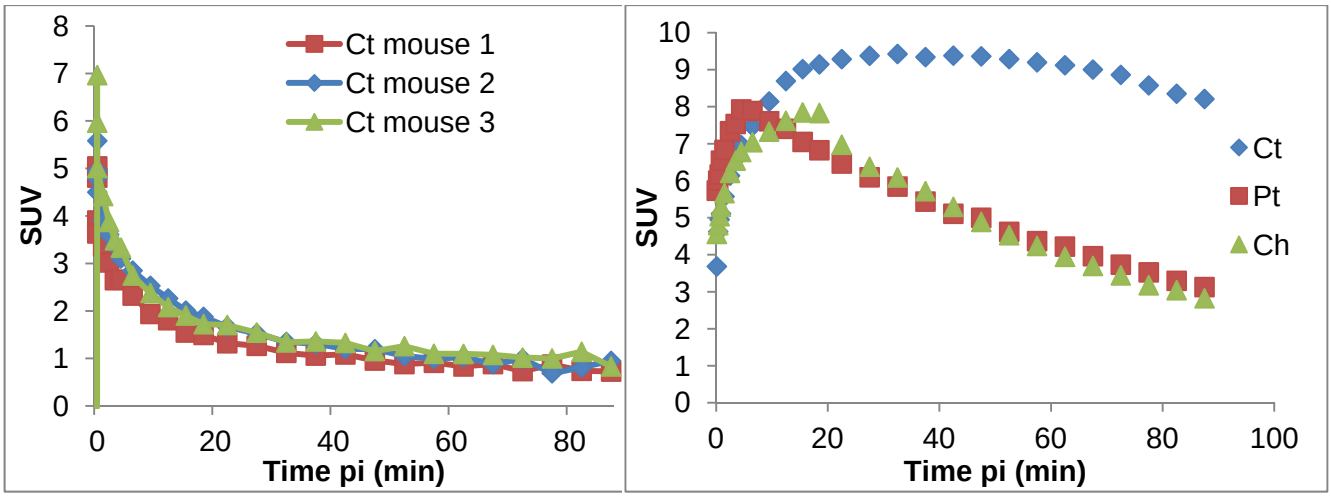

***Figure 4**. Left: Time activity curves of myocardium in three PDE5 TG mice (Control) after iv administration of [^{11}C]**37**. Right: Myocardial time activity curves in three PDE5 TG mice after iv administration of [^{11}C]**7** (Ct: Control; Pt: mouse pre-treated with tadalafil 10 mg/kg, sc; and Ch: mouse given intravenous tadalafil (10 mg/kg, iv after 20 min of tracer injection)*

On the other hand, TACs on the right panel of figure 4 represent a scenario in which radiotracers have a high affinity for PDE5 resulting in a higher B_{max}/K_d ratio. The control mice showed a steady accumulation of radioactivity in the myocardium until a maximum uptake at 30 min pi followed by slow tracer washout. Accumulation of radioactivity in the tadalafil pre-treated mice was significantly reduced and maximal uptake was achieved earlier compared to the control condition. Myocardial tracer uptake was quickly displaced after intravenous administration of tadalafil in the chased mouse. The TACs reconstructed for [^{18}F]**11** showed a similar patterns as the ones observed for [^{11}C]**7** albeit with prolonged plateau starting from 20 min and declining after 60 min. [^{11}C]**12** and [^{18}F]**17**, however, showed much faster kinetics with a maximal myocardial uptake that was reached about 5 min after tracer injection.

The use of PDE5 inhibitors has been described to be beneficial in improving memory, for treating stroke and has effects on object recognition and avoidance learning in different animal models. Nonetheless, all these claims are not without controversies. Therefore, developing radiolabeled PDE5 specific tracer(s) with the ability to cross the blood-brain barrier (BBB) will enable to assess the spatial distribution, the expression levels and the physiological role of PDE5 in the brain. Some of the PDE5 inhibitors, we evaluated, have been described to cross the BBB. However, in our study none of the radiolabeled tracers showed any significant uptake and retention in the brain except for the pyridopyrazinone

family ([^{11}C]**12** and [^{18}F]**17**). *In vitro* autoradiography experiments showed that the pyridopyrazinones [^{11}C]RPP07B and [^{18}F]FRPP07 had a self-displaceable binding in brain slices to a certain degree but their binding could not be blocked to any significant level with other PDE5 specific inhibitors such as tadalafil. In addition, *in vivo* dynamic microPET imaging of rat brain after administration of [^{11}C]**12** or [^{18}F]**17** showed a uniform and significant distribution of both tracers. Nevertheless, their retention could not be blocked by pre-treatment with cold **12** or **17**, hence providing evidence that their binding were not PDE5-specific. From our studies, the binding target of the radiolabeled pyridopyrazinones in brain tissue could not be determined and future studies are needed to determine the binding site.

Based on the results of *in vitro* and *in vivo* evaluation results, we can affirmatively conclude that among the biologically evaluated radiolabeled tracers, the vardenafil derivatives [^{11}C]**7** and [^{18}F]**11** showed the highest affinity and specificity for the PDE5 enzyme followed by the tracers of the pyridopyrazinone family [^{11}C]**12** and [^{18}F]**17**. Although initial biological evaluation of the pyrazolopyrimidinone derivative [^{11}C]**37** showed favorable properties with 45 % inhibitable binding in the lungs of wild type mice; further investigation in PDE5 TG mice showed only a moderate increase in myocardium retention compared to control mice at 30 min pi. The other investigated compounds [^{11}C]**7,** [^{11}C]**14**, [^{11}C]**21** and [^{11}C]**33** showed lower retention in lungs and accordingly there was no significant accumulation in the myocardium of PDE5 TG mice.

Based on our preclinical results, [^{11}C]**7** has been selected for further clinical investigation in selected end-stage heart failure patients awaiting cardiac transplantation. In order to use [^{11}C]**7** in human, a single dose toxicity study of **7** was conducted in rats according to the recommendation of the International Conference on Harmonization (ICH) Topic 3 guideline on Non-clinical Safety Studies for the Conduct of Human Clinical Trials for Pharmaceuticals. Necropsy, hematology and clinical chemistry parameters were fully investigated to determine the safety of **7**.

In the toxicity study, sporadic variation was detected that were statistically but not clinically significant in some cases both in control and test groups treated with **7** for some hematology and biochemical parameters. Nevertheless, systematic, consistent and treatment-related effects were not observed. The toxicity study has paved the path to further pursue the application of [^{11}C]**7** in humans.

2. Limitations and future perspectives

Selection of PDE5 inhibitors was based on reported *in vitro* PDE5 inhibitory activity (IC_{50}), selectivity (specificity) for PDE5, amenability for radiolabeling and synthetic pathways to obtain precursor and reference compounds. Though *in vivo* affinity is a more relevant predictive parameter for a potential PET radioligand, the *in vitro* PDE5 inhibitory activity (IC_{50}) of PDE5 inhibitors is generally reported in literature, particularly in articles or patents of high-throughput screening experiments as the latter is more relevant for potential therapeutic use.

The selection of the benzyl aminoquinoline derivative (**22**, Chapter II - figure 3) was based on its extremely low IC_{50} (50 pM) and high selectivity for PDE5 (at least 7800 times more selective for PDE5 vs PDEs 1 to 6). However, attempts to demethylate **22** with different classical reagents capable of breaking the aryl methyl ether bond (ArOMe) to provide the phenolic precursor for radiolabeling were not successful. It was hypothesized that every attempt to break the ArOMe bond with a Lewis acid also resulted in debenzylation of the compound at the amine bridge (figure 5). A similar boron tribromide mediated debenzylation mechanism was also proposed by Paliakov and Strekowski for a similar compound [118]. Therefore, we selected **21** a close analogue of **19** (Chapter II, figure 3) reported by the same group albeit with lower *in vitro* PDE5 inhibitory activity (0.7 nM) for radiolabeling and further biological evaluation. Hence, the results of the biological evaluation of [^{11}C]**21** might not be representative of the family. Had [^{11}C]**22** been successfully radiolabeled and evaluated, a different results might have been obtained. The same limitation (unsuitability of the lead compound for radiolabeling) applies to the pyrazolopyrimidinone derivative [^{11}C]**37** as the structure of the parent compound reported by Tollefson et al differs slightly. However, our *in vitro* PDE5 inhibitory assay showed similar IC_{50} values (3.2 nM) for both compounds **35** and **37** (Chapter II, figure 4).

We first investigated the affinity and specificity of the radiolabeled tracers with different *in vitro* and *ex vivo* techniques. However, once a radioligand is proven to have high affinity and specificity for the target enzyme (receptor) the natural course would be evaluating this tracer in animal models of diseases relevant to the intended use of the radioligands in humans. However, due to the lack of a well characterized animal model for the intended purpose, our investigation of the suitability of the radiotracers was limited to proof of concept evaluations. Though some of the radioligands were validated in PDE5 TG mice with cardiomyocyte PDE5

over-expression, it remains to be determined how the expression level of PDE5 in the PDE5 TG mice correlates to PDE5 expression levels in patients with cardiomyopathies and other PDE5 related pathologies.

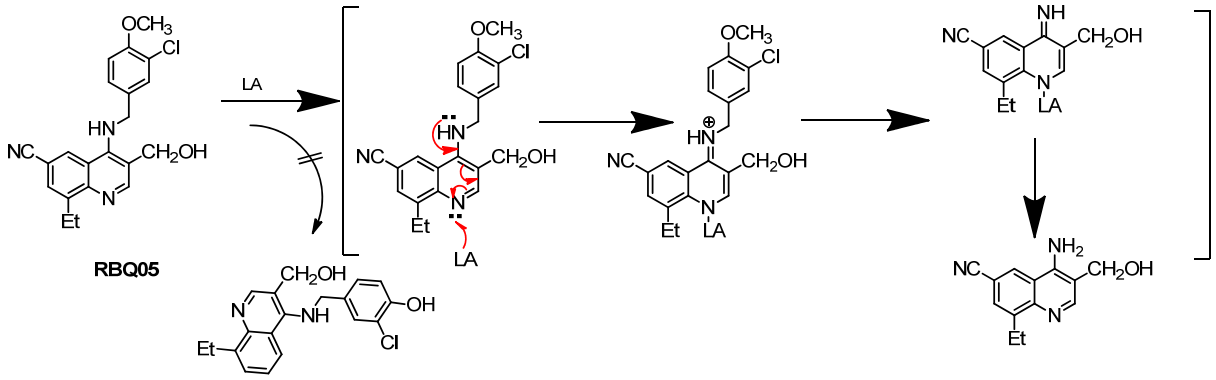

***Figure 5**. Proposed mechanism of debenzylation of **22** by Lewis acids (LA).*

Nonetheless, in light of the interest from different groups to investigate particularly [^{11}C]**7** in a selected group of cardiac patients and patients with pulmonary hypertension; the inability to evaluate this tracer in relevant animal models of disease might not preclude the application of this tracer in the preceding pathologies. In addition to the well known role of PDE5 in PAH and cardiac hypertrophy, there have been numerous reports of its direct or indirect involvement in pathologies such as apoptosis, hypercholesterolemia and atherosclerosis, Raynaud's phenomenon, cystic fibrosis, stroke, and benign prostatic hyperplasia. Future studies in animal models using radiolabeled inhibitors with favorable *in vivo* properties, might shed more light onto the possible role of PDE5 in other diseases/processes that are still under investigation such as apoptosis where the impact of labeled PDE5 tracers might be even higher. PET tracers are advantageous in this regards as it is possible to use them directly in humans once their safety is established unlike bulk pharmaceutical active ingredients where clinical trial takes years of strenuous effort.

Finally, with respect to the 4-benzylaminoquinoline derivates, it might be worth trying to search for alternative methods to provide the phenolic precursor for radiolabeling and biological evaluation. This also holds true for **14** though its close analogue [^{18}F]**17** showed a high affinity for PDE5 albeit with fast kinetics. It was anticipated that the exchange of hydroxyl in the 2-hydroxyethylpiperazine moiety by fluoride would not have much effect on the affinity of the molecule for PDE5. In support of this hypothesis is Hughes' report that in X-ray crystallographic studies, the piperazine substituent points towards the solvent and

therefore, modifications to this region of the molecule would likely have minimal effect on PDE5 affinity and selectivity [72].

3. References: Chapter I and VI

[1] Corbin JD, Francis FH. Molecular biology and pharmacology of PDE-5-inhibitor therapy for erectile dysfunction. J Androl. 2003; 6 (Suppl): S38-41

[2] Cyclicnucleotides.http://users.rcn.com/jkimball.ma.ultranet/BiologyPages/S/Second_messengers.html. Accessed on 04/11/2013

[3] Jeon YH, Heo YS, Kim CM, Hyun YL, Lee TG, Ro S, Cho JM. Phosphodiesterase: overview of protein structures, potential therapeutic applications and recent progress in drug development. Cell Mol Life Sci 2005; 62:1198-220.

[4] Kamenetsky M, Middelhaufe S, Bank EM, Levin LR, Buck J, Steegborn C. Molecular details of cAMP generation in mammalian cells: a tale of two systems. J Mol Biol. 2006; 29:362:623-39.

[5] Zaccolo M, Movsesian MA. cAMP and cGMP signaling cross-talk: role of phosphodiesterases and implications for cardiac pathophysiology. Circ Res 2007; 100:1569-78.

[6] Potter LR, Yoder AR, Flora DR, Antos LK, Dickey DM. Natriuretic peptides: their structures, receptors, physiologic functions and therapeutic applications. Handb Exp Pharmacol 2009; 191:341-66.

[7] Culotta E, Koshland DE Jr. NO news is good news. Science 1992; 18:1862-5.

[8] Baltrons MA, Pedraza C, Sardón T, Navarra M, García A. Regulation of NO-dependent cyclic GMP formation by inflammatory agents in neural cells. Toxicol Lett 2003; 139:191-8.

[9] Alderton WK, Cooper CE, Knowles RG. Nitric oxide synthases: structure, function and inhibition. Biochem J 2001; 357(Pt 3):593-615.

[10] Tsai EJ, Kass DA. Cyclic GMP signaling in cardiovascular pathophysiology and therapeutics. Pharmacol Ther 2009; 122:216-38.

[11] Kass DA, Takimoto E, Nagayama T, Champion HC. Phosphodiesterase regulation of nitric oxide signaling. Cardiovasc Res 2007; 75:303-14.

[12] Rall TW, Sutherland EW. Formation of a cyclic adenine ribonucleotide by tissue particles. J Biol Chem 1958; 232:1065-76.

[13] Francis SH, Turko IV, Corbin JD. Cyclic nucleotide phosphodiesterases: relating structure and function. Prog Nucleic Acid Res Mol Biol 2001; 65:1-52.

[14] Zoraghi R, Bessay EP, Corbin JD, Francis SH. Structural and functional features in human PDE5A1 regulatory domain that provide for allosteric cGMP binding, dimerization, and regulation. J Biol Chem 2005; 280:12051-63.

[15] Conti M, Beavo J. Biochemistry and physiology of cyclic nucleotide phosphodiesterases: essential components in cyclic nucleotide signaling. Annu Rev Biochem 2007; 76:481-511.

[16] Rybalkin SD, Yan C, Bornfeldt KE, Beavo JA. Cyclic GMP phosphodiesterases and regulation of smooth muscle function. Circ Res. 2003; 93:280-91.

[17] Sung BJ, Hwang KY, Jeon YH, Lee JI, Heo YS, Kim JH, Moon J, Yoon JM, Hyun YL, Kim E, Eum SJ, Park SY, Lee JO, Lee TG, Ro S, Cho JM. Structure of the catalytic domain of human phosphodiesterase 5 with bound drug molecules. Nature 2003; 425:98-102.

[18] Kotera J, Fujishige K, Akatsuka H, Imai Y, Yanaka N, Omori K. Novel alternative splice variants of cGMP-binding cGMP-specific phosphodiesterase. J Biol Chem. 1998; 273:26982-90.

[19] Lin CS. Tissue expression, distribution, and regulation of PDE5. Int J Impot Res 2004; 16 Suppl 1:S8-S10.

[20] Lin, Ching-Shwun; Lin, Guiting; Xin, Zhong-Cheng; Lue, Tom F. Expression, Distribution and Regulation of Phosphodiesterase 5. Curr Pharm Des 2006; 12:3439-57.

[21] Lakics V, Karran EH, Boess FG. Quantitative comparison of phosphodiesterase mRNA distribution in human brain and peripheral tissues. Neuropharmacology 2010; 59:367-74.

[22] Loughney K, Hill TR, Florio VA, Uher L, Rosman GJ, Wolda SL, Jones BA, Howard ML, McAllister-Lucas LM, Sonnenburg WK, Francis SH, Corbin JD, Beavo JA, Ferguson K. Isolation and characterization of cDNAs encoding PDE5A, a human cGMP-binding, cGMP-specific 3',5'-cyclic nucleotide phosphodiesterase. Gene 1998; 216:139-47.

[23] Yanaka N, Kotera J, Ohtsuka A, Akatsuka H, Imai Y, Michibata H, Fujishige K, Kawai E, Takebayashi S, Okumura K, Omori K. Expression, structure and chromosomal localization of the human cGMP-binding cGMP-specific phosphodiesterase PDE5A gene. Eur J Biochem 1998; 255:391-9.

[24] Francis SH, Lincoln TM, Corbin JD. Characterization of a novel cGMP binding protein from rat lung. J Biol Chem 1980; 255:620-6.

[25] Corbin JD, Beasley A, Blount MA, Francis SH.High lung PDE5: a strong basis for treating pulmonary hypertension with PDE5 inhibitors. Biochem Biophys Res Commun 2005; 334:930-8.

[26] Shimizu-Albergine M, Rybalkin SD, Rybalkina IG, Feil R, Wolfsgruber W, Hofmann F, Beavo JA. Individual cerebellar Purkinje cells express different cGMP phosphodiesterases (PDEs): in vivo phosphorylation of cGMP-specific PDE (PDE5) as an indicator of cGMP-dependent protein kinase (PKG) activation. J Neurosci 2003; 23:6452-9.

[27] Li Z, Xi X, Gu M, Feil R, Ye RD, Eigenthaler M, Hofmann F, Du X. A stimulatory role for cGMP-dependent protein kinase in platelet activation. Cell 2003; 112:77-86.

[28] Zhu CB, Hewlett WA, Francis SH, Corbin JD, Blakely RD. Stimulation of serotonin transport by the cyclic GMP phosphodiesterase-5 inhibitor sildenafil. Eur J Pharmacol. 2004; 504:1-6.

[29] Sopory S, Kaur T, Visweswariah SS. The cGMP-binding, cGMP-specific phosphodiesterase (PDE5): intestinal cell expression, regulation and role in fluid secretion. Cell Signal 2004; 16:681-92.

[30] Prickaerts J, Sik A, Van Staveren WCG, Koopmans G, Steinbush HWM, Van der Staay, de Vente J, Blokland A. Phosphodiesterase type 5 inhibition improves early memory consolidation of object information. Neurochem Int 2004; 45:915-928.

[31] Thiesson HC, Jensen BL, Jespersen B, Schaffalitzky de Muckadell OB, Bistrup C, Walter S, Ottosen PD, Veje A, Skøtt O. Inhibition of cGMP-specific phosphodiesterase type 5 reduces sodium excretion and arterial blood pressure in patients with NaCl retention and ascites. Am J Physiol Renal Physiol 2005; 288:F1044-52.

[32] Menniti FS, Ren JM, Sietsma DK, Som A, Nelson FR, Stephenson DT et al. A non-brain penetrant PDE5A inhibitor improves functional recovery after stroke in rats. Restor Neurol Neurosci 2012; 4:283-9.

[33] Dunkern TR, Hatzelmann A. The effect of Sildenafil on human platelet secretory function is controlled by a complex interplay between phosphodiesterases 2, 3 and 5. Cell Signal 2005; 17:331-9.

[34] Puzzo D, Sapienza S, Arancio O, Palmeri A. Role of phosphodiesterase 5 in synaptic plasticity and memory. Neuropsychiatr Dis Treat 2008; 2:371-387.

[35] Menniti FS, Faraci WS, Schmidt CJ. Phosphodiesterases in the CNS: targets for drug development. Nat Rev Drug Discov. 2006; 5:660-70.

[36] Prickaerts J, van Staveren WC, Sik A, Markerink-van Ittersum M, Niewöhner U, van der Staay FJ, Blokland A, de Vente J. Effects of two selective phosphodiesterase type 5 inhibitors, sildenafil and vardenafil, on object recognition memory and hippocampal cyclic GMP levels in the rat. Neuroscience 2002; 113: 351–361.

[37] Prickaerts J, de Vente J, Honig W, Steinbusch HW, Blokland A. cGMP, but not cAMP, in rat hippocampus is involved in early stages of object memory consolidation. Eur J Pharmacol 2002; 436:83-7.

[38] Schultheiss D, Müller SV, Nager W, Stief CG, Schlote N, Jonas U, Asvestis C, Johannes S, Münte TF. Central effects of sildenafil (Viagra) on auditory selective attention and verbal recognition memory in humans: a study with event-related brain potentials. World J Urol. 2001; 19:46-50.

[39] Zhu CB, Hewlett WA, Francis SH, Corbin JD, Blakely RD. Stimulation of serotonin transport by the cyclic GMP phosphodiesterase-5 inhibitor sildenafil. Eur J Pharmacol 2004; 504: 1-6.

[40] Fukuo K, Hata S, Suhara T, Nakahashi T, Shinto Y, Tsujimoto Y, Morimoto S, Ogihara T. Nitric oxide induces upregulation of Fas and apoptosis in vascular smooth muscle. Hypertension 1996; 27(3 Pt 2):823-6.

[41] Taimor G, Hofstaetter B, Piper HM. Apoptosis induction by nitric oxide in adult cardiomyocytes via cGMP-signaling and its impairment after simulated ischemia. Cardiovasc Res 2000; 45:588-94.

[42] DeMeester L, Qiu Y, Buchman G, Hotchkiss S, Dunnigan K, Karl E, et al. Nitric oxide inhibits stress-induced endothelial cell apoptosis. Crit Care Med 1998; 26:1500−09.

[43] Thompson HJ, Jiang C, Lu J, Mehta RG, Piazza GA, Paranka NS, et al. Sulfone metabolite of sulindac inhibits mammary carcinogenesis. Cancer Res 1997; 57:267-71.

[44] Lim JT, Piazza GA, Han EK, Delohery TM, Li H, Finn TS, et al. Sulindac derivatives inhibit growth and induce apoptosis in human prostate cancer cell lines. Biochem Pharmacol 1999; 58:1097-1107.

[45] Piazza GA, Thompson WJ, Pamukcu R, Alila HW, Whitehead CM, Liu L, et al. Exisulind, a novel proapoptotic drug, inhibits rat urinary bladder tumorigenesis. Cancer Res 2001; 61:3961-8.

[46] Piazza GA, Rahm AK, Finn TS, Fryer BH, Li H, Stoumen AL, et al. Apoptosis primarily accounts for the growth-inhibitory properties of sulindac metabolites and involves a mechanism that is independent of cyclooxygenase inhibition, cell cycle arrest, and p53 induction. Cancer Res 1997; 57:2452-9.

[47] Thompson WJ, Piazza GA, Li H, Liu L, Fetter J, Zhu B, et al. Exisulind induction of apoptosis involves guanosine 3', 5'-cyclic monophosphate phosphodiesterase inhibition, protein kinase G activation, and attenuated beta-catenin. Cancer Res 2000; 60:3338-42.

[48] Zhu B, Vemavarapu L, Thompson WJ, Strada SJ. Suppression of cyclic GMP-specific phosphodiesterase 5 promotes apoptosis and inhibits growth in HT29 cells. J Cell Biochem 2005; 94:336-50.

[49] Whitehead CM, Earle KA, Fetter J, Xu S, Hartman T, Chan DC, et al. Exisulind-induced apoptosis in a non-small cell lung cancer orthotopic lung tumor model augments docetaxel treatment and contributes to increased survival. Mol Cancer Ther 2003; 2:479-88.

[50] Wharton J, Strange JW, Moller GM, Growcott EJ, Ren X, Franklyn AP, et al. Anti-proliferative effects of phosphodiesterase type 5 inhibition in human pulmonary artery cells. Am J Respir Crit Care Med 2005; 172:105-13.

[51] Zhu B, Strada S, Stevens T. Cyclic GMP-specific phosphodiesterase 5 regulates growth and apoptosis in pulmonary endothelial cells. Am J Physiol Lung Cell Mol Physiol 2005; 289:L196-206.

[52] Kass DA, Champion HC, Beavo JA. Phosphodiesterase type 5: expanding roles in cardiovascular regulation. Circ Res 2007; 101:1084-95.

[53] Viagra: A chronology. http://www.about-ed.com/viagra-history. accessed on 08/11/2013.

[54] Black SM, Sanchez LS, Mata-Greenwood E, Bekker JM, Steinhorn RH, Fineman JR. sGC and PDE5 are elevated in lambs with increased pulmonary blood flow and pulmonary hypertension. Am J Physiol Lung Cell Mol Physiol 2001; 281:L1051-7.

[55] Buckley MS, Staib RL, Wicks LM, Feldman JP. Phosphodiesterase-5 inhibitors in management of pulmonary hypertension: Safety, tolerability, and efficacy. Drug Healthc Patient Saf 2010; 2:151-161.

[56] Humbert M, Morrell NW, Archer SL, Stenmark KR, MacLean MR, Lang IM, Christman BW, Weir EK, Eickelberg O, Voelkel NF, Rabinovitch M. Cellular and

molecular pathobiology of pulmonary arterial hypertension. J Am Coll Cardiol 2004; 16:43(12 Suppl S):13S-24S.

[57] Dorfmüller P, Perros F, Balabanian K, Humbert M. Inflammation in pulmonary arterial hypertension. Eur Respir J 2003; 22:358–63.

[58] Lamé MW, Jones AD, Wilson DW, Segall HJ. Monocrotaline pyrrole targets proteins with and without cysteine residues in the cytosol and membranes of human pulmonary artery endothelial cells. Proteomics 2005; 5:4398-413.

[59] Molkentin JD, Forc T. Molecular signaling networks underlying cardiac hypertrophy and failure. In: Dec GW editor. Heart failure: A comprehensive guide to diagnosis and treatment. New York: Marcel Dekker; 2005, p. 23-43.

[60] Opie LH, Commerford PJ, Gersh BJ, Pfeffer MA. Controversies in ventricular remodelling. Lancet 2006; 367:356–67.

[61] Nagendran J, Archer SL, Soliman D, Gurtu V, Moudgil R, Haromy A, St Aubin C, Webster L, Rebeyka IM, Ross DB, Light PE, Dyck JR, Michelakis ED.Phosphodiesterase type 5 is highly expressed in the hypertrophied human right ventricle, and acute inhibition of phosphodiesterase type 5 improves contractility. Circulation. 2007;116:238-48.

[62] Pokreisz P, Vandenwijngaert S, Bito V, Van den Bergh A, Lenaerts I, Busch C, Marsboom G, Gheysens O, Vermeersch P, Biesmans L, Liu X, Gillijns H, Pellens M, Van Lommel A, Buys E, Schoonjans L, Vanhaecke J, Verbeken E, Sipido K, Herijgers P, Bloch KD, Janssens SP. Ventricular phosphodiesterase-5 expression is increased in patients with advanced heart failure and contributes to adverse ventricular remodeling after myocardial infarction in mice. Circulation 2009; 119:408-16.

[63] Vandenwijngaert S, Pokreisz P, Hermans H, Gillijns H, Pellens M, Bax NA, Coppiello G, Oosterlinck W, Balogh A, Papp Z, Bouten CV, Bartunek J, D'hooge J, Luttun A, Verbeken E, Herregods MC, Herijgers P, Bloch KD, Janssens S. Increased cardiac myocyte PDE5 levels in human and murine pressure overload hypertrophy contribute to adverse LV remodeling. PLoS One 2013; 8:e58841.

[64] Shan X, Quaile MP, Monk JK, French B, Cappola TP el al. Differential expression of PDE5 in failing and nonfailing human myocardium. Circ Heart Fail 1012; 5:79-86.

[65] Lu Z, Xu X, Hu X, Lee S, Traverse J. Oxidative stress regulates left ventricular PDE5 expression in the failing heart. Circulation 2010; 121:1474-83.

[66] Laber U, Kober T, Schmitz V, Schrammel A, Meyer W, Mayer B, Weber M, Kojda G. Effect of hypercholesterolemia on expression and function of vascular soluble guanylyl cyclase. Circulation 2002; 105:855–60.

[67] Oelze M, Mollnau H, Hoffmann N, Warnholtz A, Bodenschatz M, Smolenski A, Walter U, Skatchkov M, Meinertz T, Munzel T. Vasodilator-stimulated phosphoprotein serine 239 phosphorylation as a sensitive monitor of defective nitric oxide/cGMP signaling and endothelial dysfunction. Circ Res 2000; 87:999–1005.

[68] Giovannoni MP, Vergelli C, Graziano A, Dal Piaz V. PDE5 inhibitors and their applications. Curr Med Chem 2010; 17:2564-87.

[69] Acker BA, Hughes RO, Jacobsen EJ, Hwang-Fun RT, Tollefson MB, Walker JK, et al. Novel pharmaceuticals. World patent 2006; WO 2006/0461135A2.

[70] Tollefson MB, Acker BA, Jacobsen EJ, Hughes RO , Walker JK, Foker DN, et al. 1-(2-ethoxyethyl)-1H-pyrazolo[4,3-d]pyrimidines as potent phosphodiesterase 5 (PDE5) inhibitors. Bioorg Med Chem Lett 2010; 20:3120-24.

[71] Hughes RO, Bell AS, Brown DG, Owen d, Palmer MJ, Phillips CP, et al. Pyridine[3,4-B]pyrazinones. US Patent 2007; US2007/0249615A1.

[72] Hughes RO, Rogier DJ, Jacobsen EJ, Walker JK, Macinnes A, Bond BR, et al. Hughes RO, Rogier DJ, Jacobsen EJ, Walker JK, Macinnes A, Bond BR, et al. Design, synthesis, and biological evaluation of 3-[4-(2-hydroxyethyl)piperazin-1-yl]-7-(6-methoxypyridin-3-yl)-1-(2-propoxyethyl)pyrido[3,4-b]pyrazin-2(1H)-one, a potent, orally active, brain penetrant inhibitor of phosphodiesterase 5 (PDE5). J Med Chem 2010; 6:2656-60.

[73] Menniti FS, Ren JM, Coskran TM, Liu J, Morton D, Siestsma DK, et al. Phosphodiesterase 5A inhibitors improve functional recovery after stroke in rats: optimized dosing regimen with implication for mechanism. J Pharmacol Exp Ther 2009; 3:842-50.

[74] Bell AS, Palmer MJ. Novel phosphodiesterase type 5 modulators: a patent survey (2008 - 2010). Expert Opin Ther Pat 2011; 21:1631-41.

[75] Haning H, Niewohner N, Schenke T, Es-Sayed M, Schmidt G, Lampe T, et al. Imidazo[5,1-f][1,2,4]triazin-4(3H)-ones, a new class of potent PDE 5 inhibitors. Bioorg Med Chem Lett 2002; 12:865-68.

[76] Niewohner U, Es-Sayed M, haning H, Schenke T, Schlemmer KH, Keldenich J, et al. 2-Phenyl substituted imidazotriazinones as phosphodiesterase inhibitors. US Patent 2002; US6362178B1.

[77] Dungan A, Grondin P, Ruault C, Le Monnier de Gouvile A-C, Coste H, Kirilovsky J, et al. The discovery of tadalafil: A novel and highly selective PDE5 inhibitor. 2: 2,3,6,7,12,12a-hexahydropyrazino[1´,2´:1,6]pyrido[3,4,-b]indole-1,4,-dione analogues. J Med Chem 2003; 46:4533-42.

[78] Bi Y, Yu Guixue, Rotella DP, Macor JE (2003) Quinoline inhibitors of cGMP phosphodiesterase. US patent, US 6576644 B2.

[79] Bi Y, Stoy P, Adam L, He B, Krupinski J, Normandin D, et al. Quinolines as extremely potent and selective PDE5 inhibitors as potential agents for treatment of erectile dysfunction. Bioorg Med Chem Lett 2004: 14: 1577-80.

[80] Fiorito J, Saeed F, Zhang H, Staniszewski A, Feng Y, Francis YI, et al. Synthesis of quinoline derivatives: discovery of a potent and selective phosphodiesterase 5 inhibitor for the treatment of Alzheimer's disease. Eur J Med Chem 2013; 60:285-94.

[81] Piazza GA, Alberts DS, Hixson LJ, Paranka NS, Li H, Finn T, Bogert C, Guillen JM, Brendel K, Gross PH, Sperl G, Ritchie J, Burt RW, Ellsworth L, Ahnen DJ, Pamukcu R. Sulindac sulfone inhibits azoxymethane-induced colon carcinogenesis in rats without reducing prostaglandin levels. Cancer Res 1997; 57:2909-15.

[82] Corbin, J.D. Mechanisms of action of PDES inhibition in erectile dysfunction. Int J Impot Res 2004, 16:(suppl I)S4-S7.

[83] Antoniu SA. Sildenafil citrate for the treatment of pulmonary arterial hypertension. Expert Opin Pharmacother. 2006; 7:825-8.

[84] Leibovitch L, Matok I, Paret G. Therapeutic applications of sildenafil citrate in the management of paediatric pulmonary hypertension. Drugs 2007, 67:57-73.

[85] Doggrell SA. Phosphodiesterase 5A as a target in cardiac disease. Expert Opin Ther Targets. 2005; 9(5):1097-100.

[86] Takimoto E, Champion HC, Li M, Belardi D, Ren S, Rodriguez ER, Bedja D, Gabrielson KL, Wang Y, Kass DA. Chronic inhibition of cyclic GMP phosphodiesterase 5A prevents and reverses cardiac hypertrophy. Nat Med 2005; 11:214-22.

[87] Hassan MAH, Ketat AF. Sildenafil citrate increases myocardial cGMP content in rat heart, decreases its hypertrophic response to isoproterenol and decreases myocardial leak of creatine kinase and troponin T. BMC Pharmco 2005; l5:6-10.

[88] Salloum FN, Ockaili RA, Wittkamp M, Marwaha VR, Kukreja RC; Vardenafil: a novel type 5 phosphodiesterase inhibitor reduces myocardial infarct size following ischemia/reperfusion injury via opening of mitochondrial KATP channels in rabbits. J Mol Cell Cardiol 2006; 40:405-11.

[89] Szabo G, Radovits T, Veres G, Krieger N, Loganathan S, Sandner P, et al. Vardenafil protects against myocardial and endothelial injuries after cardiopulmonary bypass. Eur J Cardiothorac Surg 2009; 36:657-64.

[90] Guazzi M, Vicenzi M, Area R, guazzi MD. PDE5 inhibition with sildenafil improves left ventricular diastolic function, cardiac geometry, and clinical status in patients with stable systolic heart failure: results of a 1-year, prospective, randomized, placebo-controlled study. Circ Heart Fail 2010; 1:8-17.

[91] Levien, T.L. Phosphodiesterase inhibitors in Raynaud's phenomenon. Ann. Pharmacother 2006; 411:1388-93.

[92] Friedman EA, Harris PA, Wood AL, Stein CM, Kurnik D. The effects of tadalafil on cold-induced vasoconstriction in patients with Raynaud's phenomenon. Clin Pharmacol Ther 2007, 81:503-9.

[93] McPherson MA, Pereira MM, Lloyd Mills C, Murray KJ, Dormer RL. Cyclic nucleotide PDE5 inhibitor corrects defective mucin secretion in submandibular cells containing antibody directed against cystic fibrosis transmemberane conductance regulator protein. FEBS Lett 1999; 464:48-52.

[94] Lubamba B, Lecourt H, Lebacq J, Lebecque P, De Jonge H, Wallemacq P, Leal T. Preclinical evidence that sildenafil and vardenafil activate chloride transport in cystic fibrosis. Am J Respir Crit Care Med 2008; 177:506-15.

[95] Prickaerts J, Steinbusch HW, Smits JF, de Vente J. Possible role of nitric oxide-cyclic GMP pathway in object recognition memory: effects of 7-nitroindazole and zaprinast. Eur J Pharmacol. 1997; 337:125-36.

[96] Baratti CM, Boccia MM. Effects of sildenafil on long-term retention of an inhibitory avoidance response in mice. Behav Pharmacol. 1999; 10:731-7.

[97] Bednar MM. The role of sildenafil in the treatment of stroke. Curr Opin Investig Drugs. 2008; 9:754-9

[98] Bortolotti M, Mari C, Lopilato C, Porrazzo G, Miglioli M. Effects of sildenafil on esophageal motility of patients with idiopathic achalasia. Gastroenterology 2000; 118:253-7.

[99] Richalet JP, Gratadour P, Robach P, Pham I, Déchaux M, Joncquiert-Latarjet A, Mollard P, Brugniaux J, Cornolo J. Sildenafil inhibits altitude-induced hypoxemia and pulmonary hypertension. Am J Respir Crit Care Med 2005; 171:275-81.

[100] Gonzalez RR, Kaplan SA. Tadalafil for the treatment of lower urinary tract symptoms in men with benign prostatic hyperplasia. Expert Opin Drug Metab Toxicol 2006; 2:609-17.

[101] Zhang Z, Klyachko V, Jackson MB. Blockade of phosphodiesterase Type 5 enhances rat neurohypophysial excitability and electrically evoked oxytocin release. J Physiol 2007; 584(Pt 1):137-47.

[102] Andrés JI, De Angelis M, Alcázar J, Celen S, Bormans G. Recent advances in positron emission tomography (PET) radiotracers for imaging phosphodiesterases. Curr Top Med Chem 2012; 12:1224-36.

[103] DaSilva JN, Lourenco CM, Meyer JH, Hussey D, Potter WZ, Houle S. Imaging cAMP-specific phosphodiesterase-4 in human brain with R-[11C]rolipram and positron emission tomography. Eur J Nucl Med Mol Imaging 2002; 29:1680-3.

[104] Celen S, Koole M, De Angelis M, Sannen I, Chitneni SK, Alcazar J, Dedeurwaerdere S, Moechars D, Schmidt M, Verbruggen A, Langlois X, Van Laere K, Andrés JI, Bormans G. Preclinical evaluation of 18F-JNJ41510417 as a radioligand for PET imaging of phosphodiesterase-10A in the brain. J Nucl Med 2010; 51:1584-91.

[105] Li P, Wennogle LP, Zhao J, Zheng H. Phosphodiesterase 1-Targeting Tracers and Methods. PCT Int. Appl. WO2011043816, 2011.

[106] Jakobsen S, Kodahl GM, Olsen AK, Cumming P. Synthesis, radiolabelling and in vivo evaluation of [11C]RAL-01, a potential phosphodiesterase 5 radioligand. Nucl Med Biol 2006; 33:593-97.

[107] Mankoff D. A definition of molecular imaging. J. Nucl. Med. 2007, 48, 18N, 21N.

[108] Saha GB. Fundamentals of nuclear pharmacy. 5th ed. New York; Springer, 2004.

[109] Saha GB. Basics of PET imaging: Physics, Chemistry, and Regulations. Cleveland, Springer, 2005.

[110] Miller PW, Long NJ, Vilar R, Gee AD. Synthesis of ^{11}C, ^{18}F, ^{15}O and ^{13}N radiolabels for positron emission tomography. Angew Chem Int Ed Engl 2008; 47:8998-9033.

[111] Allard M1, Fouquet E, James D, Szlosek-Pinaud M. State of art in ^{11}C labelled radiotracers synthesis. Curr Med Chem. 2008; 15:235-77.

[112] Wester H (ed). Munich molecular imaging handbook series Volume 1: Pharmaceutical radiochemistry (1). Fürstenfeldbruck; Scintomics, 2010.

[113] Sampson C. 3rd ed. Text book of Radiopharmacy: Theory and practice. Amsterdam; Gordon and Breach Science Publishers, 1999.

[114] Van Veghel D. Development and biological evaluation of PET-tracers for in vivo visualisation of the endovanilloid/endocannabinoid system. Doctoral dissertation in Pharmaceutical Sciences 2013; Laboratory for Radiopharmacy, KU Leuven.

[115] Tolmachev V and Stone-Elander S. Radiolabelled proteins for positron emission tomography: Pros and cons of labelling methods. Biochim Biophys Acta 2010, 1800:487-510.

[116] Serdons K, Verbruggen A and Bormans GM. Developing new molecular imaging probes for PET. Methods 2009; 48:104-11.

[117] Verhoeff NP. Pharmacological implications for neuroreceptor imaging. Eur J Nucl Med 1991; 18:482-502.

[118] Paliakov E, Strekowski L. Boron tribromide mediated debenzylation of benzylamino and benzyloxy groups. Tetrahedron Letters 2004; 45: 4093-95.

Curriculum Vitae

Rufael Chekol was born on 18th of February, 1977 in Wellega, Ethiopia. In 1995, he completed his secondary school at Aste Gelawdios High School in Adama, Oromiya, Ethiopia. Afterwards, he started his studies in Pharmacy at School of Pharmacy, Addis Ababa University, and obtained Bachelor of Pharmacy in 2001. Between 2002 and 2008, he worked in a hospital (Shashemene General Hospital) as head of pharmacy department and college (Hayome Medical School) as an instructor. In September 2008, he started his postgraduate studies at the Laboratory of Radiopharmacy (KU Leuven) under the promotership of Prof. Alfons Verbruggen and obtained a Master degree in Postgraduate Studies in Pharmaceutical Research (Distinction) in 2009. Subsequently in October 2009, he started his PhD thesis work on 'Development of Radiolabeled PET Tracers for *in vivo* Visualization of Phosphodiesterase Type 5 (PDE5)' at the Faculty of Pharmaceutical & Pharmacological Sciences, Laboratory of Radiopharmacy, KU Leuven under guidance of his promoter Prof. Guy Bormans and co-promoters Prof. Alfons Verbruggen and Prof. Olivier Gheysens.

List of publications

Papers in international peer-reviewed journals

Chekol R, Gheysens O, Cleynhens J, Pokreisz P, Vanhoof G, Ahamed M, Janssens S, Verbruggen A, Bormans G. Evaluation of PET radioligands for *in vivo* visualization of phosphodiesterase 5 (PDE5). Nucl Med Biol. 2014; 41:155-162.

Gheysens O, Akurathi V, **Chekol R**, Dresselaers T, Celen S, Koole M, Dauwe D, Cleynhens BJ, Claus P, Janssens S, Verbruggen AM, Nuyts J, Himmelreich U, Bormans GM (2013). Preclinical evaluation of carbon-11 and fluorine-18 sulfonamide derivatives for *in viv*o radiolabeling of erythrocytes. EJNMMI Research, 4, doi: 10.1186/2191-219X-3-4.

Bauwens, M., **Chekol, R.**, Vanbilloen, H., Bormans, G., Verbruggen, A. (2010). Optimal buffer choice of the radiosynthesis of Ga-68-Dotatoc for clinical application. *Nuclear medicine communications, 31* (8), 753-758.

Chekol R; Gheysens O; Dauwe D; Postnov A; Pokreisz P; Janssens S; Verbruggen A; Bormans G. [^{11}C]NMVardenafil: A PET radioligand for in vivo visualization of phosphodiesterase type 5 (PDE5). J Nuc Med. 2014. S*ubmitted.*

Chekol R; Gheysens R; Cleynhens R; Pokreisz P; Vanhoof G; Ahamed M; Janssens S; Verbruggen A; Bormans G. Radiolabeled pyridopyrazinone derivatives for PET imaging of phosphodiesterase-5A (PDE5). J Med Chem. 2014. S*ubmitted.*

Publication and presentation at international congresses

Chekol, R, Gheysens, O, Cleynhens, J, Janssens, S, Verbruggen, A, Bormans, G. [^{11}C]RPP07B a potential radioligand for *in vivo* visualization of PDE5 in myocardium and brain. J Nucl Med. 2013; 54 (Supplement 2):385. SNM anuual meeting 2013, Vancouver, BC, Canada. *Oral presentation.*

Chekol R, Gheysens O, Cleynhens J, Janssens S, Verbruggen A, Bormans G. [^{11}C]JC4714 as a potential radioligand for in vivo visualization of phosphodiesterase 5. ISRS 2013, Jeju, S. Korea. *Poster presentation.*

Chekol R, Gheysens O, Cleynhens J, Janssens S, Verbruggen A, Bormans G. Fluorine-18 and carbon-11 labeled vardenafil derivatives for *in vivo* visualization of phosphodiesterase 5 in myocardium. SNM 2012, J Nucl Med 2012; 53 (Supplement 1):72. *RPSC Young Investigator Award Symposium (1st place). Oral presentation.*

Chekol R, Gheysens O, Cleyhens J, Janssens S, Verbruggen A, Bormans G. (2011). Radiosynthesis and biological evaluation of a carbon-11 labelled vardenafil derivative as a PDE5 specific tracer. *J Labelled Comp Radiopharm 2011; 54, S152-S152*. ISRS 2011. *Poster presentation. Amsterdam 2011.*

Chekol R, Gheysens O, Cleyhens J, Janssens S, Verbruggen A, Bormans G. Labelling and preliminary biological evaluation of [C-11]RBQ08 as a specific PDE5 radiotracer. *J Labelled Comp Radiopharm 2011; 54:S153-S153*. ISRS 2011. *Poster presentation. Amsterdam 2011.*